The Application of Vector Control to PWM Drives

Dipl.-Ing.(FH) Dirk W. Schaper

A Thesis submitted in partial fulfilment of the requirements of the University of Glamorgan for the degree of Master of Philosophy

June 1993

University of Glamorgan

Acknowledgments

I am most greatful for the continuous help, discussions and interest of my Director of Studies, Dr. M.G. Jayne, and my second supervisors Prof. Dr.-Ing. Peter F. Brosch and Mr. S. Gardener, during the period of research to which this thesis relates. I am also thankful to Mr. J. Warrington from Black Clawson Vanguard Drives for his support and encouragement.

My gratitude is also extended to the Fachhochschule Hannover, the collaborating establishment, for offering me this opportunity to study in Wales and supporting me whilst here. I would especially like to name Prof. Dr.-Ing. Brosch and Prof. Dipl.-Ing. Friedrich in thanks for the employment they provided for my financial support.

I would also like to thank the technical and secretarial staff of the Department of Electronics and Information Technology for their assistance throughout and I wish to express my special thanks to my fellow researcher Mr. Ceri Evans for his support.

I am also greatful to my family, who supported and encouraged me throughout, and who allowed me to take this opportunity.

Abstract

This thesis describes the results of an investigation into the performance and behaviour of inverter fed induction motor drive systems, where the main aim of the investigation was to produce a means of simulation, whereby the transient response of drives could be studied in detail.

It is shown that a useful simulation of an inverter drive can be achieved by means of a standard software package and a Personal Computer (PC). The thesis demonstrates that once the mathematical model for the drive system is established, a software package called MATLAB can be employed to study the performance of such electrical drive systems. Two types of induction motor drives were investigated in detail by means of this package. The first drive consisted of an open loop Pulse Width Modulated (PWM) inverter induction motor drive system, whereas the second was a PWM Vector Control System.

The thesis also contains the results of experimental investigations into the performance of the drive system, where the control strategies were implemented by means of a transputer. The experimental results demonstrate good correlation with the simulated results.

The thesis also contains the design and development of a flux trajectory observation system which may be employed to study the behaviour of the drive system, when supplied with modulated voltage waveforms which contain harmonics.

Table of Contents

1. Introduction

1.1. Historical review of classical Drives

Variable speed electrical drives are used extensively in industry, commerce and domestic premises. The considerable increase in the application of such drive systems to commerce and domestic premises can mainly be attributed to the increased automation of offices and kitchens in domestic premises. The demands of such drives are of course determined by the application, which varies considerably from heavy industry to domestic premises. The requirements of such drives, however, may be categorized as follows:

1) the drive must be capable of a wide range of speed control, whilst maintaining the required torque;

2) the drive system must sustain good dynamic performance whilst requiring minimum maintenance.

By looking back at the development of drive technology, one sees that the first attempt of providing a drive system resulted in the steam engine. These systems were mainly used to replace men and animal power or more unreliable power generators such as wind or water powered systems. The steam engine was mainly applied to heavy industrial processes. The development of electrical power, however, brought with it a widespread increase in the requirement for drive systems. Whilst electrical power could be generated by the direct current (DC) type and the alternating current (AC) type, the first freely available power was the DC type mainly because DC machines were developed before the now well known AC types. The wide utilisation of DC power was restricted because of the difficulties inherent in the distribution of DC power. This problem, however, was overcome with the invention of the polyphase AC machine by Tesla [1.1.1]. Two new machines were developed by Tesla, the synchronous and the asynchronous induction machine. Simultaneously, the Transformer was developed

[1.1.2] which also played an important role in transferring power with minimal losses over great distances.

The three phase AC system of distribution of constant frequency and of fixed voltage then formed the basis for electrical energy distribution to modern industry and went on a road of success to its present level.

The relative advantages and disadvantages of the synchronous and asynchronous machine may be summarized as follows:

The synchronous machine is only able to run at a speed proportional to its supply frequency. This machine is not of great use for variable speed drive systems. Nowadays there are applications where it is used with electronics, to run as a brushless DC motor, but its major application is in the area of power generation.

The asynchronous machine requires little maintenance especially in the case of the cage rotor machine. But its application was mainly for constant speed because of the inadequate means of varying its supply frequency.

The DC machine with its characteristics forms the ideal drive. Its disadvantage, however, is the need for maintenance of the brushes and commutators and its relatively high cost, when compared with the induction motor.

It should be stressed that in order for the attractive characteristics of the DC machine to be utilized the motor requires variable DC voltages. In high power applications this requirement was satisfied by the Ward-Leonard system, which added great cost to the overall variable speed DC motor drive.

With the introduction of semiconductor power devices in the 1950's [1.1.3] it was anticipated that the disadvantages of variable speed drive systems such as the Ward-Leonard set could be removed. Following the introduction of power semiconductor devices rapid development in this domain took place, which resulted in the introduction of such

devices as the transistor, thyristor and gate turn off thyristor (GTO). After a number of years the advances made in MOS technology also brought forward other power semiconductor devices such as the power MOS-FET and insulated gate bipolar transistors (IGBT). These advances provided the basis for two areas of influence on drive technology. The first area of influence was the development of efficient DC to AC converters and inverters whereas the second influence was in the micro electronic field, which resulted in the development of the microprocessor.

The availability of power semiconductor switching devices allowed efficient inverters to be built. This became of great significance, because it allowed induction machines to be supplied with variable voltage and variable frequency.

The type of inverter system used for variable speed induction motor drives was known as the DC-link inverter. Such systems consisted of an AC to DC converter (CON), an intermediate DC-link, and a forced commutated inverter (INV) as illustrated in Figure 1.

The AC to DC converter basically consists of diodes, which are used to transform three phase supply voltages to a DC voltage. The intermediate circuit, known as the DC-link, is used to store the rectified energy. If the intermediate circuit is made to contain a very large value of inductance the inverter system is often referred to as a current source inverter. If the DC-link mainly consists of capacitors this system is know as a voltage source inverter. The output inverter consists of a configuration of power semiconductor devices which converts DC to AC. The choice of switching device depends very much upon the power requirement of the application. Which type of inverter to choose depends very much upon the application and the number of quadrants the drive system is required to perform in. It is generally found that current source inverters are mainly applied to only large power variable speed drives. The voltage source inverter, however, is the most used type in industry and is applied to a wide range of variable speed applications.

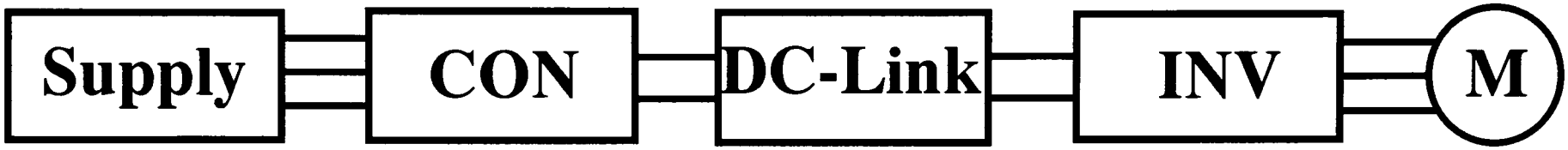

Fig. 1: Block diagram of an inverter drive system

Thus the advances made in power semiconductor devices and the converters to which they are applied has resulted in a widespread increase in the use of cage rotor induction motors for variable speed applications. The reasons for the choice of cage rotor induction motor over the DC motor are maintenance and cost based.

The induction machine is well known and its construction and design is mainly optimized. There are actually no great new developments to be expected so far as induction motor technology is concerned. The inverter is also now well known, but there is still some development in the area of power semiconductors, which generally results in the device having improved power rating, switching speed and switching losses. Also new switching power devices with integrated control modules are becoming available, little significant improvement can be expected in converter technology.

The area of electrical drive systems where considerable improvement is still taking place is control strategy. Fundamental to electrical drive control strategy is the mathematical modelling of the components which make up the drive system. Considerable progress has been made over the last decade in the derivation of mathematical models of all of the components in an electrical drive system. An area, however, where progress has been limited is the use of the mathematical models developed in simulation software packages. One of the prime areas where considerable difficulty has been experienced in the mathematical modelling of the induction motor is where the induction motor is subjected to vector control. The difficulty experienced can mainly be attributed to the manipulation of the matrix equations involved in the modelling. The manipulation and solving of these equations have involved considerable computing time, prior to the availability of a software simulation package knows as MATLAB.

The investigation reported in this thesis was mainly devoted to the implementation and transformation of electrical drive component models, so that they may be usefully applied to MATLAB.

There is a lot of research going on in the area of control strategies. Modern microprocessor technology opens a wide range of possibilities. It is in this area where developments are to be expected and this is the area this work will concentrate on.

1.2. PWM

Modern inverter technology began with the advent of power semiconductors in the 1950's [1.2.1-1.2.3]. Before that time the use of AC machines was mainly limited to constant speed applications. The availability of semiconductor devices, however, provided the opportunity for synthesizing alternating voltage waveforms which basically provided the basis for much of the variable speed drive system research which is taking place.

In the early years of inverter technology the semiconductor switching devices were mainly connected in configurations which provided the generation of basic alternating waveforms such as square waves. It was soon realized, however, that because of the harmonic content of these waveforms induction motors did not perform efficiently and with sufficient stability, when supplied with such waveforms. In order to overcome these undesirable features considerable research was carried out into the modulation techniques which could provide an alternating variable voltage/variable frequency waveform with low harmonic content.

Since all power converters can be shown to be modulators it was realized that techniques used in the field of communication could be employed in power converters. Such technologies as pulse amplitude modulation (PAM), pulse position modulation (PPM) and pulse width modulation (PWM) were investigated in-depth to discover whether such techniques could meet the requirements of variable speed DC-link inverter drive systems.

In order to minimize the harmonic content of modulated waveforms other communication techniques such as natural and regular sampling were also employed [1.2.4]. Many other harmonic elimination techniques such as notch control were also employed [1.2.5-1.2.7].

1.3. Vector Control

In 1973 a new control strategy for variable speed induction motor drives known as vector field control was developed by Leonhard and Blaschke [1.3.1,1.3.2] at the University of Brunswick. Basically the research viewed the machine in terms of its transfer functions and developed a technique which gave independent control of torque and speed by decoupling the rotational machine parameters from the fixed machine parameters. This strategy demanded information about the rotor flux position and such information was gained by direct measurement of the flux in the air gap by allocation of a search coil in the stator. However, because this technique could not be employed without making modifications to off-the-shelf induction motors, other strategies were developed whereby the required information could be determined from the phase currents. This latter technique is called indirect vector field control whilst the first technique is referred to as direct vector field control[1.3.3-1.3.16].

Although vector control techniques considerably improve the response time of induction motor drive systems it does not compensate for variation in the motor parameters such as the variation of resistance with temperature. A further control technique which has been considerably researched over recent years, to compensate for temperature variation of parameters in the induction motor, is known as adaptive control [1.3.17-1.3.29].

2. Theory

2.1. Introduction

The recent developments in microelectronics technology have made components available with very large memories and very fast computing times. The corresponding fall in the price of these machines has meant, that most engineers can now enjoy the privilege of having a powerful computer at home. The concept of computer integrated manufacturing, CIM, is now becoming established in many industries and thus will allow engineers to participate in the industrial activities from their home as well as from their place of work. Part of the CIM development is of course the simulation of a design or of a process. Although the mathematical theories used for system simulation have in the main been known for many years, the inclusion in software packages for simulation studies have yet to be fully exploited.

2.2. The Induction Motor

2.2.1 Introduction to Induction Motor

Electrical machines are available in the form of DC machines, synchronous and asynchronous induction machines. However, of all electrical machines the cage rotor induction machine has one feature that distinguishes it from all other types. The secondary currents in induction machines are created only by induction, hence its name. Thus there is no need for an external source for excitation and subsequently for commutators or slip rings to transfer this source to the rotor [2.2.1.1].

The DC machine provides the best characteristics, it allows an independent control of speed and torque. The commutators needed to transfer the excitation energy to the rotor, however, bring with them the need for maintenance.

Also, although the synchronous machine is particularly useful for constant speed applications it does suffer from the requirement of start-up facilities. The construction of the stator is similar to that of the cage rotor induction machine, but the rotor design is different and requires slip rings to transfer the excitation energy. This machine also has the disadvantage of the need for maintenance and for start-up technology. However, the synchronous machine has a safe place in the field of energy generation, where constant speed is required over a wide power range.

Induction machines are available as single phase or polyphase machines. The single phase induction machine really is a two phase machine, having a main winding and an auxiliary winding for the generation of the starting torque. Its field of use is the area of low power applications, where it is not cost effective to install three phase supply systems, as in the domestic premises, because it only requires a single phase supply. Since there are converters available now that allow single phase input and three phase output this type of machine will increasingly be replaced by polyphase induction machines. So far the replacement is slow due to the size and cost of the converter required. But with the increasing integration of electronic components for converter drives the replacement will increase and the use of single phase induction machines will be reduced to specialised areas, where inverter drives are to expensive.

There are two standard types of polyphase induction machine available. The wound rotor induction machine has a rotor winding similar to the stator winding. The windings are normally in star connection and the free ends of this connection are brought to the outside by using slip-rings. The connection via the slipring is used to inject and extract power from the rotor mainly during the start up period to increase the torque in this area. After start up the sliprings are normally short circuited and it operates like a cage rotor induction motor. This type of machine needs maintenance for its slip rings, but they are not used as much as those in the synchronous machine, because they are not continuously needed. Like the synchronous machine the wound rotor induction machine requires some start up technology.

The difference between the cage rotor or squirral-cage rotor induction machine and the wound rotor induction machine is the rotor. The rotor used for this machine simply consists of conducting bars shorted together by endrings. As far as the manufacturing side is concerned this is the simplest type of rotor to produce. Hence this machine is cheaper to produce than any other machine and the simple design without sliprings or commutators leaves it virtually maintenance free. The only parts to maintain are the bearings.

A special form of cage rotor induction machine is the reluctance machine. Its cage rotor has salient poles generated by cutting out the material in distinct areas or by using areas with materials of different magnetic characteristic. This machine combines the start up ability of the induction machine with the constant speed behaviour of the synchronous machine. Constant speed applications, e.g. textile industry, are the ideal working field for this motor and considerable research is taking place in this field.

The preferred motor for variable speed drive systems is the cage rotor induction motor because it is maintenance free, is available off-the-shelf and has a low price compared with other motors. However, one of the problems of such machines is that they require sufficient power electronic converter systems to vary their speed and control their torque.

2.2.2 Theory of Induction Motor

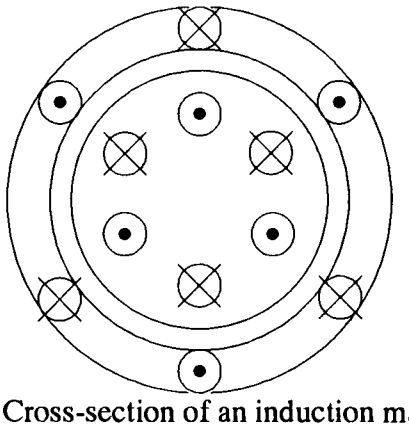

Fig. 2: Cross-section of an induction machine

A cross-section of an induction machine is shown in figure 2. It can be seen that the stator contains several coils, which form the three phase AC distributed winding. Similarly it may also be seen that the rotor winding mainly consists of copper or aluminium bars shorted together at their ends by means on endrings.

To find a mathematical model describing the machine, one starts with the basic mathematical description of a coil. This description is given by the following equation:

$$V = R * i + \frac{d(L*i)}{dt} \qquad \text{eqn. 2.2.1}$$

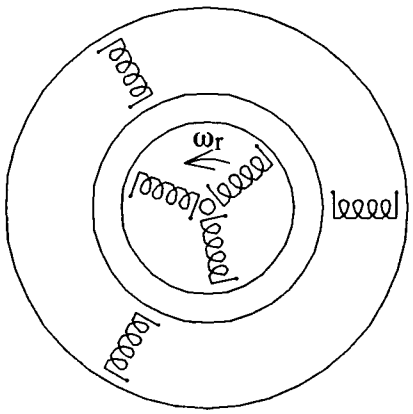

Fig. 3: 6 coil model of the induction machine

Analytically the machine can be described as two sets of interacting circuits as shown in figure 3. For these interacting coils equation 2.2.1 can be written as:

$$v = R * i + \omega_r G * i + L * \frac{di}{dt} \qquad \text{eqn. 2.2.2}$$

where $\omega_r G$ represents the coupling inductance produced by the rotation of the rotor.

The six coil induction machine in figure 3 has an equivalent circuit per phase as illustrated in the following figure.

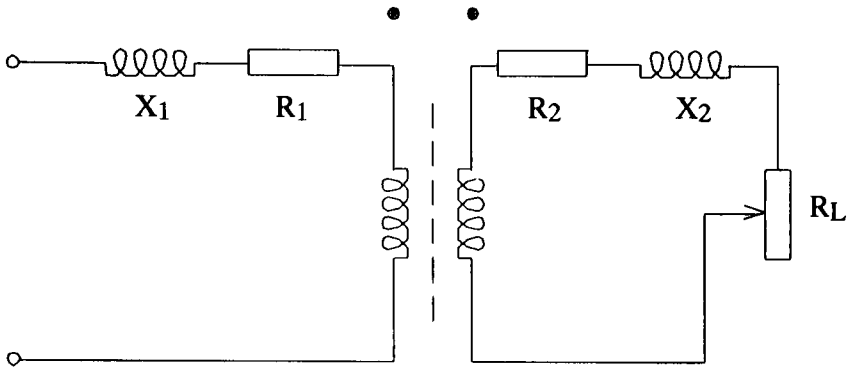

Fig. 4: Single phase equivalent circuit

By transforming all of the rotor quantities to the primary one can illustrate an induction motor in terms of its equivalent circuit of one phase as shown in figure 5.

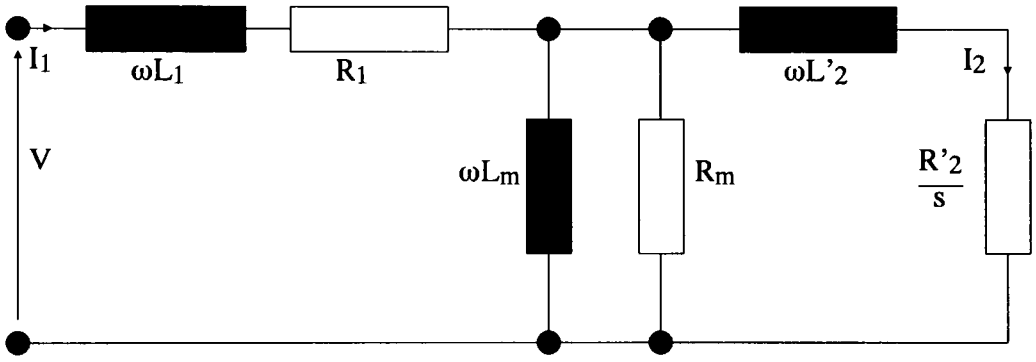

Fig. 5: Stator based single phase equiv. circuit

In the single phase equivalent circuit shown in figure 5, L_1 is the stator leakage inductance, R_1 the stator resistance, L_m the magnetizing inductance, R_m the magnetizing resistance, L'_2 the rotor leakage inductance and R'_2/s is the rotor equivalent resistance including the load resistance. The magnetizing resistance R_m can be used to represent the mechanical and iron losses associated with the machine. The resistance R_m, however, due to its high value is often neglected so far as simulation studies are concerned. However, where large iron losses can be anticipated such as in the case of supplying the motor with voltage waveforms high in harmonic distortion the resistance becomes significant and must be taken into account when the simulation studies of heat

losses and temperature rise are required. By ignoring the resistance R_m the equivalent circuit shown in figure 5 is simplified to the equivalent circuit shown in figure 6.

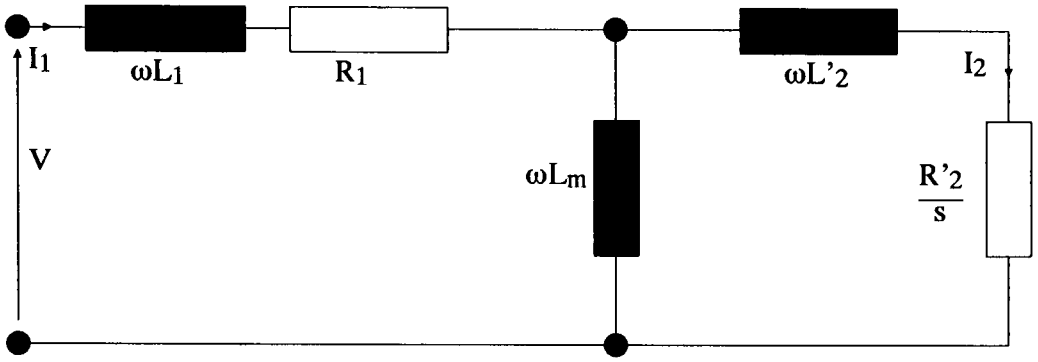

Fig. 6: Equivalent circuit used for Simulation

The winding resistances R_1 and R'_2 are often neglected when their value is small compared with the leakage reactances ωL_1 and $\omega L'_2$, which is often agreed to be the case when the machine is operated at high frequencies.

As far as the investigation into the influence of harmonics is concerned the equivalent circuit can even be simplified more by employing the following assumptions.

From the manufacturers data, shown in the appendix, it can be seen that the values of the winding resistances are about the same size as the values of their corresponding leakage inductances for the rated frequency. This means that for higher harmonics the value of the resistance becomes smaller than the value of the reactance and from the tenth harmonic onwards it is dimensionally smaller and thus it can be justified to neglect the value of the resistors. Similarly the value of the magnetizing reactance ωL_m becomes very large and can be neglected.

By neglecting the above terms the equivalent circuit shown in figure 6 can be modified to that shown in figure 7.

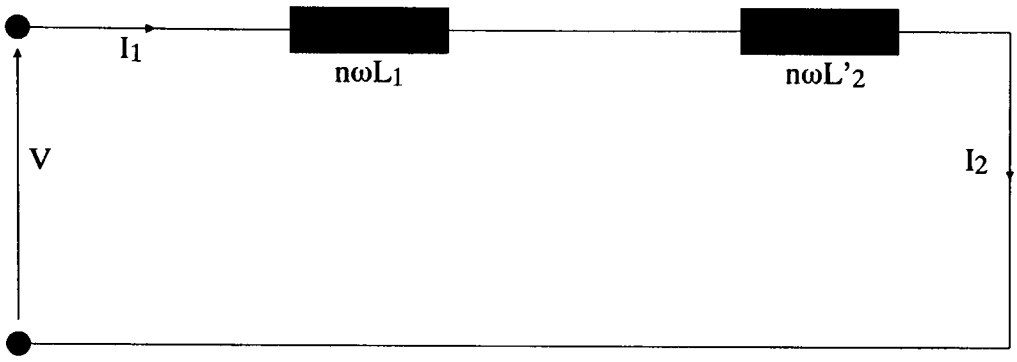

Fig. 7: Equivalent circuit for higher harmonics

In order to carry out a steady state and transient analysis of the behaviour of induction machines under various conditions of operation the unified machine theory developed by Kron [2.2.1.1, 2.2.2.1-2.2.2.5] may be usefully applied.

The work of Kron demonstrated that any machine system can be shown to be equivalent to an electrical network as illustrated in figure 4. For a three phase induction motor the equations defining the stator and rotor voltages in terms of the stator and rotor currents and the generalized machine parameters are as follows:

$$\begin{bmatrix} V_{as} \\ V_{bs} \\ V_{cs} \\ V_{ar} \\ V_{br} \\ V_{cr} \end{bmatrix} = \begin{bmatrix} R_1+pL_1 & 0 & 0 & pL_mG_a & pL_mG_b & pL_mG_c \\ 0 & R_1+pL_1 & 0 & pL_mG_c & pL_mG_a & pL_mG_b \\ 0 & 0 & R_1+pL_1 & pL_mG_b & pL_mG_c & pL_mG_a \\ pL_mG_a & pL_mG_c & pL_mG_b & R_2+pL_2 & 0 & 0 \\ pL_mG_b & pL_mG_a & pL_mG_c & 0 & R_2+pL_2 & 0 \\ pL_mG_c & pL_mG_b & pL_mG_a & 0 & 0 & R_2+pL_2 \end{bmatrix} * \begin{bmatrix} i_{as} \\ i_{bs} \\ i_{cs} \\ i_{ar} \\ i_{br} \\ i_{cr} \end{bmatrix} \quad \text{eqn. 2.2.3}$$

where G_a, G_b and G_c are $\cos(\Theta_r)$, $\cos(\Theta_r+2\pi/3)$ and $\cos(\Theta_r-2\pi/3)$ respectively.

The 6x6 matrix defining the voltage equation, however, is inconvenient in the present state.

There are techniques available for transforming the 3 phase system to a 2 phase system, which reduces the matrix to a 4x4 one as shown in equation 2.2.7. This reduces the number of variables and the amount of computer memory required for simulation of the induction motor. The transformation techniques used allow analysis of the motor in different frames of reference. For example a d-q frame rotating synchronously with the supply frequency may be used. This frame of representation transforms ac values into dc values as explained in the following [2.2.2.6-2.2.2.13].

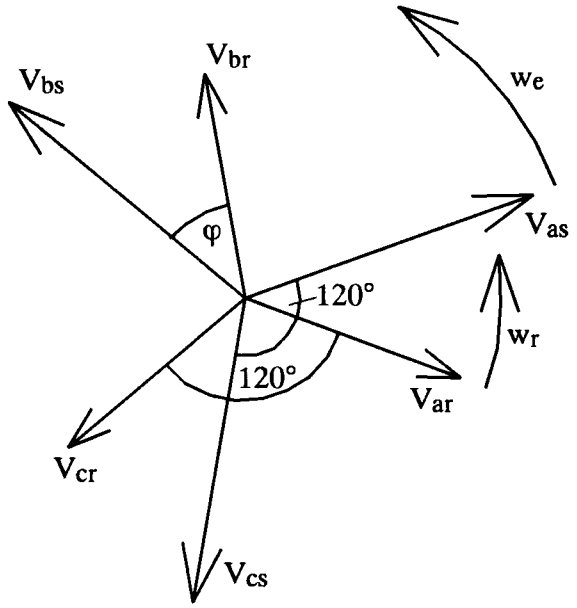

Fig. 8: Stator and rotor vector diagrams

Applying this transformation to the interacting coils in both sets and putting them into matrix form leads to the matrix described in equation 2.2.3 earlier. The whole mathematical treatment is based on the generalized machine theory. Figure 8 shows the two three phase systems, the stator, index s, and the rotor, index r, respectively. The three phase system consists of the three phases a-b-c, each in 120° phase shift. The stator field is rotating with the electrical speed ω_e and the rotor field is rotating with the mechanical speed ω_r. The angle between both system, φ, is generated by the difference between electrical and mechanical speed.

The three phase a-b-c system can be transformed to a two phase α-β system. The relationship of both systems is show in figure 9. This transformation from 3 to 2 phases is performed for both, stator and rotor separately.

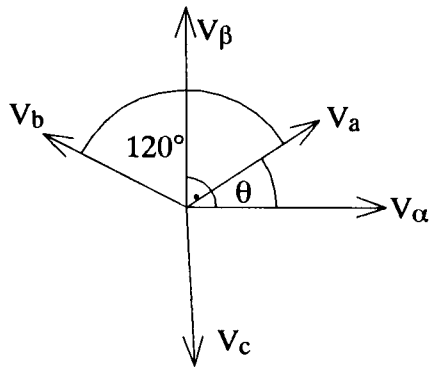

Fig. 9: The three and two phase systems

The mathematical description of this transformation is given in the following equation:

$$\begin{bmatrix} v_a \\ v_b \\ v_c \end{bmatrix} = \begin{bmatrix} \cos\theta & \sin\theta & 1 \\ \cos(\theta+120°) & \sin(\theta+120°) & 1 \\ \cos(\theta-120°) & \sin(\theta-120°) & 1 \end{bmatrix} * \begin{bmatrix} v_\alpha \\ v_\beta \\ v_o \end{bmatrix} \qquad \text{eqn. 2.2.4}$$

Where v_o is a zero sequence voltage system introduced to simplify the mathematical treatment of the matrix equation.

The results of the transformation of these two a-b-c systems are two α-β systems for rotor and stator. Figure 9 shows a displacement between the two and the three phase system, called θ, caused by the choice of the reference frame. The mathematical formula in equation 2.2.4 can be simplified by choosing a reference frame, where the α-axis is in phase with the a-axis, thus θ becomes equal to zero. The then resulting system can be seen in the following figure:

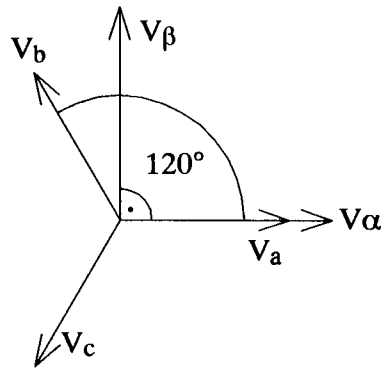

Fig. 10: The three and two phase systems in phase

The equation 2.2.4 then becomes:

$$\begin{bmatrix} v_a \\ v_b \\ v_c \end{bmatrix} = \begin{bmatrix} 1 & 0 & 1 \\ -\frac{1}{2} & +\frac{\sqrt{3}}{2} & 1 \\ -\frac{1}{2} & -\frac{\sqrt{3}}{2} & 1 \end{bmatrix} * \begin{bmatrix} v_\alpha \\ v_\beta \\ v_o \end{bmatrix} \qquad \text{eqn. 2.2.5}$$

To transform the rotor and stator α-β frame systems into a system with a single d-q frame of reference requires a common reference to be chosen. The reference frame can either be fixed to the rotor or the stator or be synchronously rotating, or indeed, be a frame rotating with any other velocity. There are several options in use. However for the motor a stator fixed d-q frame was chosen. This produces a 1 to 1 transformation for the stator, where say α-β becomes d-q. Only the α-β frame of the rotor has to be transformed to the stator d-q frame. This transformation is shown in figure 11. The mathematical description for the Transformation is given in equation 2.2.6.

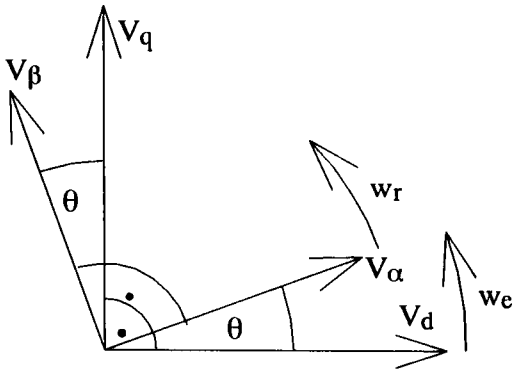

Fig. 11: Transformation to a single d-q frame

$$\begin{bmatrix} v_d \\ v_q \end{bmatrix} = \begin{bmatrix} \cos \omega_r t & \sin \omega_r t \\ -\sin \omega_r t & \cos \omega_r t \end{bmatrix} * \begin{bmatrix} v_\alpha \\ v_\beta \end{bmatrix} \qquad \text{eqn. 2.2.6}$$

By transforming the matrix equation given in equation 2.2.3 to the two axis frame of reference the matrix equation given in equation 2.2.7 is obtained. This 4x4 Matrix can easily be dealt with in computer simulation since it keeps the demand for memory in an acceptable range.

$$\begin{bmatrix} V_{ds} \\ V_{qs} \\ V_{dr} \\ V_{qr} \end{bmatrix} = \begin{bmatrix} R_1+pL_1 & 0 & pL_m & 0 \\ 0 & R_1+pL_1 & 0 & pL_m \\ pL_m & \omega_r L_m & R_2+pL_2 & \omega_r L_2 \\ -\omega_r L_m & pL_m & -\omega_r L_2 & R_2+pL_2 \end{bmatrix} * \begin{bmatrix} i_{ds} \\ i_{qs} \\ i_{dr} \\ i_{qr} \end{bmatrix} \qquad \text{eqn. 2.2.7}$$

The transformation equations shown here for the voltage are valid for the current in the same way.

The literature available on the unified theory of analysis of machines presents considerable confusion because the American literature tends to displace the direct and quadrature axis with respect to that used in much of the British literature. It would therefore be helpful if an international standard existed for the frames of reference.

The voltage equation 2.2.7 can be transformed to the following form:

$$v = R * i + \omega_r G * i + L * \frac{di}{dt} \qquad \text{eqn. 2.2.8}$$

where $R = \begin{bmatrix} R_1 & 0 & 0 & 0 \\ 0 & R_1 & 0 & 0 \\ 0 & 0 & R_2 & 0 \\ 0 & 0 & 0 & R_2 \end{bmatrix}$, $G = \begin{bmatrix} 0 & 0 & 0 & 0 \\ 0 & 0 & 0 & 0 \\ 0 & L_m & 0 & L_2 \\ -L_m & 0 & -L_2 & 0 \end{bmatrix}$, $L = \begin{bmatrix} L_1 & 0 & L_{m7} & 0 \\ 0 & L_1 & 0 & L_m \\ L_m & 0 & L_2 & 0 \\ 0 & L_m & 0 & L_2 \end{bmatrix}$.

Equation 2.2.8 can then be transformed to the standard state space representation:

$$\dot{x} = A\,x + B\,u \qquad \text{eqn.2.2.9.}$$

From

$$\frac{di}{dt} = A * i + B * v \qquad \text{eqn.2.2.10}$$

this transformation gives

$$A = -(R + \omega_r G) * L^{-1} \qquad \text{eqn. 2.2.11}$$

and

$$B = L^{-1} \qquad \text{eqn.2.2.12.}$$

The system described by equation 2.2.10 describes a real system that is of the continuous form. In the simulation it is necessary to work with a discrete system. The continuous system described has to be transformed into a discrete one and the process of discretization is shown in figure 12. A software package called MATLAB which has recently become available incorporates a function called ***C2D*** which carries out the translation from the continuous to the discrete.The syntax used for this translation is given by:

$$(\Phi,\Gamma)=\text{c2d}(A,B,dt) \qquad \text{eqn.2.2.13}$$

where A and B are the same as described before and dt is the time increment. This function provides a solution to the continuous system.

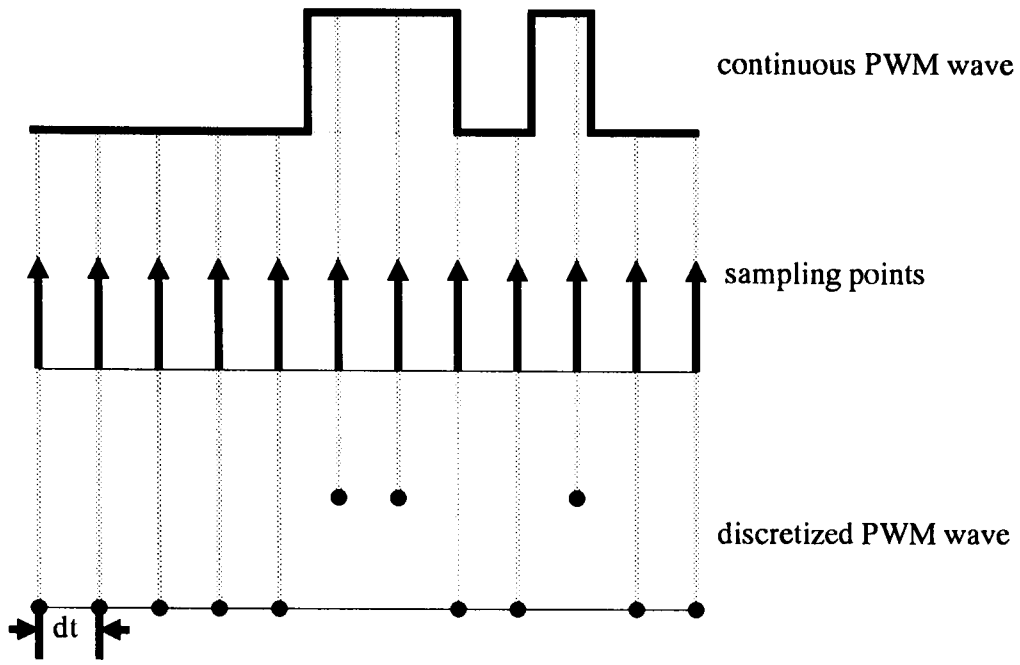

Fig. 12: Discretizing a PWM wave

With Φ and Γ the solution is given by the following set of equations:

$$\begin{aligned} x(1) &= \Phi * x(0) + \Gamma * u(0) \\ &\bullet \\ &\bullet \\ x(p+1) &= \Phi * x(p) + \Gamma * u(p) \\ &\bullet \\ &\bullet \\ x(n+1) &= \Phi * x(n) + \Gamma * u(n) \end{aligned} \qquad \text{eqn. 2.2.14}$$

This set of equations provides a means of producing a solution to equations 2.2.3 and 2.2.8. However the initial condition still has to be determined. The way of obtaining the initial condition depends on the aim of the simulation. For the simulation of a start up the initial condition is specified as 0. Alternatively the initial condition for a motor operating in the steady state condition can be calculated by employing the inherent symmetry of the voltage waveform. For a balanced three phase system and a voltage waveform with half wave symmetry the initial condition can be determined by equation 2.2.15. For a voltage waveform with no symmetry equation 2.2.16 has to be used [2.2.2.14, 2.2.2.15].

$$x\left(t+\frac{T}{6}\right) = \begin{bmatrix} \frac{1}{2} & \frac{\sqrt{3}}{2} & 0 & 0 \\ -\frac{\sqrt{3}}{2} & \frac{1}{2} & 0 & 0 \\ 0 & 0 & \frac{1}{2} & \frac{\sqrt{3}}{2} \\ 0 & 0 & -\frac{\sqrt{3}}{2} & \frac{1}{2} \end{bmatrix} * x(t) \qquad \text{eqn. 2.2.15}$$

$$x\left(t+\frac{T}{3}\right) = \begin{bmatrix} -\frac{1}{2} & -\frac{\sqrt{3}}{2} & 0 & 0 \\ \frac{\sqrt{3}}{2} & -\frac{1}{2} & 0 & 0 \\ 0 & 0 & -\frac{1}{2} & -\frac{\sqrt{3}}{2} \\ 0 & 0 & \frac{\sqrt{3}}{2} & -\frac{1}{2} \end{bmatrix} * x(t) \qquad \text{eqn. 2.2.16}$$

For a voltage wave with half wave symmetry p is the point number representing the time $t+\frac{T}{6}$. Equation 2.2.14 can then be written as:

$$\begin{aligned} x(1) &= \Phi * x(0) + \Gamma * u(0) \\ &\bullet \\ &\bullet \\ x(i+1) &= \Phi * x(i) + \Gamma * u(i) \\ &\bullet \\ &\bullet \\ x(p) &= \Phi * x(p-1) + \Gamma * u(p-1) \end{aligned}$$

and eqn. 2.2.17

$$x(p) = \begin{bmatrix} \frac{1}{2} & \frac{\sqrt{3}}{2} & 0 & 0 \\ -\frac{\sqrt{3}}{2} & \frac{1}{2} & 0 & 0 \\ 0 & 0 & \frac{1}{2} & \frac{\sqrt{3}}{2} \\ 0 & 0 & -\frac{\sqrt{3}}{2} & \frac{1}{2} \end{bmatrix} * x(0)$$

This system can now be solved and the initial condition is given by the following equation:

$$x(0) = \left(\begin{bmatrix} \frac{1}{2} & \frac{\sqrt{3}}{2} & 0 & 0 \\ -\frac{\sqrt{3}}{2} & \frac{1}{2} & 0 & 0 \\ 0 & 0 & \frac{1}{2} & \frac{\sqrt{3}}{2} \\ 0 & 0 & -\frac{\sqrt{3}}{2} & \frac{1}{2} \end{bmatrix} - \Phi^p \right)^{-1} * \sum_{i=1}^{p} \Gamma * \Phi^{p-i} * u(i-1) \qquad \text{eqn. 2.2.18}$$

Once this initial condition is found the complete solution can be calculated.

The electromagnetic torque T_e is given by:

$$T_e = n * i * G * i^t \qquad \text{eqn. 2.2.19}$$

where n is the number of polepairs, i is the current vector, i^t the transpose of i and G as used previously.

The mechanical speed ω_r can be calculated from

$$\omega_r = \int_0^{\infty} \frac{n}{J} (T_e - T_L)\, dt \qquad \text{eqn. 2.2.20}$$

where n, T_e are as previously defined, T_L is the load torque and J is the inertia.

2.3 Theory of PWM

With the introduction of power semiconductor devices the possibility for the generation of variable voltage variable frequency voltage waveforms arose. The initial enthusiasm generated by this feature was soon dampened by the effects of the harmonics of the fundamental component inherent in the square wave waveform used. Considerable research effort has been spent to find an optimised generation process. This research has shown that a generation process called PWM with a triangular carrier wave is the preferable solution to this problem.

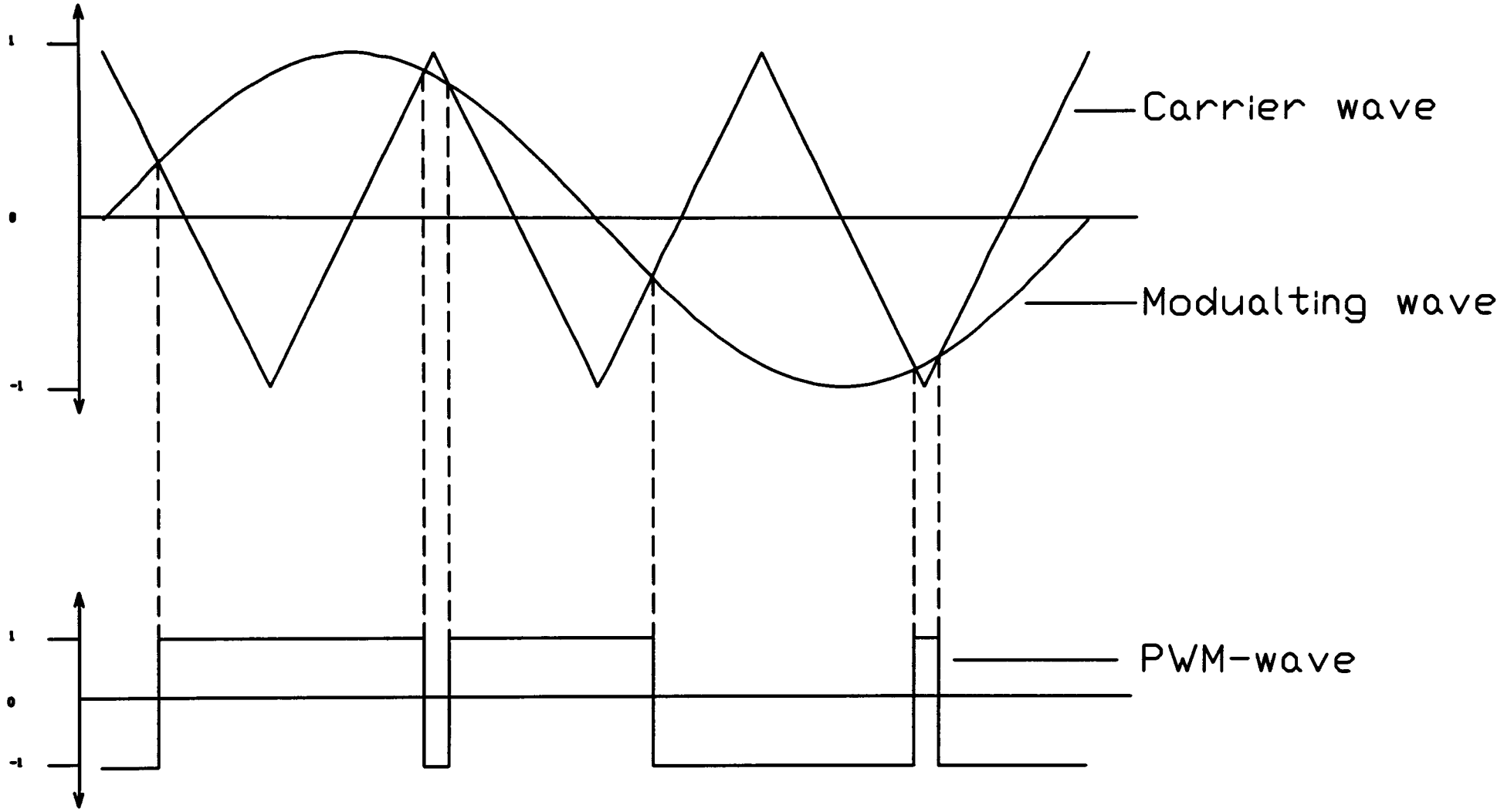

Fig. 13: Natural sampled PWM

To generate a PWM wave, a modulating wave has to be chosen. The frequency of this wave is the fundamental frequency of the resulting PWM wave and the amplitude of this wave, determines the amplitude of the fundamental component of the resulting PWM wave. A triangular carrier wave is chosen. The number of carrier wave cycles per modulating wave is called the frequency ratio (R). The period of a carrier cycle is called T_c, the amplitude of carrier wave is kept to unity whereas the amplitude of the modulating wave is M times unity. The intersection between the carrier and modulating wave defines the switching point or time for the PWM wave. This generation process is shown in figure 13

However, it was found that the harmonic content of this waveform was still not satisfactory. Consequently other methods were investigated. A process where a sampled modulating wave was used was investigated and found to produce an improved PWM wave as far as harmonic content is concerned. To distinguish both methods the earlier one was called natural sampled PWM, while the later one was called regular sampled PWM. There are several types of triangular carrier wave possible. A positive slope, a negative slope or a double slope waveform could be chosen. The processes of generating PWM waves with positive slope and negative are shown in figures 14 and 15 respectively. However, a double slope triangular wave as carrier wave has been shown to be the better solution. A double slope carrier waveform opens a new possibility for the sampling process of the modulating wave. The sampling could be performed per carrier cycle, thus called regular sampled symmetric PWM, or per carrier half cycle, then called regular sampled asymmetric PWM. The harmonic spectrum contained in the asymmetric type of PWM has been found to be superior to that of the symmetric type [1.2.4], however, the latter remains in use [2.2.2.11]. The process of generating regular sampled symmetric PWM is shown in figure 17. Figure 18 shows the same for regular sampled asymmetric PWM.

The switching points for a PWM wave in an inverter can be obtained by generating the desired modulating wave (sampled) and the carrier wave and simply comparing these waves by means of hardware. The introduction of microprocessor technology, however, allowed the real time calculation of these sampling points. This could be done by simply

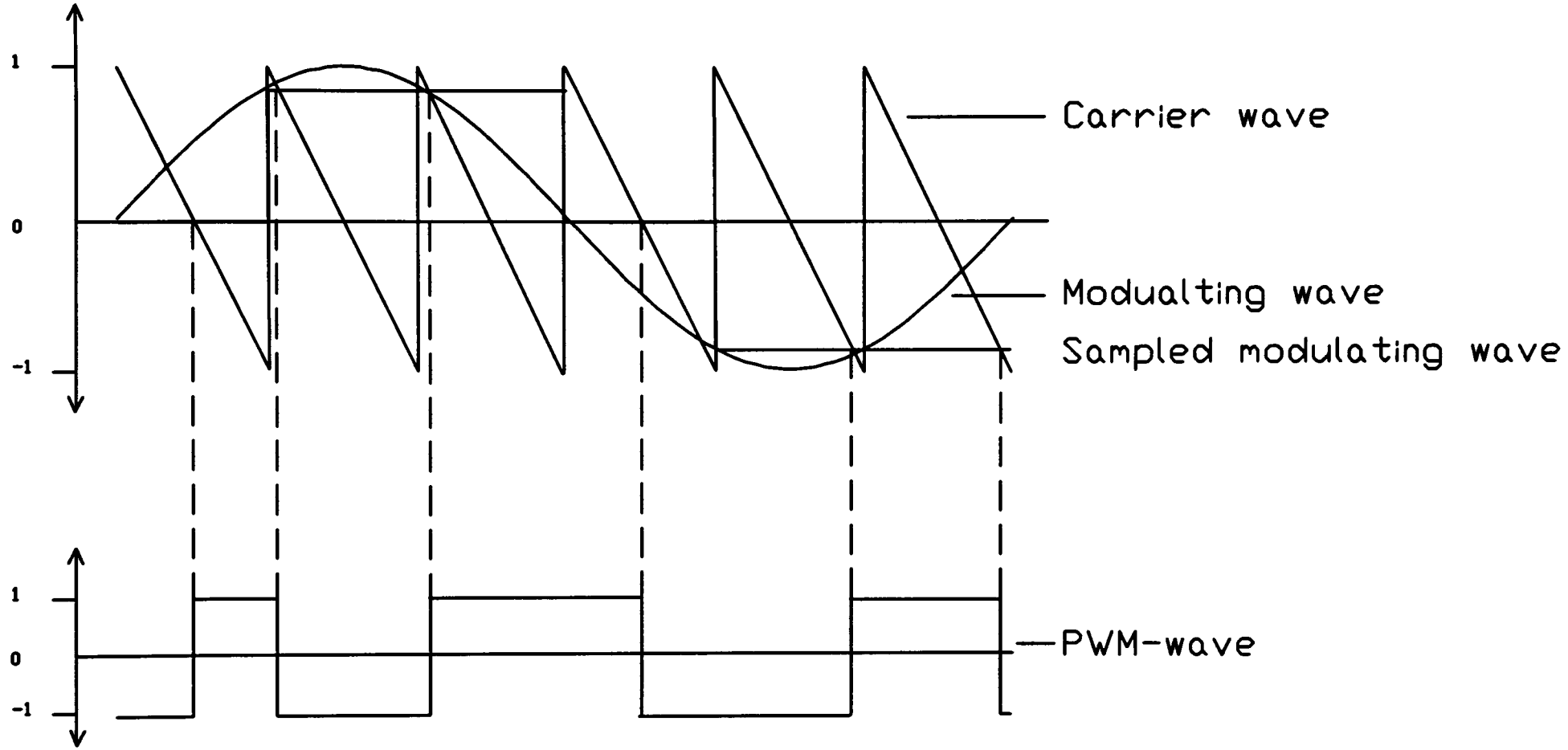

Fig. 14: Regular sampled leading edge PWM

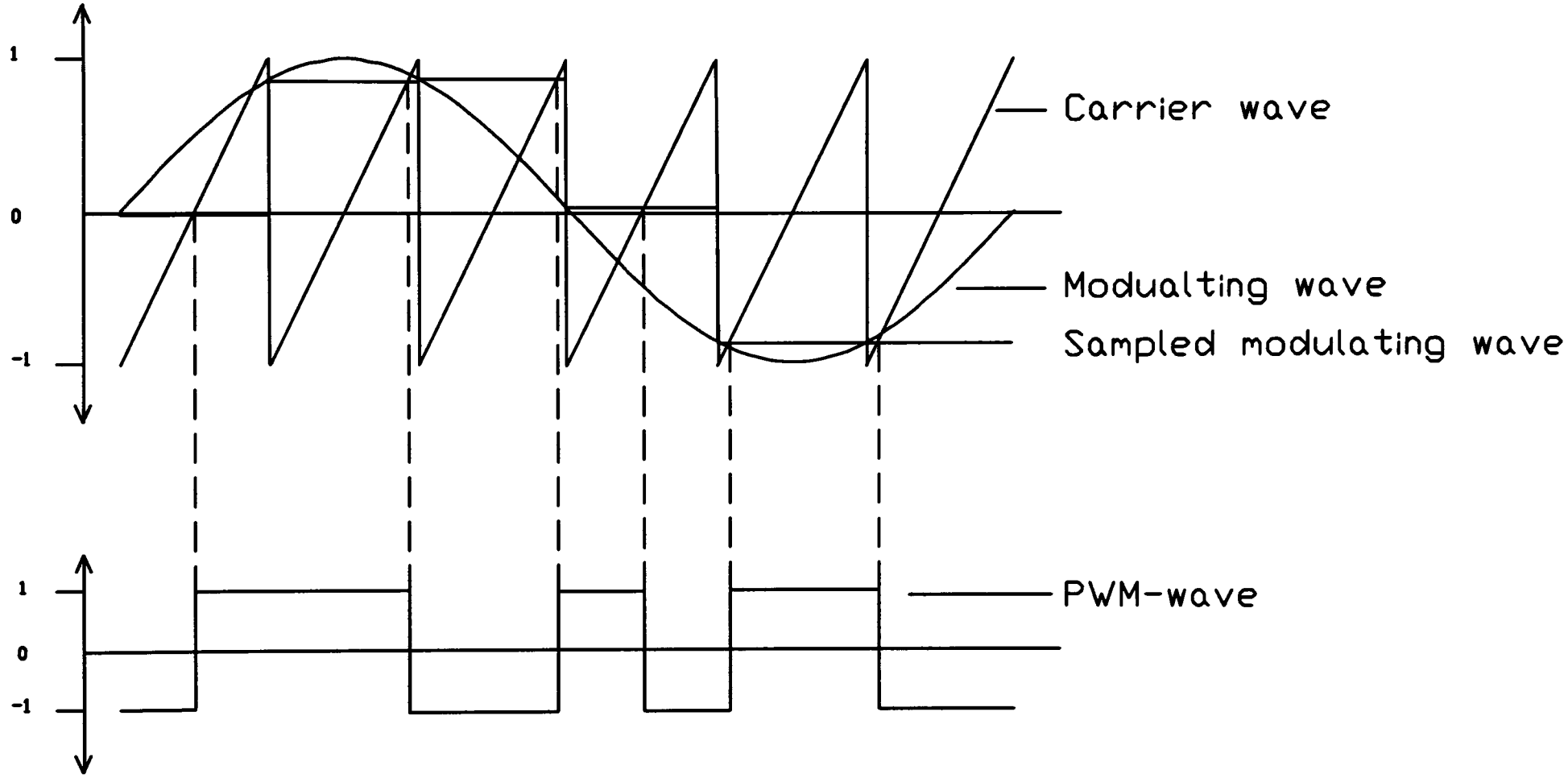

Fig. 15: Regular sampled trailing edge PWM

calculating the different waves and just comparing the amplitudes to obtain the switching points. It has been shown, that the switching time for a phase can be found by the following equations [2.3.1], where T_{an} is the switching time for the nth carrier half cycle of phase a and T_{bn} and T_{cn} are the same for phase b and c respectively.

$$T_{a_n}=\left(\frac{T_c}{2}\right)*\left\{1+(-1)^{n+1}*\left(\frac{M}{2}\right)*\left(\sin\frac{n\pi}{R}+\sin\frac{(n+1)\pi}{R}\right)\right\} \qquad \text{eqn. 2.3.1}$$

$$T_{b_n}=\left(\frac{T_c}{2}\right)*\left\{1+(-1)^{n+1}*\left(\frac{M}{2}\right)*\left(\sin\frac{n\pi}{R}-120°+\sin\frac{(n+1)\pi}{R}-120°\right)\right\} \qquad \text{eqn. 2.3.2}$$

$$T_{c_n}=\left(\frac{T_c}{2}\right)*\left\{1+(-1)^{n+1}*\left(\frac{M}{2}\right)*\left(\sin\frac{n\pi}{R}-240°+\sin\frac{(n+1)\pi}{R}-240°\right)\right\} \qquad \text{eqn. 2.3.3}$$

The generation of PWM waveforms by means of power electronic converters requires considerable explanation so far as the different voltages existing in the converter. The PWM waveforms shown in the figures 13, 14, 15, 17 and 18 are the switching signals used to switch the semiconductor devices in the power converter and are mainly two level voltages signals.

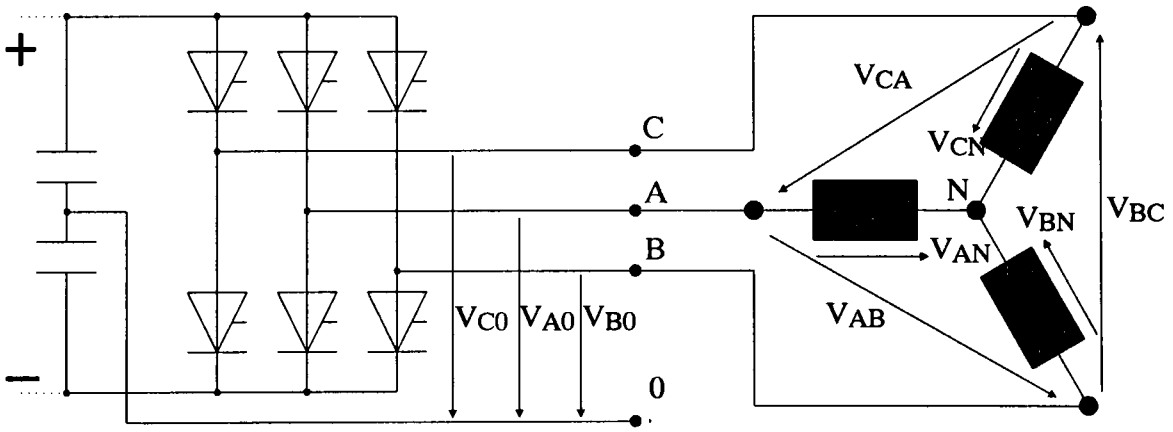

Fig. 16: The voltages in a PWM inverter drive

The voltages shown in the drive circuit of figure 16, however, are of the three level and five level types. For example the voltages V_{CO}, V_{AO} and V_{BO} which are the voltages of the output lines with respect to an artificial DC supply neutral are two level. The voltages

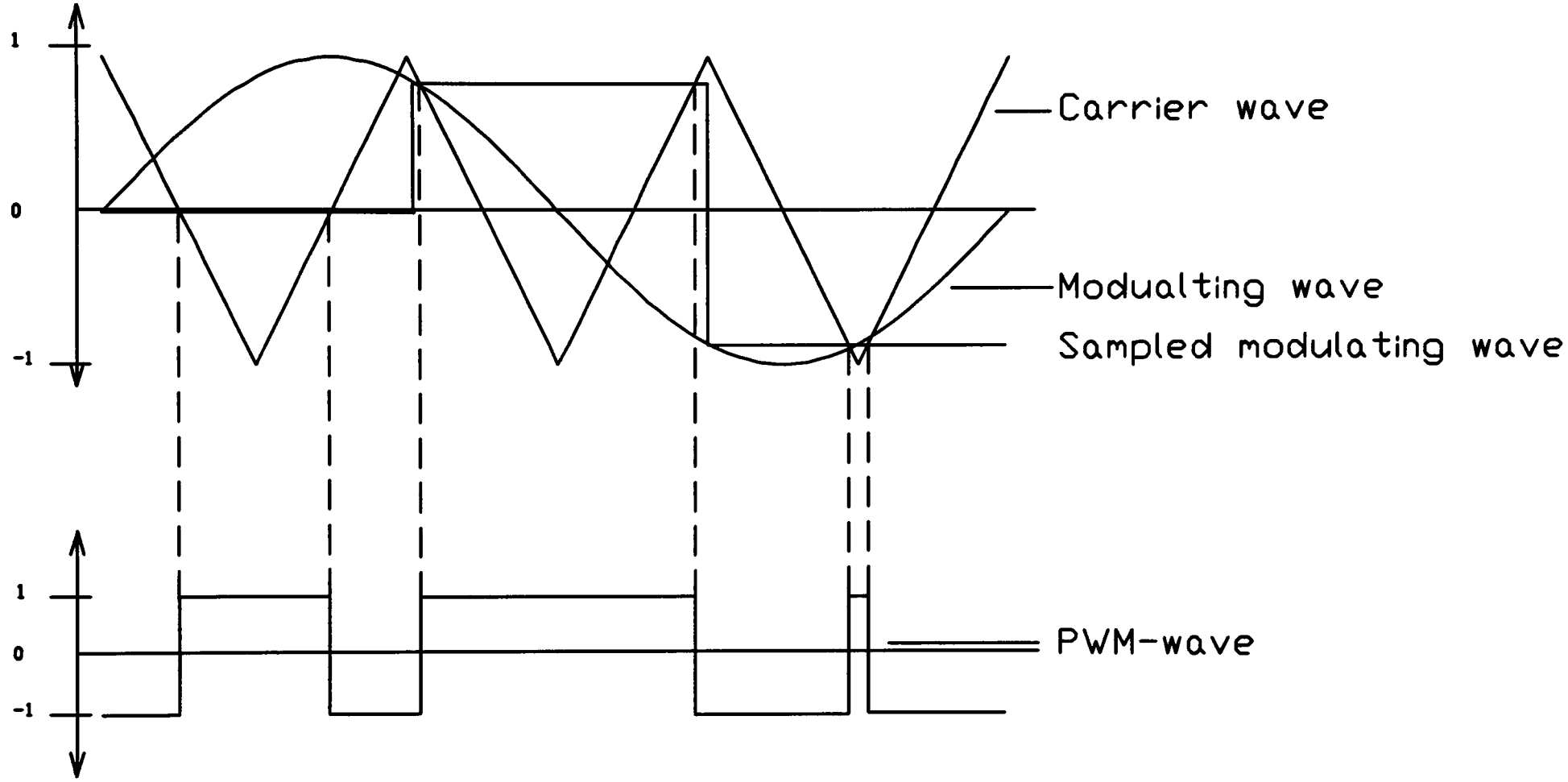

Fig. 17: Regular sampled symmetric PWM

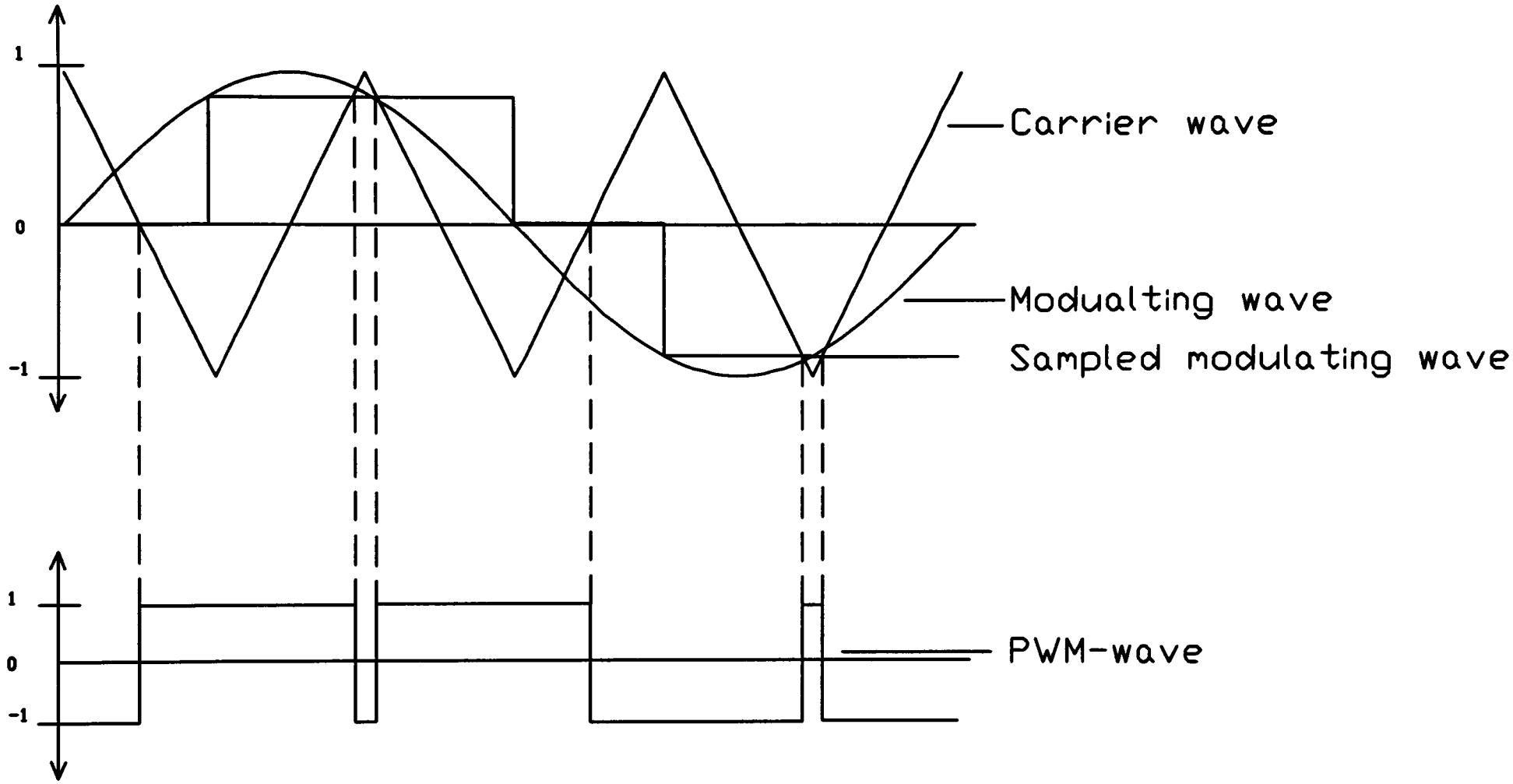

Fig. 18: Regular sampled asymmetric PWM

between the lines C, A and B, however, defined by V_{CA},V_{AB} and V_{BC} are three level voltages, because:

$$V_{CA} = V_{C0} - V_{A0}$$

$$V_{AB} = V_{A0} - V_{B0}$$

$$V_{BC} = V_{B0} - V_{C0}$$

The voltages between the lines C, A and B and the neutral of the load machine are five level and can be determined by the application of Miller's theorem. The simulation results of these voltage waveforms is discussed in chapter 3, where the various voltage levels are illustrated.

2.4. The Fourier Transform

The importance of harmonic analysis of complex waves has been described earlier. The most common way to handle such waves is by applying Fourier transform techniques.

The basic theory of Fourier analysis was proposed by J. B. J. Fourier in the early 1800's. It opened the possibility of analyzing a wave in the frequency domain [2.4.1-2.4.3]. Such analysis is of great importance to inverter drives, since they deal with non sinusoidal waveforms. These waveforms contain harmonics of the fundamental repetition waveform. Many of the harmonics which exist in the spectra of these waveforms can have determinant effects on the performance of the induction motor

In the 1960's J. W. Cooly and J. W. Tukey presented an algorithm called the fast fourier transform (FFT). This algorithm allowed Fourier analysis to be performed at a fast speed which greatly assists the calculation of the Fourier or harmonic components. Therefore the FFT technique was applied to numerous instruments for the measurement and

analysis of waveforms. There is now a wide variety of instruments and tools available which allow a rapid analysis of a waveform. The idea of Fourier analysis is that a periodic wave can be described as a series of sine and cosine terms such as:

$$Y = \frac{a_o}{2} + (a_1 * cos(x_1) + b_1 * sin(x_1)) + (a_2 * cos(x_2) + b_2 * sin(x_2)) + \ldots \qquad \text{eqn. 2.4.1}$$

For a waveform of period T the series can be written as:

$$x(t) = a_o + \sum_{n=1}^{\infty} (a_n * cos(n * \omega_o * t) + b_n * sin(n * \omega_o * t)) \qquad \text{eqn. 2.4.2}$$

where $\omega_o = \frac{2\pi}{T}$. a_o is the DC-term and is given by:

$$a_o = \frac{1}{T} * \int_0^T x(t)\, dt \qquad \text{eqn. 2.4.3}$$

whilst a_n and b_n are given by:

$$a_n = \frac{1}{T} * \int_0^T x(t) * cos(n * \omega_o * t)\, dt \qquad \text{eqn. 2.4.4}$$

$$b_n = \frac{1}{T} * \int_0^T x(t) * sin(n * \omega_o * t)\, dt \qquad \text{eqn. 2.4.5}$$

By substituting the terms for $\cos(n\omega_o t)$ and $\sin(n\omega_o t)$ in equation 2.4.2 with the terms $\frac{e^{j*n*\omega_o*t} + e^{-j*n*\omega_o*t}}{2}$ and $\frac{e^{j*n*\omega_o*t} - e^{-j*n*\omega_o*t}}{2*j}$ respectively, it can therefore be written as:

$$x(t) = \sum_{-\infty}^{\infty} c_n * e^{j*n*\omega_o*t} \qquad \text{eqn. 2.4.6}$$

where c_n is given by

$$c_n = \frac{1}{T} * \int_{-T/2}^{T/2} x(t) * e^{-j*\omega_o*t}\, dt \qquad \text{eqn. 2.4.7}$$

Therefore equation 2.4.7 can be used to determine the magnitude and phase of the harmonic components in the waveform described. Taking the expression in equation 2.4.6 to the limit, it can be transformed to the frequency domain and becomes:

$$x(t) = \int_{-\infty}^{\infty} X(f) * e^{j*\omega_o*t}\, df \qquad \text{eqn . 2.4.8}$$

The expression described by equation 2.4.8 is known as the inverse Fourier transform. By transforming this equation to the frequency domain it becomes:

$$X(f) = \int_{-\infty}^{\infty} x(t) * e^{-j*\omega_o*t}\, dt \qquad \text{eqn. 2.4.9}$$

which is known as the direct Fourier transform. As mentioned earlier there are algorithms available, that allow a quicker transformation with reasonable accuracy, but which also have certain limits.

2.5. Theory of Vector Control

The PWM voltage waveforms discussed in earlier sections provide an excellent means of generating a variable voltage variable frequency supply for the speed control of induction motors operating in the steady state condition. However, so far as the dynamic behaviour of an electrical drive is concerned considerable thought must be given to the speed control system. One method of speed control which considerably improves dynamic response is known as vector field control and will be discussed further in the proceeding paragraphs of this chapter. Vector field control has proven to be a good solution to the problem and is nowadays widely used in inverter systems.

Vector field control, also called field oriented control, was developed by Leonhard and Blaschke at the Institute of Control of the University of Brunswick [1.3.1]. The approach adopted by Leonhard and Blaschke basically consisted of representing the induction motor in terms of its transfer functions. They then looked at means whereby the induction machine could be controlled such that its behaviour would be equivalent to that of a DC machine, where it is well known that, because the DC machine has two separate input quantities for the control of speed and torque, it provides a better overall dynamic response then the induction machine. This analysis commenced with the production of a vector diagram for an idealised machine with compensation coils and is illustrated in figure 19.

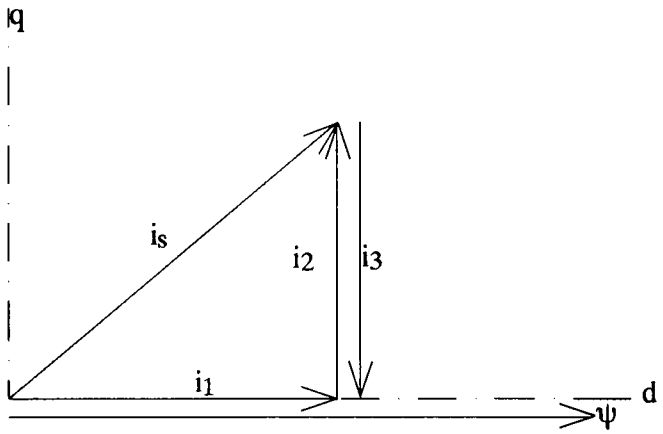

Fig. 19: Vector diagram of a DC-machine

In this figure i_s is the total DC motor stator current, whereas i_1 the component of that current, that flows in the stator coil and sets up the flux Ψ. The component of the current i_2 is the component of i_s which is assumed to flow in the compensation coil. The current i_3, however, is that current which is assumed to flow in the armature winding. The torque generated by this idealized machine is then considered to be proportional to the difference between the currents of i_3 and i_2. The speed of the idealized motor, however, is dependent upon and partly proportional to the component of current i_1 which sets up the flux. Leonhard and Blaschke then set about identifying a similar structure in an induction motor which could be used for speed and torque control processes. This resulted in the vector field control models of an induction motor which are available today.

The analysis used in vector field control strategies of induction machines is described further in the following paragraphs of this chapter.

With the usual assumptions such as symmetrical stator and rotor construction, neglecting slot effects and disregarding iron losses and eddy currents, the complex current vectors for stator and rotor were found to be given by:

$$\underline{i}_S(t) = \underline{i}_{S1}(t) + \underline{i}_{S2}(t) * e^{j2\pi/3} + \underline{i}_{S3}(t)\, e^{j4\pi/3} \qquad \text{eqn. 2.5.1}$$

$$\underline{i}_R(t) = \underline{i}_{R1}(t) + \underline{i}_{R2}(t) * e^{j2\pi/3} + \underline{i}_{R3}(t)\, e^{j4\pi/3} \qquad \text{eqn. 2.5.2}$$

Blaschke then introduced a flux reference defined as:

$$\underline{i}_{mR}(t) = \underline{i}_S(t) + (1+\sigma_R) * \underline{i}_R(t)\, e^{j\varepsilon} = |\underline{i}_{mR}|\, e^{j\rho} \qquad \text{eqn. 2.5.3}$$

Thus a vector diagram analogous to that of the DC-machine is generated, with the same orthogonal torque and speed components, as shown in figure 20.

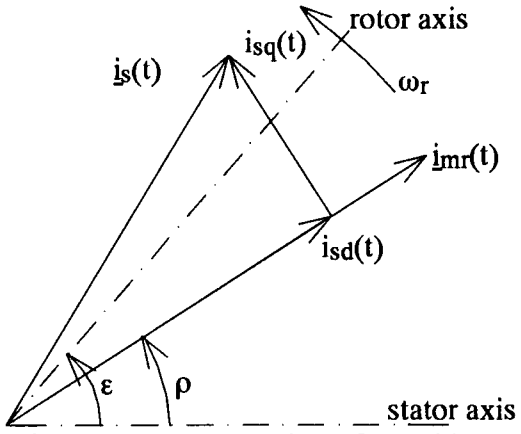

Fig. 20: Vector diagram for AC-machine

However, this approach with Hall sensors or search coils in the induction machine has some disadvantages. The fitting of these devices increases the cost for the drive system dramatically and they are not immune to noise caused by slot ripple and the influence of temperature variation. Measures to compensate for these effects cause other difficulties. The measurement of the flux itself at two orthogonal points in the system does not necessary lead to an accurate representation of the decoupled flux components.

Therefore means were investigated which avoid the use of flux sensing devices. To distinguish between both kinds of vector control, the method using flux sensors is called direct vector control, while the other is called indirect vector control.

A simplified block diagram of direct vector control is shown in figure 21 and a simplified block diagram of indirect vector control is shown in figure 22

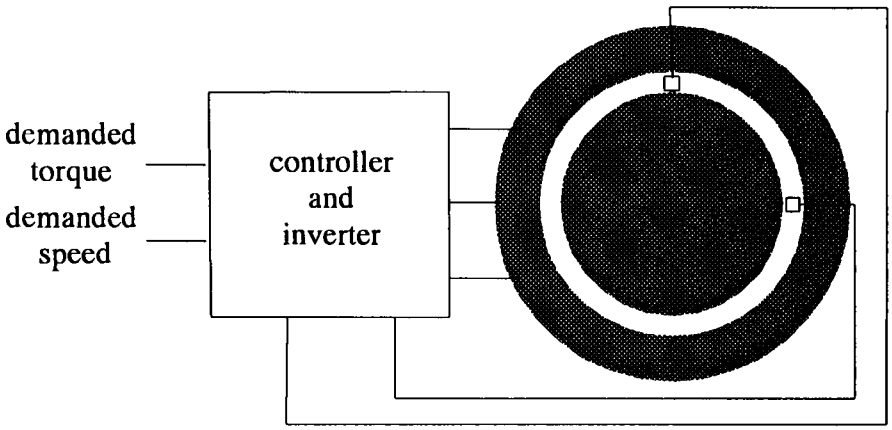

Fig. 21: Block diagram of direct vector control

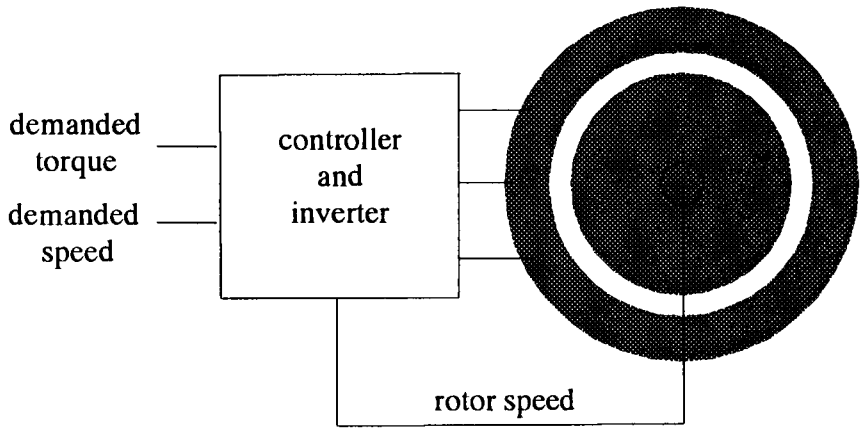

Fig. 22: Block diagram of indirect vector control

2.5.1. Indirect Vector control

To achieve a vector control strategy without sensors it was decided to look at the machine in terms of its representation as a control diagram for the motor in α - β frame as shown in figure 23. The reason for this aproach was to develop a model for the system

without sensors by compensating for the terms in the motor model in figure 23. This produces a model with two inputs, the supplied voltages $V_{1\alpha}$ and $V_{1\beta}$, and one output, the mechanical torque T. Looking at figure 23 from the control system point of view this can be achieved by standard compensation techniques. This entails introducing standard compensation terms for the control model. However, because of the complex intercoupling of the transfer function terms in the motor model of figure 23 considerable effort has been devoted to this problem. This considerable research effort dedicated to this strategy has resulted in the availability of a decoupled vector control strategy [1.3.9, 2.5.1]. In this strategy, the assumption is made that the secondary flux is controlled only in the α axis, whilst the secondary current is only controlled in the β axis. This means that the secondary current in the α axis $i_{2\alpha}$ is 0 and the secondary flux in the β axis $\lambda_{2\beta}$ is 0, which is achieved by a control method called slip frequency control where the slip frequency

$$\omega_s = \omega_r + \frac{Mr_2}{L_2\lambda_{2\alpha}} i_{2\beta}$$

and the primary current in the α axis

$$i_{1\alpha} = constant.$$

Under these conditions it has been shown [2.5.1] that the primary current in the α axis is given by

$$i_{1\alpha ref} = \frac{\lambda_{2\alpha ref}}{M}$$

whereas the primary current in the β axis is given by

$$i_{1\beta ref} = \frac{l_2}{M\lambda_{2\alpha ref}} T_{ref},$$

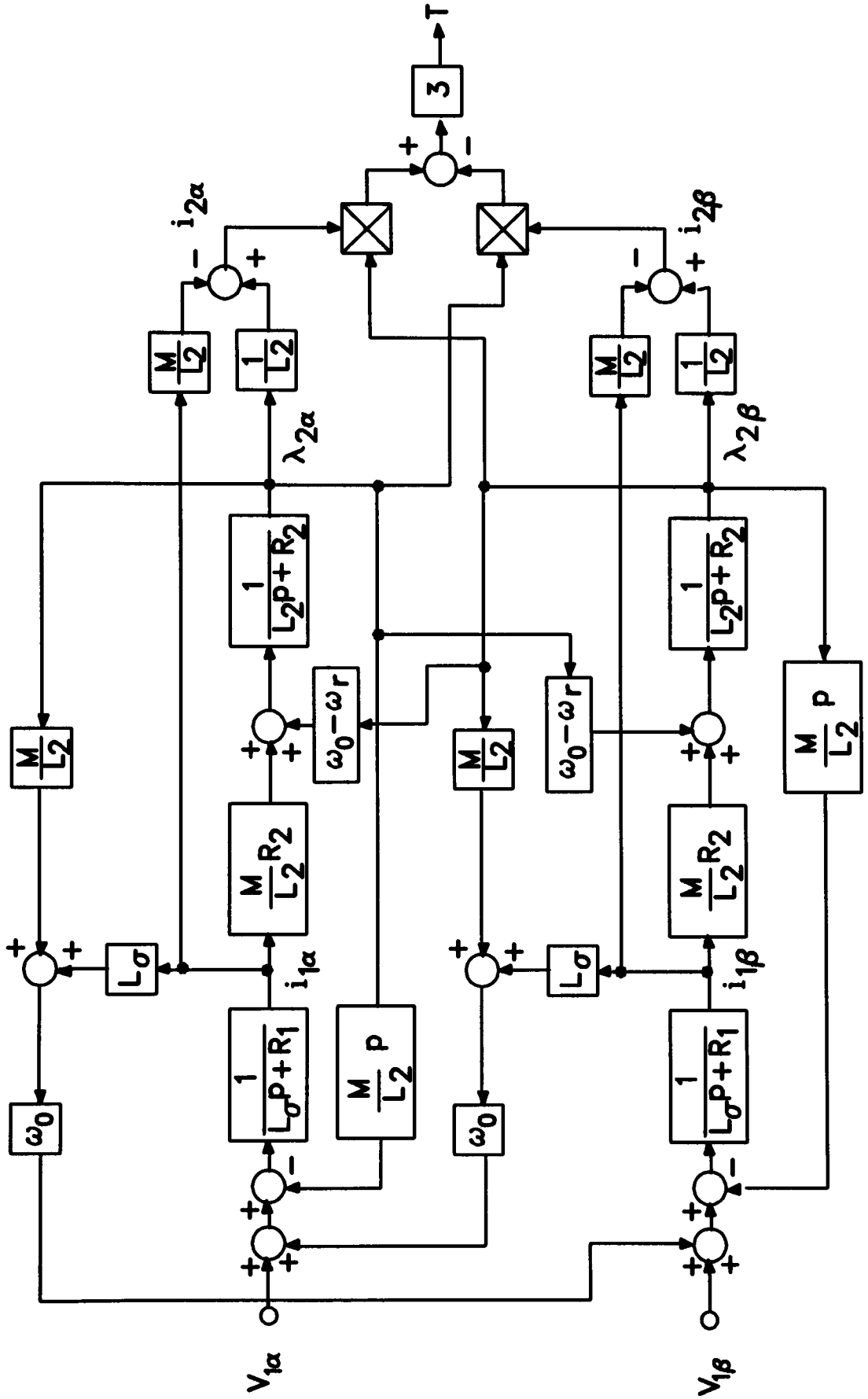

Fig. 23: Control block diagram of induction machine

where the index *ref* shows that these are control reference values not real motor values. Following the control rules shown earlier $i_{1\alpha ref}$ is constant. The slip frequency can then be obtained by

$$\omega_s = \omega_r + \frac{Mr2}{L_2 \lambda_{2\alpha ref}} i_{1\beta ref},$$

whilst the primary voltages for α and β axis can be obtained by

$$e_{1\alpha} = r_1 i_{1\alpha ref} - L\sigma\omega_s i_{1\beta ref}$$

and

$$e_{1\beta} = r_1 i_{1\beta ref} + L_1 \omega_s i_{1\alpha ref}$$

respectively. Thus the resulting voltage vector control used in the simulations is shown in figure 24.

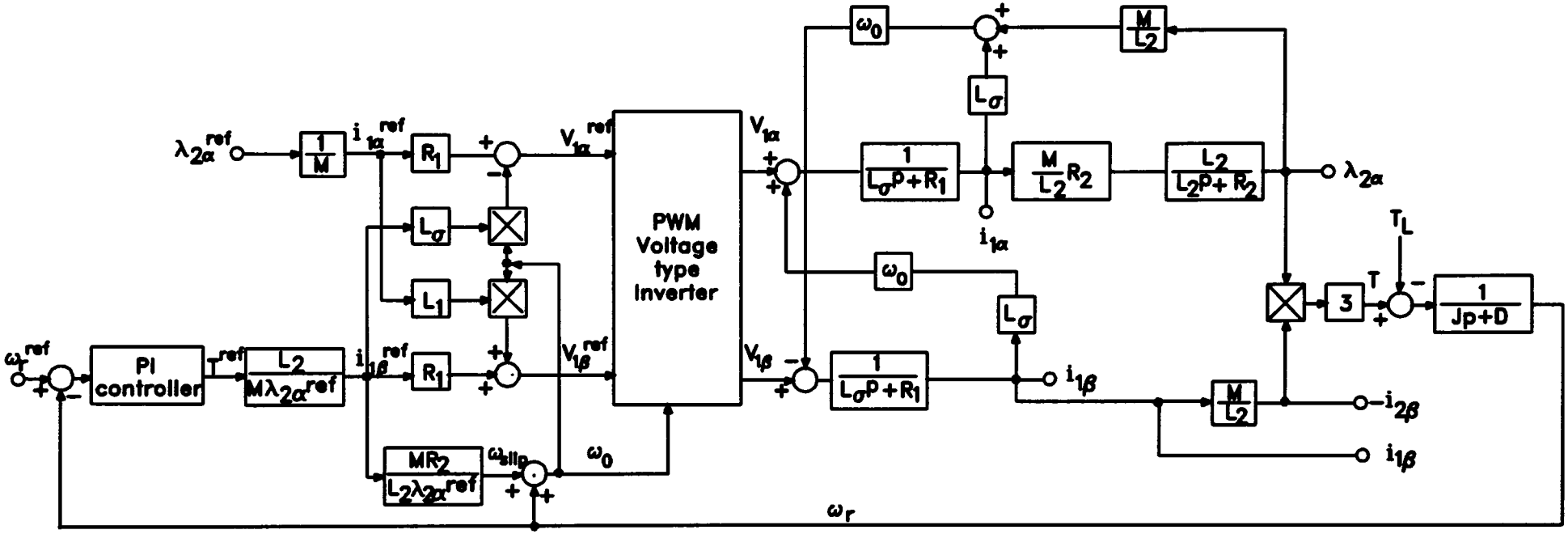

Fig. 24: Vector field control model

3. Simulation

3.1. Software packages

Prior to making simulation studies several questions had to be answered. One was which type of computer to use? The next question was what is a suitable software package? There were two options available at that time. One was the main frame computer and the other was the PC.

On the main frame computer a software package called CTRL-C was available. This package is a matrix orientated software for mathematical calculations. The main frame is of course the more powerful and one would think should provide the quicker solution. But during term time the main frame was so heavily used, that it turned out to be unacceptablely slow. Thus this solution was soon dropped and the sight turned to the PC. The PC offers more flexibility, subject to the availability of the software of course, for the user, because one can work at home on the machine outside office hours.

The question now was whether to buy software from outside or to go for the software packages available in the Department. One of the problems with selecting a software package is the determination of the suitability of the package for solving the problem in hand. The suitability of a package can only really be established by gaining experience with the use of the package. It was therefore decided to look at two packages available within the department, one known as SYMBOL2 and the other known as MATLAB, to determine their suitability for the simulation of a PWM vector control induction motor drive. The result of this investigation suggested that SYMBOL2 was not really suitable, whereas MATLAB turned out to be particularly useful because of its matrix manipulation properties. MATLAB was therefore used in the remainder of this investigation.

3.2. MATLAB

MATLAB stands for MATrix LABoratory and is, as the name indicates, a software package specially designed for matrix computations. During the period of study, three different versions of MATLAB were in use. For the quality of this package it has to be said, that with every higher version it was not necessary to learn the basics again - unlike other software such as OCCAM. It started with the simple PC-MATLAB, designed for PC-XT, which was, due to the capacity of this computer type, very limited in its power. For instance the maximum length of a vector was 4144 elements. Shortly after an updated version of PC-MATLAB became available. MATLAB was supplied as PC-MATLAB to keep up "Compatibility", but it also contained a version called AT-MAT-LAB, that was no longer able to run on 86/88 computers. It runs only on 286 and higher computers exploiting their advanced features. With AT-MATLAB the length of a vector was limited to 8288 elements. Finally a version called 386-MATLAB became available, that broke with "Compatibility" and runs only on 386 and 486 computers. Its vector length is only limited by the available memory. MATLAB is also available for other types of computers such as main frames and Mac's.

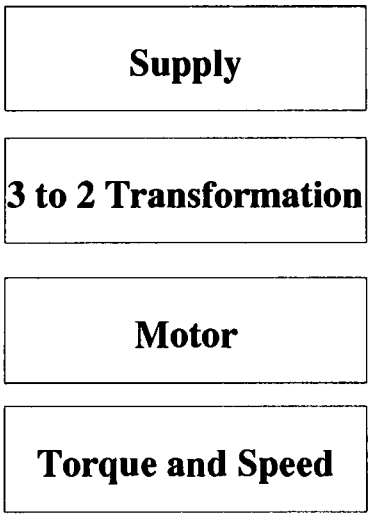

Fig. 25: The motor model built up by modules

MATLAB offers a lot of features, that make it a very comprehensive package. It incorporates graphic features that allow display of the data, printing features for most of the printers available and communication capability to other software such as FORTRAN, C, PASCAL and SYMBOL2.

The program is structured into suitable blocks that are saved as MATLAB *.M files as shown in figure 25. The main advantage of the MATLAB structure is that any parameter can be changed in a module or M-file without having to changed the other modules or M-files. This provides the facility for indepth investigations into any part of the system, for example current, torque or speed, by running that particular module or M-file only.

3.3. Simulation of Motor Characteristic

The torque speed characteristic of the motor used in the experimental electrical drive setup was simulated by means of MATLAB for operation from a three phase 240 V, 50 Hz supply. This simulation, the result of which is illustrated in figure 26, also made use of the Park vector representation in the MATLAB package. The exact parameters and data of the machine under investigation can be found in Appendix A.

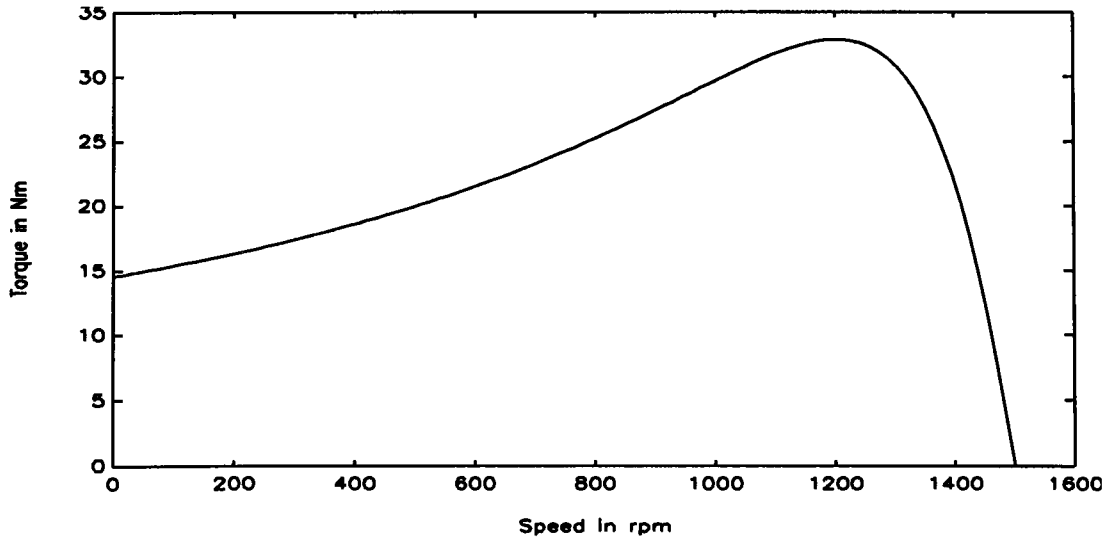

Fig. 26: Simulated motor characteristic

In order to cross-check the simulation result illustrated in figure 26 the motor torque speed characteristic was also simulated by making use of the equivalent circuit in figure 6 and treating the circuit as a voltage divider. The result of this simulation agreed closely with that illustrated in figure 26.

Further simulations of the motor torque speed characteristic were made when the frequency of the supply to the motor was held constant at 50 Hz and the amplitude of the supplied stator voltage varied from 10 V to 240 V in 10 V steps. The result of this simulation is illustrated in figure 27. It is interesting to note from figure 27 that the reduction of the magnitude of the stator voltage whilst frequency is held constant brings about a reduction in the pull-out torque, which is of course to be expected.

Similar simulation studies of the motor torque speed characteristics were made when the applied stator voltage was held constant at 240 V whilst the frequency of the main supply was varied from 2 Hz to 50 Hz in 2 Hz steps. The results of this investigation are illustrated in figure 28. It can be seen from this figure that the synchronous speed of the motor decreases in proportion to the decrease in frequency whilst the pull-out torque increases because of the increased volt-frequency ratio.

However, it should be noted that for the simulations described above a simplified motor model is used, that neglects effects such as iron losses and saturation. The neglection of these effects is of course justifiable at rated voltage and frequency, but of course are not acceptable for low values of frequencies and voltages. An experimental verification of the simulated results illustrated in figures 27 and 28 would have proved interesting but unfortunately could not be made with the torque transducer facilities and the power supply systems available. The experimental verification of all illustrated results, however, will be discussed in chapter 6.

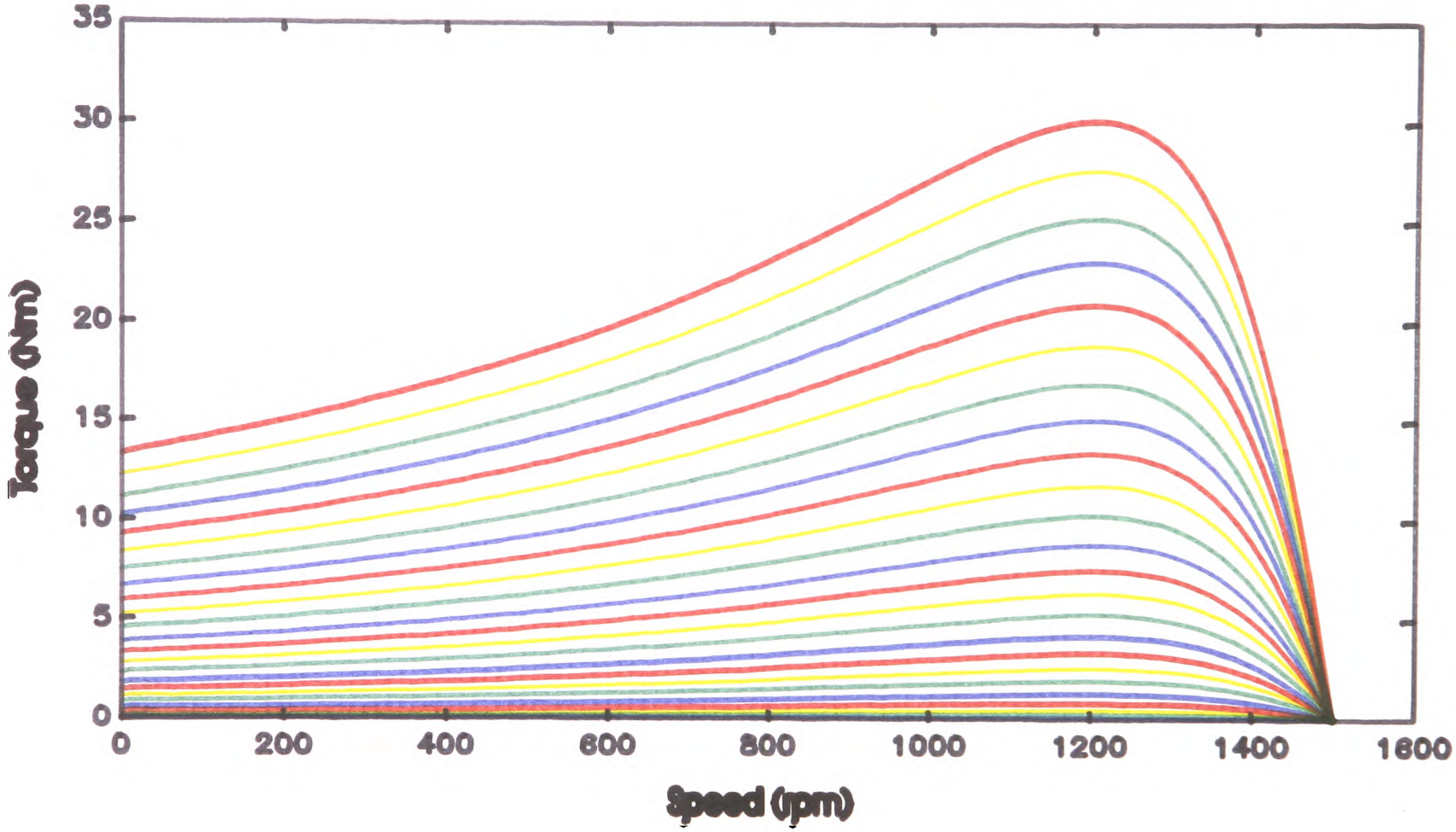

Fig. 27: The motor characteristic with variable V

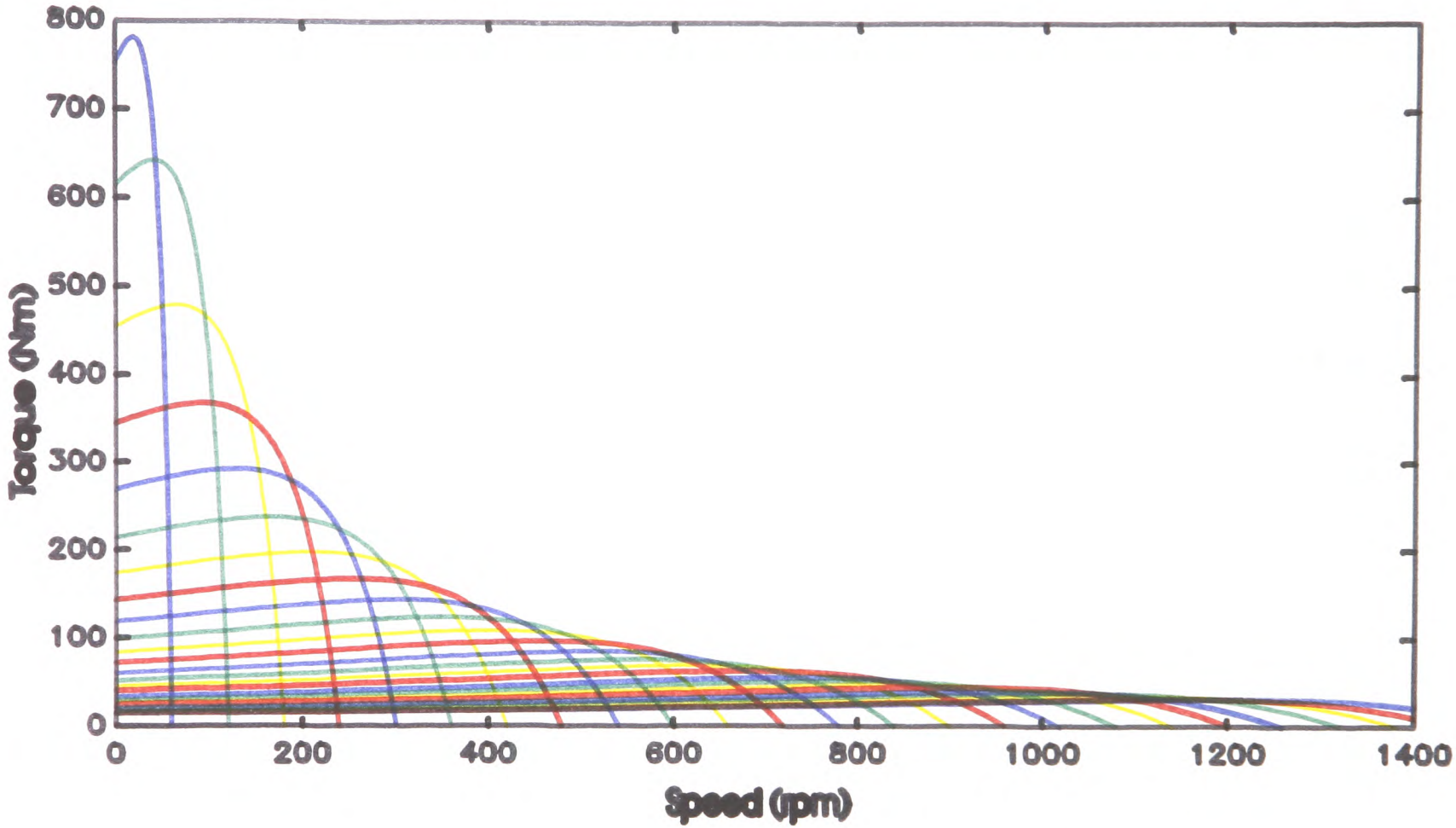

Fig. 28: The motor characteristic with variable f

3.4. Simulation of direct on-line start-up of the Motor

In this section the dynamic behaviour of the motor was under investigation. The direct on-line start-up (DOL) of the induction machine was simulated, when supplied by a 240V 50Hz three phase system. Since the manufacturer did not supply any information about the value of the motor inertia, it was necessary to investigate the machine behaviour at different inertia values.

On each of the following pages a set of three figures is shown. The top figure illustrates the simulation result of the torque speed characteristic, the middle one the speed characteristic and the bottom one the torque characteristic. The first four sets show the results when the inertia is increased for a load of the type $T_L \sim n$, where the proportional factor has a very little value and thus a very small torque is applied in steady state condition. In the then following sets the load is of the type T_L= *constant.* These sets are grouped to sets of four where the inertia value is the same, but the applied load has the value of 0, 4, 8 and 10 Nm respectively. The values of the inertia are the same as used in the first 4 sets and can be obtained from the figures.

All these figures show, that the DOL can be divided into two phases. In the first phase the machine follows one mathematical function and passes across to a sliding function at a certain point, furthermore referred to as synchronisation point, into another mathematical function. The existence of these two functions can be explained by the fact, that the initial condition for the motor is defined as zero. From the machine characteristic for this voltage as presented earlier it can be anticipated, that this situation zero speed at zero torque is alien for the machine. This means, that the machine first tries to overcome this situation to reach a familiar point in the area of the characteristic. At this point the machine now synchronises its behaviour to the machine characteristic and is therefore referred to as the synchronisation point. From here on the behaviour is the same as for a speed change along the characteristic, but not necessarily on it, depending on the value of the inertia. However, it can be seen that for higher values of the inertia, the start-up characteristic in the first phase approaches the motor characteristic as far as the average value is concerned and then runs quite accurately along it

during the second phase, where a little overswing is visiable around the working point. This swinging vanishes for very high values of inertia. Looking at the functions involved in both phases, the characteristic can be divided into two parts. The first part is the picking up of speed, the second one is the decreasing of the overshot speed and so on. The period and amplitudes of these functions are very much dependent on the inertia value. In the first part the inertia reacts as a resistance to the development of speed, while in the second part it acts as resistance to the decrease in speed. With the switching on of the supply voltage the machine generates current and the flux thus induced generates speed. However, not all of the current goes into speed, a part is consumed in magnetization, generating heat and torque. Since heat and magnetization are neglected in this simulation, all of the current generates torque. This might not be the case for a real machine and thus can only be judged by comparison with experimental results.

As stated earlier the duration of the first function for the build up of speed is dependant on the inertia value, and from the simulation results it can be seen that for small values the period is small. This appears to be logical because a small value means a small resistance and thus a fast reaction time. The amplitude, however, appears to be not only dependent on the inertia value, but also on the interaction with the torque developed in the motor. Obviously the value of speed reached in the first upswing is higher than desired and thus the machine starts to brake. The inertia does now resist the decrease in speed and thus the period of this braking is the longer, the bigger the value of the inertia.

For the further deliberation, the inertia values looked at will be split in three groups. Representative figures are shown here, more are available from the appendix. These groups show three different behaviour patterns. The first group are inertia values (J) smaller than 0.002 kgm^2, the second, which is rather a value then a group, is J = 0.002 kgm^2 and the third are values bigger then 0.002 kgm^2.

In the first group (figures 29-31, 41-52) the inertia is so small, that it reaches the area of the synchronisation point very quickly. This synchronisation point, however, appears to be the working point, because in the second phase the underlying function is a straight line. It can be seen that the number of cycles performed until synchronisation is the

greater the smaller the value of inertia. This can be explained by the fact that a small value of inertia provides less resistance to the startup oscillation and thus allows a more free oscillation. However, the working point is reached with synchronisation and from then on the inertia is dominant in decreasing the oscillation to a stable condition. A low value of inertia now allows a fast decrease of speed, while a higher value resists the decrease and thus prolongs the time needed for ending the oscillation. This leads straight away to the second group (figures 32-34, 53-64). Here, a situation is found where from synchronisation onwards the decreasing function equals the increasing function and thus the working point is never reached, but the average of this oscillation function is the operating point. This appears to be a resonance point of the system.

For the third group (figures 35-40, 65-88), this synchronisation point is away from the working point. It can be anticipated that the underlying function for the startup more closely approaches the machine characteristic the higher the value of the inertia. However, with the increase of the value of the inertia the time until the operation point is reached increases dramatically. The operation along the motor characteristic starts to oscillate again around the working point. The amplitude of this oscillation decreases with the increase of the inertia value to a point where it vanishes. The addition of load can be seen to force the machine to a negative value for the initial speed.

From all this, it can be concluded that an inertia value below 0.002 kgm^2 is desirable as far as the startup time is concerned. However, every load attached to a machine has an inertia value of its own and this adds to the motor inertia. And this could mean that a drive could arise, that would work at the resonance point. This would be a very undesirable situation for any application, but fortunately every machine has its inertia value built in by the physical parameters of the machine. An other desire is that the machine reaches its characteristic and runs along it stablely to the working point. This means the real behaviour has to be a compromise between both demands, a very fast oscillation in the first phase and then running along the characteristic with moderate oscillation around the working point. The oscillation around the working point is not unfamiliar to the author from investigation into the startup behaviour of inverter induction motor drives undertaken at the Fachhochschule Hannover. The inertia value

taken as the presumed real value is 0.02 kgm^2. This is confirmed by data sheets for off-the-shelf motors of the same building size from Siemens and AEG. The unavailability of a suitable torque transducer made it impossible to confirm the simulation results with experimental results.

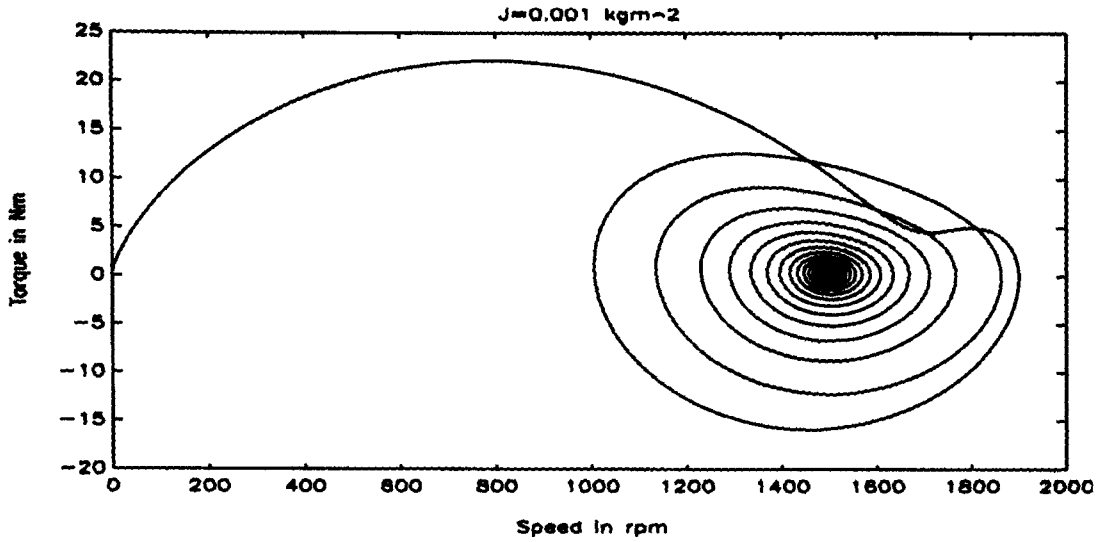

Fig. 29: Direct on line start up

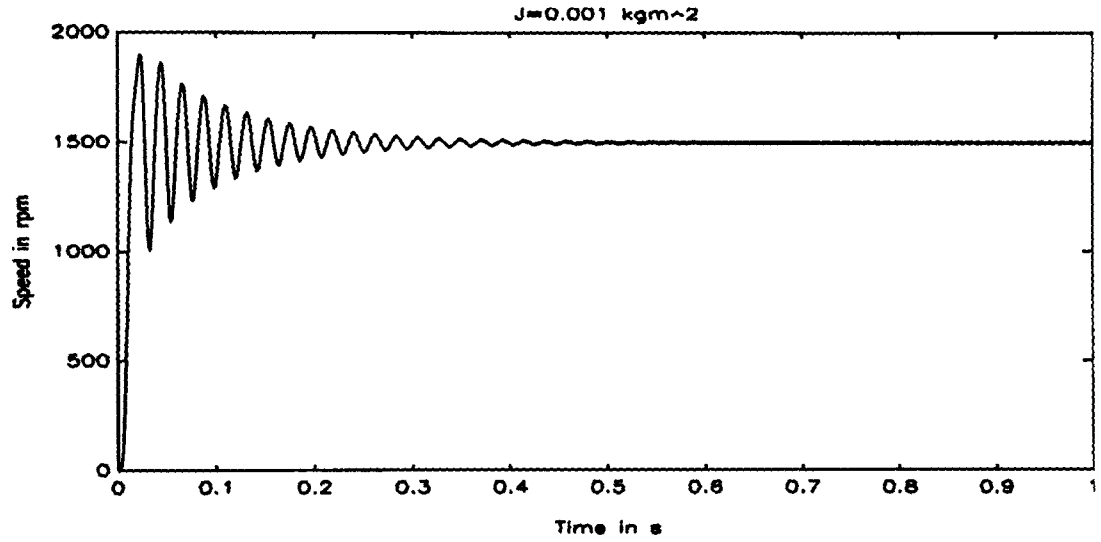

Fig. 30: The speed at inertia = 0.001 kgm^2

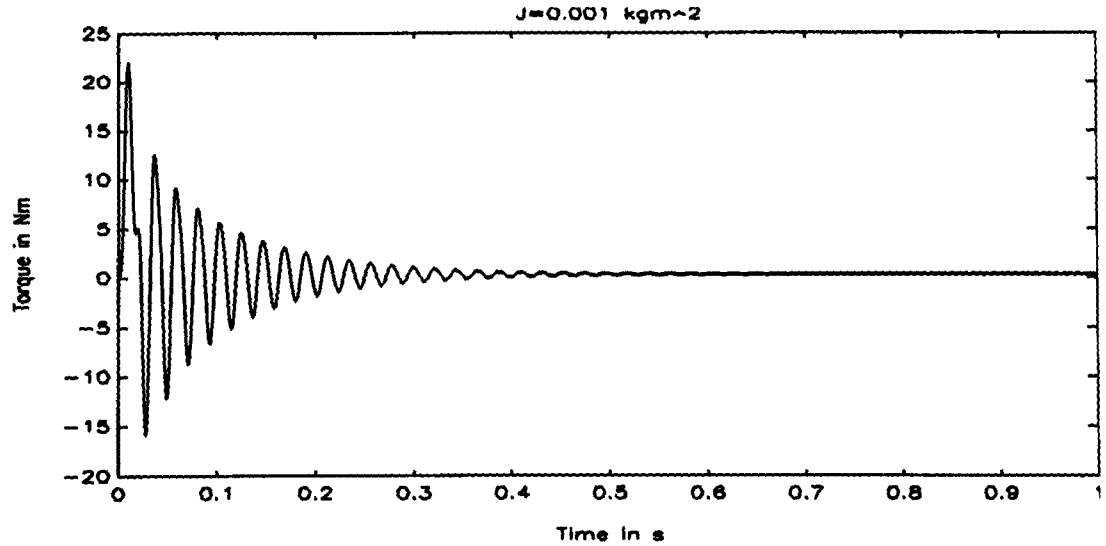

Fig. 31: Torque characteristic of DOL

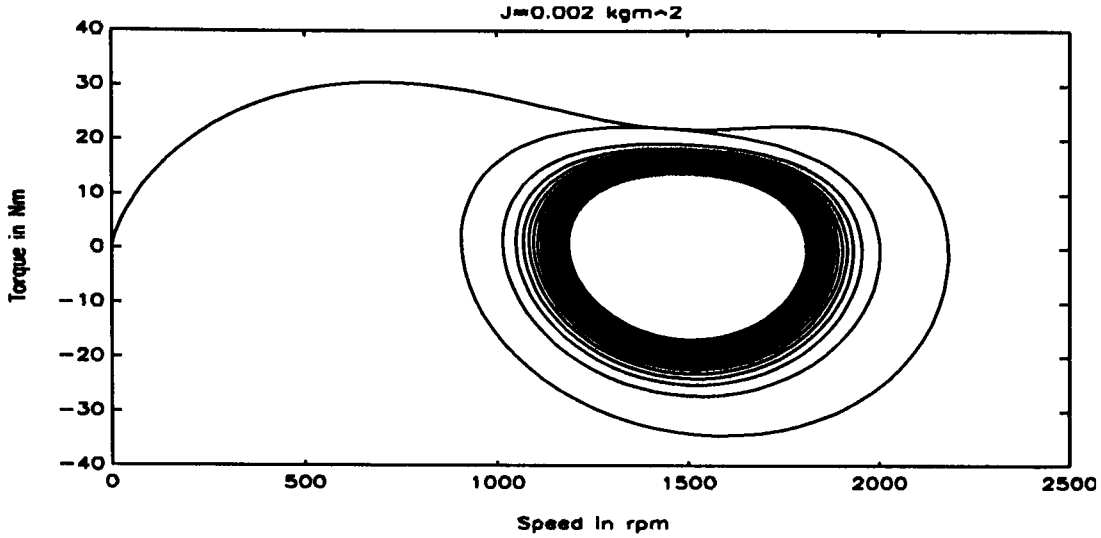

Fig. 32: Direct on line start up

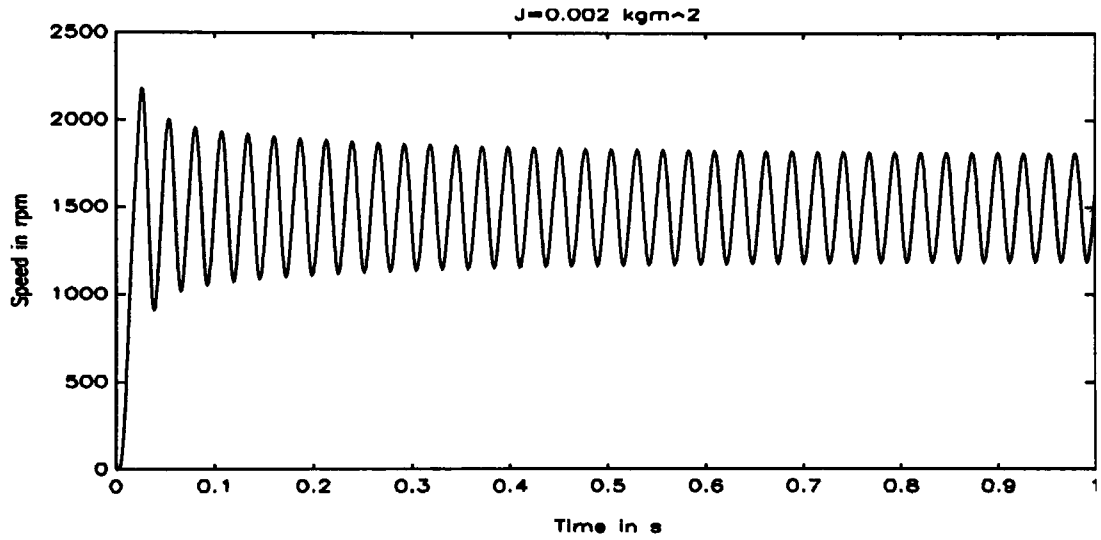

Fig. 33: The speed at inertia = 0.002 kgm^2

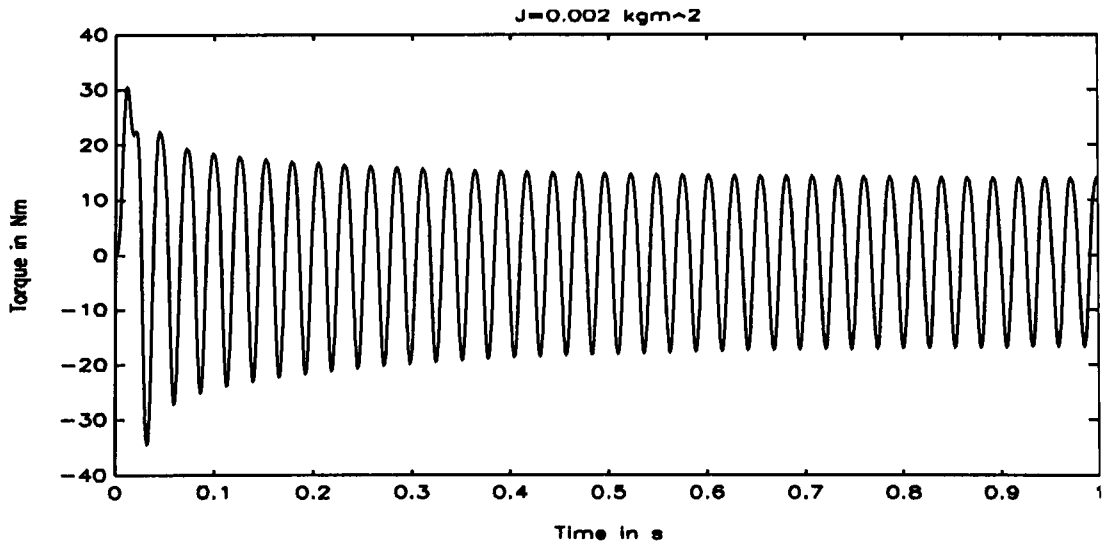

Fig. 34: Torque characteristic of DOL

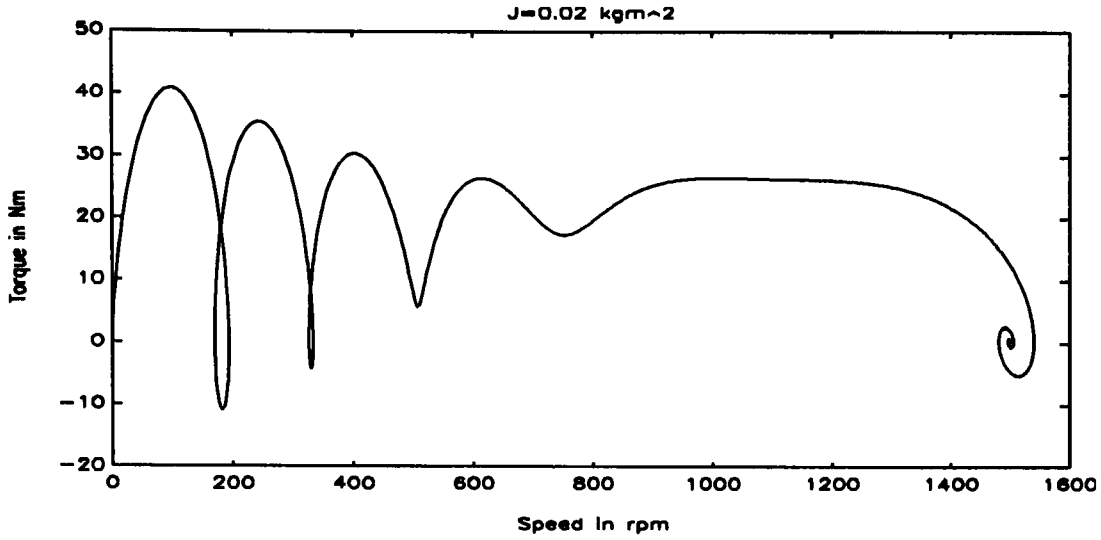

Fig. 35: Direct on line start up

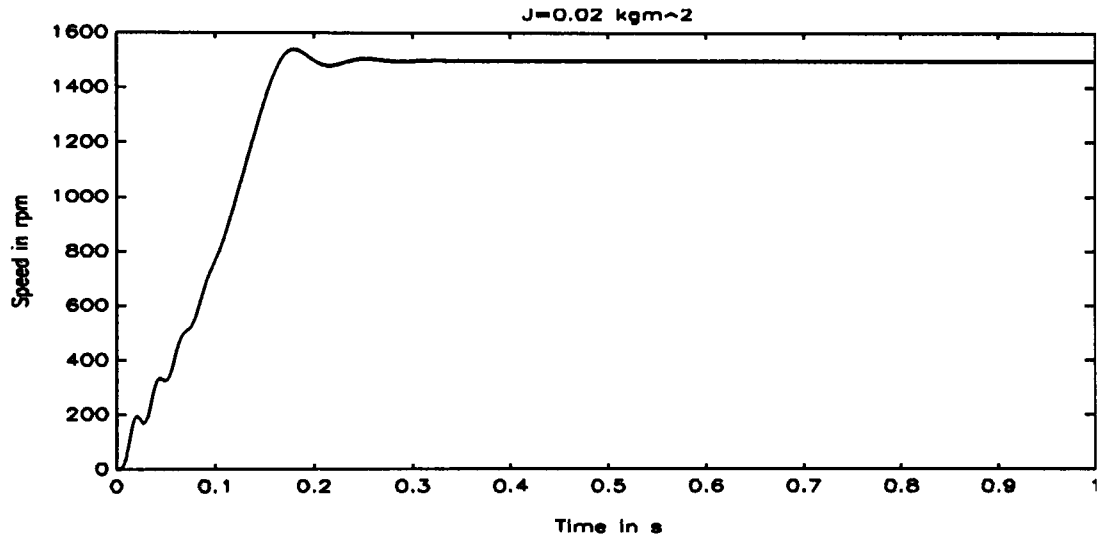

Fig. 36: Speed characteristic for DOL

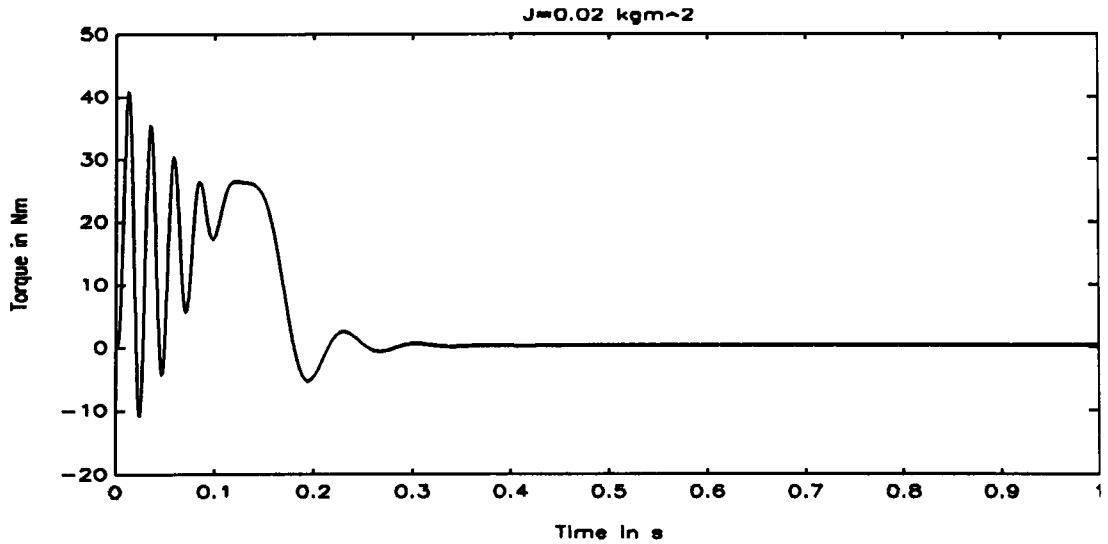

Fig. 37: Torque characteristic of DOL

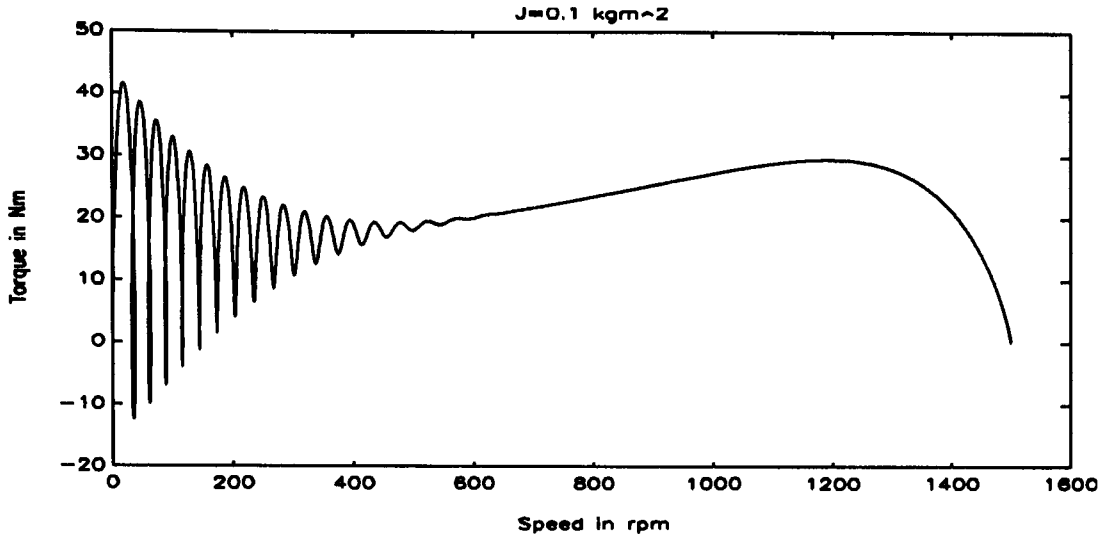

Fig. 38: Direct on line start up

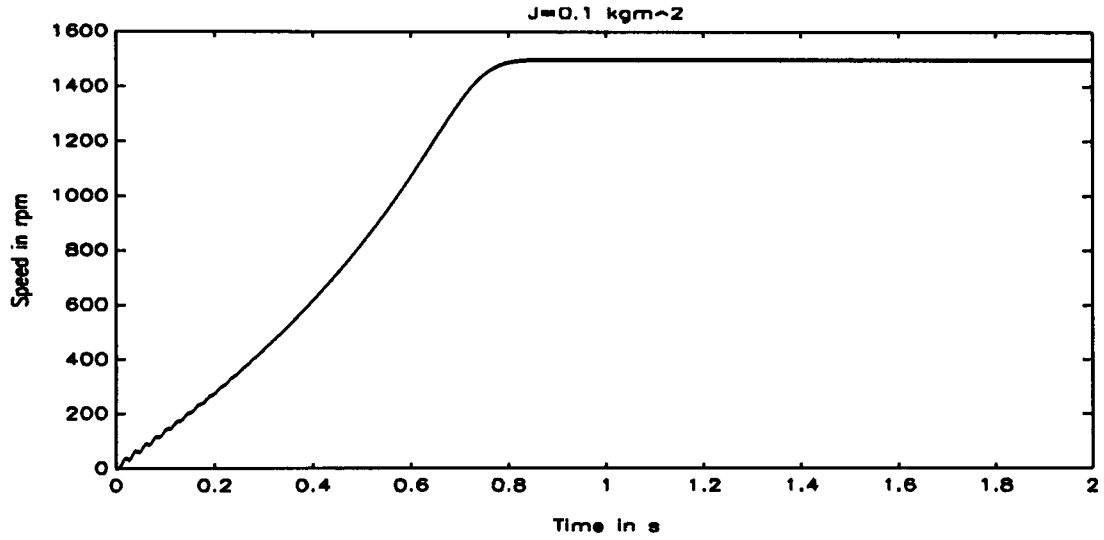

Fig. 39: The speed at inertia = 0.1 kgm^2

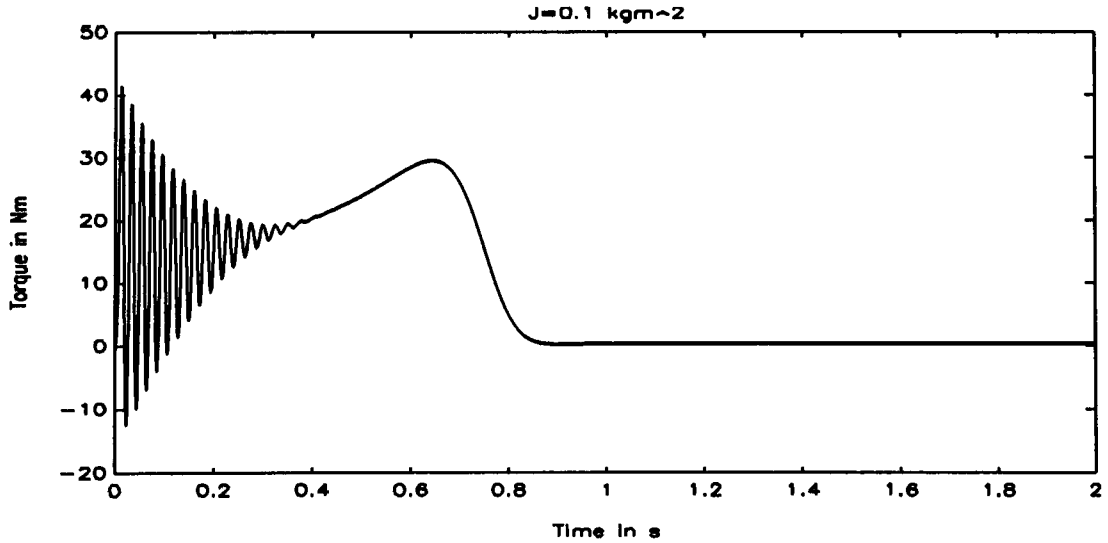

Fig. 40: Torque characteristic of DOL

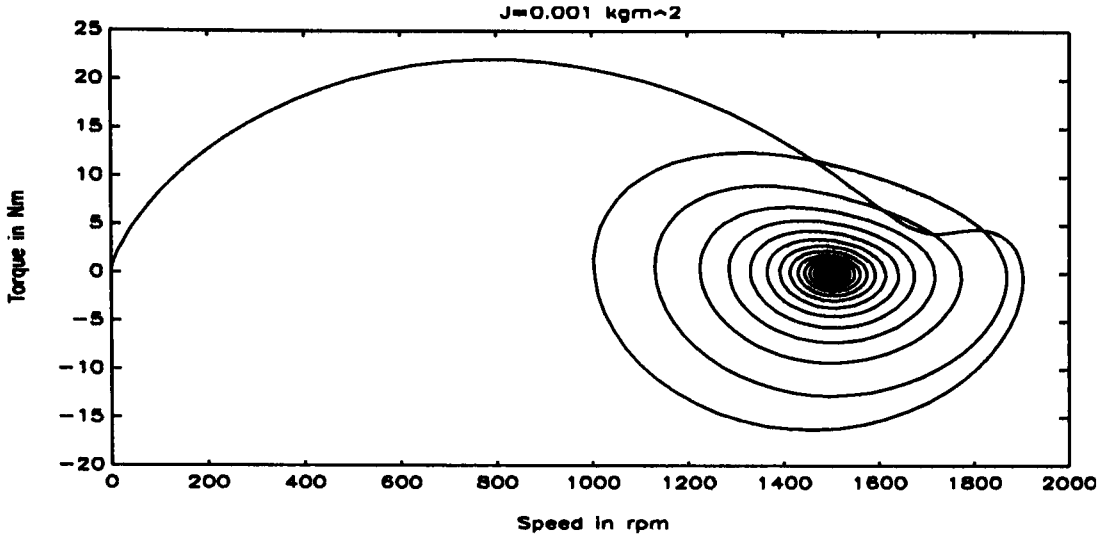

Fig. 41: Torque = 0 Nm

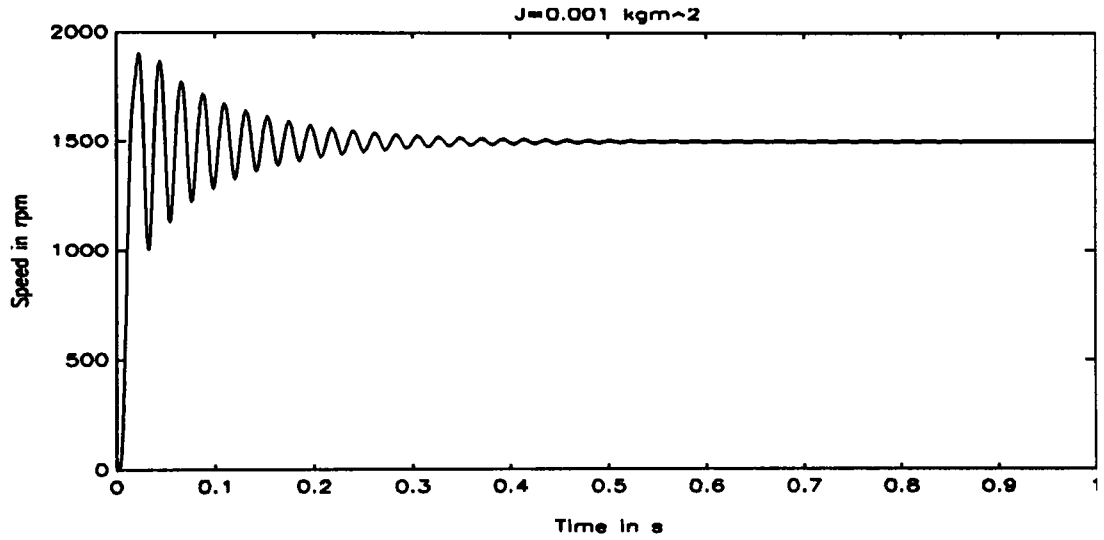

Fig. 42: Torque = 0 Nm

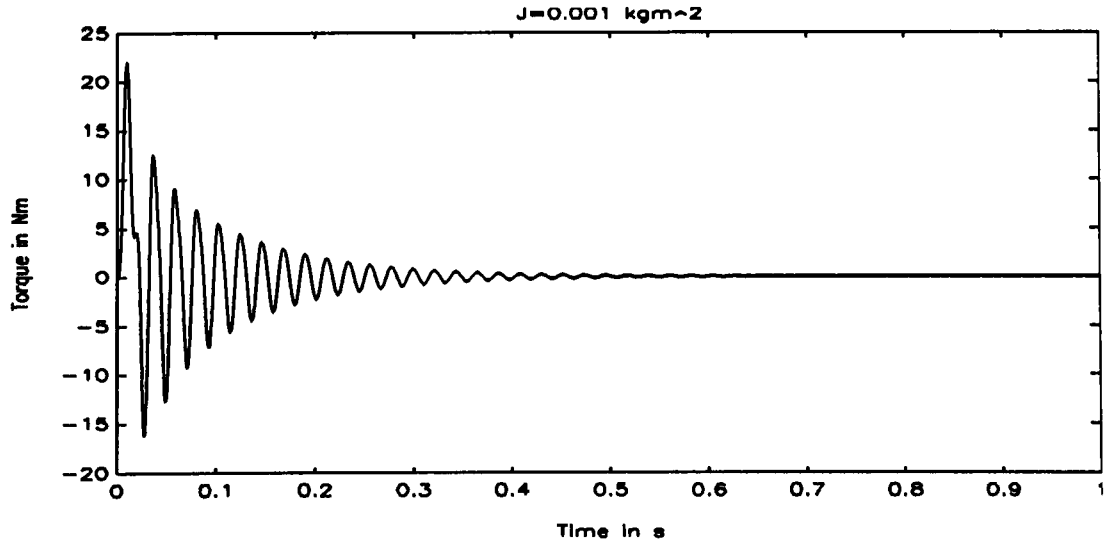

Fig. 43: Torque = 0 Nm

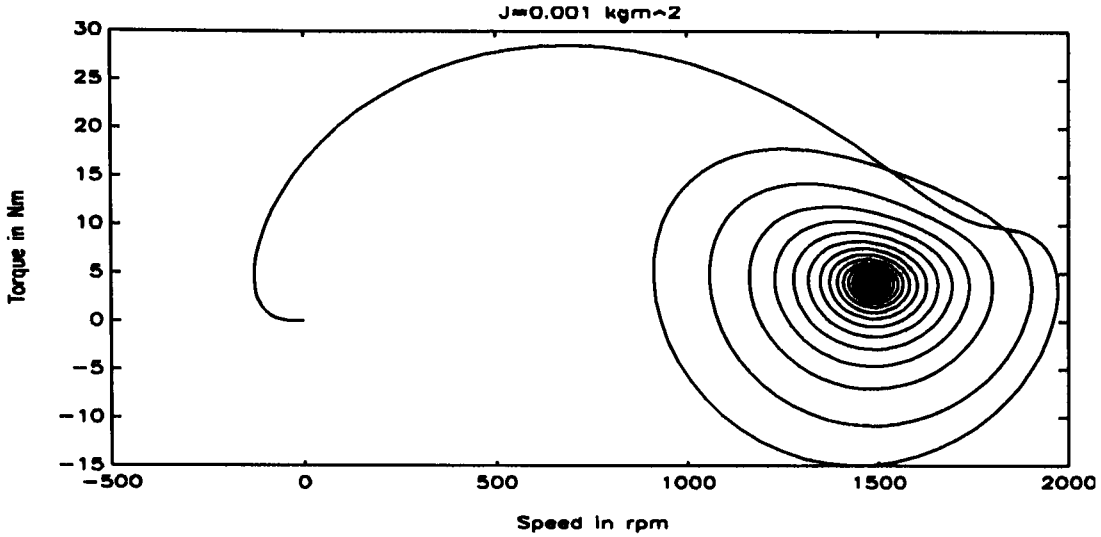

Fig. 44: Torque = 4 Nm

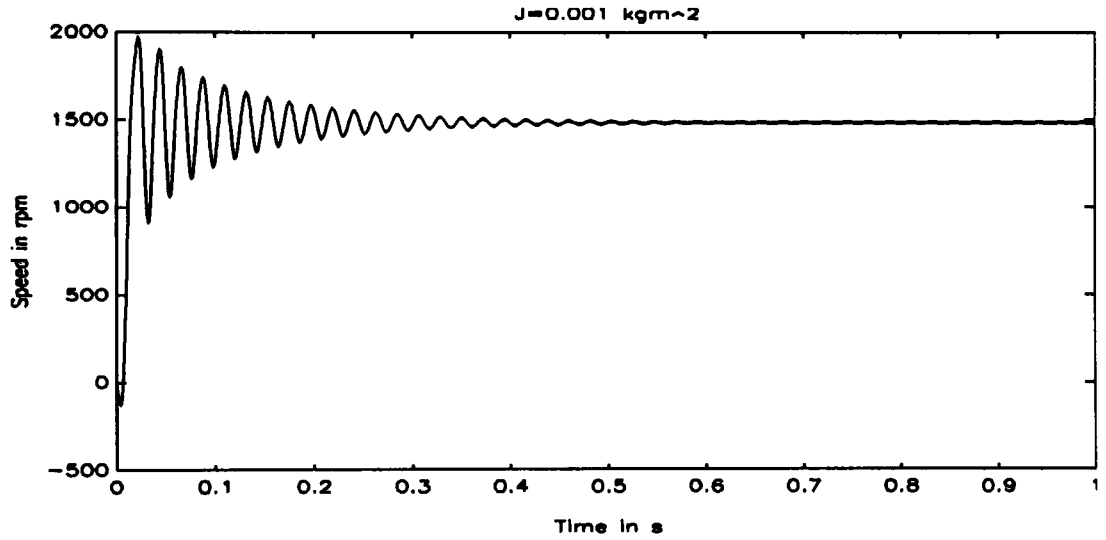

Fig. 45: Torque = 4 Nm

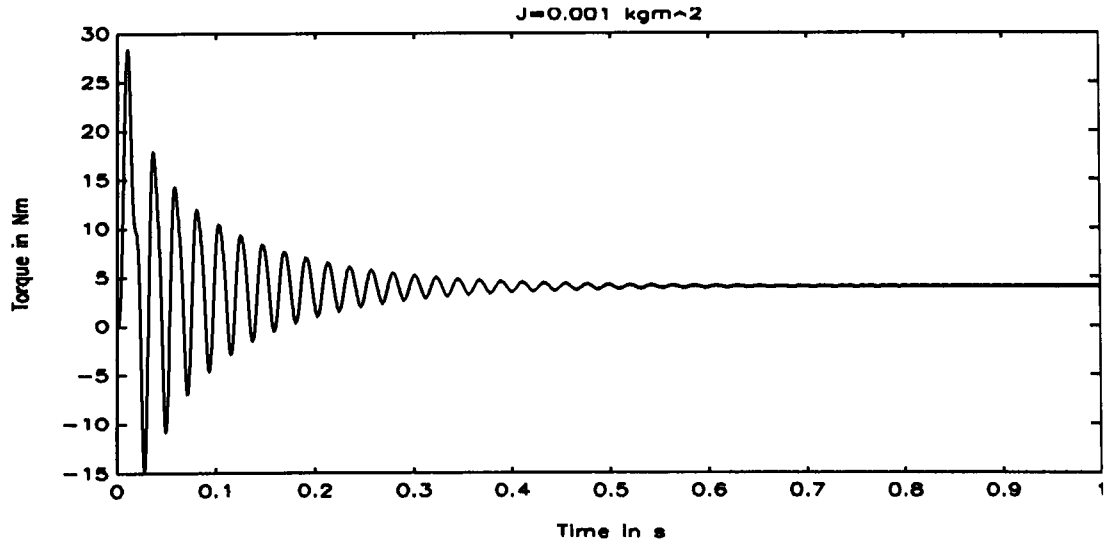

Fig. 46: Torque = 4 Nm

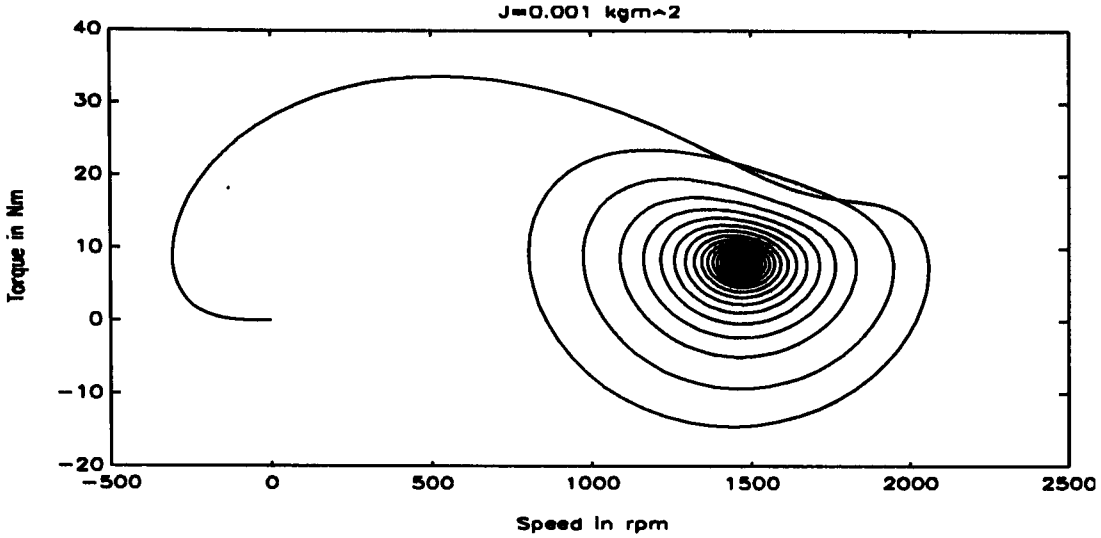

Fig. 47: Torque = 8 Nm

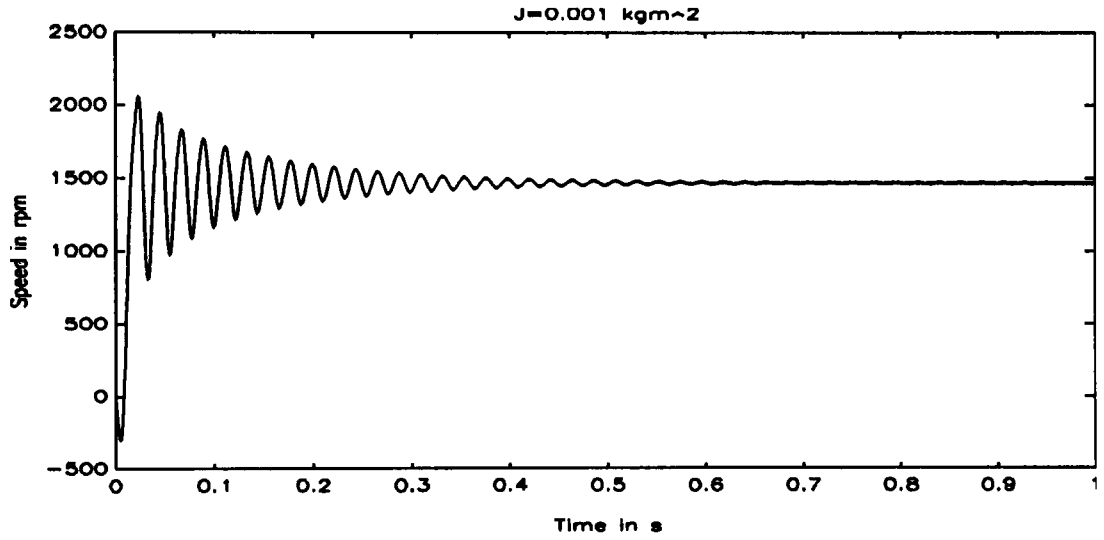

Fig. 48: Torque = 8 Nm

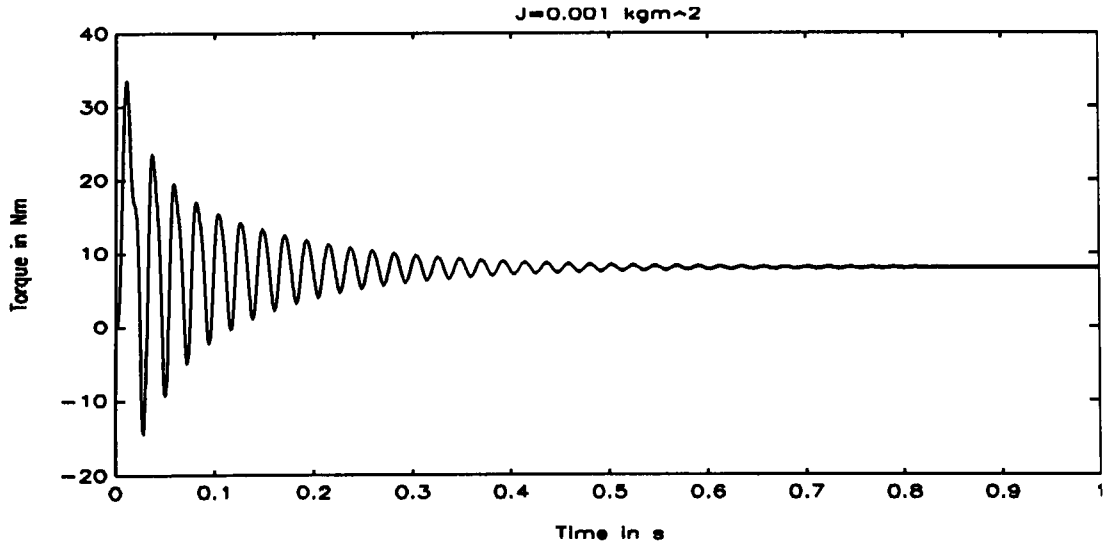

Fig. 49: Torque = 8 Nm

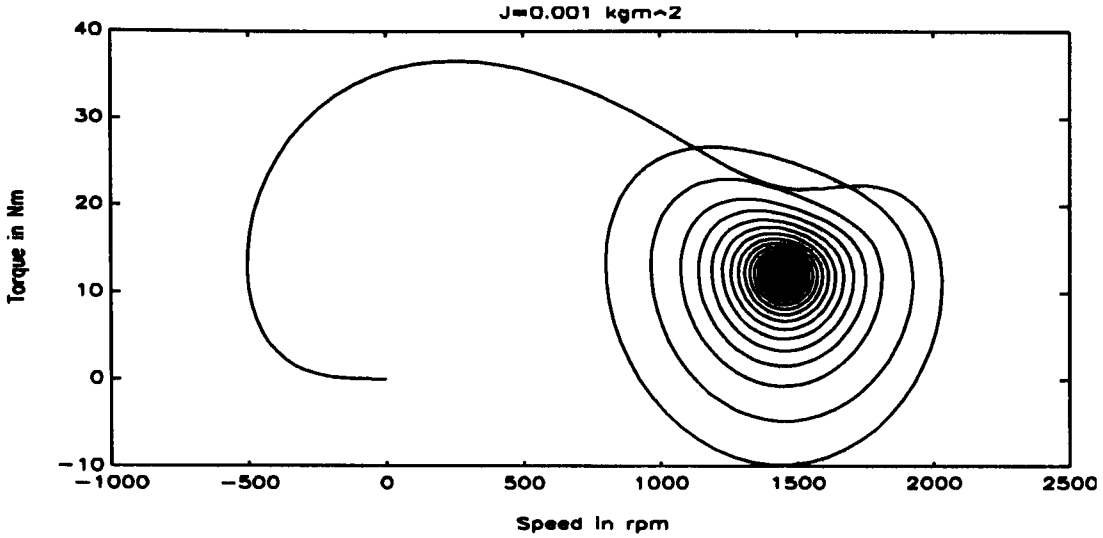

Fig. 50: Torque = 12 Nm

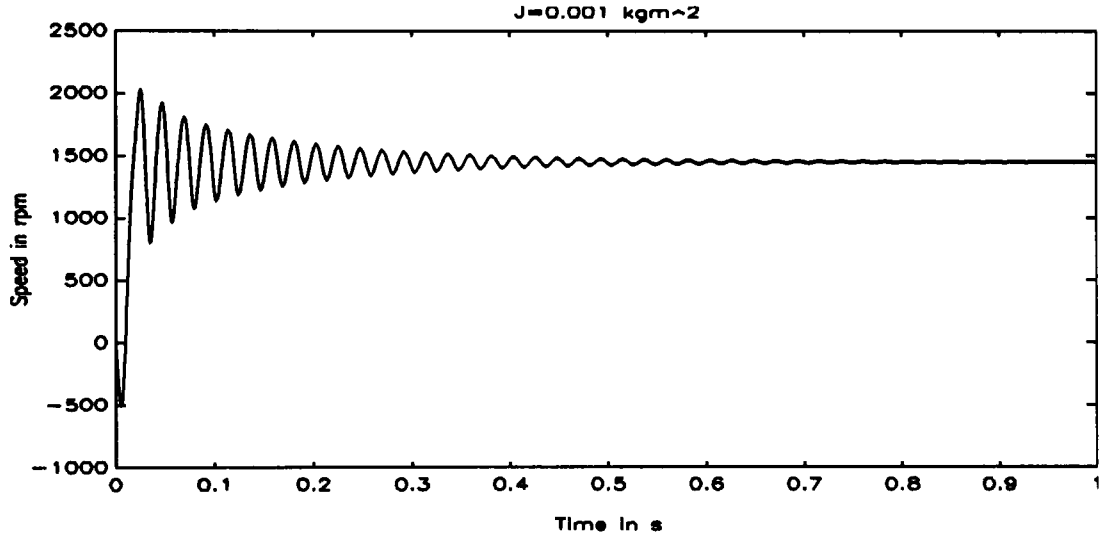

Fig. 51: Torque = 12 Nm

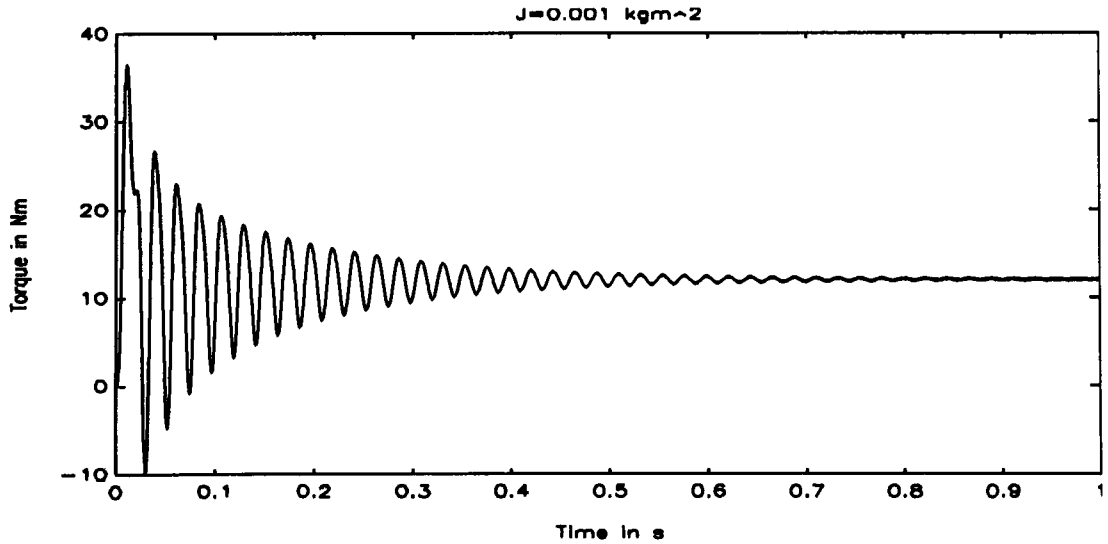

Fig. 52: Torque = 12 Nm

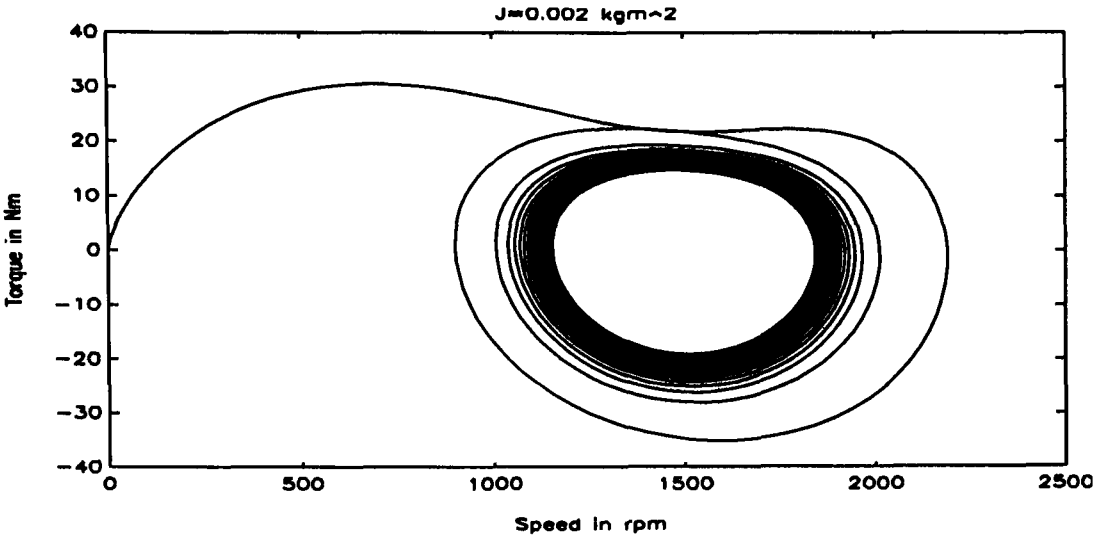

Fig. 53: Torque = 0 Nm

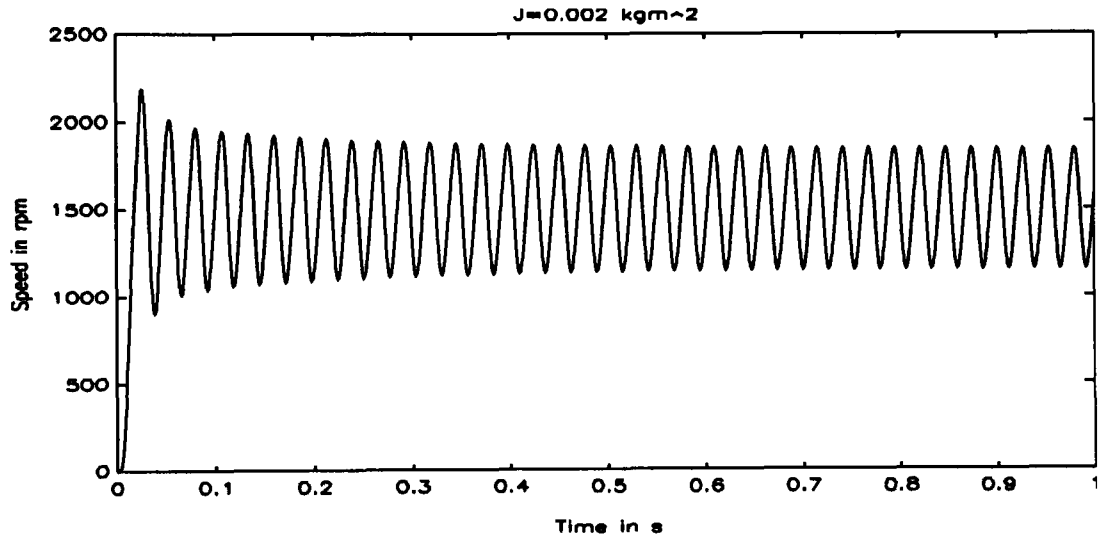

Fig. 54: Torque = 0 Nm

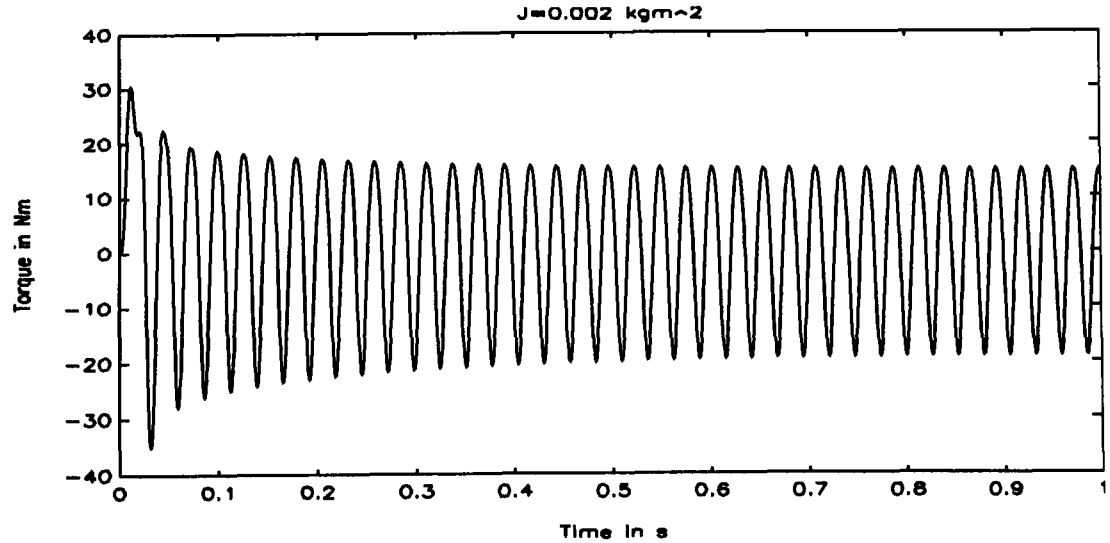

Fig. 55: Torque = 0 Nm

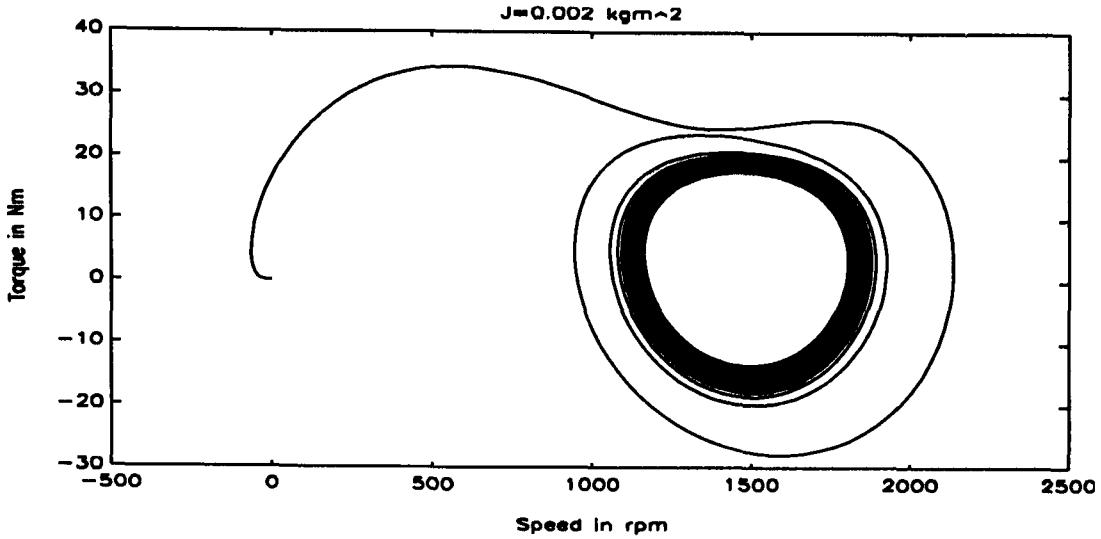

Fig. 56: Torque = 4 Nm

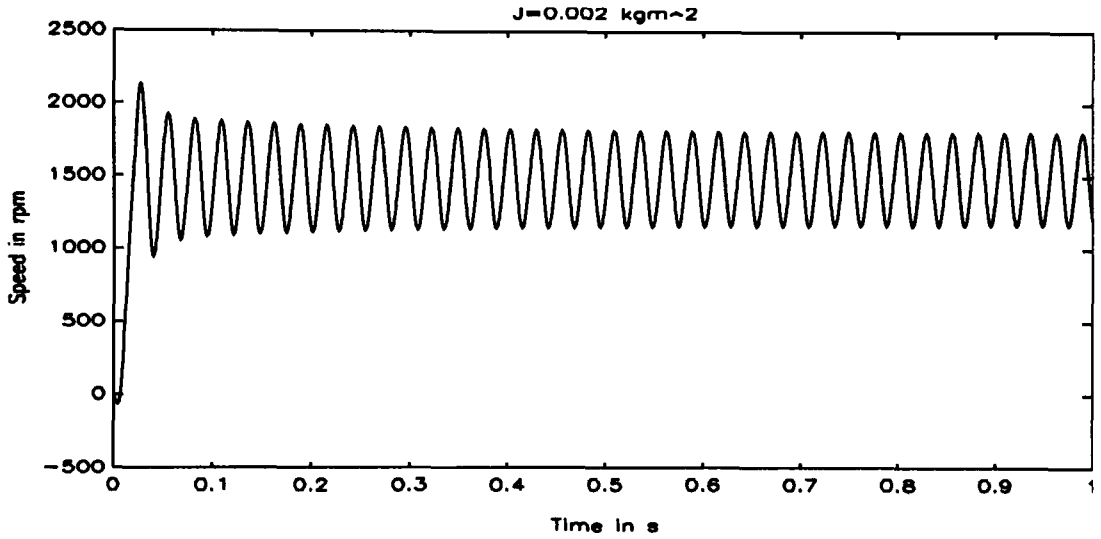

Fig. 57: Torque = 4 Nm

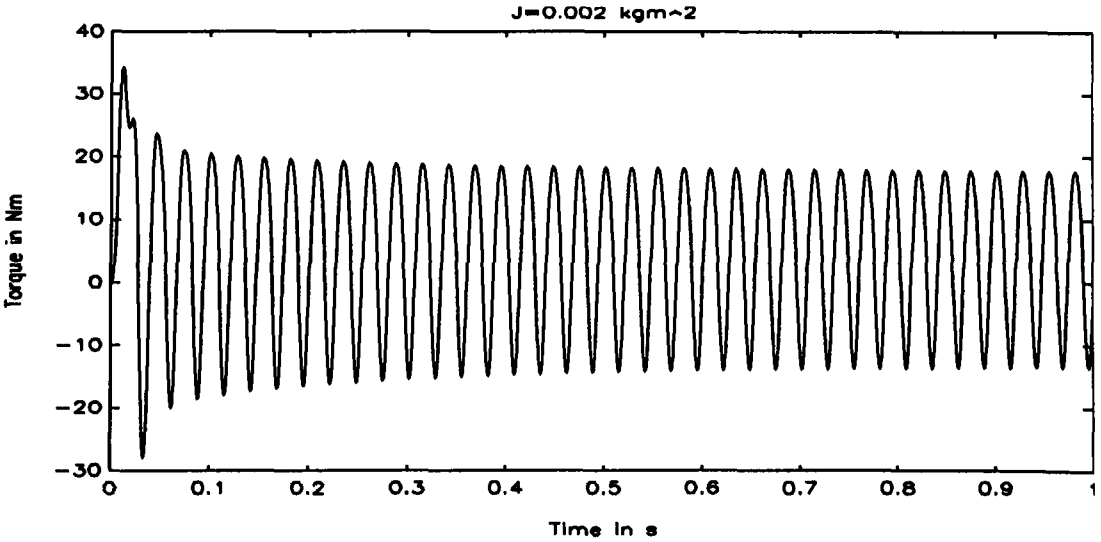

Fig. 58: Torque = 4 Nm

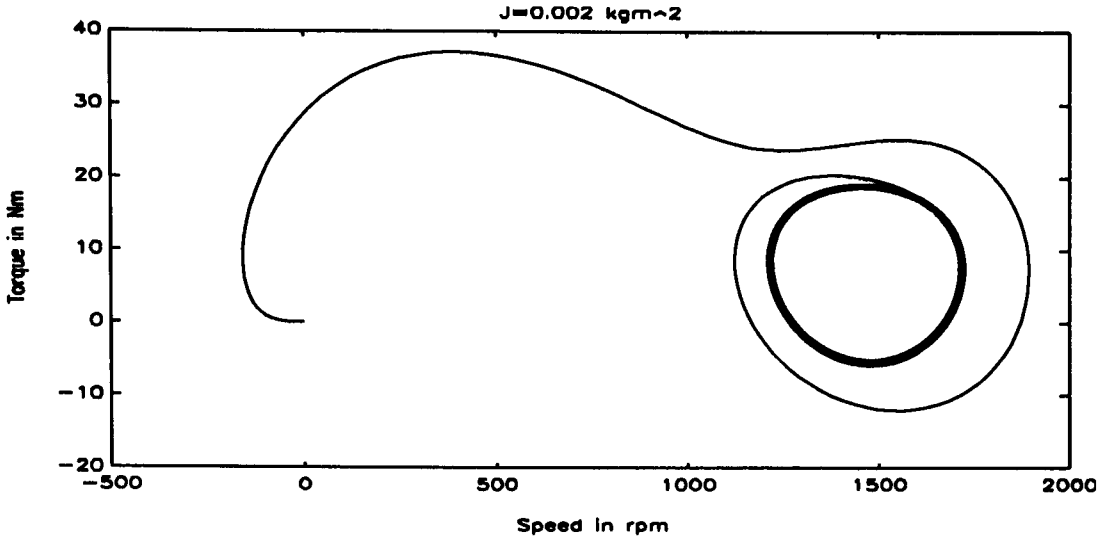

Fig. 59: Torque = 8 Nm

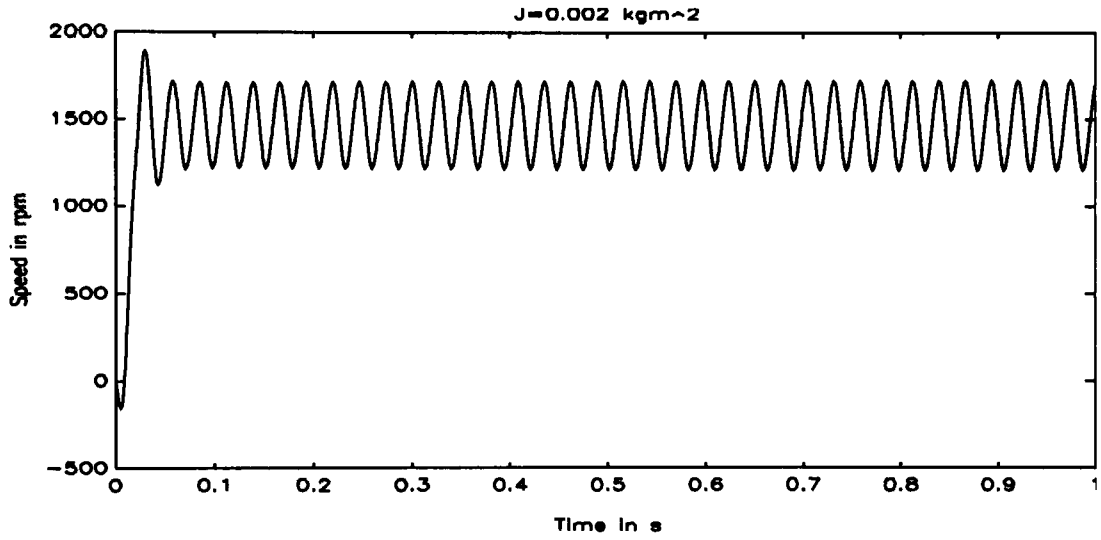

Fig. 60: Torque = 8 Nm

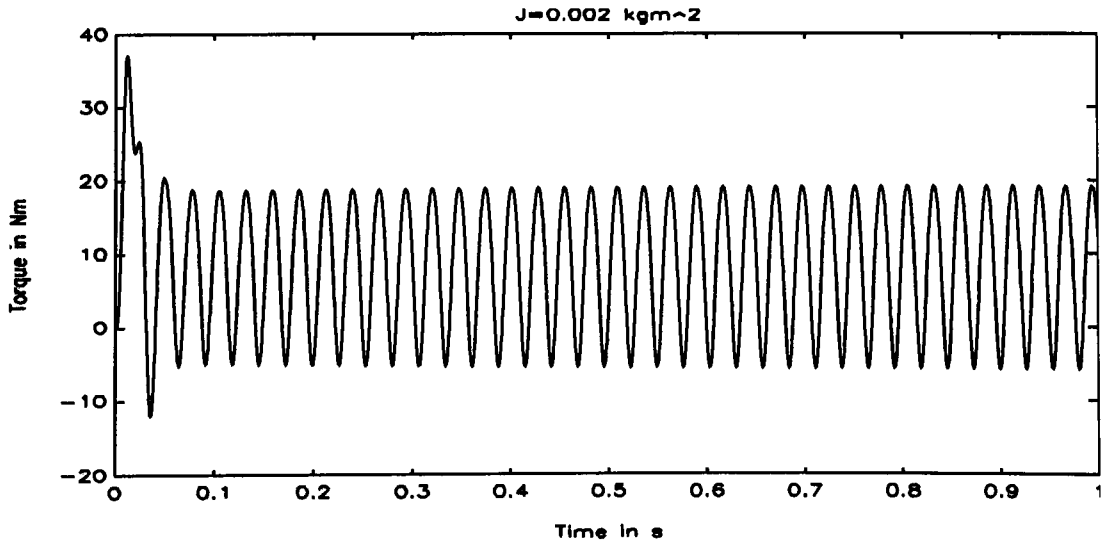

Fig. 61: Torque = 8 Nm

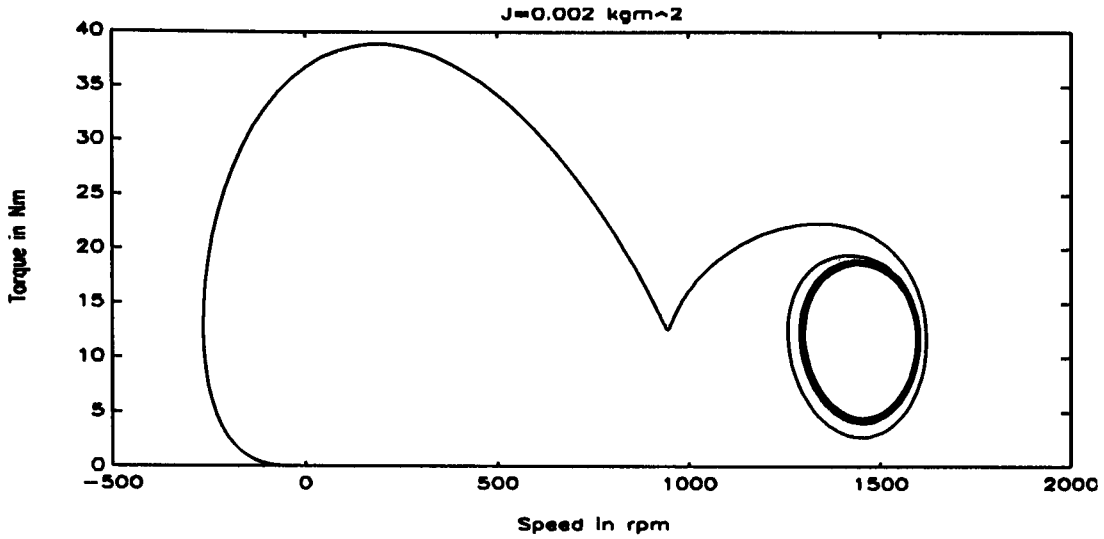

Fig. 62: Torque = 12 Nm

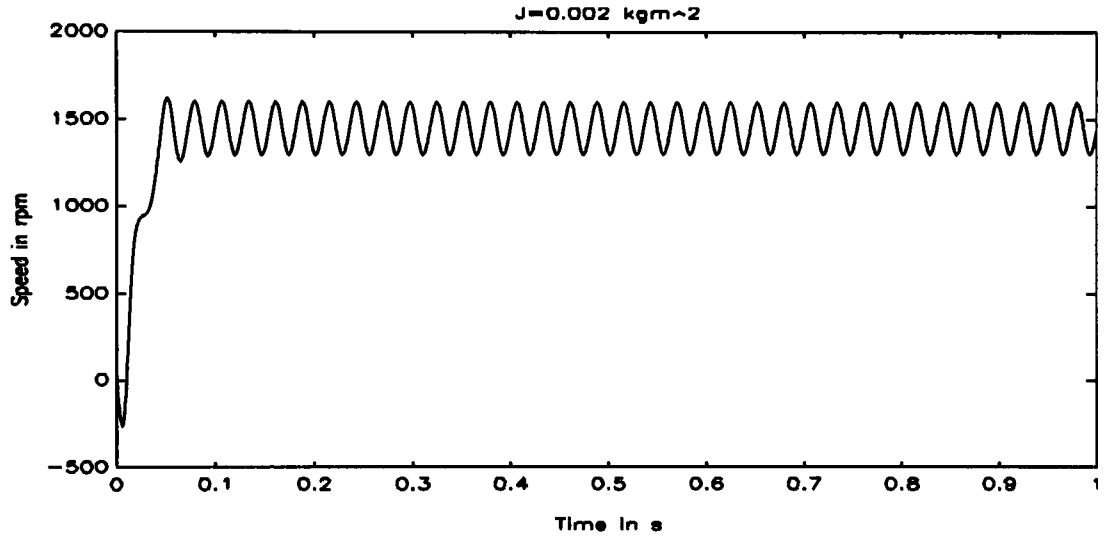

Fig. 63: Torque = 12 Nm

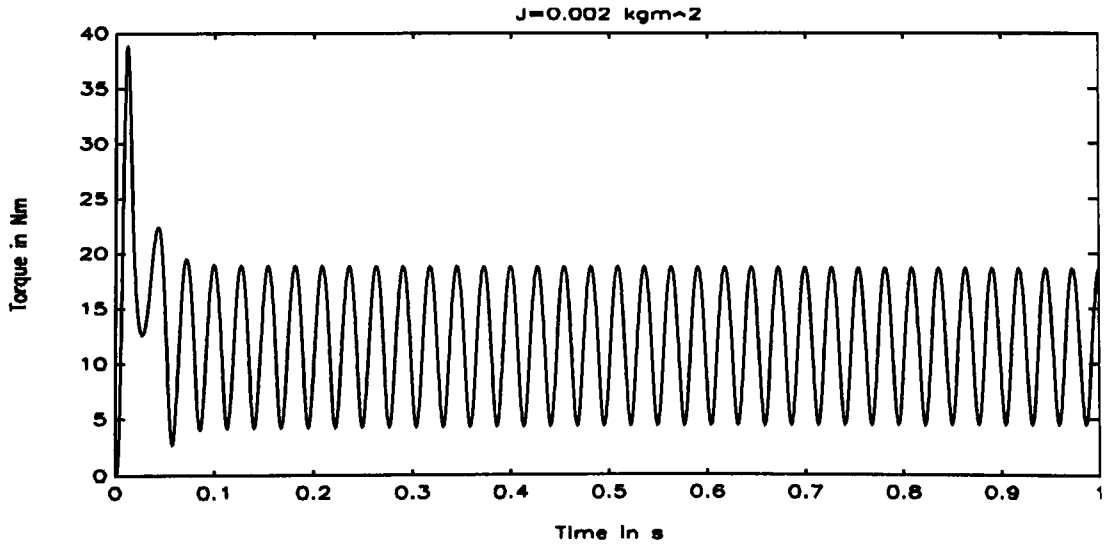

Fig. 64: Torque = 12 Nm

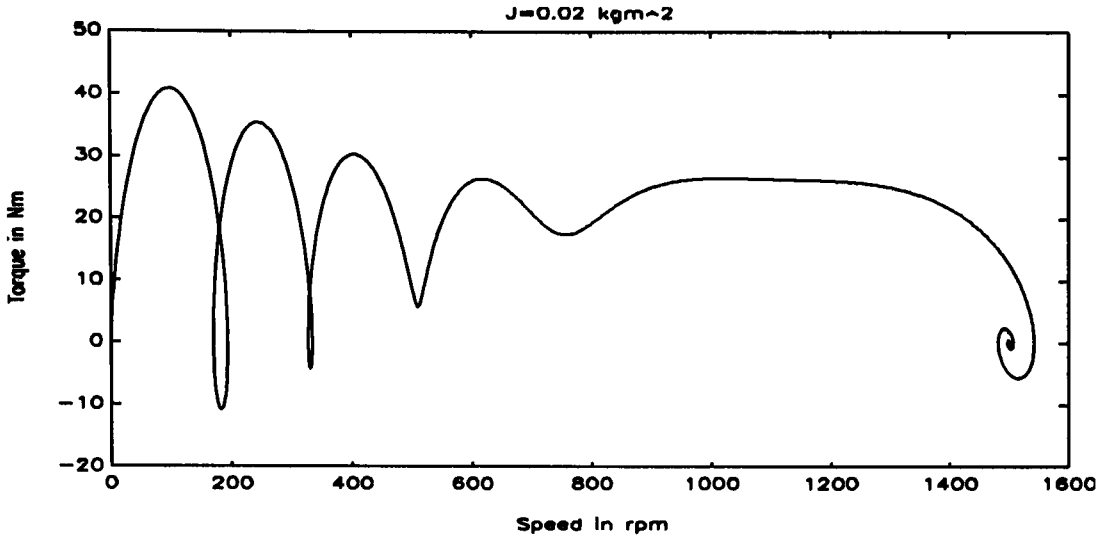

Fig. 65: Torque = 0 Nm

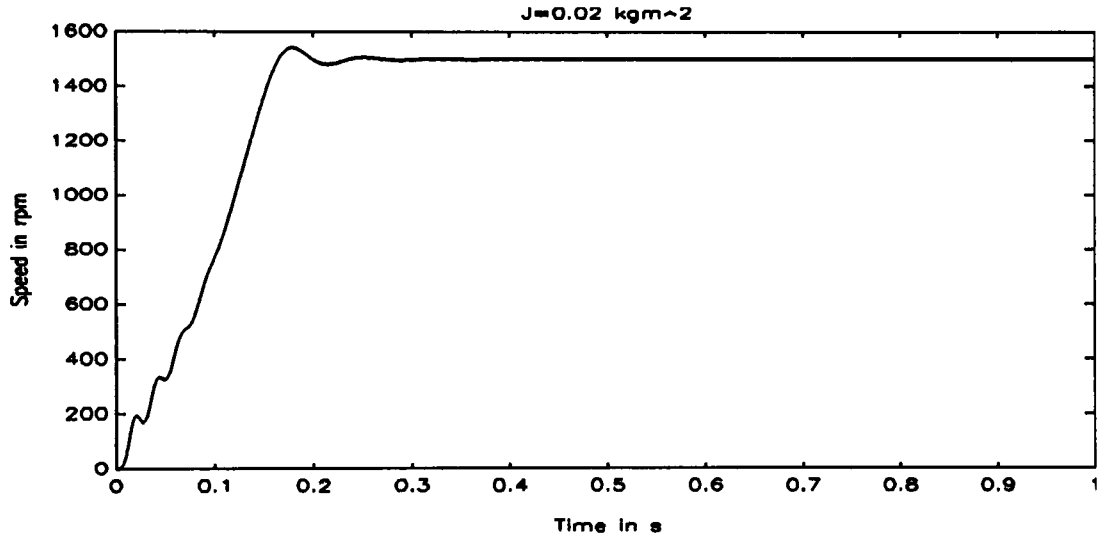

Fig. 66: Torque = 0 Nm

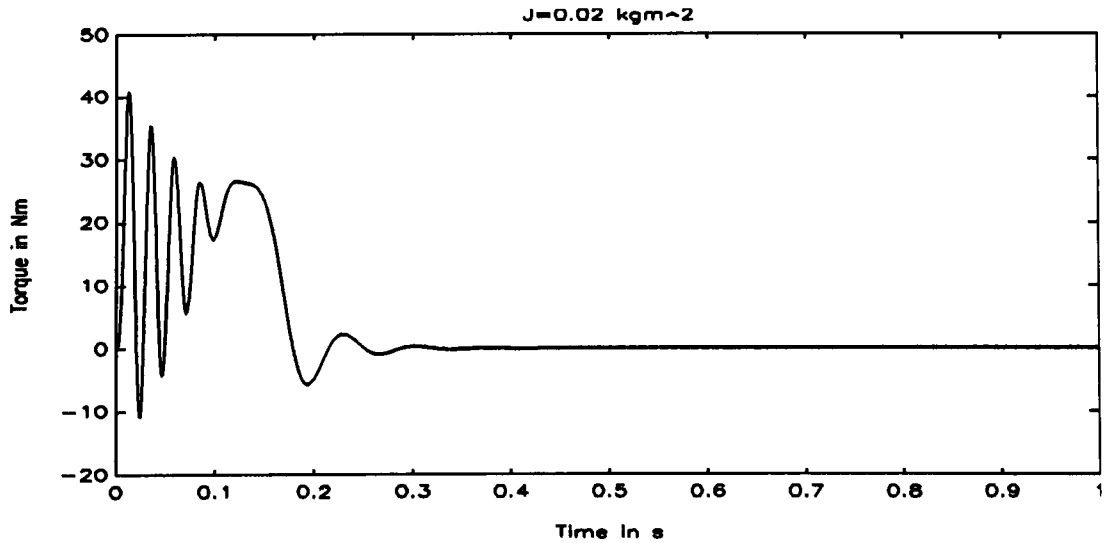

Fig. 67: Torque = 0 Nm

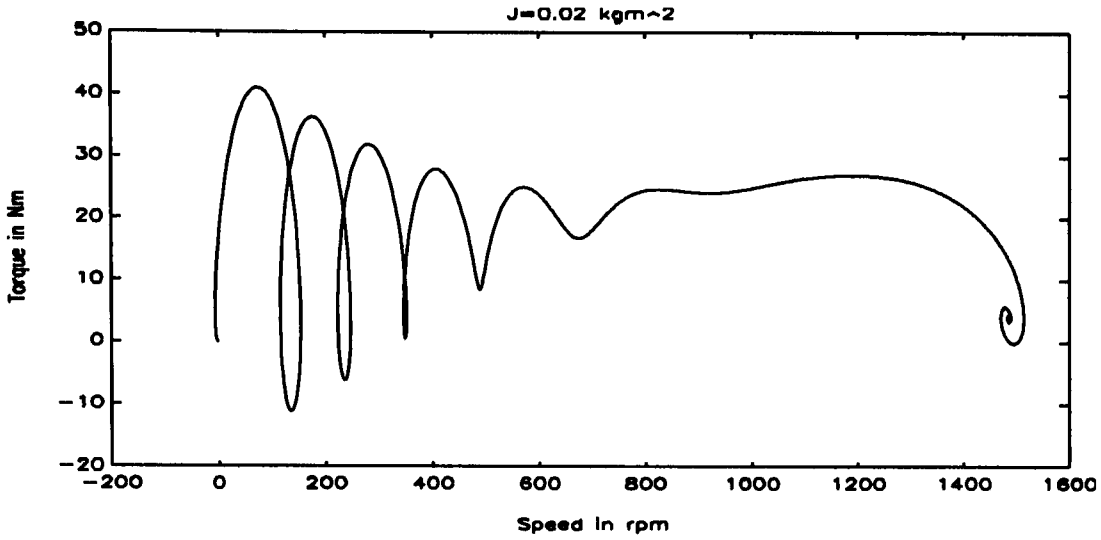

Fig. 68: Torque = 4 Nm

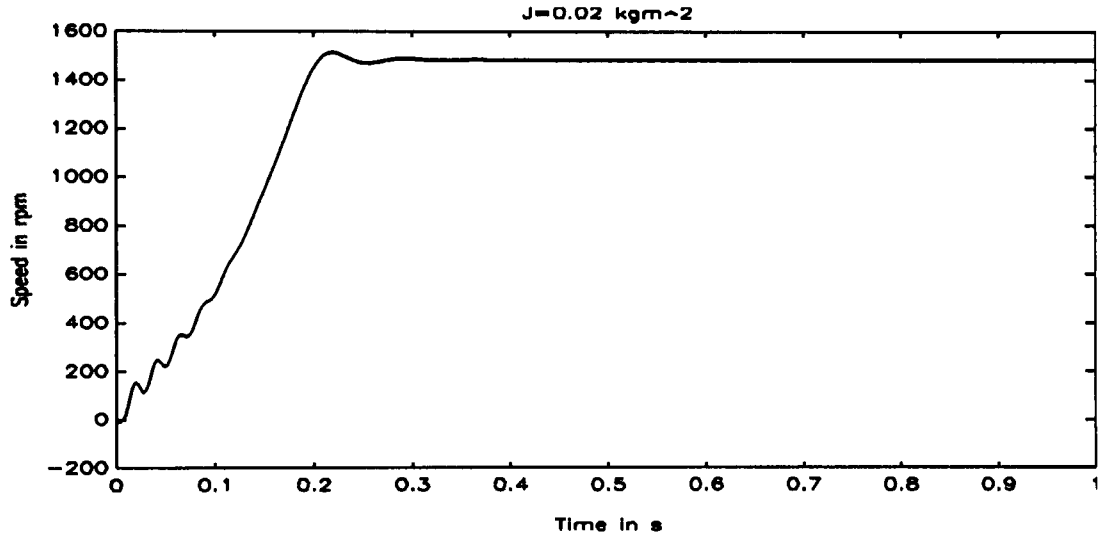

Fig. 69: Torque = 4 Nm

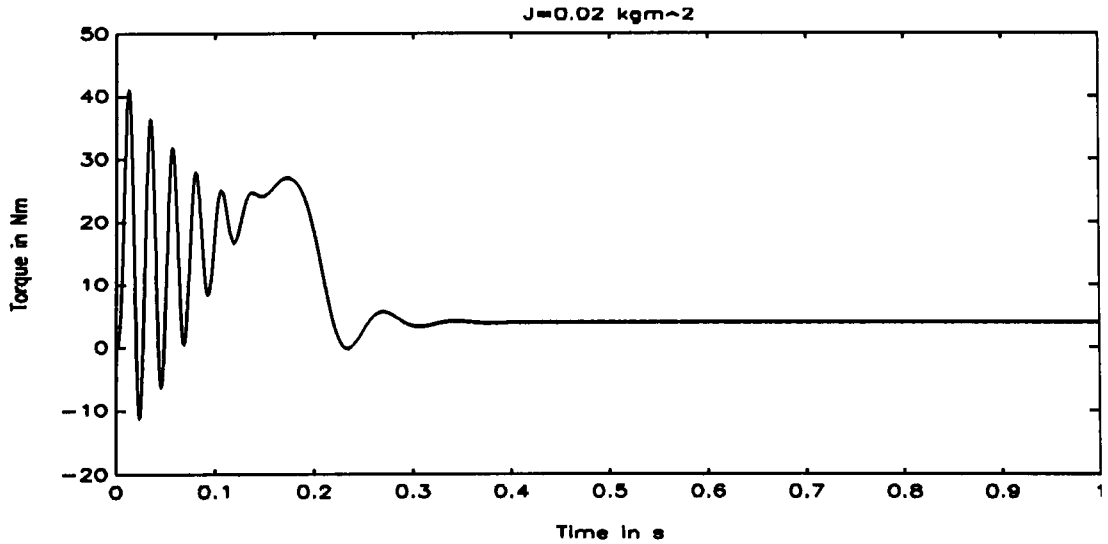

Fig. 70: Torque = 4 Nm

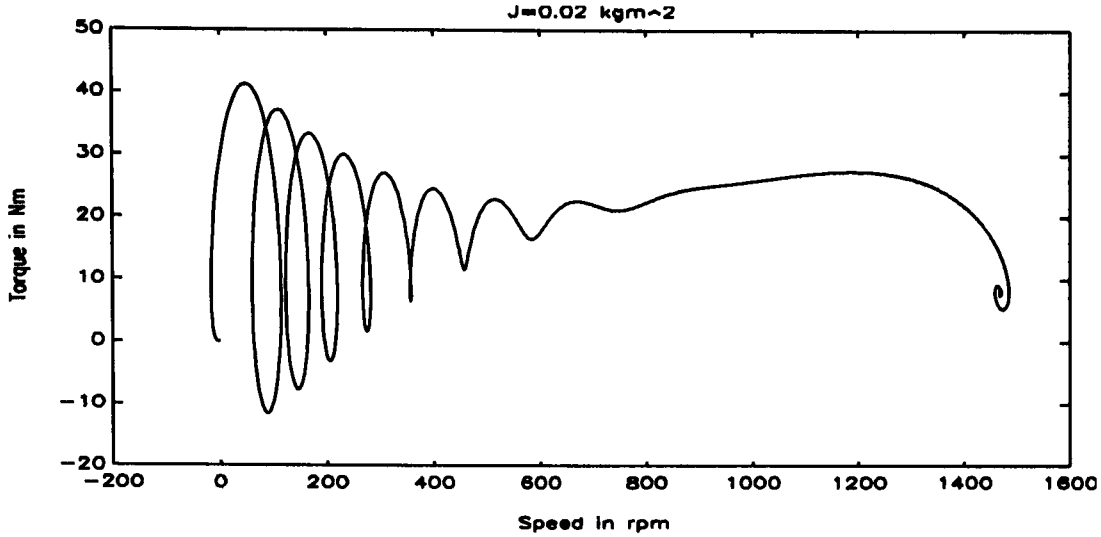

Fig. 71: Torque = 8 Nm

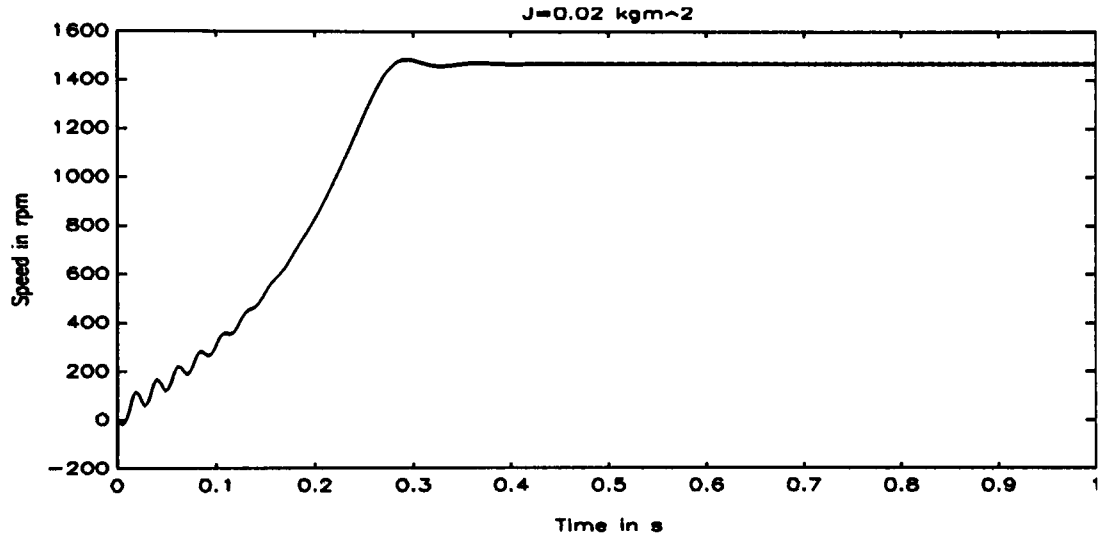

Fig. 72: Torque = 8 Nm

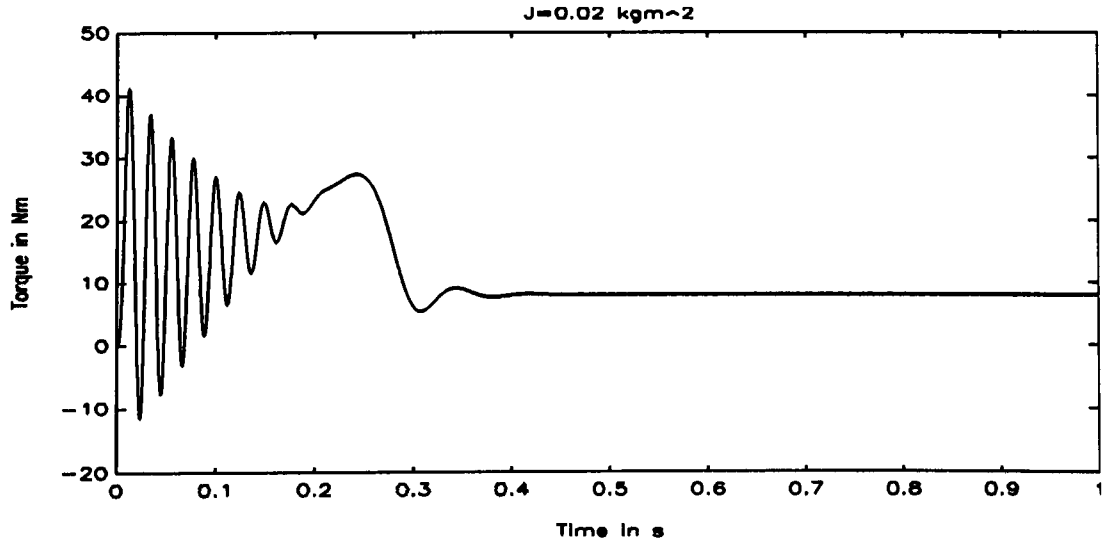

Fig. 73: Torque = 8 Nm

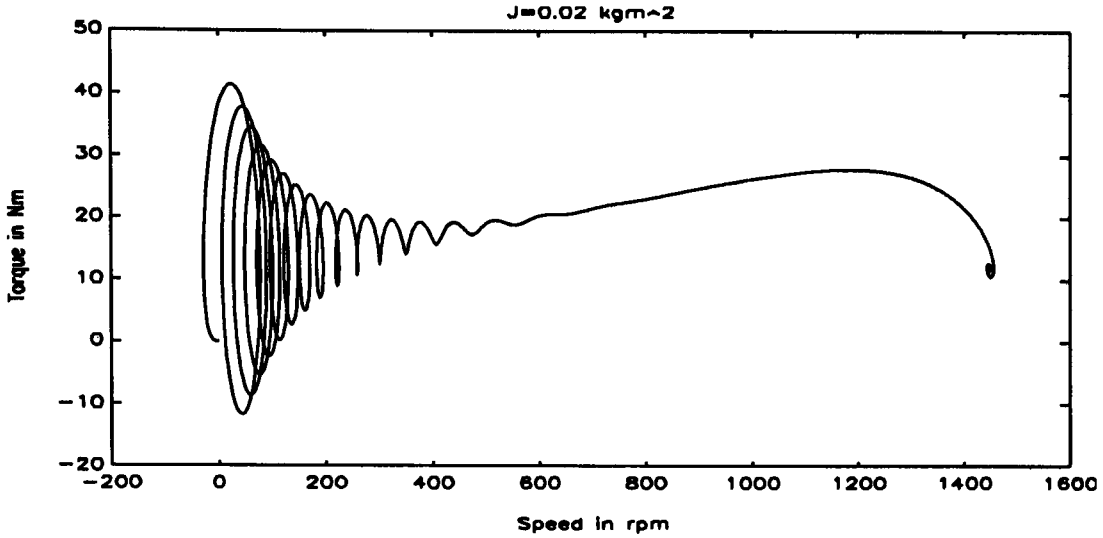

Fig. 74: Torque = 12 Nm

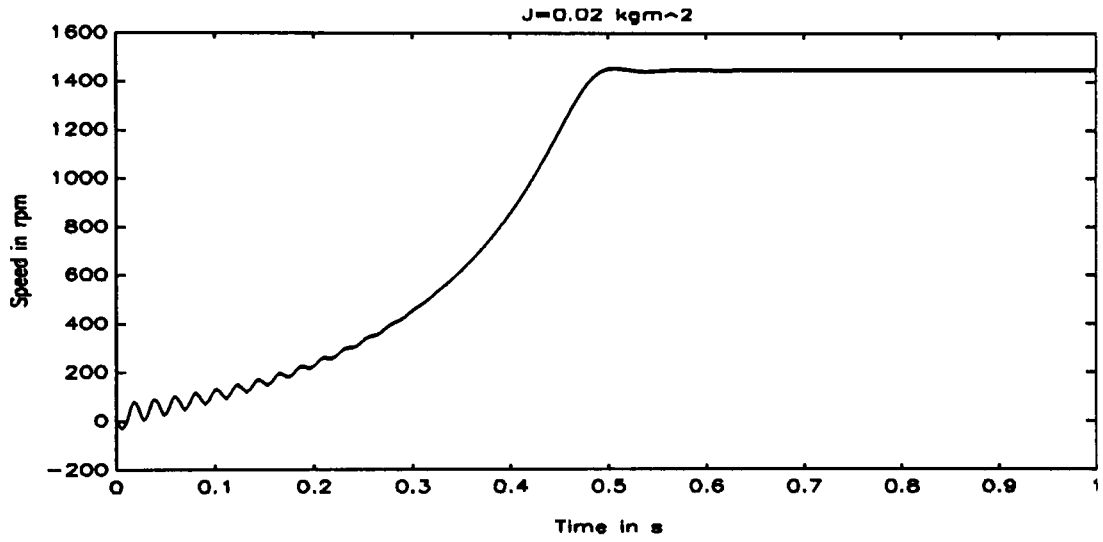

Fig. 75: Torque = 12 Nm

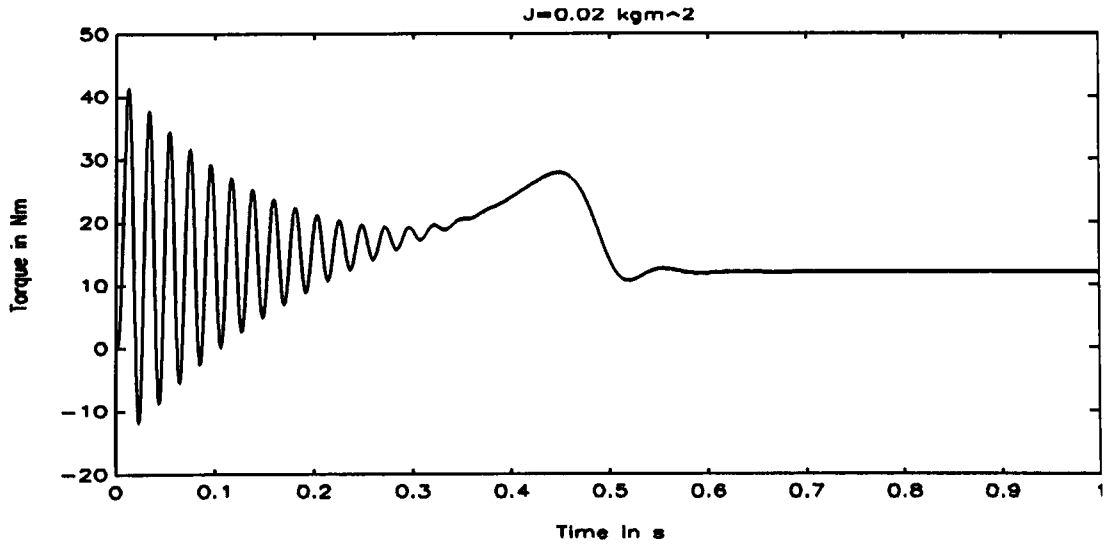

Fig. 76: Torque = 12 Nm

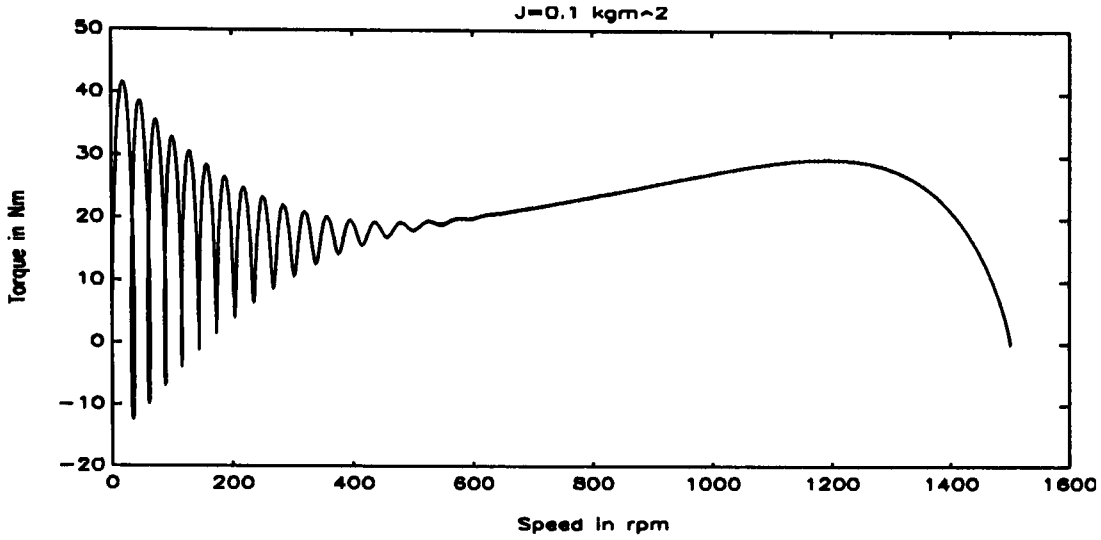

Fig. 77: Torque = 0 Nm

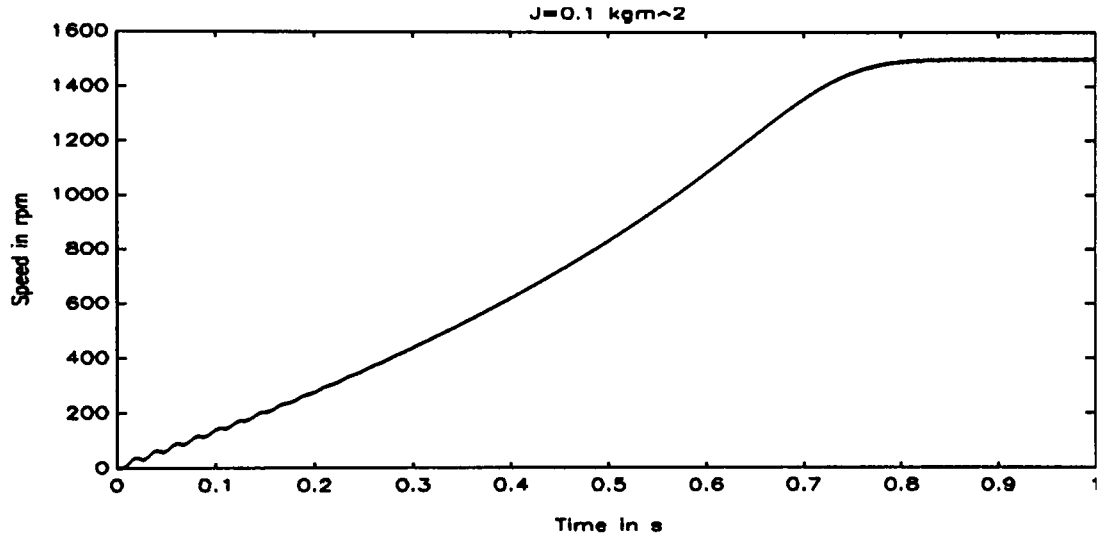

Fig. 78: Torque = 0 Nm

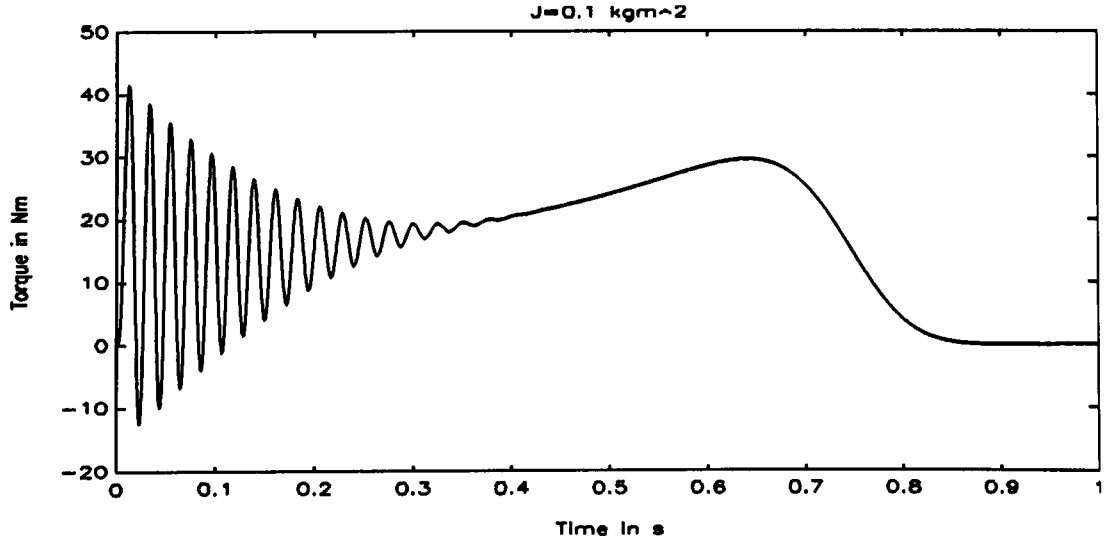

Fig. 79: Torque = 0 Nm

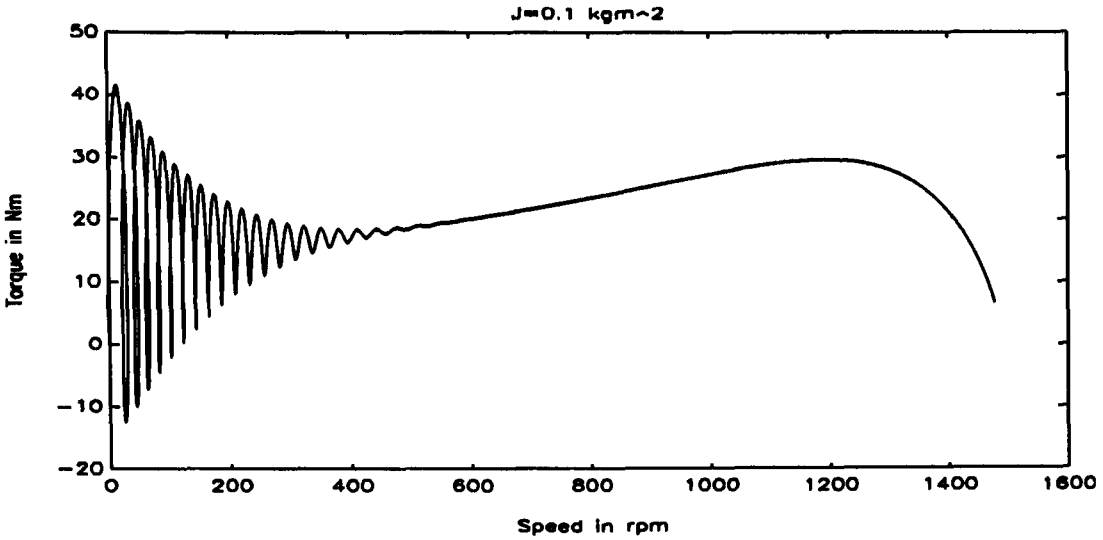

Fig. 80: Torque = 4 Nm

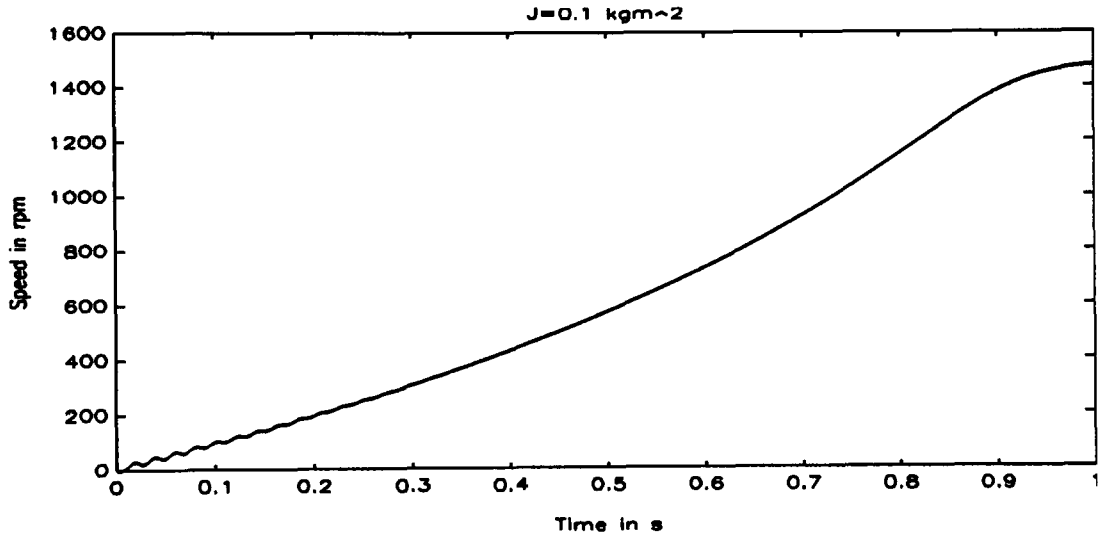

Fig. 81: Torque = 4 Nm

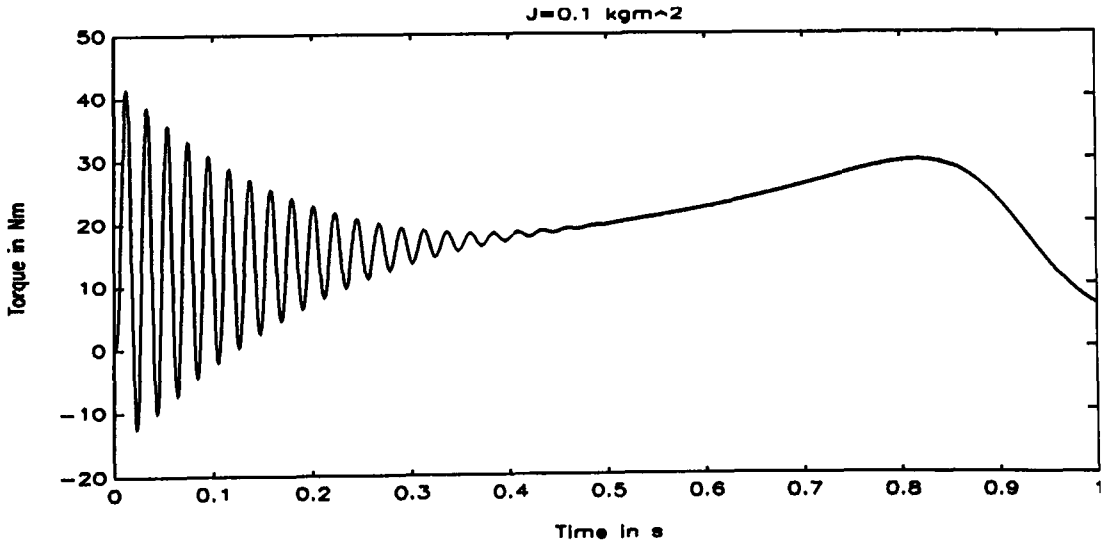

Fig. 82: Torque = 4 Nm

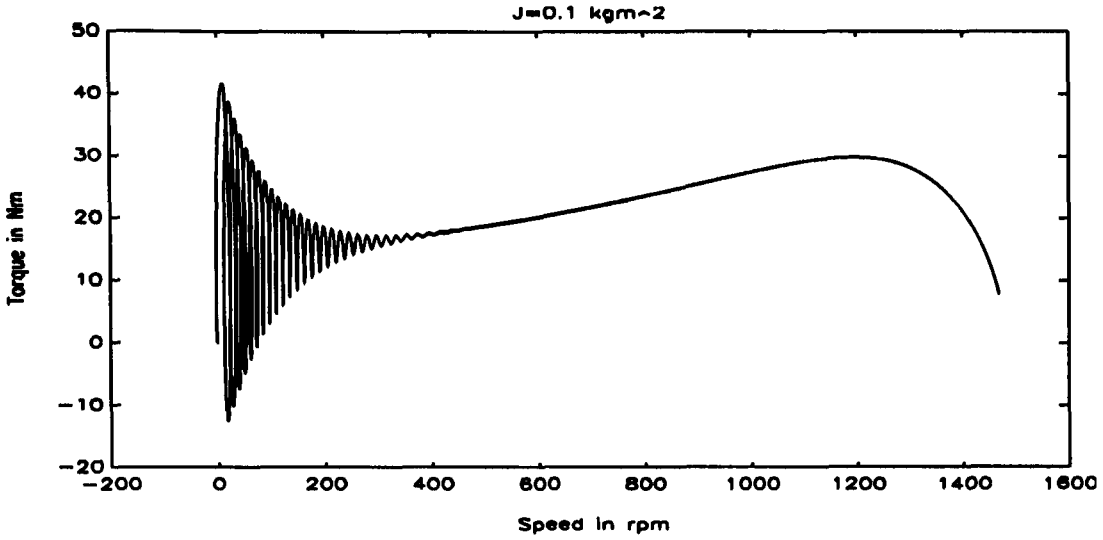

Fig. 83: Torque = 8 Nm

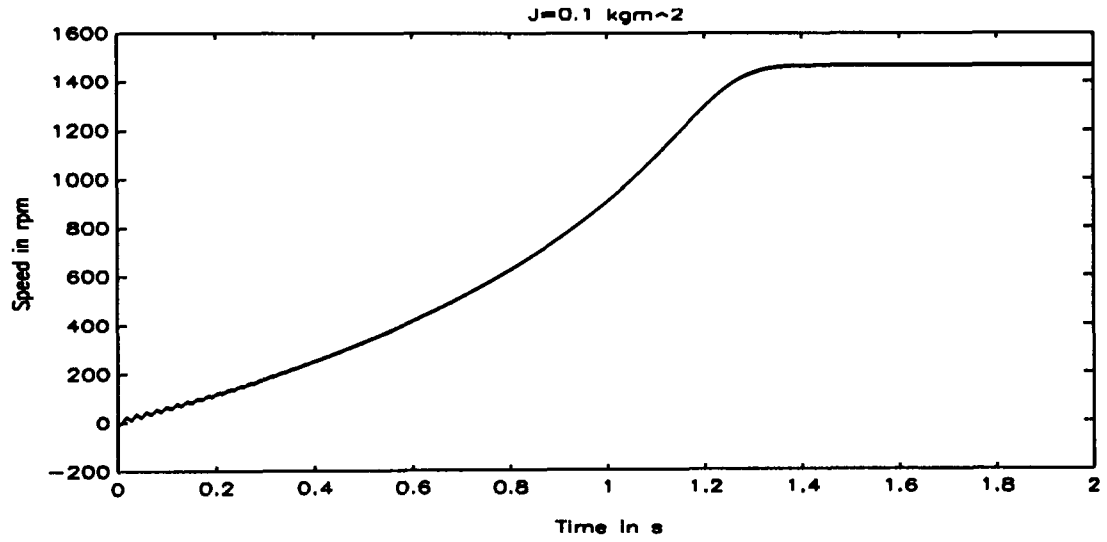

Fig. 84: Torque = 8 Nm

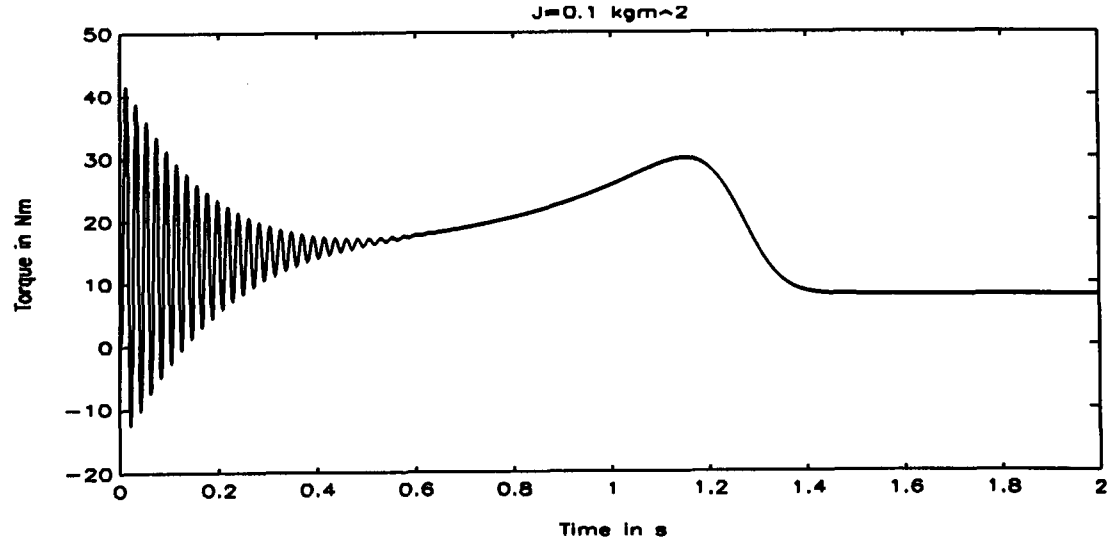

Fig. 85: Torque = 8 Nm

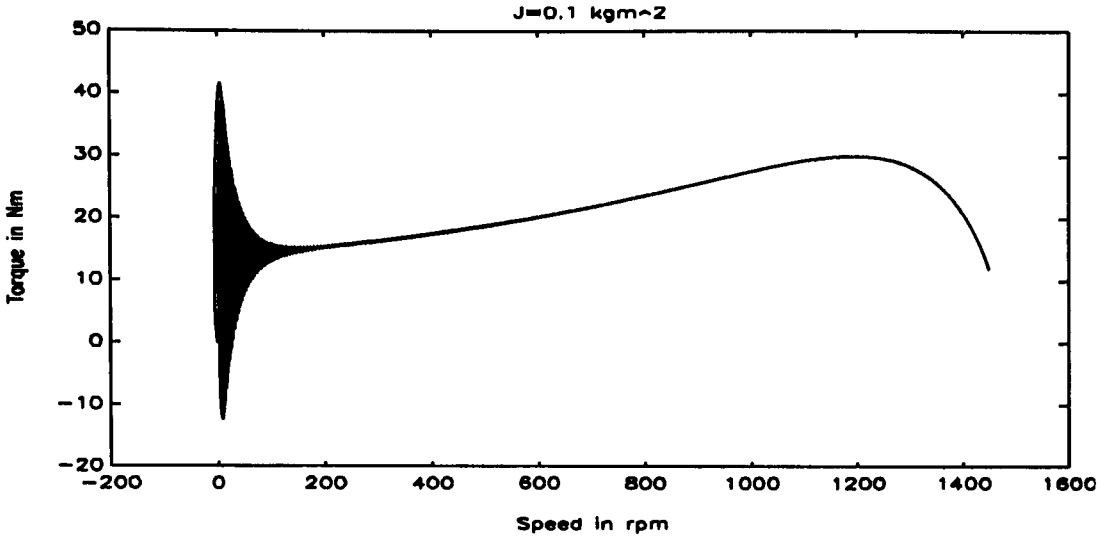

Fig. 86: Torque = 12 Nm

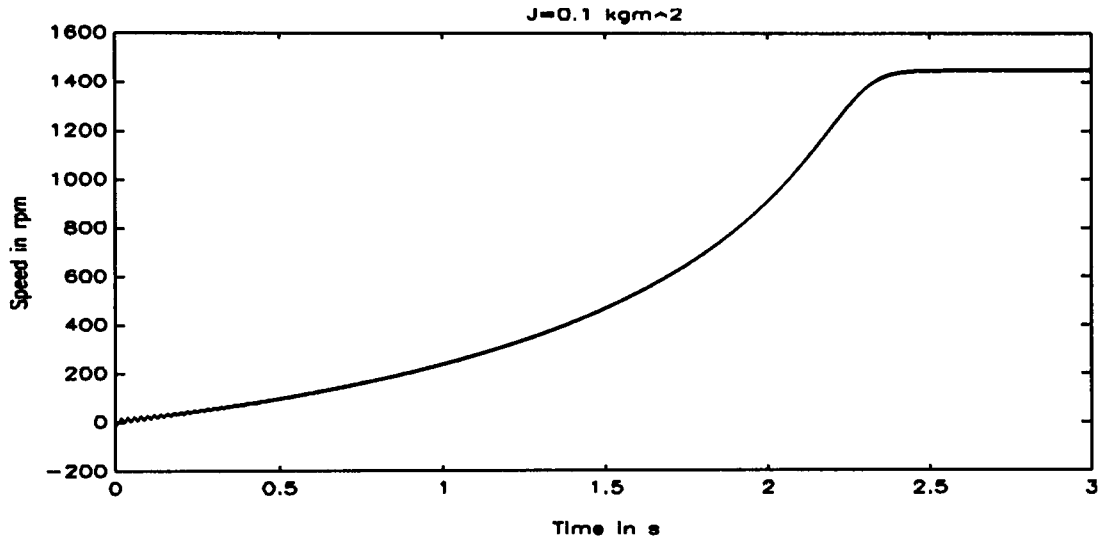

Fig. 87: Torque = 12 Nm

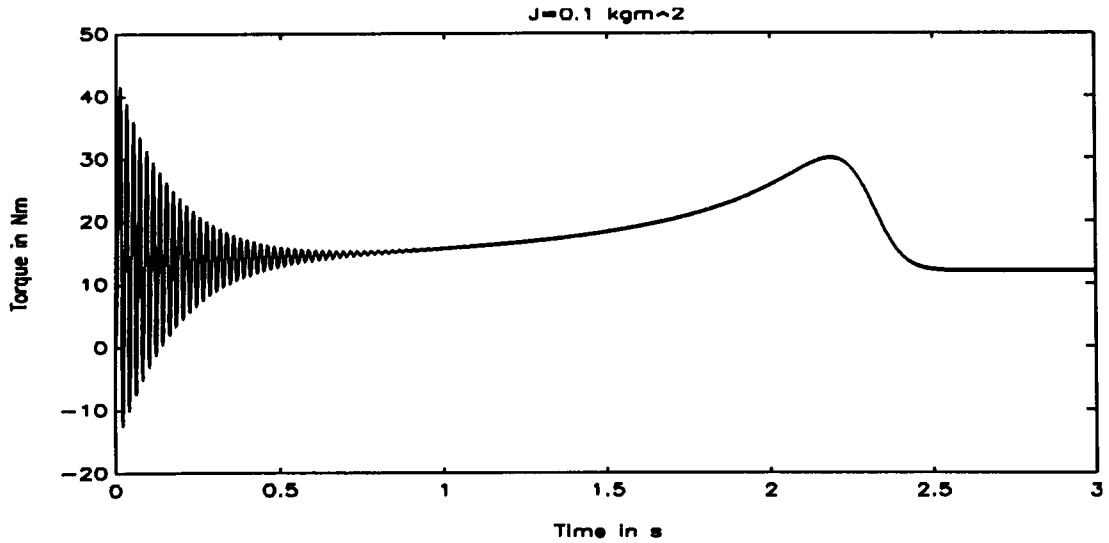

Fig. 88: Torque = 12 Nm

3.5. Simulation of PWM

The generation of regular sampled asymmetric PWM using MATLAB is illustrated in figure 89. This figure is also an example of the graphic capabilities of MATLAB, it is a screen dump plotted on a HP plotter with functions provided by the software. For this figure the sinusoidal modulating wave is generated first, then this wave is sampled in equidistant intervals corresponding to a half cycle of the carrier wave and this sample and hold process produces the sampled modulating wave. The carrier wave is then generated and the sampled modulating wave compared with it. The points of intersection between the sampled modulating wave and carrier wave are then the switching points for the PWM voltage waveform.

The inverter PWM voltage waveforms for all three phases are generated by the same process except that a 120° displacement is introduced into the modulating waveforms for each phase. The resulting PWM voltage waveforms are of course of the two level and correspond to the voltage between an outputline and the artificial neutral of the DC-supply as explained in figure 16. The PWM voltage waveforms between any two output lines of the converter can be determined from the difference between any two line to DC-neutral voltage waveforms, that is to say

$V_{ab} = V_{a0} - V_{b0}$
$V_{bc} = V_{b0} - V_{c0}$
$V_{ca} = V_{c0} - V_{a0}$.

The result of taking the difference between the two level PWM waveforms is a three level PWM voltage waveform. Similarly when the output to the converter is connected to a star connected load such as an induction motor then the line to load neutral voltage waveform can be determined from Miller's theorem and results in a 5 level PWM voltage waveform.

The results of the simulation of the voltages described above are illustrated in figures 90, 91 and 92 for Regular Sampled Asymmetric PWM with modulation index 1, frequency ratio 9 and modulating frequency 50 Hz. It is apparent from figure 90 that

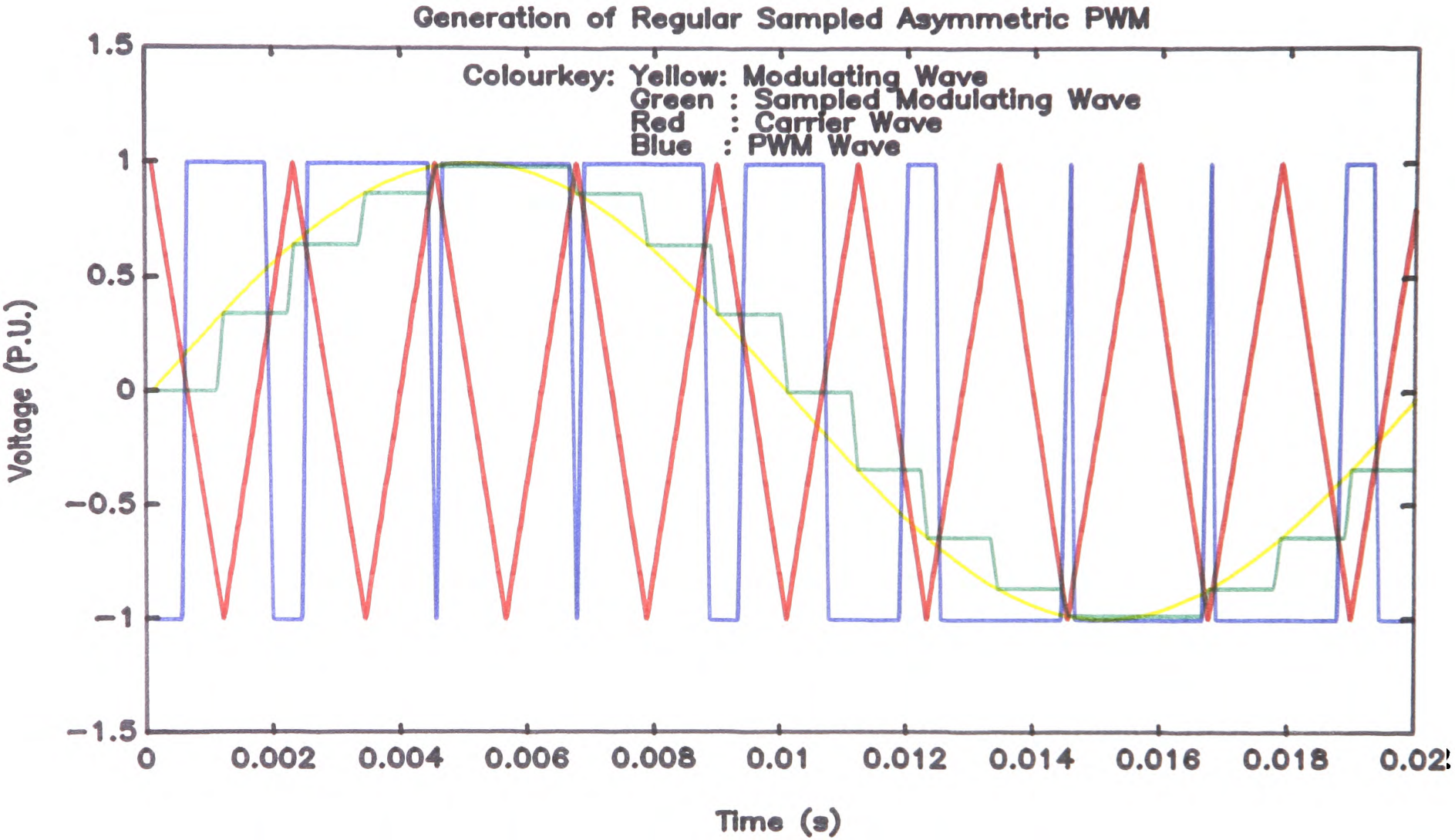

Fig. 89: MATLAB plot of generation of a PWM wave

the PWM waveform is two level whereas from figure 91 it can be seen that the line to line voltage is three level whereas the line to load neutral point voltage illustrated in figure 92 is a five level PWM waveform. The number of levels in a PWM voltage waveform along with the number of pulses in the waveform have a very significant bearing on the harmonic content of the waveform. It is therefore particularly important that an investigation is made into the harmonic content of the various PWM voltage waveforms existing in a three phase three wire star connected system. It is to this aspect of the investigation that the following section is devoted.

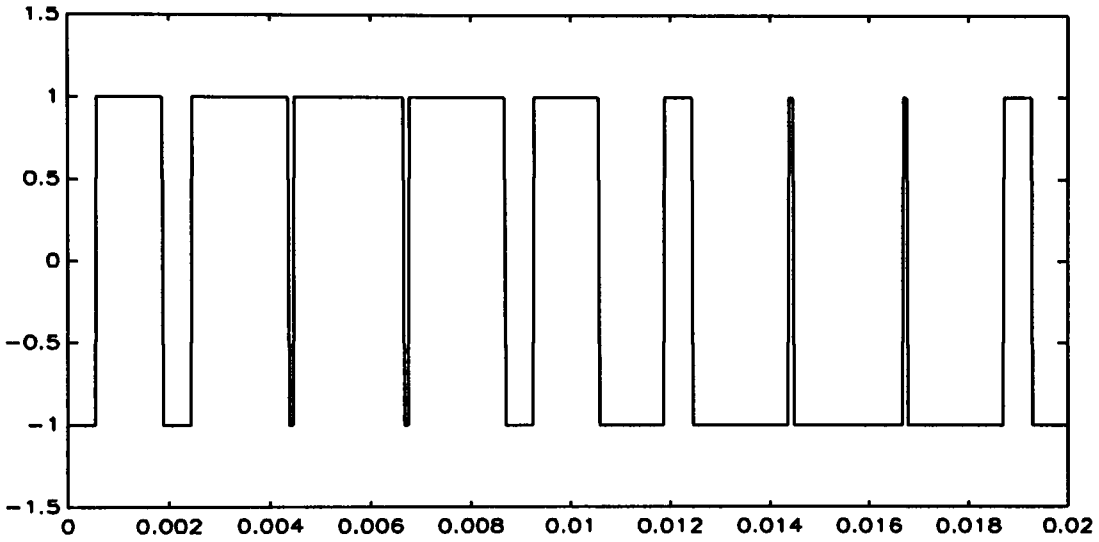

Fig. 90: The PWM voltage wave of Phase A, V_{a0}

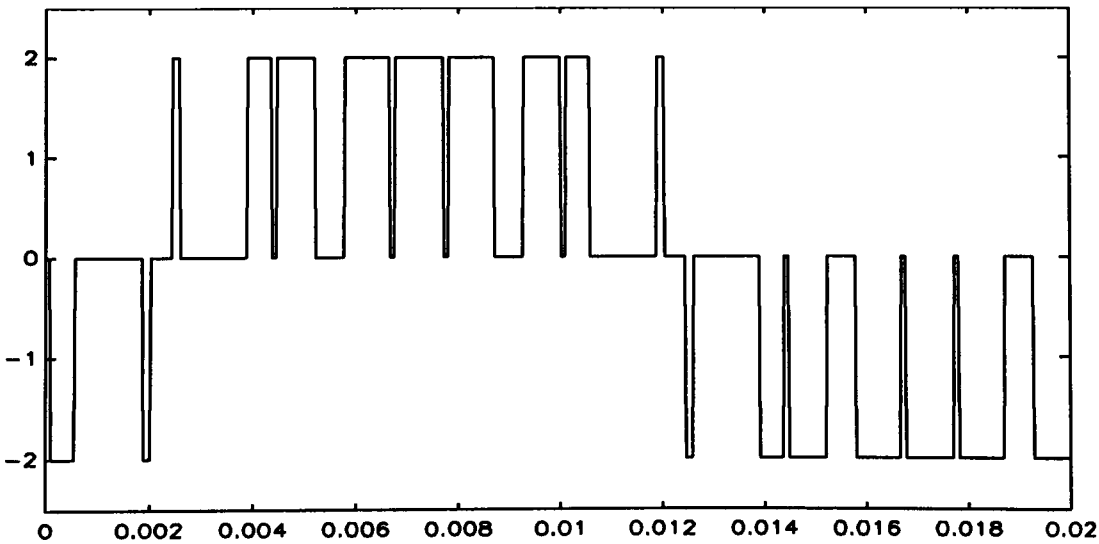

Fig. 91: Line to line voltage, V_{ab}

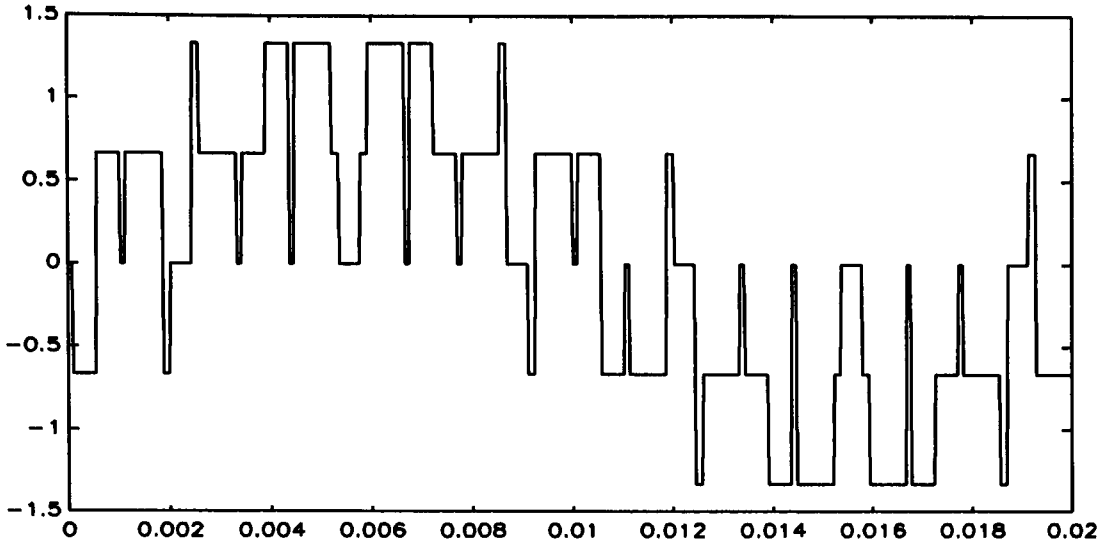

Fig. 92: Line to starpoint voltage, V_{aN}

3.6. Fourier Analysis

In this step the harmonic analysis of the PWM voltage waveform is performed. The voltage waveform under investigation was the line to artificial DC-link two level voltage. In the following figures examples for these results of the harmonic content of the PWM voltage waveforms are shown. More figures supporting the conclusion drawn can be obtained in the appendix.

Figure 93 shows the harmonic spectrum of a regular sampled symmetric PWM voltage waveform at frequency ratio R=9. In comparison the harmonic spectrum of a regular sampled asymmetric PWM voltage waveform is shown in figure 94. The difference in harmonics contents between both waveforms is self evident. The result of this comparison shows the superiority of asymmetric PWM over symmetric PWM, lending asymmetric PWM to be the preferred generation process to be used.

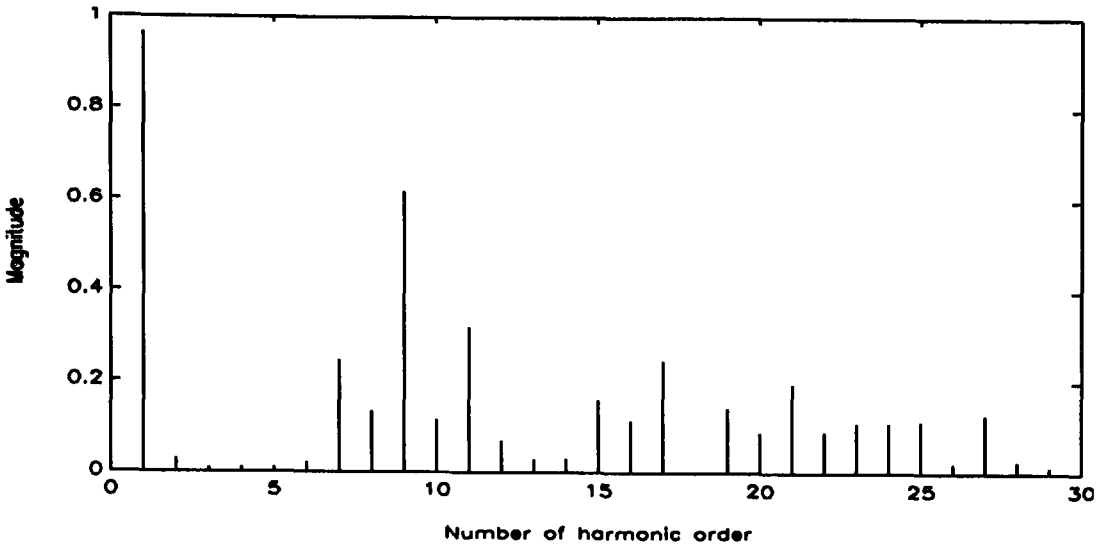

Fig. 93: FFT of Va0, symmetric PWM with R=9

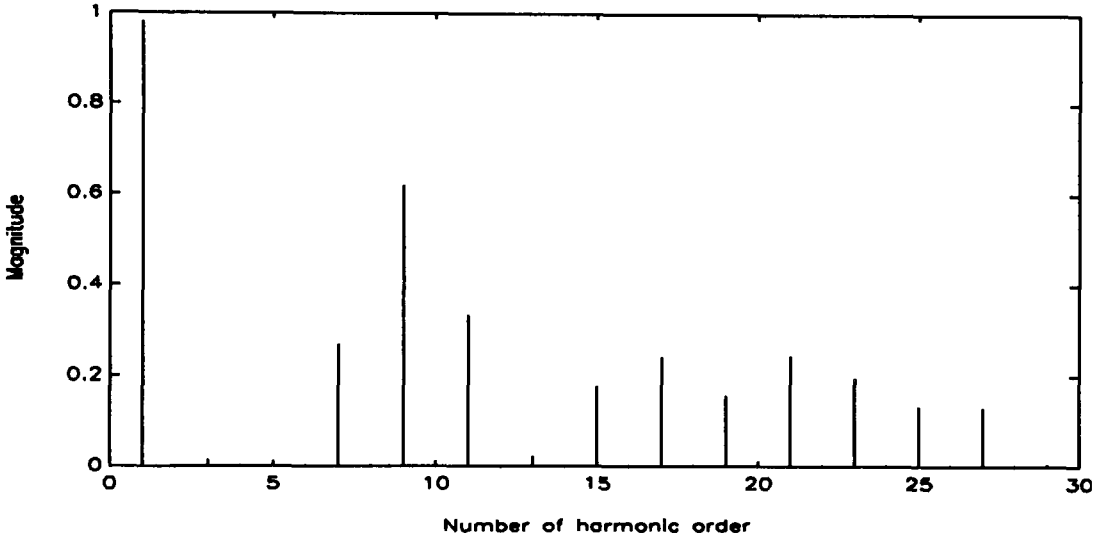

Fig. 94: FFT of Va0, asymmetric PWM with R=9

In figures 95 and 96 the harmonic spectrum of regular sampled asymmetric PWM with frequency ratios R=8 and R=10 are shown. Comparing these to figure 94 it can bee seen that regular sampled asymmetric PWM with triplen frequency ratios contains less harmonic components then the one with non triplen frequency ratios. Figure 97 shows the harmonic spectrum of the three level line to line voltage for regular sampled asymmetric PWM at frequency ratio R=9. In comparison to figure 94 it can be seen that triplen harmonics being present in the line to DC-link neutral point waveform are eliminated in the line to line voltage. The shifting of the harmonic spectrum to higher frequencies for higher frequency ratios can be seen from figure 98.

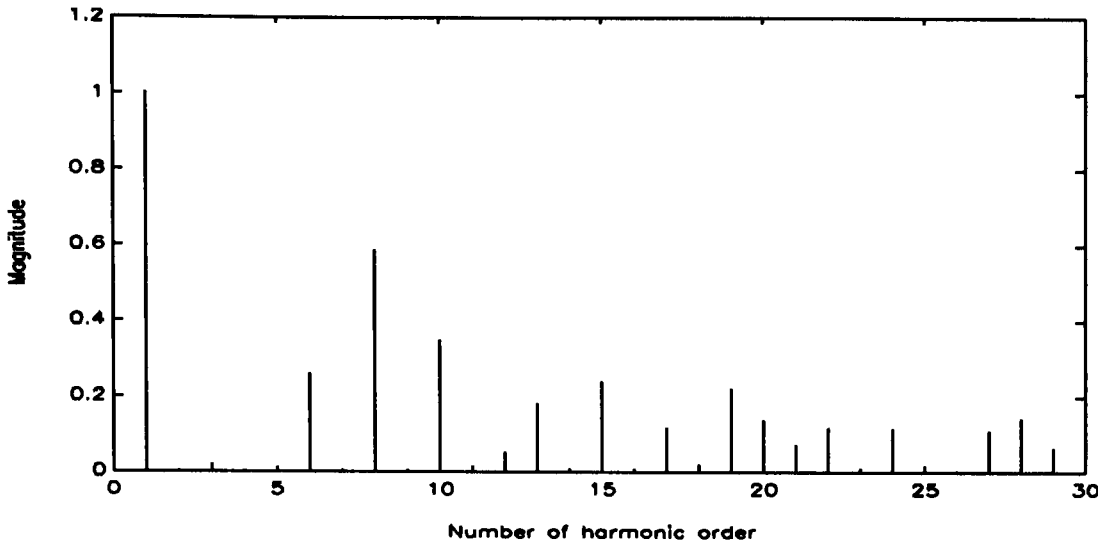

Fig. 95: FFT of Va0, asymmetric PWM with R=8

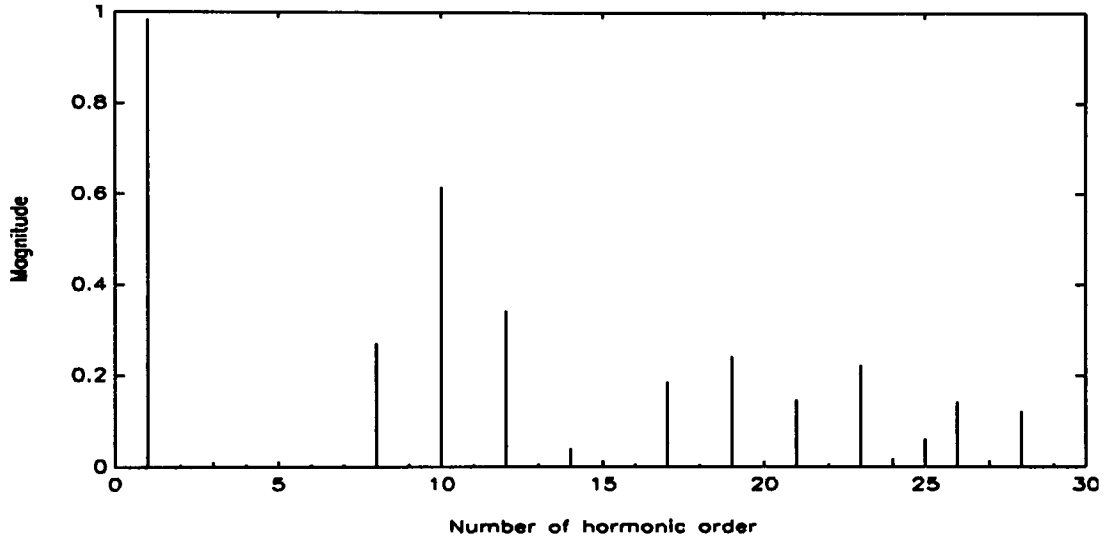

Fig. 96: FFT of Va0, asymmetric PWM with R=10

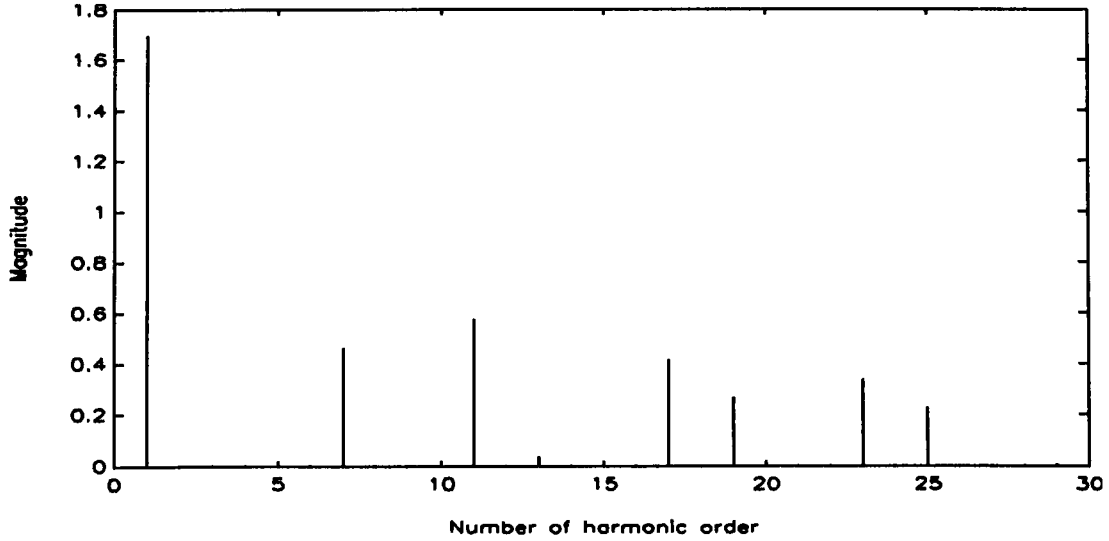

Fig. 97: FFT of line to line PWM with R=9

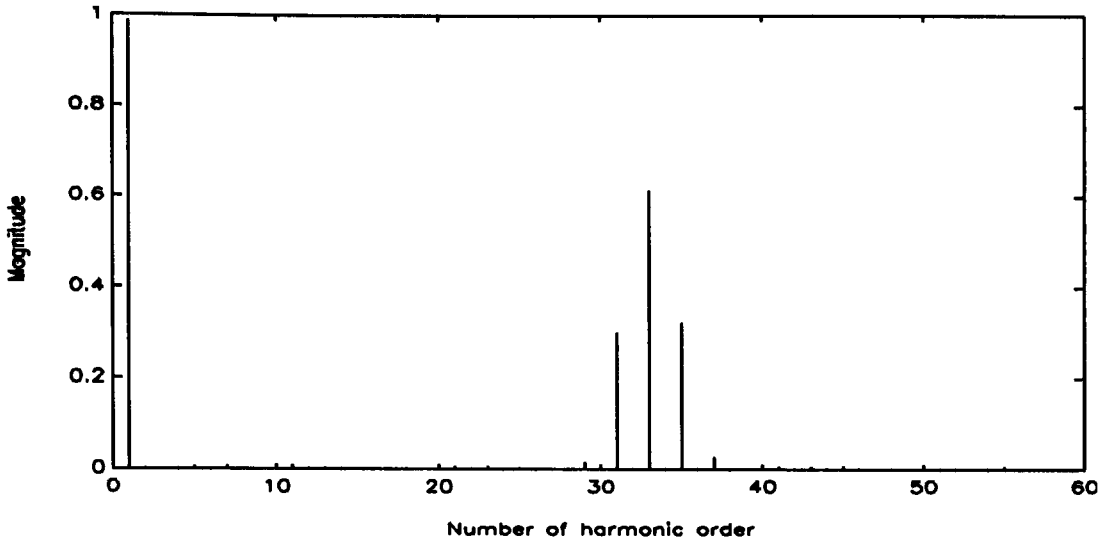

Fig. 98: FFT of Va0, asymmetric PWM with R=33

3.7. Simulation of the motor operating in steady state condition

In this section the simulation results for a motor operating in steady state condition are presented. This simulation uses the mathematical solution for the state space equation as described in chapter 2. In the first step of simulation the voltage waveforms of a 3 phase inverter using the Regular Sampled Asymmetric PWM strategy were generated for one modulation cycle. The modulation index is 1, the frequency ratio is 9 and the modulating frequency is 50 Hz. The three line to line voltages resulting from this simulation are illustrated in figure 99.

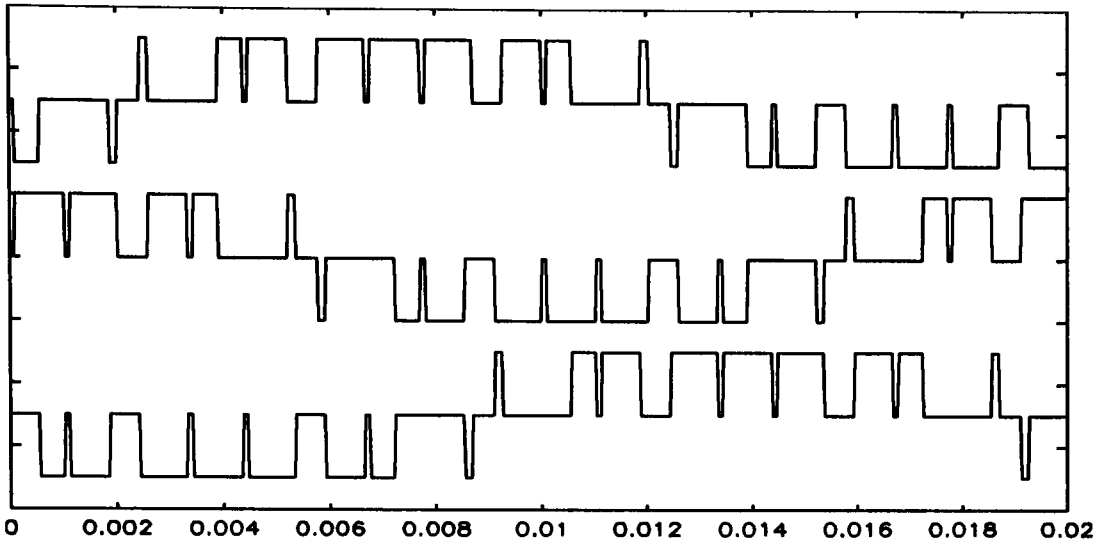

Fig. 99: The three line to line voltages

These voltage waveforms were then transformed to the d-q frame of reference. The thus resulting voltages waveforms V_{ds} and V_{qs} are illustrated in figure 100 and 101 respectively. The simulation then produces the currents in d-q frame of reference and these stator currents I_{ds} and I_{qs} are shown in the same figures as the voltages.

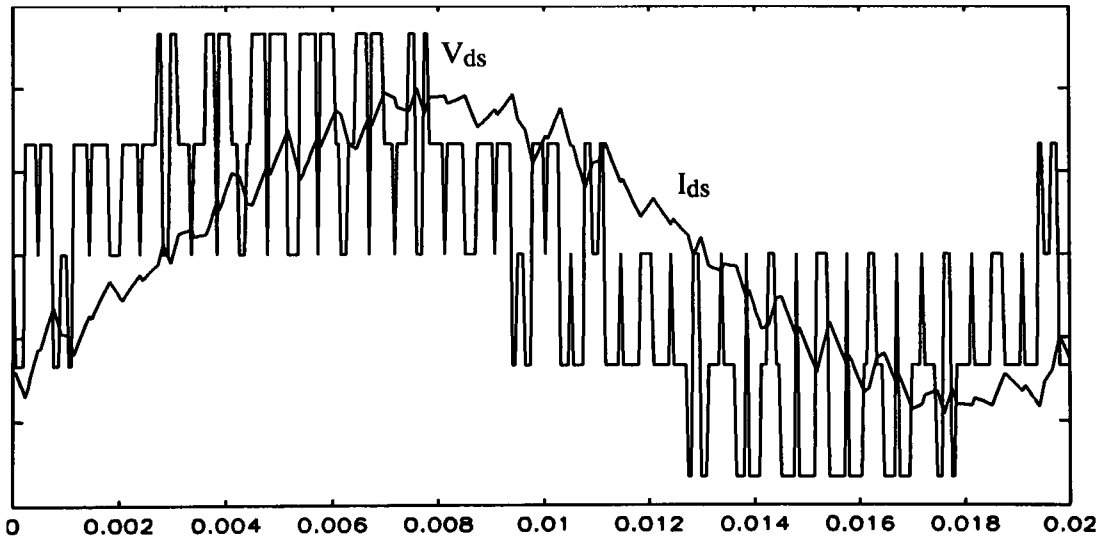

Fig. 100: Direct axis stator voltage and current

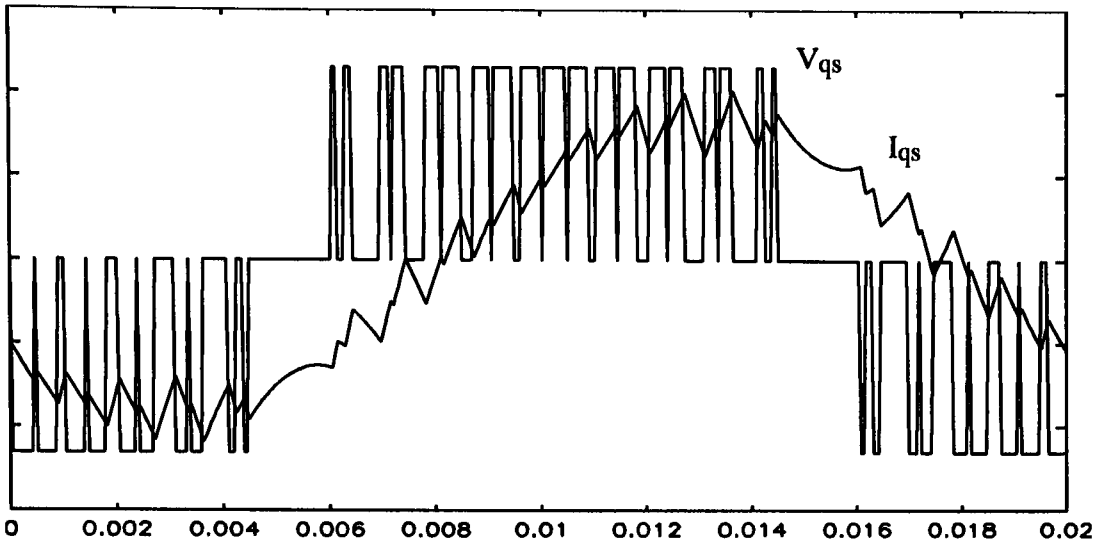

Fig. 101: Quadrature axis stator voltage and current

Another way of displaying these currents is in the form of the current trajectory as shown in figure 102, where the d values of the current are plotted against the q values. Transforming the results from the d-q frame of reference to the a-b-c frame of reference produces the stator currents of which the stator current of phase A is shown in figure 103. Attention is drawn to the similarity of these results shown in figures 102 and 103 to the results presented in paper 2.2.2.14. However it should be noticed, that in this paper regular sampled symmetric PWM was used.

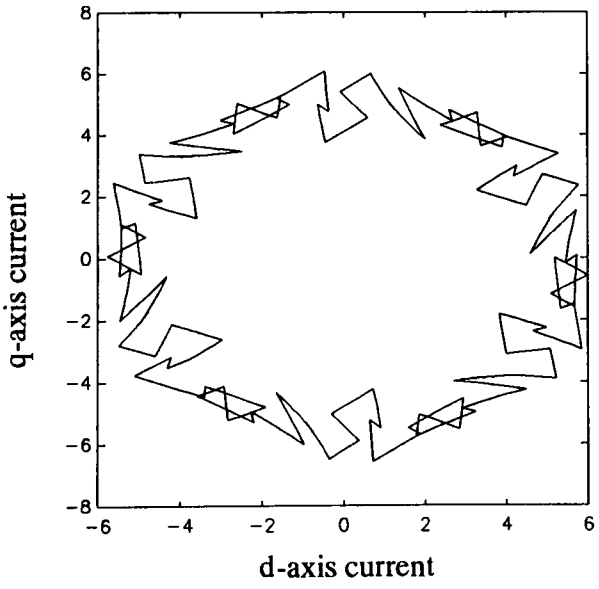

Fig. 102: The steady state stator current trajectory

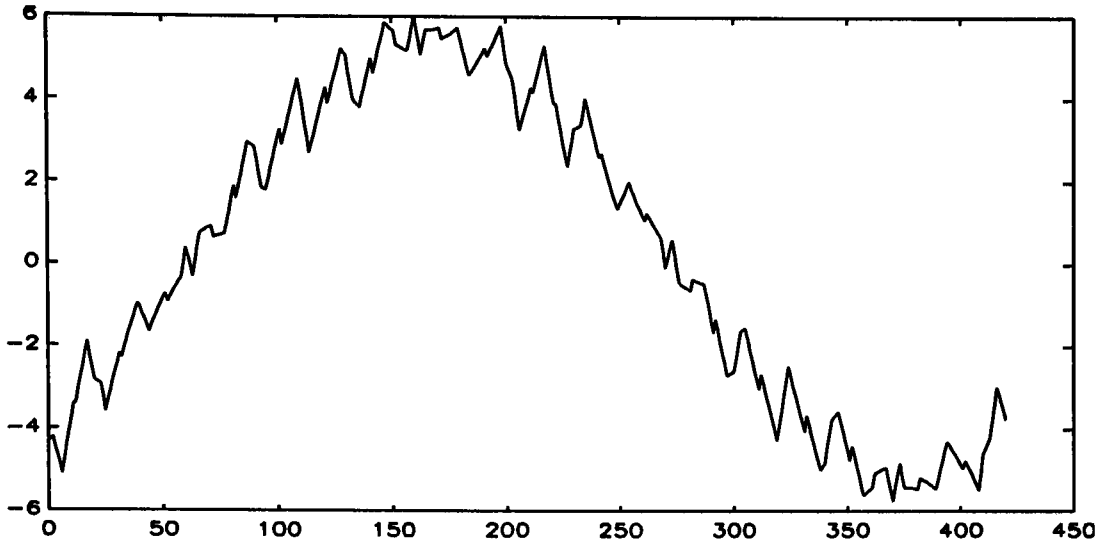

Fig. 103: The steady state phase A current

The flux was also obtained from this simulation the importance of which will be shown in the next chapter.

3.8. Flux Trajectory

In this section the motor stator flux when represented in d-q frame of reference is illustrated. For figures 104-109 the flux direct axis component, Ψ_{ds}, of the flux on the x-axis is plotted versus the quadrature axis component, Ψ_{qs}, on the y-axis. Figure 109 shows the flux trajectory for a sine wave. This trajectory of course is a perfect circle which is what is required to make the motor run smoothly. In figure 104 the flux trajectory is shown for a square wave. This is a polygon and every thing else but round. With this type of supply the motor produces an oscillating torque. In figures 105, 106, 107 and 108 the flux trajectories for regular sampled asymmetric PWM are shown with increasing frequency ratios from 6 to 72. For low triplen values the flux trajectory looks like a low order polygon, similar to the case of the square wave. By increasing the frequency ratio, the flux trajectory becomes more and more circular. It can be seen that low even triplen harmonics have a distortion of the hexagon form, producing a form that is even more removed from the circle and subsequently disadvantageous.

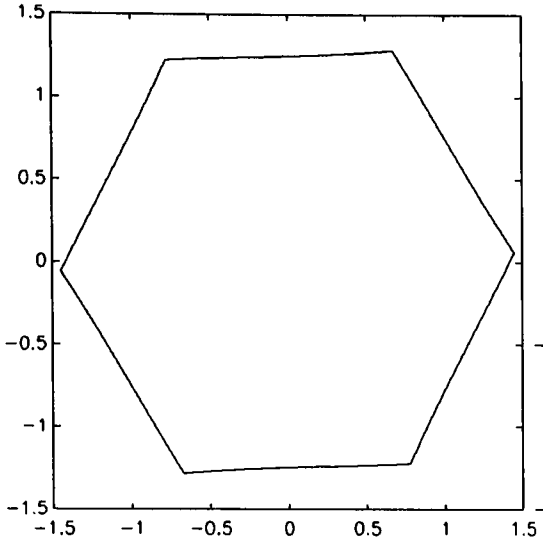

Fig. 104: Square wave

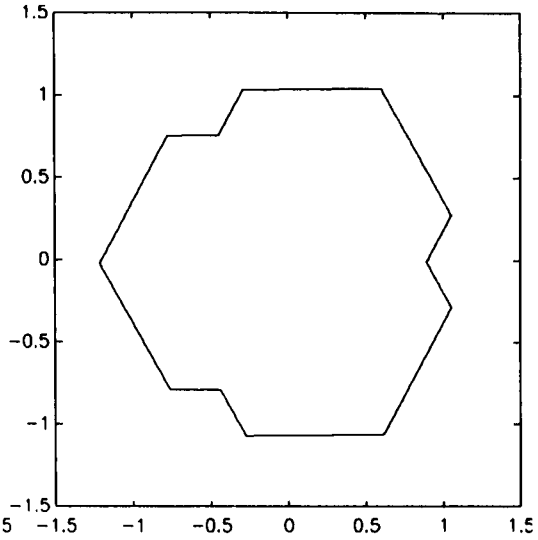

Fig. 105: Frequency ratio = 6

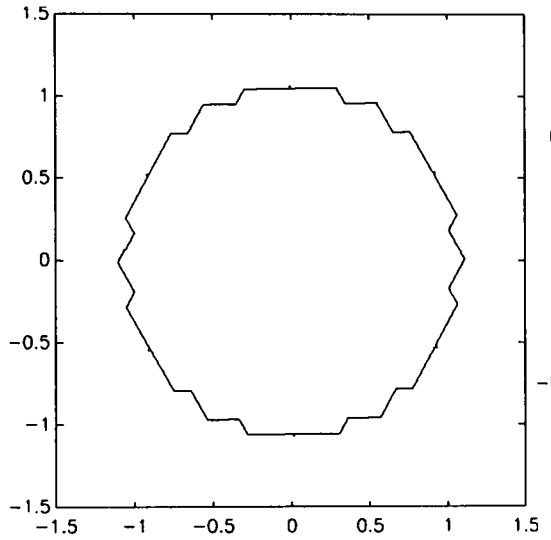

Fig. 106: Frequency ratio = 21

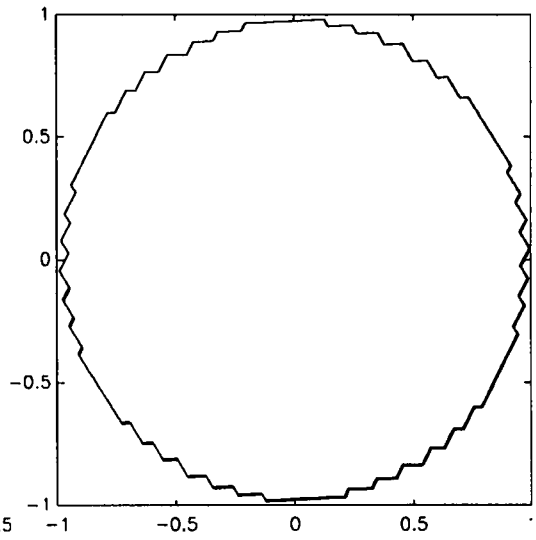

Fig. 107: Frequency ratio = 51

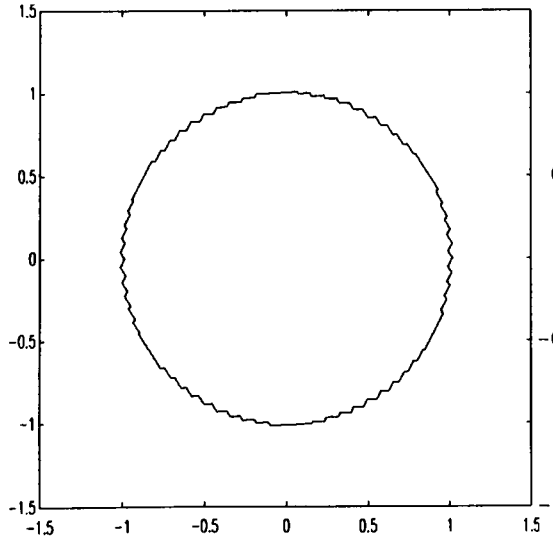

Fig. 108: Frequency ratio 72

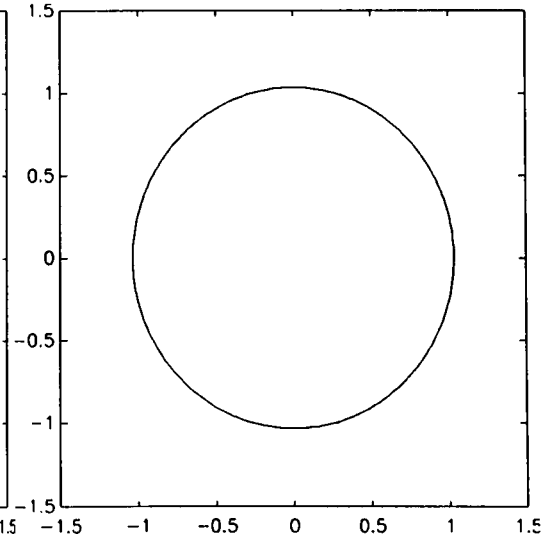

Fig. 109: Sine wave

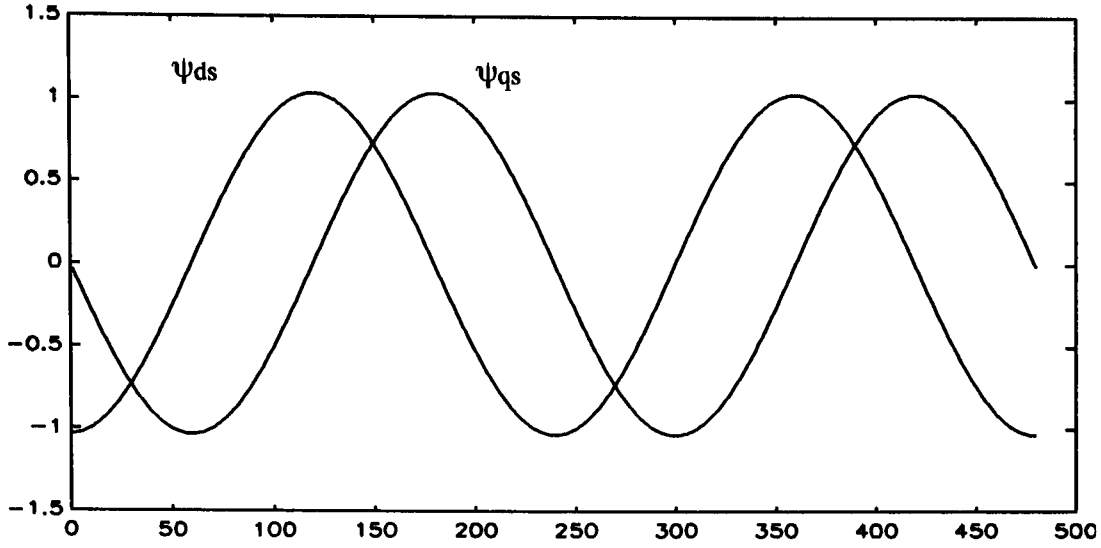

Fig. 110: Sine wave

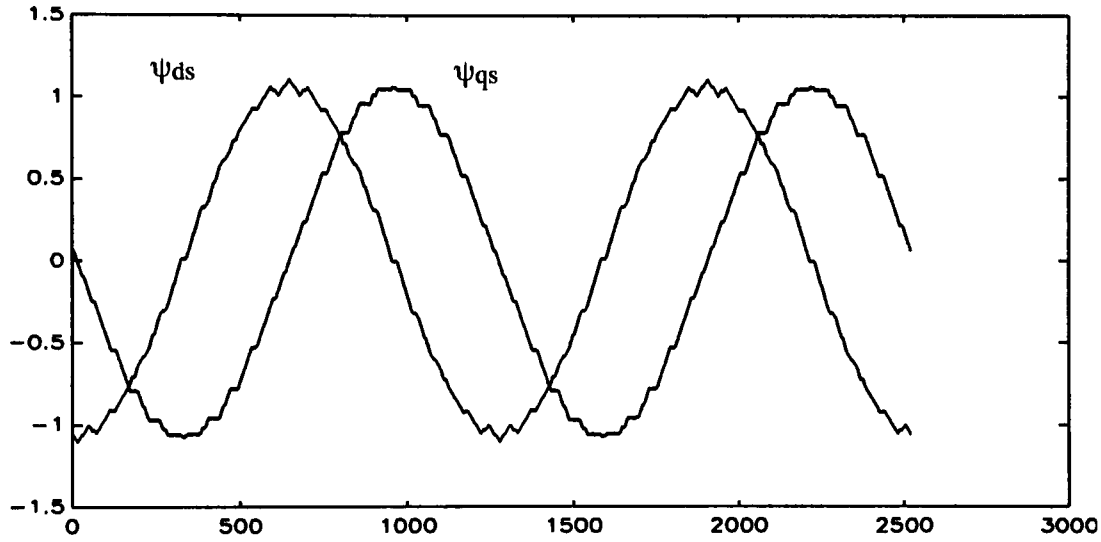

Fig. 111: Frequency ratio 21

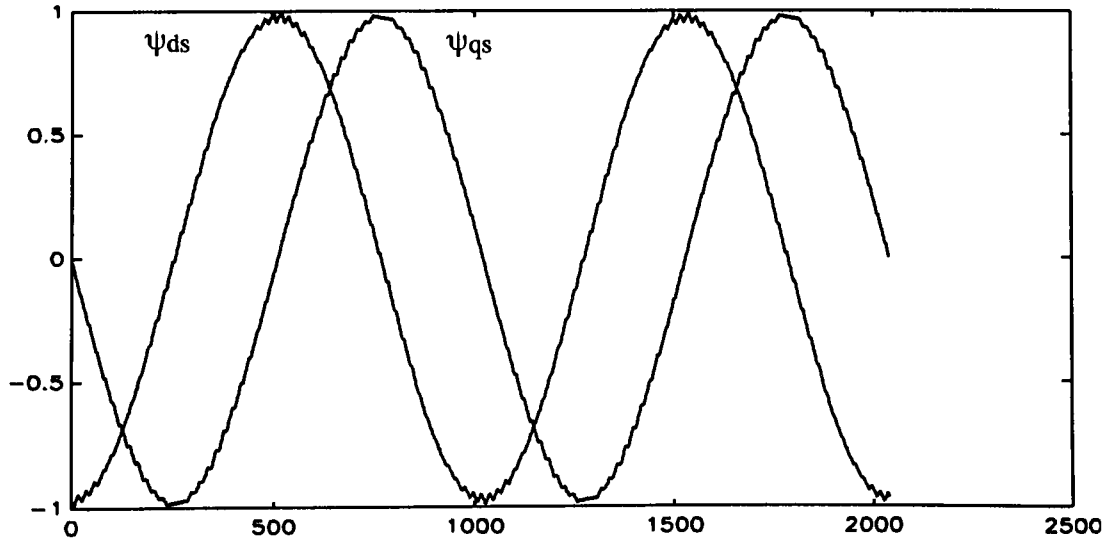

Fig. 112: Frequency ratio 51

The direct and quadrature fluxes corresponding to figures 109, 106 and 107 are illustrated versus time in figures 110, 111 and 112 respectively.

3.9. Simulation of Direct on-line start-up with PWM supply

The simulation result of a direct on-line start-up of the motor when supplied by a variable voltage variable frequency inverter are illustrated in this section. For reason of comparison with the results shown in the section for sinusoidal supply two values of inertia were chosen. A regular sampled asymmetric PWM voltage waveform with modulating frequency 50 Hz, frequency ratio R=9 and modulating index 1 was used as supply voltage. The load is of the type $T_L \sim n$ with the same proportional value as used in the simulation of direct on-line start-up with sinusoidal supply.

The simulation results for a motor with inertia J=0.02 kgm^2 are shown in the figures 113, 114 and 115. Comparing these results with the results for sinusoidal waves, shown in figures 35, 36 and 37, it can be seen, that the basic shape of the torque stays the same, but it is greatly distorted by ripple torques, while there is almost no disturbance to be seen in the speed. For inertia J=0.1 kgm^2 the result is shown in figure 116. The comparison of this result with the one obtained for sinusoidal supply with the same inertia as shown in figure 38 confirm the conclusions.

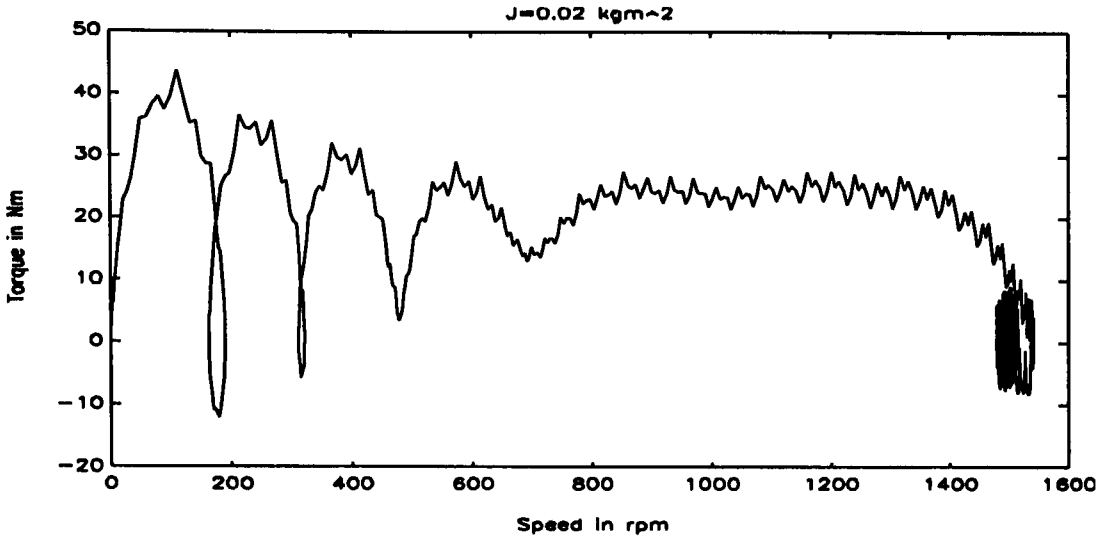

Fig. 113: The torque- speed characteristic for PWM

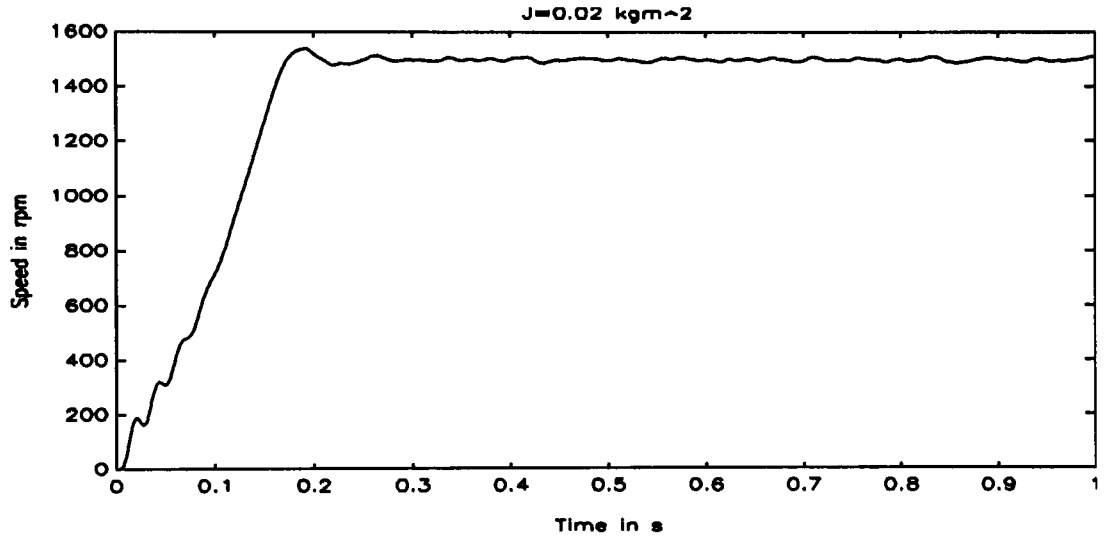

Fig. 114: The speed characteristic for PWM

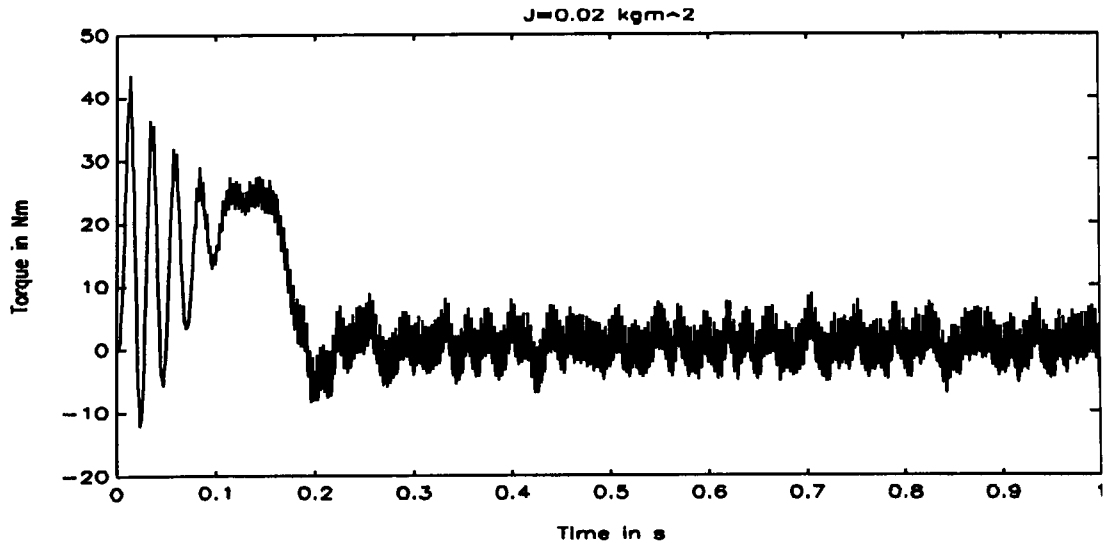

Fig. 115: The torque characteristic for PWM

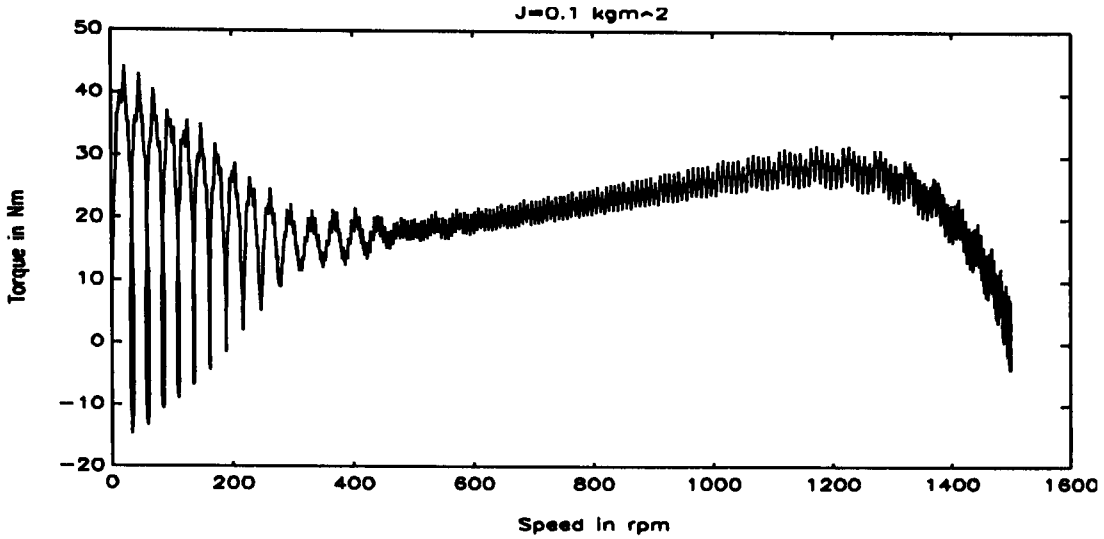

Fig. 116: The characteristic at higher inerta

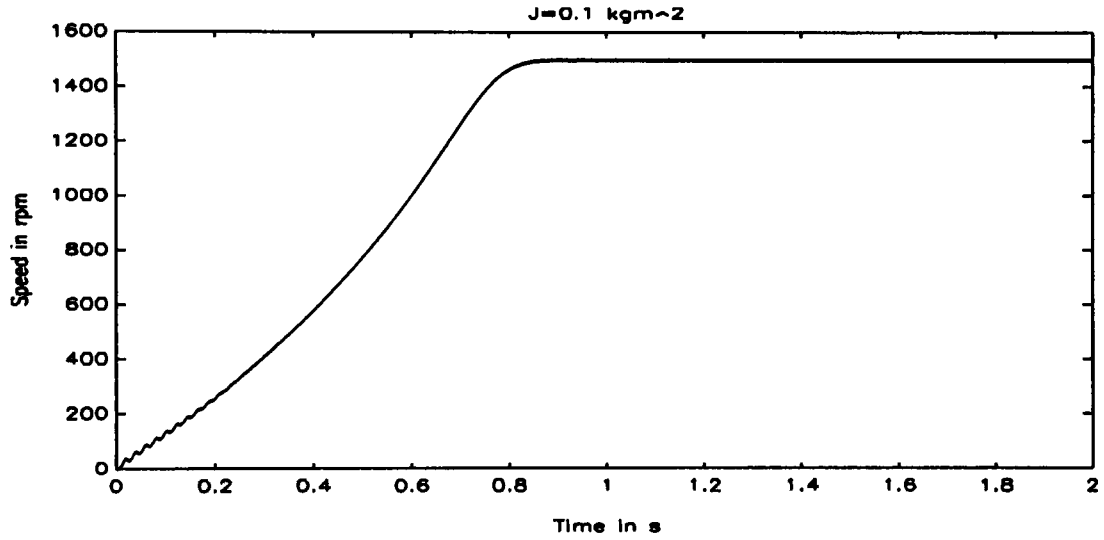

Fig. 117: The speed characteristic for PWM

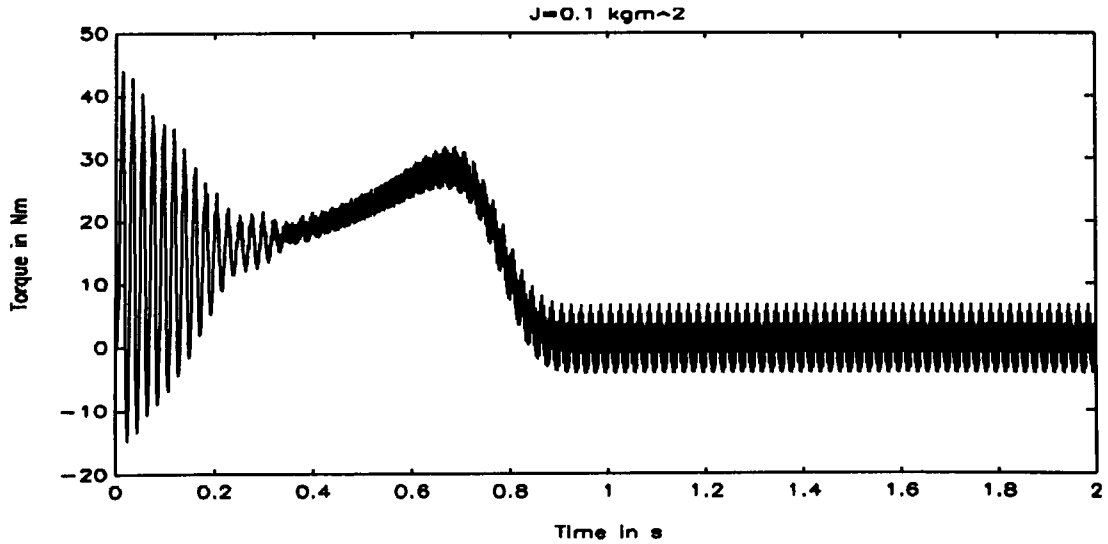

Fig. 118: The torque characteristic for PWM

3.10. Vector Field Control

In this step the vector control model was developed and tested. An indirect decoupled vector control model as explained in chapter 2 was used. The inputs for that controller were magnetizing current and the demanded speed. In addition the controller needed the actual rotating speed of the motor as feedback. This controller was working in a synchronously rotating α-β frame of reference, meaning it was working with dc values. The outputs of the controller were the demanded voltages in this α-β frame and the electrical speed. These outputs had to be translated to supply voltage and frequency to be supplied to the PWM inverter working in the standard a-b-c frame of reference. The PWM inverter then generated the three phase voltages. These phase voltages had to be translated to a d-q frame of reference. The d-q voltages then were supplied to the motor model. The motor model produced from these values the resulting torque and the mechanical speed. The speed was finally fed back to the controller to close the loop.

First the harmonics contained in the PWM voltage waveform were neglected to avoid problems caused by these harmonics. This practically meant that the motor was supplied by a variable voltage variable frequency sine wave. This allowed testing of the control model without getting into problems caused by the harmonics contained in the PWM wave. It also avoided errors generated by calculation and translation involved in the model. The load used in these simulations is of the form $T_L \sim n$ with the same value of the proportional factor as used previously.

In the following figures torque, speed and torque speed characteristics are shown for different values of the gain at an inertia of J=0.02 kg m^2. The figures show that the gain of the controller has great influence on the performance of the overall system. It can be seen that the speed of the startup is greatly improved compared to PWM without control at the cost of higher torque during this startup period. The torque characteristic shows two peaks whose size are obviously depending on the gain. There is a gain, where the maxima of both these peaks are almost equal (gain = 0.09). For gains with a higher value than that the first peak will be bigger that the second and the steady state speed will be reached slightly faster, while for smaller values the amplitude of the second peak will

be higher and the speed slightly slower. The choice of the gain will very much depend on the demand of the real application.

The vector field control strategy used is based on speed control and this effect can clearly be seen when comparing the speed characteristic of this simulations with the ones of the direct on line start up presented earlier. There is no more oscillation to be seen in the speed. The speed runs on a tangential route to its final value. This is a great improvement of the dynamic behaviour of the drive system. Looking at the torque characteristic it can be seen, that there are two high peaks and at the end of the second peak there is a disturbance of the curve. The first of these peaks is caused by the fact that the system starts up from the zero point, as discussed in the section about the direct on-line startup. Contrary to this situation, there is now only one peak instead of an oscillation. This first peak will not be present when the machine changes speed, other than from the startup position. The second peak is the reaction of the machine to the speed change command, this is present if a speed change is performed and the disturbance of the curve will be more significant in this case.

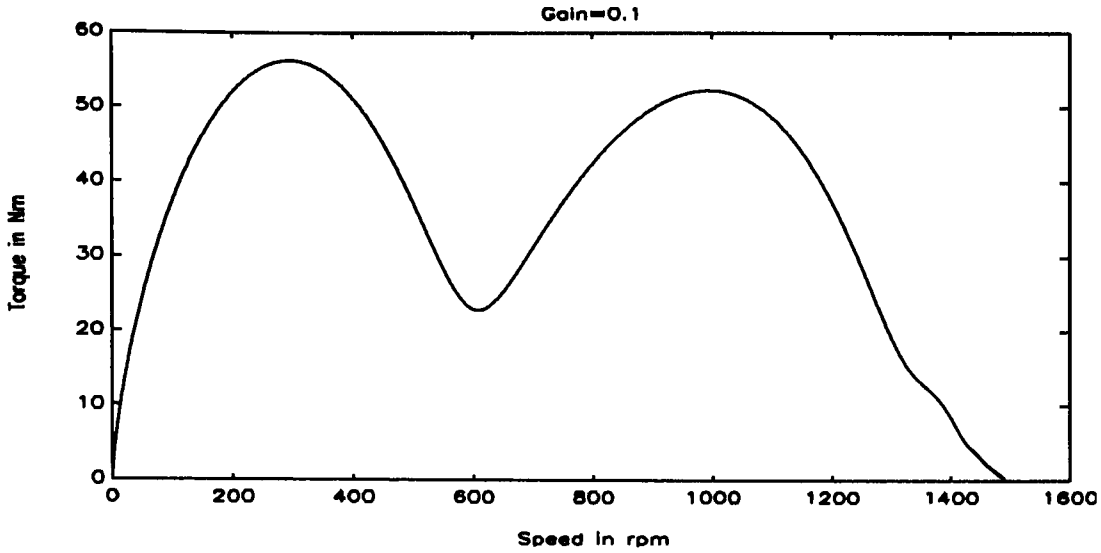

Fig. 119: The torque-speed characteristic

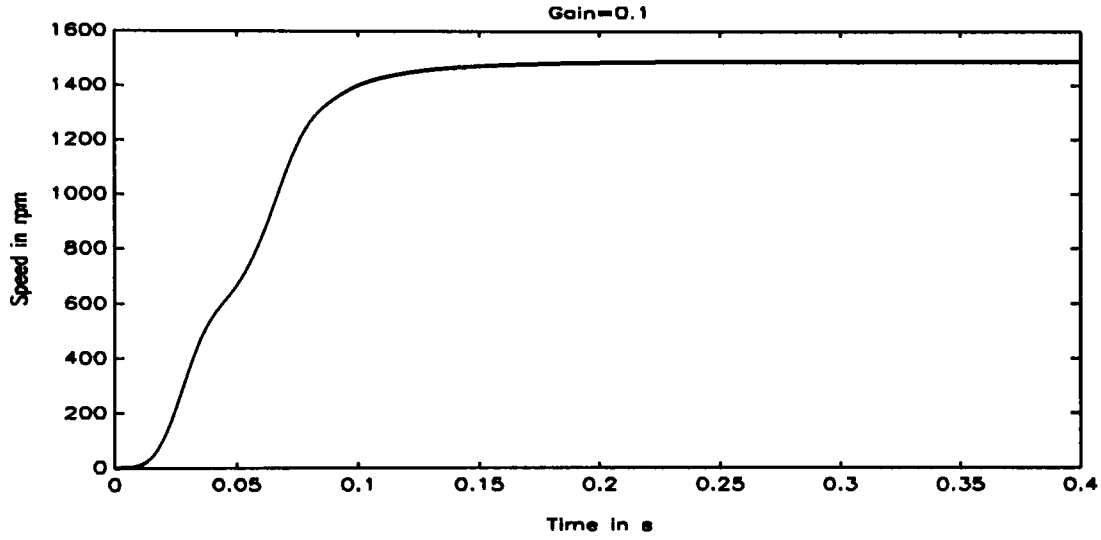

Fig. 120: The speed characteristic

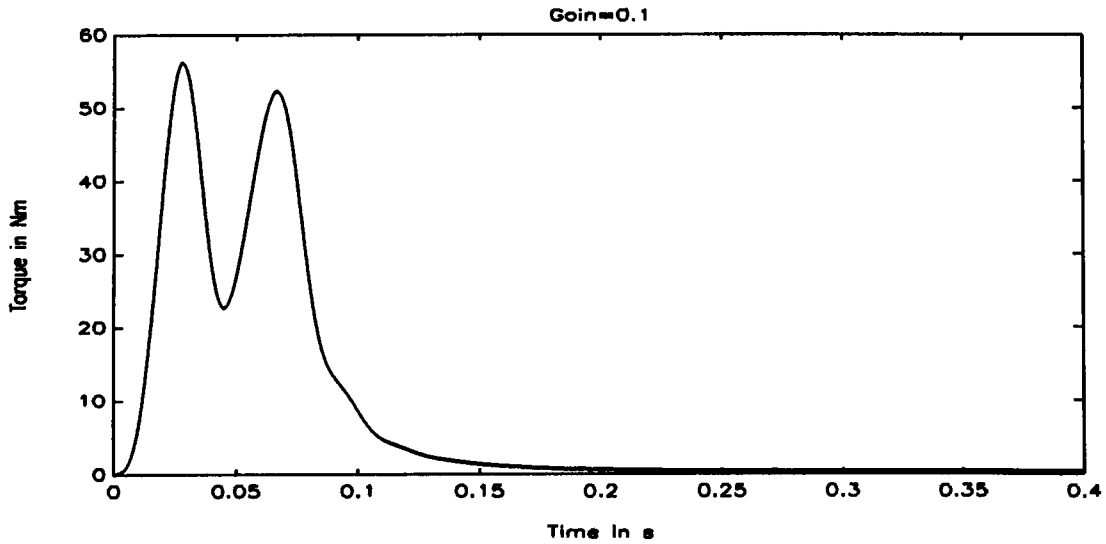

Fig. 121: The torque characteristic

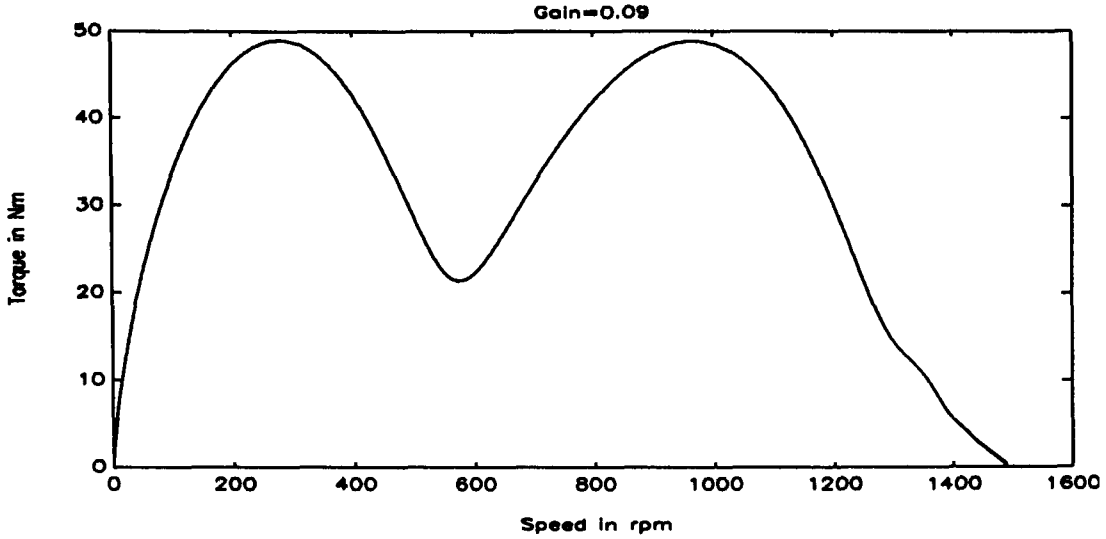

Fig. 122: The torque-speed characteristic

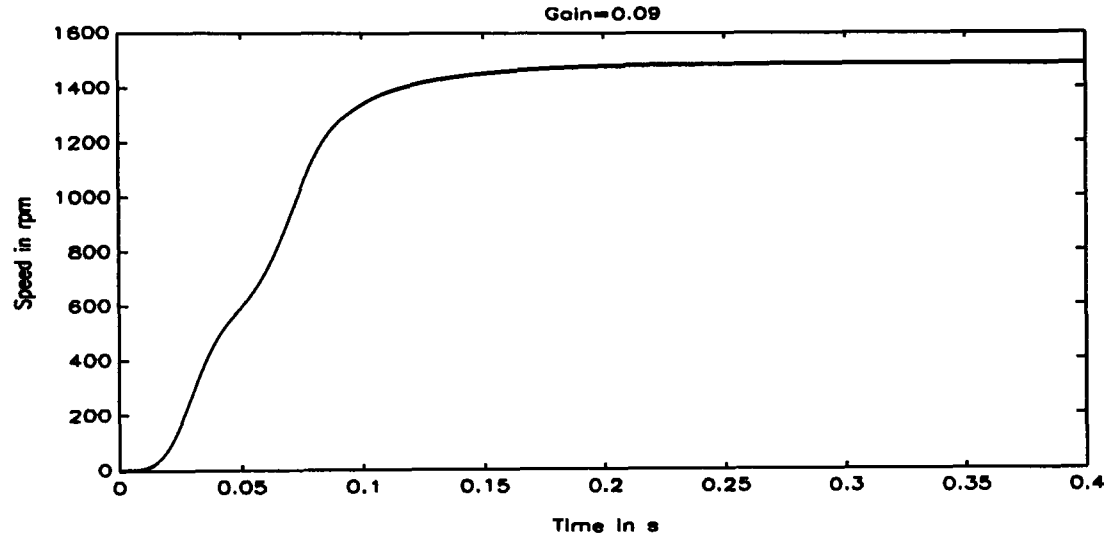

Fig. 123: The speed characteristic

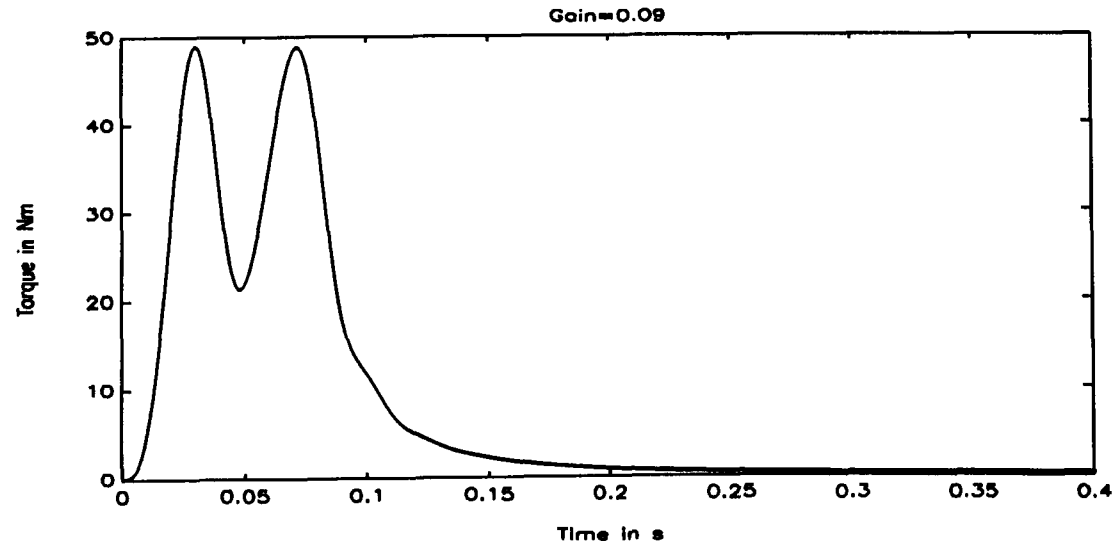

Fig. 124: The torque characteristic

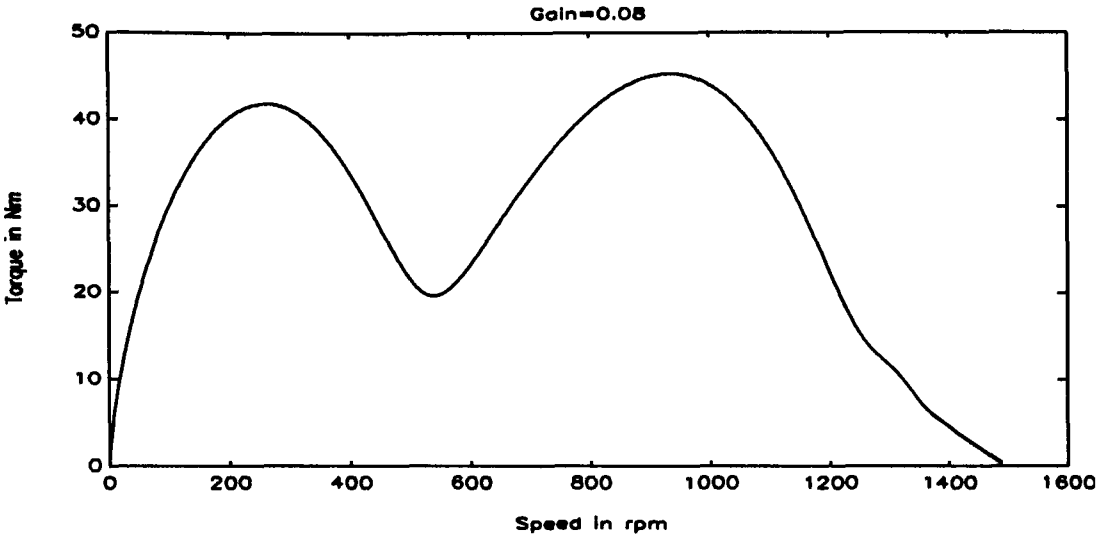

Fig. 125: The torque-speed characteristic

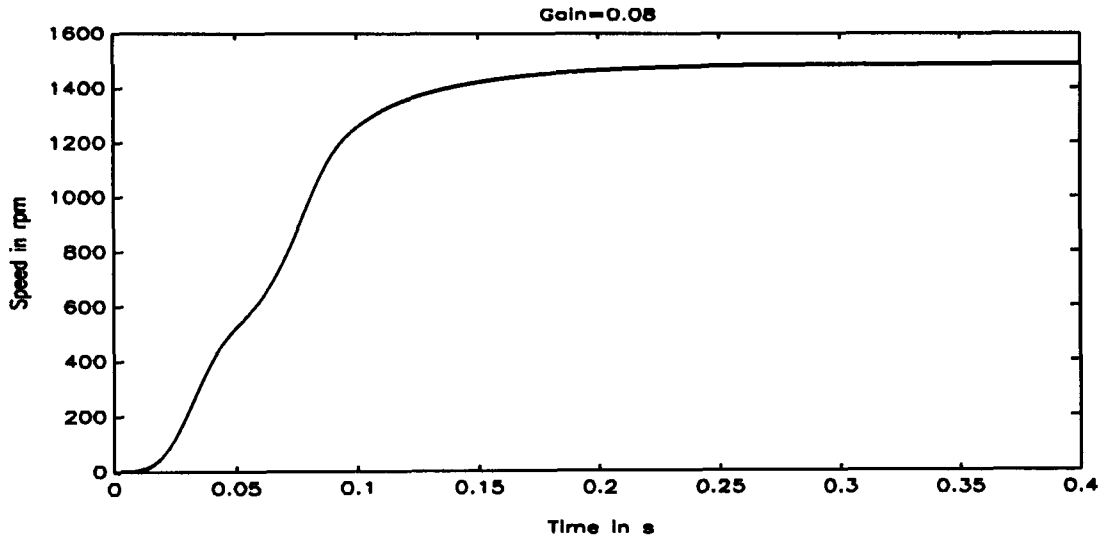

Fig. 126: The speed characteristic

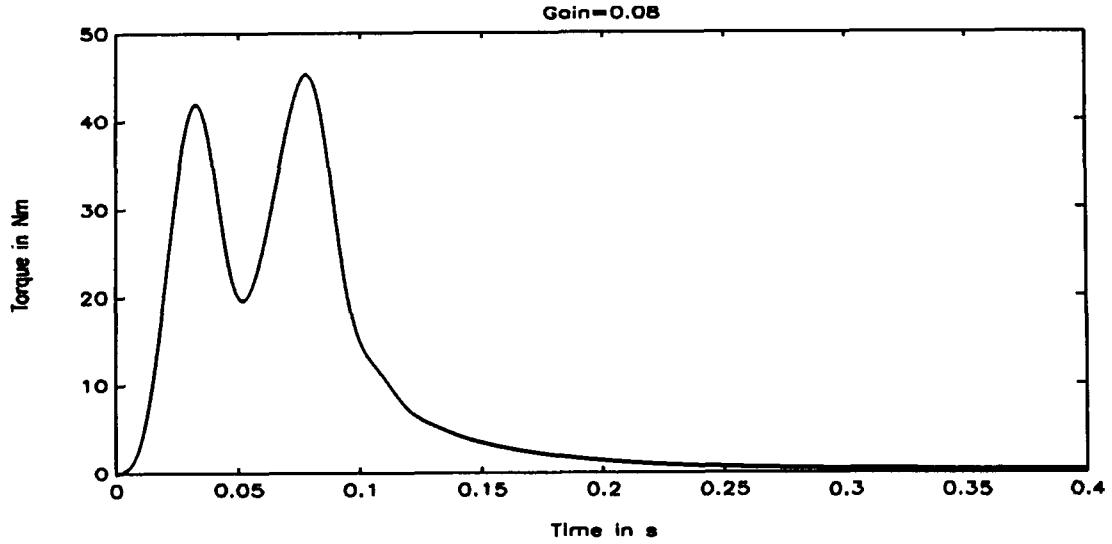

Fig. 127: The torque characteristic

3.11. Vector Control with PWM

In this step the full PWM generator was included in the simulation of the vector field control model. From the experience with the motor model when supplied by PWM voltage waveforms compared to a sinusoidal voltage supply, it is expected that the characteristics resulting from this simulation will have a similar shape to the ones without harmonics but will be more disturbed. But also there is some effect on the dynamic performance of the controller to be expected. The load used here is the same as used for the simulation in the previous section.

The simulation with the inclusion of a regular sampled asymmetric PWM generator proved to involve a problem and it paid off to have simulated the system neglecting the harmonics involved in the PWM wave first. The problem involved in this simulation is that the fundamental frequency of the PWM wave continuously changes. Since it is worked with a discretized system, this would mean changing the sampling frequency all the time or taking a very high number of sampling points. The latter possibility proved to be limited by the available resources, while the earlier one proved to involve drastic calculation errors, preventing the system from working properly. To overcome this problem in another project it was proposed to use a constant carrier frequency and this again allowed a constant sampling frequency to be used [4.3.1]. However, the great disadvantage of this method is that the frequency ratio used is quite unlikely to be a multiple of three. Thus there will be a PWM waveform used that contains harmonic elements that could be avoided by using a variable carrier frequency.

This method is not very satisfactory. Therefore another way was looked at to overcome this problem. There are two considerations made. The first is, that during a dynamic period the harmonic content of a wave does not really matter and the second is, that what is supplied to the motor is not voltage but pulses of voltage time. These deliberations lead straight towards the idea of translating the sinusoidal wave for a period directly to a pulse that has the same voltage time ratio. This translation is done by discretizing the sinewave obtained from the control model during the time of a control cycle, called T_S, into a number of intervals with the time δt. The amplitudes of the

sinewave resulting from the discretization are now added together and multiplied by δt, producing the voltage time pulse required during the time Ts. This of course has to be performed for all three phases.

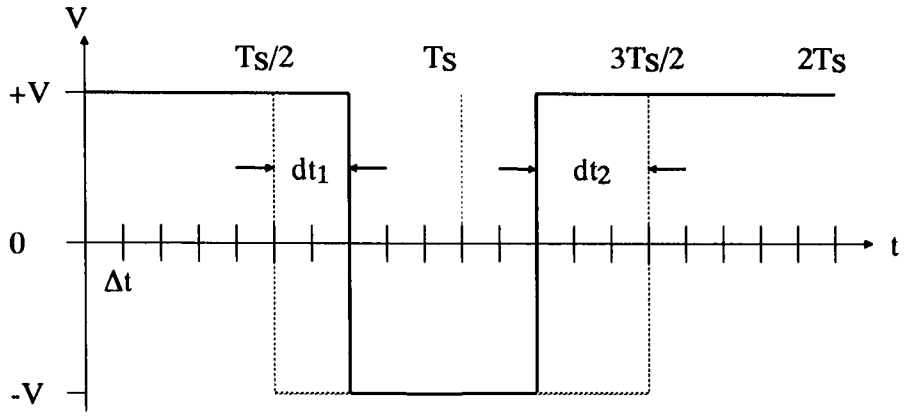

Fig. 128: A process to generate a PWM voltage wave

The process of generating the PWM voltage waveform is performed as follows. The time for a control cycle Ts is divided into an even number of intervals with the time Δt, this time can be the same as δt, but this is not essential. The whole process of generating described here is illustrated in figure 128. If the required voltage time pulse would be zero, the voltage would be a value +V for the time Ts/2, which equals half the number of the Δt intervals in the figure, and after this time it would switch to -V for the remaining 5 Δt intervals. In the next control cycle the voltage would start with -V and after half the time switch to +V, and from then again starting with +V and so on. The voltage discribed here is of the two-level type phase to DC-neutral voltage and would be the same for all three phases. From this two-level voltage would result the three level phase to phase voltage and this would be zero in this case and subsequently there would be no voltage time pulse transferred to the machine. For a no zero voltage time pulse the pulse is calculated as described earlier for each phase and this value is now divided by +V resulting in the switching time dt. This switching time, however, has at least for the simulation to correspond to a multiple of Δt. The question, if this switching time has to be added or subtracted from the zero switching time Ts/2 is dependant on the period it is performed in. If it is done in a cycle starting with +V a positive value of dt, called dt_1

in the figure, will result in an addition of this value to $T_S/2$, whilst the same one in a cycle starting with -V, then called dt_2, would result in a subtraction. For a negative value of dt_1 it will result in a subtraction whilst a negative value of dt_2 would result in an addition.

Obviously this method finds its limits with the switching frequency allowed for the semiconductors in the experimentation and the time chosen for a control cycle and of course by the computing power available for the drive. In the simulation stage the limits are given by the number of variables available. This method of generating a PWM wave has so far not been investigated, because it requires a great number of calculation of sine wave values and this was not possible, because the computing power at affortable cost was made available only in recent years. The same is valid for fast switching devices. However, the accuracy of this method is very much dependant on the accuracy of both the computing process and the available switching speed.

The results of this simulation are presented in the following figures with the standard format. These results propose, that this method of generating a PWM voltage waveform is suitable during the dynamic phase of the operation, but it can be seen, that during steady state operation there is an increasing disturbance of the waves. This is of course due to the harmonics contained in the generated wave. It is possible to reduce this problem during simulation with an increase in the number of sampling point at every level (δt, Δt, T_S). However, before an indepth investigation in this field is concerned, it appears to be sensible to test this method by means of experimentation, to get an idea about the limits, such as recovering time of the semiconductors, given by the real system, which are neglected during the simulation phase. For this project, however, it is currently not possible, because the system used is no longer available in that form and a suitable transducer is not available.

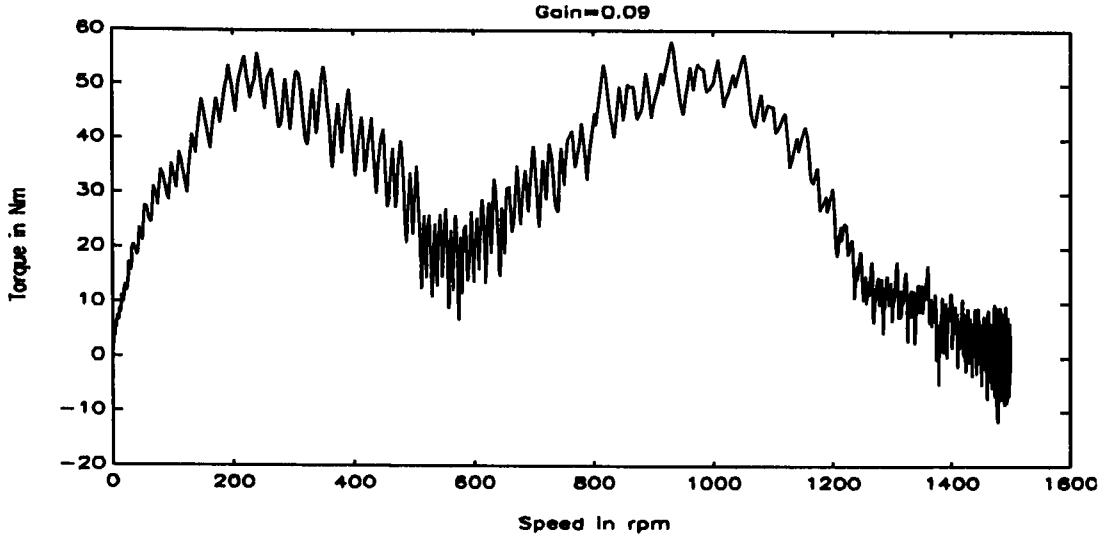

Fig. 129: The torque-speed characteristic

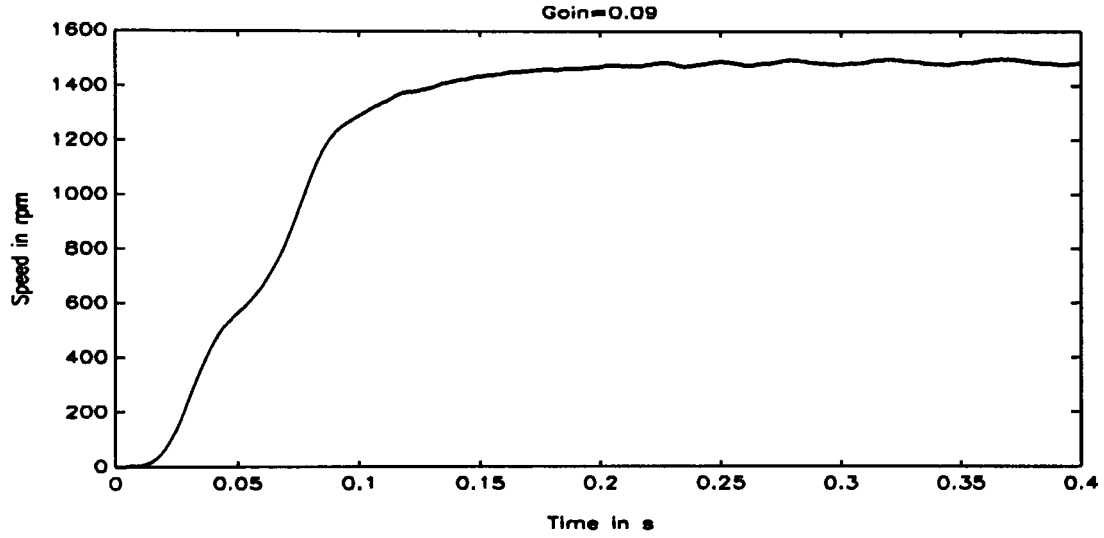

Fig. 130: The speed characteristic

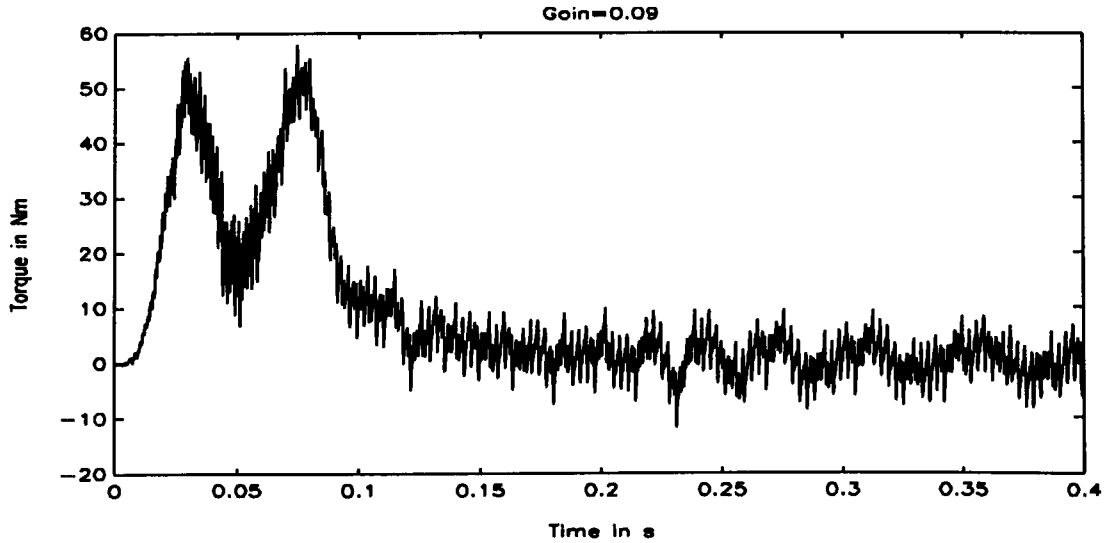

Fig. 131: The torque characteristic

4. Experimentation

4.1. Introduction

The motor under investigation in this thesis was also used in a PhD project. The machine is a 2.2 kW, 3-Phase, 4 Pole cage rotor induction machine fitted with an encoder with 1024 pulses/rev and forced ventilation at the non-drive end. The supply voltage is 240V/415V, the slip is 4.91% at 50 Hz. The manufacturer supplied the following information about the machine:

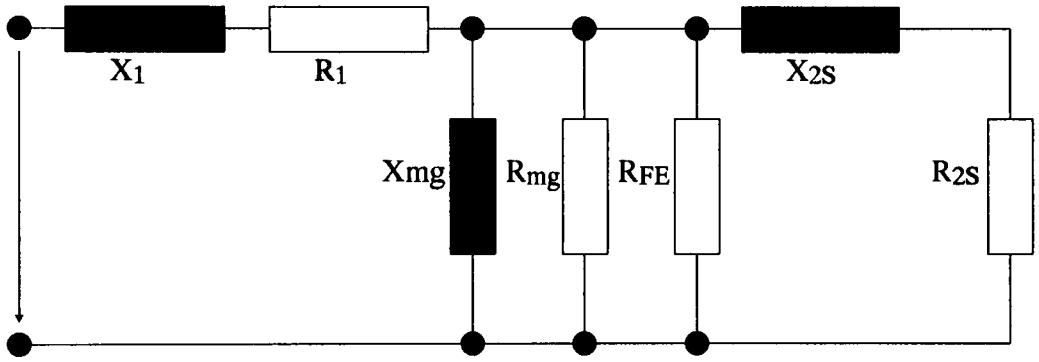

Fig. 132: The equivalent circuit from manufacturer

X_1, stator leakage inductance	: 3.661Ω
R_1, stator resistance	: 3.76Ω
X_{mg}, magnetising reactance	: 84.2Ω
R_{mg}, equivalent resistance for mechanical losses	: 1387Ω
R_{FE}, equivalent resistance for iron losses	: 1153Ω
X_{2S}, rotor leakage inductance (referred to stator)	: 8.765Ω
R_{2S}, rotor resistance (referred to stator)	: 2.571Ω

First the motor was investigated when supplied with a sinusoidal voltage wave. The investigation of the variable voltage variable frequency system was performed with a transputer based PWM inverter developed in the same PhD project. Finally a device was build to display the flux trajectory as shown in chapter 3.

4.2. Motor test

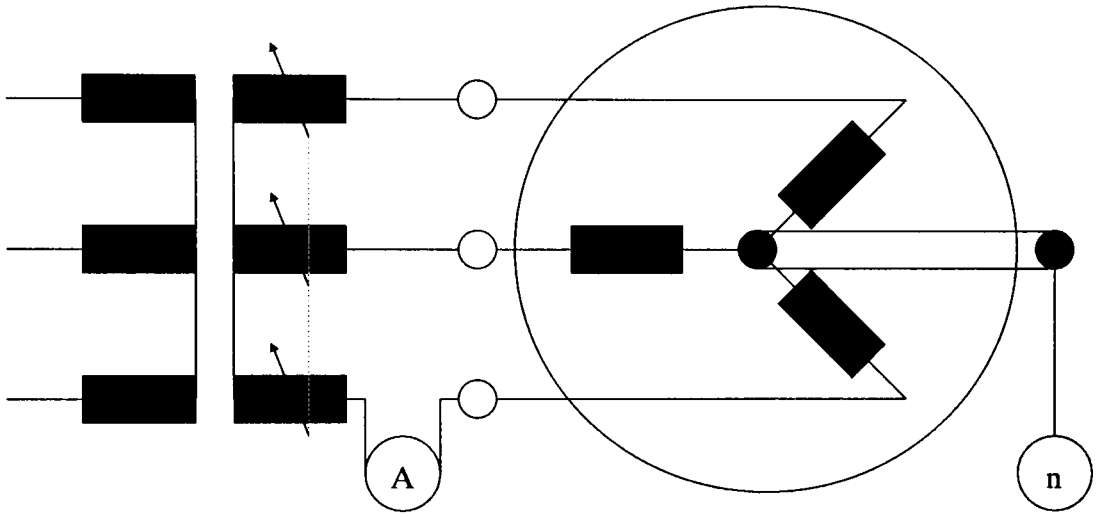

Fig. 133: Setup for motor characteristic

Due to the unavailability of a direct torque measurement setup the motor characteristic had to be determined by indirect means. The motor was connected to a load machine with built in speedometer and supplied by the rated values via a regulated transformer. In one phase the current was measured and recorded together with the speed. The torque was then determined from the measured current values.

4.3. Transputer based Inverter Drive

The transputer based inverter can be divided in four parts, the actual inverter, the main transputer system, the host PC with internal interface transputer and the interface circuit between main transputer, inverter and motor. The experimental setup is in figure 135 and a block diagram of the setup is shown in figure 134.

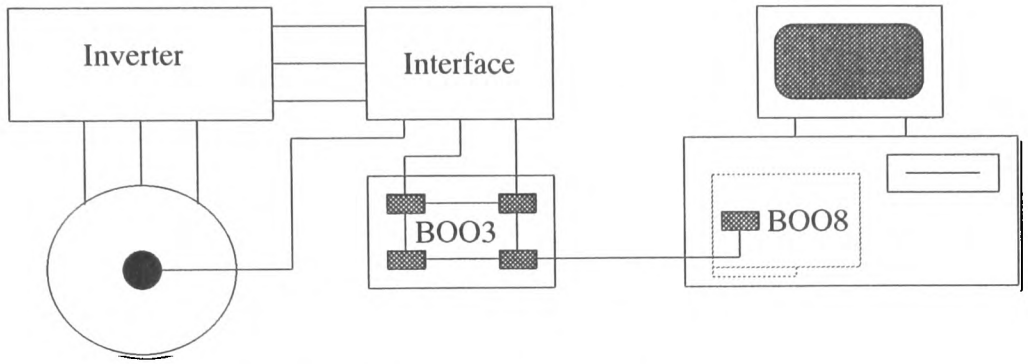

Fig. 134: Block diagram of inverter drive system

Fig. 135: The Transputer Based Inverter Drive

The inverter drive is a 2.2kW three phase bridge inverter [4.3.1] based on MOSFETs as power semiconductor switching devices. The choice of MOSFETs as switching devices was determined by the power rating and the operating frequency. In the power rating of this inverter there are normally bipolar transistors or MOSFETs in use, with the latter offering the lower switching losses. At low frequencies increased conduction losses occur in the MOSFET. These losses can be reduced by the addition of devices such as diodes in the circuit. MOSFETs require less complicated gate driving electronic circuitry and in respect of future development are simpler to replace with higher ratings.

MOSFETs are available as p-chanel and n-chanel devices allowing switching between positive and negative potential respectively, a feature needed in a bridge inverter, where the three lower switches have the negative in common, usually the ground of the supply voltage, whilst the three upper switches have the positive, normally phase, in common. However, the specifications for n-chanel and p-chanel MOSFETs regarding their switching behaviour are significantly different, which would result in additional control electronics. At the time of the design of the inverter p-chanel MOSFETs were not yet available at the same power rating as the n-chanel complements required for the inverter. Thus only n-chanel MOSFETs were chosen to be used. This, however, demanded three additional isolated power supplies for the three upper switching devices. In addition to the electronics for this, means of protection, isolation and safety were necessary. For example, to separate the different power levels between switching devices and switching logic, opto-isolators were used, also providing some feedback separation, and an interlocking logic was designed to avoid any two switches in one branch conducting in the same time and thus generating a short circuit.

The transputer is a form of optimised single chip computer designed for parallel operation. The name transputer is derived from TRANSistor and comPUTER indicating its unique design. A transputer is a central processing unit with a floating point unit, a memory controller, some memory and a special communication controller on board. The communication controller is of special design, because it is a serial communication line with a special and fixed communication protocol, the port is called a link and consists of two lines, and each transputer has four of them. These links provide an easy

to use and fast interface to connect to other transputers or by means of a link adapter to other components. The transputer is designed for parallel processing. Different processes can be performed on one transputer or on several transputers, where the communication between the transputers is provided by means of the links, not requiring any additional programming.

Alongside the transputer came the programming language ***OCCAM*** specially designed for the features of the transputer, which will be explained later. ***OCCAM*** is provided as part of a system called Transputer Development System (TDS) which provides all the necessary means to run the system. In the PC a transputer board called B008 was used. The B008 board contains a T800 transputer on a standard PC peripheral card providing host for up to eight transputer modules. A transputer module consists of a transputer and 256K, 1M or 2M ram and is called T(ransputer)RAM. To run the TDS (in version 2) on a PC, a transputer with a minimum of 2M RAM is necessary which is provided by the B008 board and a TRAM called B414. The setup of TDS and B008 is only necessary for the development stage of a transputer program, however, in this case it is used to provide an interface between the inverter and the "outer world".

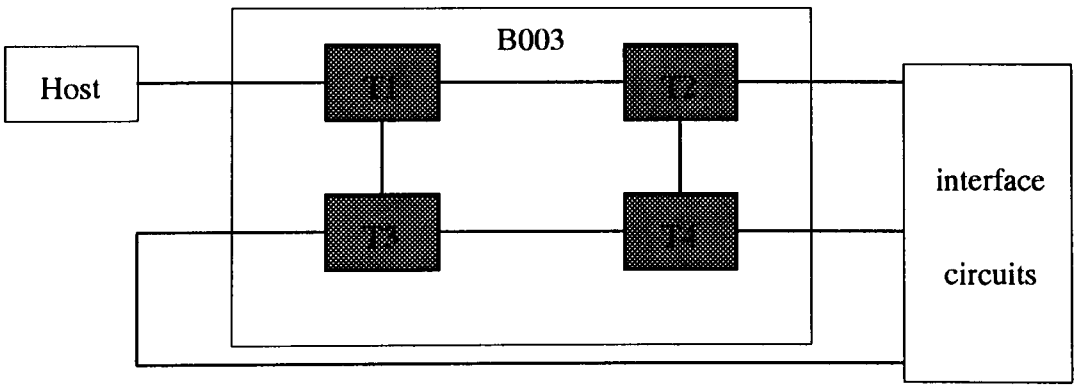

Fig. 136: Block diagram of the B003 board

The main transputer board operating the inverter is a board called B003. This board consists of four T414 transputers with 256K ram each. The transputers are interconnected by means of layout forming a square. Each transputer has two links connected to another transputer, this provides a basic cell to build up a transputer array, as used in

highly parallel application such as graphics. A block diagram of the B003 board is shown in figure 136.

OCCAM is the programming language specially designed for transputers. Its main distinct feature compared to other programming languages are the two commands ***SEQ*** and ***PAR***. ***SEQ*** stands for SEQential working of the following commands, which is the normal procedure. ***PAR***, however, stands for PARallel working of the following commands. Writing programs in ***OCCAM*** is very convenient because of the structure of the program in a multi-level system, the so called Folders. Folders allow a complex procedure to be represented in the program level by just its name, while the actual procedure code is on a level below, accessed by its procedure name, just as in a real filing system. This provides an environment with a very clear program structure.

The allocation of a process to a physical location in a transputer system is done at the start of the ***OCCAM*** program. Since processes can run in parallel on one processor it is possible to run a program for the experimental stage only in the TDS with the B008 board. Once the implementation stage is reached the program can easily be transferred to a multiprocessor system by reassigning the processes to other processors at the beginning of the program without effecting the program performance itself. The only side effect of assigning processes to processors is the program performance, where for the most time effective work of the system the best allocation has to be decided, however, this does not effect the performance of the program code.

The interface circuit finally provides the feedback of the speed produced by the encoder to the host computer and contains the timers which are programmed by the transputers with the switching commands for the power semiconductors. For the timers there is a special application performed. Normally there is one timer per phase switching the output voltage after counting down the programmed time and then requesting a new switching time from the controller via interrupt request. This method has the disadvantage, that there might be interference by two timers requesting an interrupt at the same time and thus disturbing the correct generation of the PWM waveform. To overcome this problem a method has been proposed to use a fourth timer counting the half carrier

wave time and then requesting the change of all four times from the controller, consequently avoiding any chance of interference and thus producing a more accurate PWM waveform. In this inverter a solution is used that employs the three timers for the three phases, with the fourth timer provided via software, this being a modified four timer method.

4.4. Flux Trajectory Display Device

If a motor is supplied by a pulse type voltage waveform, the waveform of the current generated in the motor will be more sinusoidal then the supplied voltage waveform, because the machine acts as a low pass filter, filtering the higher harmonics out. The same is of course valid vice versa for the resulting voltage waveform if a pulse current waveform is supplied. This behaviour also is evident from the equivalent circuit of the motor, which looks like a low pass filter.

To display the flux trajectory of a motor, all that has to be done is to simulate this filtering process. However, the supply voltage waveform for this process has to be of the d-q frame of reference. To achieve this the three phase voltage waveforms have to be transformed to a d-q frame of reference and the mathematical formula governing this process is shown in equation 4.4.1.

$$\begin{bmatrix} v_a \\ v_b \\ v_c \end{bmatrix} = \begin{bmatrix} 1 & 0 & 1 \\ -\frac{1}{2} & +\frac{\sqrt{3}}{2} & 1 \\ -\frac{1}{2} & -\frac{\sqrt{3}}{2} & 1 \end{bmatrix} * \begin{bmatrix} v_d \\ v_q \\ v_o \end{bmatrix} \qquad \text{eqn. 4.4.1}$$

Based on this theory a device was built to show the flux trajectory of the motor caused by the supplied voltage on an oscilloscope [4.4.1,4.4.2]. One bit of the device is therefore performing a transformation of the three phase voltage system to a d-q system, whilst the other one is performing the filtering process for higher frequencies.

This device uses the supplied voltages, that are related to the flux, and separates them into their real and imaginary parts. The real part is then supplied as the x-input and the imaginary as the y-input to display a Lissajous figure. For a pure sine wave input it generates a smooth circle. Since the PWM waveform is not a pure sine wave a distorted circle is generated. For a quasi square wave the result would be a hexagon. Thus the smoothness of this circle gives an indication of how good the supply is, indicating how smooth the motor runs. It also can indicate a change of strategy used for inverters over their full range of supply.

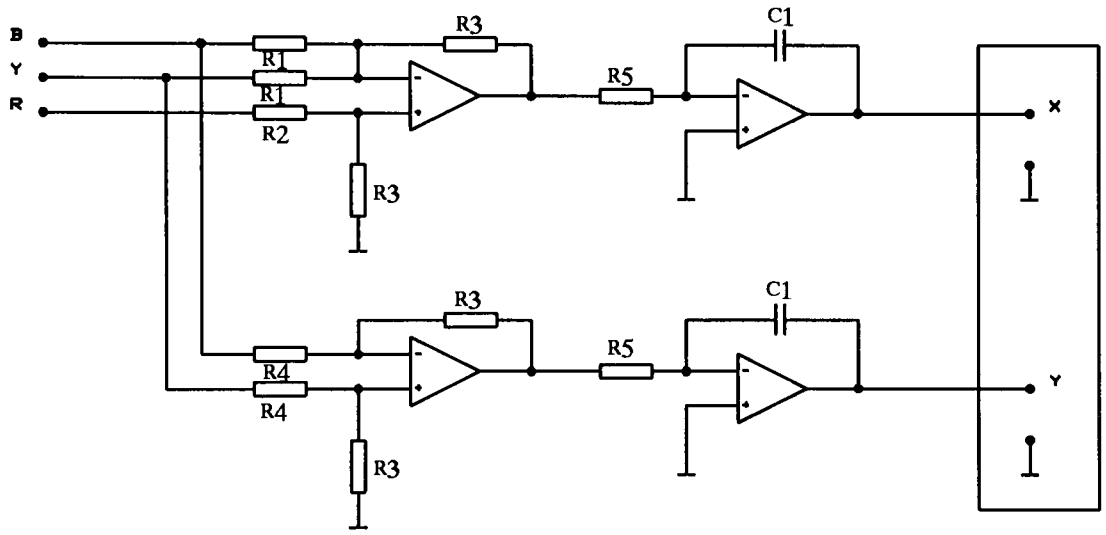

Fig. 137: Diagram of flux trajectory display device

The device consists of two branches one for the imaginary part the other for the real one. Each branch consists of two operational amplifiers. The first is a summator that performs the actual mathematical addition as described in equation 4.4.1. The second one is an integrator that filters the higher harmonics out of the voltage since they are not present in the flux. This device unfortunately has some problems. It is very sensitive to the environment, this makes adjustment very difficult and distortion can be seen on some pictures later. But this problem will be overcome since a project in Hannover is

currently working on an improved version, that will also provide potential separation between Line voltages and scope output.

5. Experimental Results

5.1. Motor characteristic

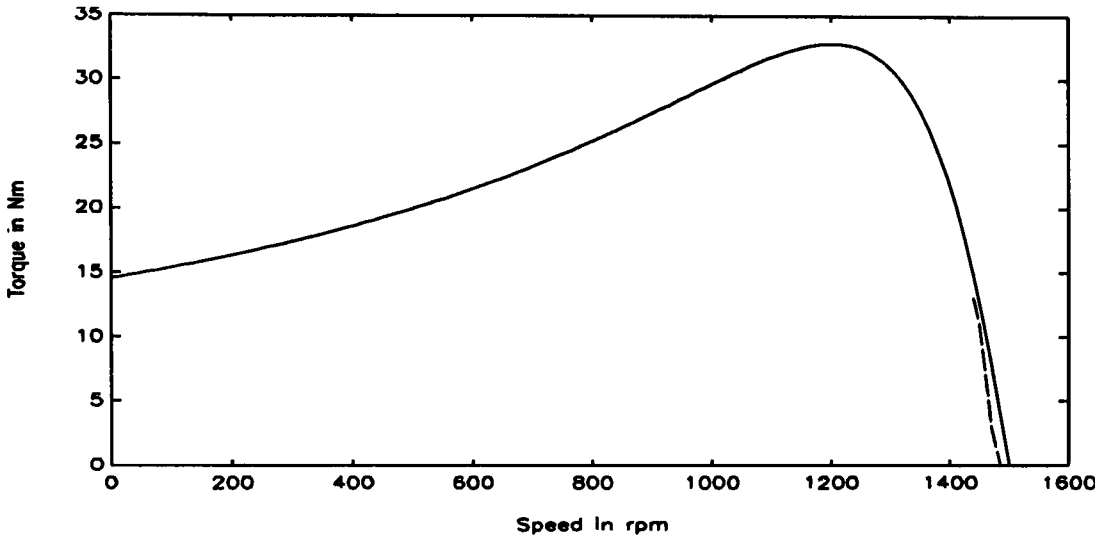

Fig. 138: The motor characteristics

The machine data were measured up to the rated value and it was not possible to measure the torque directly, it was deduced by the measured current. In figure 138 the experimental results are shown by the dotted line, the simulation results by the solid line. It can be seen that the simulation results are a little bit higher than the experimental results. But taking into account the measurement accuracy, the fact that the simulation uses ideal behaviour and that the supplied machine data are average values for this machine series, it can be concluded, that the simulation matches the reality.

5.2. PWM waves

In figure 139 a photograph is shown of the scope picture of the three phase three level line to line voltages generated by the inverter when operating with regular sampled

asymmetric PWM at frequency 50 Hz, modulating index 1 and frequency ratio 9. This figure compares to figure 99 in the simulation section, where a simular picture is shown.

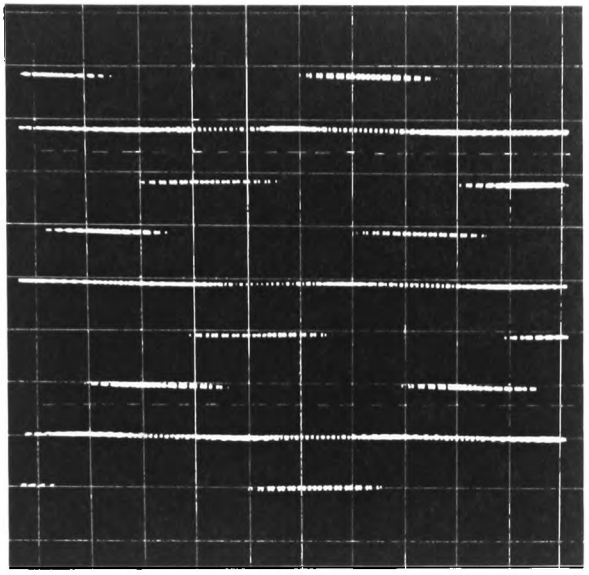

Fig. 139: Scope picture of line to line PWM voltage

The experimental results for the phase A current are shown in figure 140 for the motor when supplied by a three phase regular sampled asymmetric PWM voltage waveform with R=21 , M=1 and 50 Hz frequency and opertating in steady state condition. This result compares fovourable to the one presented in figure 103 in the simulation section.

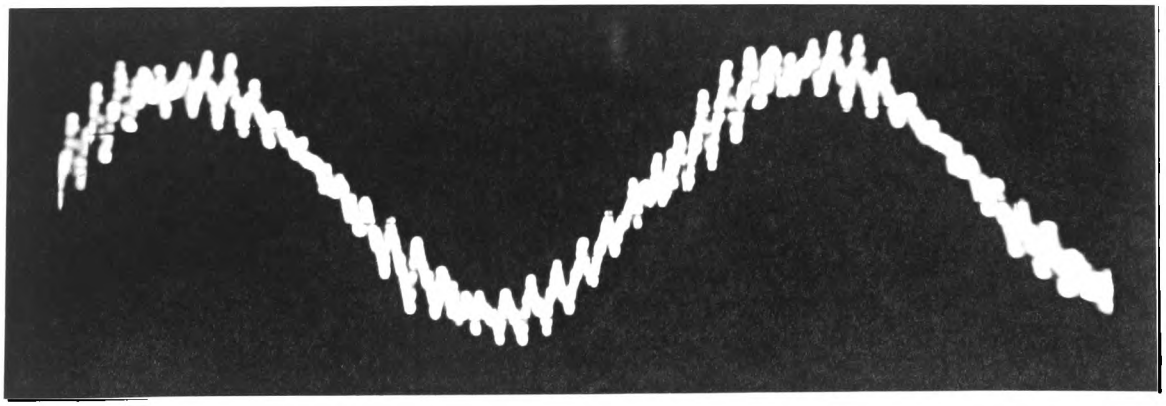

Fig. 140: Motor line current of phase A

5.3. FFT

In this section the results of a Fourier analysis of the generated PWM voltage waveforms performed with a harmonic analyzer are presented and compared with the simulation results. In figure 141 harmonic spectrum of a natural sampled PWM voltage waveform is presented. The simulation result for the same waveform is shown in figure 142 and it can be seen that it compares favourably to its experimental complement.

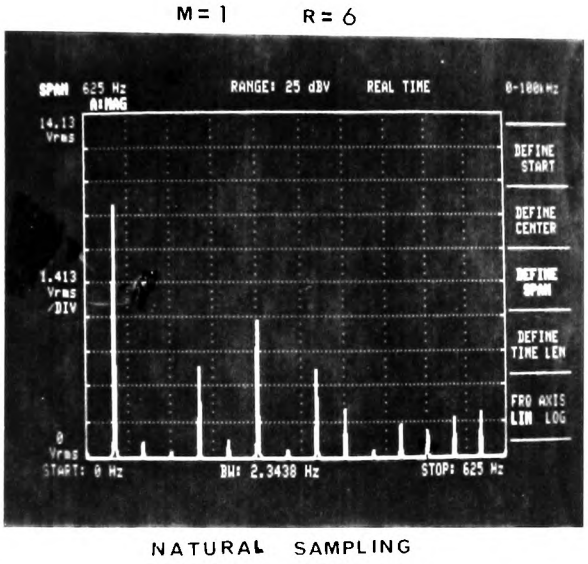

Fig. 141: Spectral analysis of natural sampled PWM

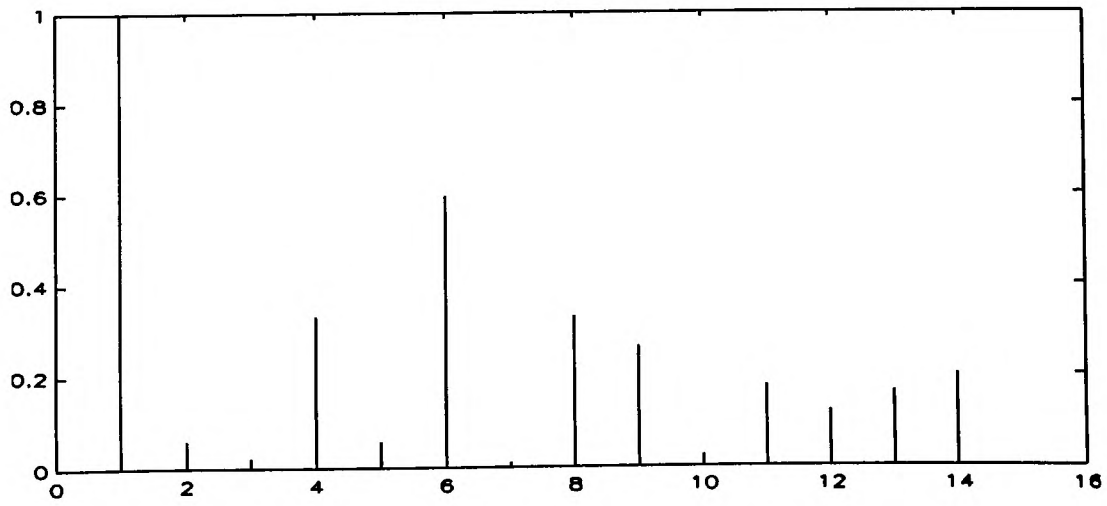

Fig. 142: FFT of simulated natural sampled PWM

The spectra of PWM voltage waveforms generated by means of regular sampled asymmetric PWM are shown in figures 143 and 145 respectively. The modulating index for both waveforms is one and the fundamental frequency is 50 Hz. The frequency ratio for the first figure is 6 and for the latter 21. In figures 144 and 146 the corresponding simulation results are shown. As previously the experimental results compare favourably to the simulation results.

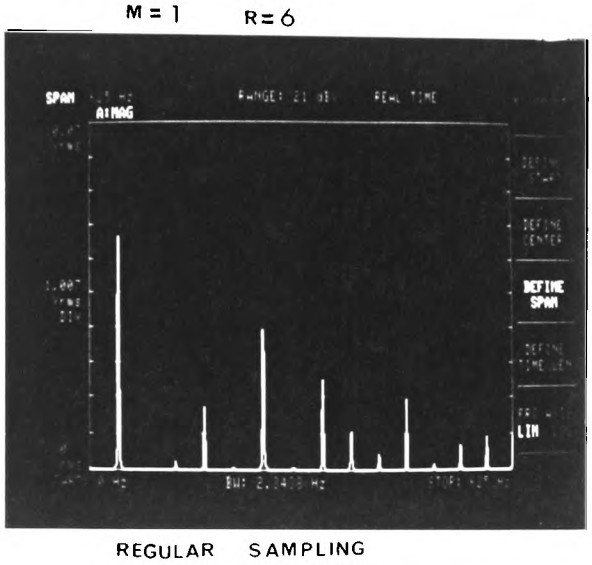

Fig. 143: Spectral analysis of regular sampled PWM

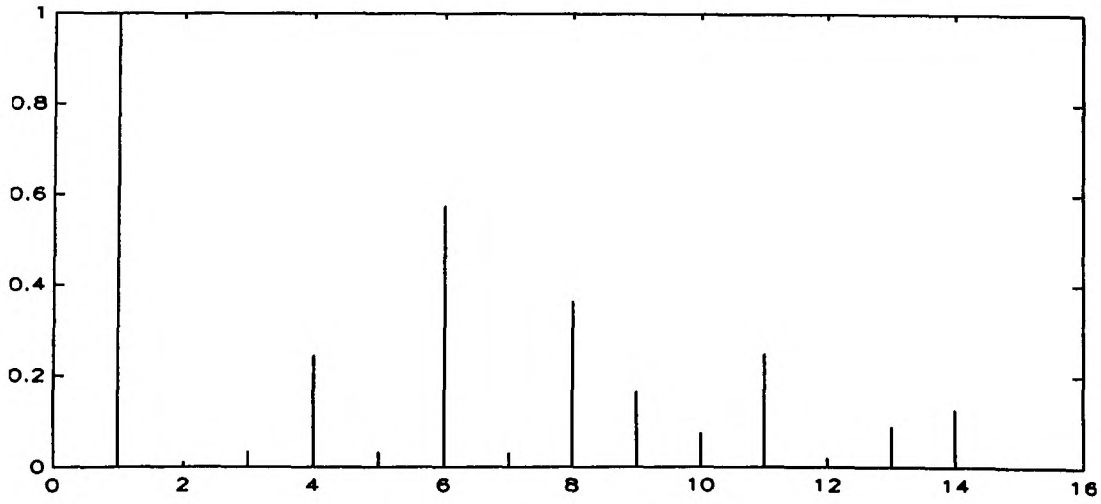

Fig. 144: FFT of simulated regular sampled PWM R=6

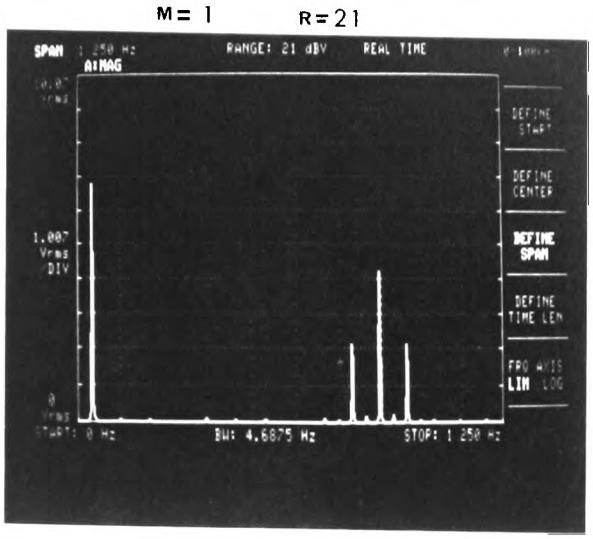

Fig. 145: Spectral analysis of regular sampled PWM

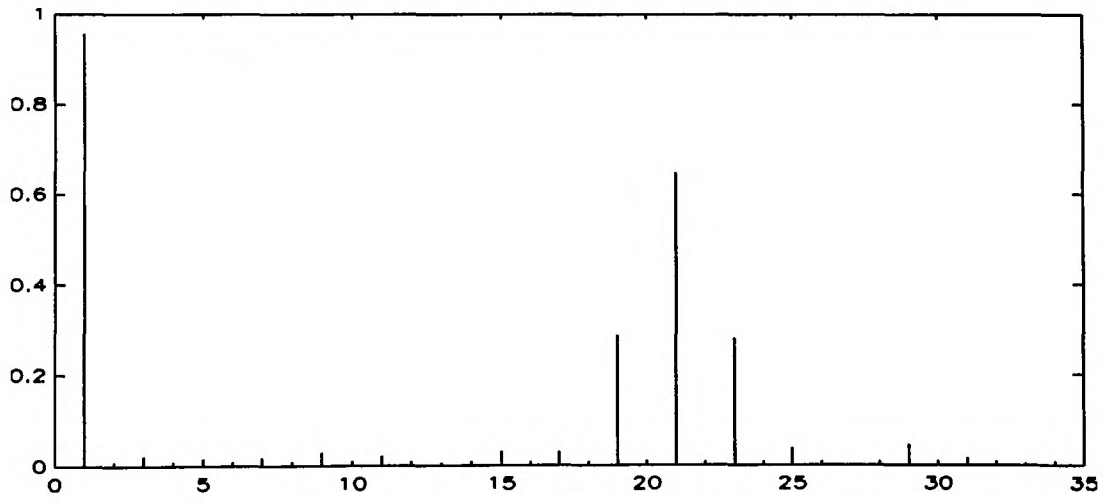

Fig. 146: FFT of simulated regular sampled PWM R=21

5.4. Flux trajectory

In this section the results of the flux trajectory generated by the device described in chapter 4 are illustrated. Attention is drawn to the fact that due to a different definition of the d-q axis system used in Britain and in Germany, the Y and X axis are swapped compared to the simulation results presented in chapter 3.

In figures 147 and 149 the results of the flux trajectory display are shown. These results compare favourably to figures 106 and 107 that are the simulation results presented in chapter 3. Figures 148 and 150 show the quadrature and direct axis flux components corresponding to figures 147 and 149 , respectively and of course these results compare well to their counterparts in the simulation section, which are figures 111 and 112. Finally in figure 151 the flux trajectory of a soft start with a constant V/f ratio is shown. This figure, however, can be seen to be distorted and illustrates some of the dificulties involved in using this very sensitive divice. Nevertheless it can be seen that the softstart produces a flux that is slowly winding up towards the full operation value.

From these results, it can be concluded that this device provides a simple method of obtaining information about the supply source used to operate a machine.

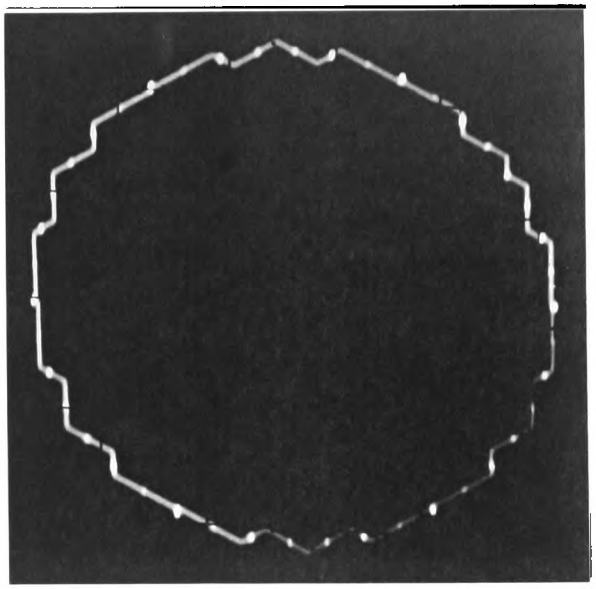

Fig. 147: Flux trajectory at R=21

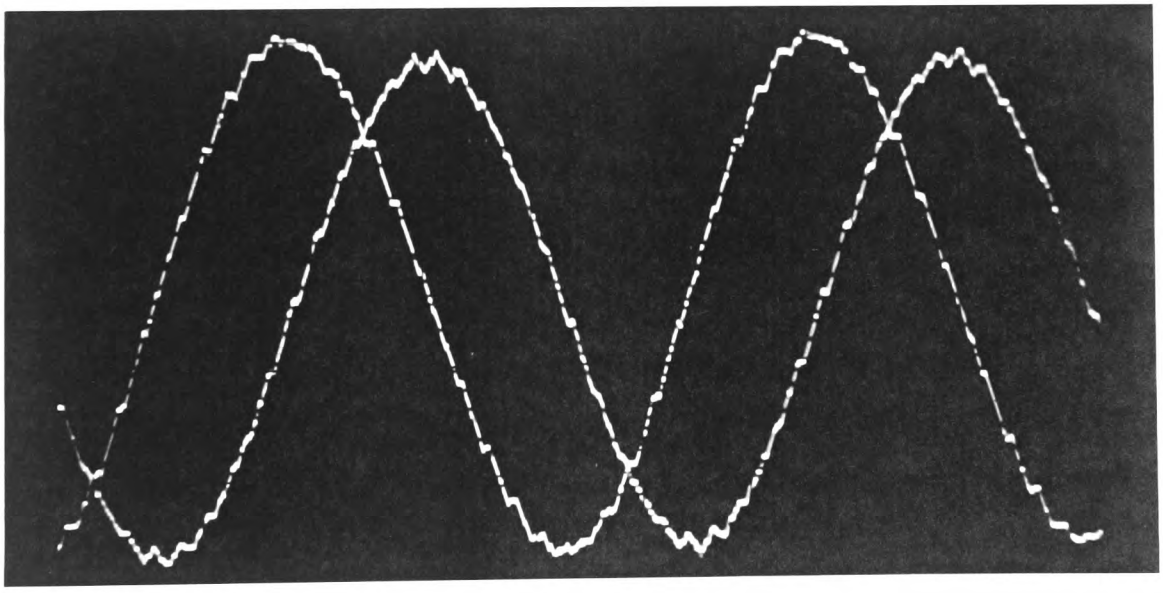

Fig. 148: D and q axis flux at R=21

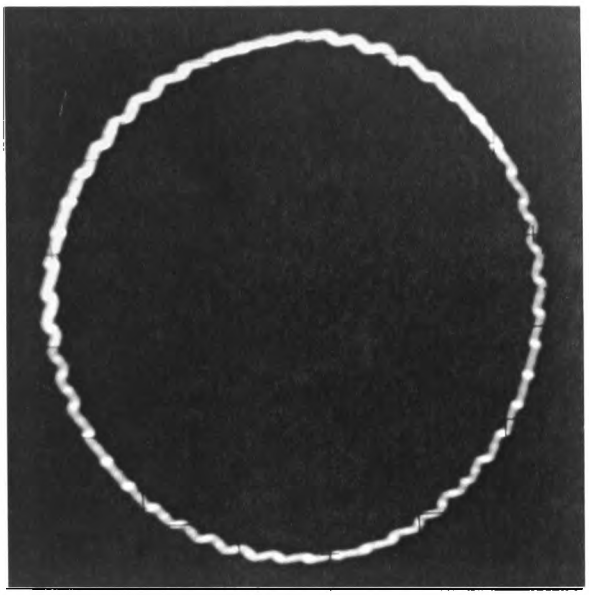

Fig. 149: Flux trajectory at R=51

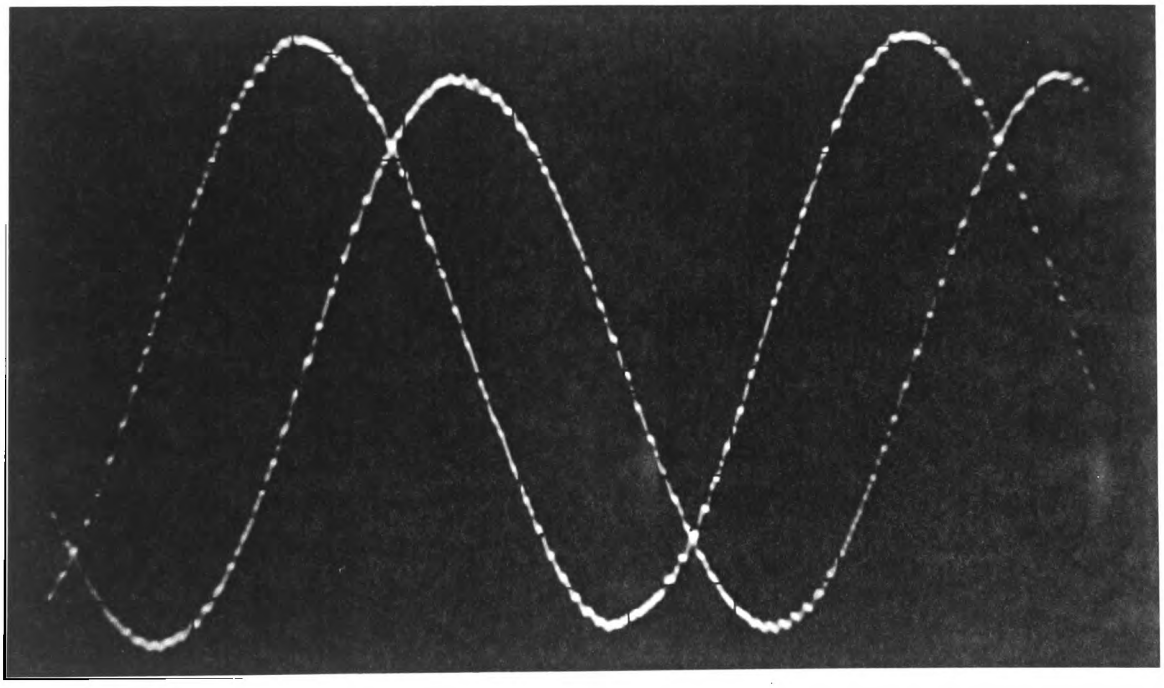

Fig. 150: D and q axis flux at R=51

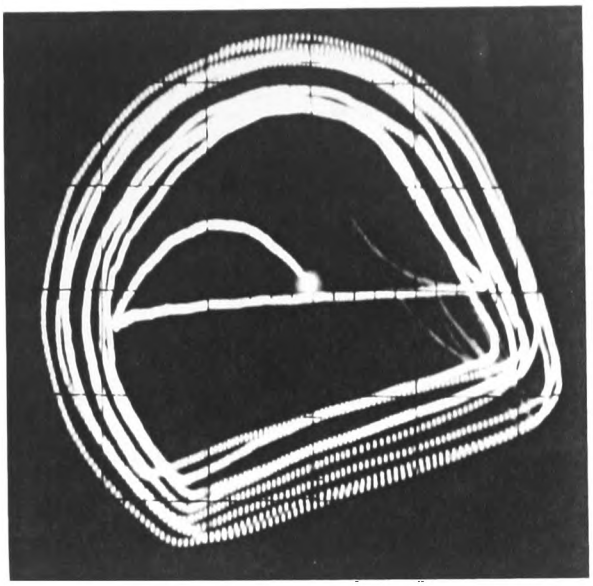

Fig. 151: Flux trajectory of a soft-start

6. Conclusion and Further Work

6.1. Conclusion

This thesis contains an investigation into the performance and behaviour of an inverter cage rotor induction motor drive system by means of simulation on a personal computer. The various ways of describing a machine in mathematical terms are established. To generate a variable frequency variable voltage supply Pulse Width Modulation (PWM) strategy was examined. To analyze the quality of different methods of generating a PWM waveform the Fourier transform was investigated. Finally the theory of vector field control was reviewed.

The software package MATLAB was found to be most useful for translating mathematical theory into a computer program. This software package allows the simulation to be performed on an up to date personal computer rather then on the mini- or main frame computers that are normally used for such complex simulation studies.

From the theory two motor models were developed, one for steady state operation using the Park vector and the second for the dynamic behaviour. With the steady state model, the motor characteristic was generated when supplied by a three phase mains supply. The second model was used to investigate the influence of the variation of the value of the inertia on the start-up behaviour of the machine. A regular sampled symmetric PWM inverter and a regular sampled asymmetric PWM inverter were simulated. The harmonic content of the voltage waveforms generated was analyzed by means of the Fast Fourier Transform. Regular sampled asymmetric PWM was found to be superior to regular sampled symmetric PWM. An open loop PWM inverter drive was then simulated, to see the impact of the harmonics contained in these pulse type waveforms on the behaviour of the drive system, when compared to sinusoidal supplies. Finally, a voltage type indirect vector field controlled PWM inverter induction motor drive was simulated.

The motor characteristic was experimentally investigated and the result of this investigation favourably confirms the simulation results. The open loop PWM inverter was investigated by means of a transputer based induction motor inverter drive. The harmonic analysis of the output of the PWM inverter was performed with a spectrum analyzer. The comparision of the experimental results with the results obtained from the simulation showed good correlation.

A device was built to display the flux trajectory generated in the motor on an oscilloscope, when supplied by a three phase voltage. The experimental results obtained from this show a good correlation with the results for the flux trajectory obtained from the simulation of the drive.

This thesis has demonstrated, that a useful simulation of an induction motor inverter drive is possible with modern engineering tools. With the current increase in computing power and the availability of more powerful software packages it will become more and more common use to simulate complex drive systems. This will allow engineers, in the future, to simulate an application before actually implementing a design, with a reasonable accuracy being achieved. With the widespread increase of fast, large memory computers, and the availability of the necessary communication tools, it might soon be the case, that manufacturers will provide the necessary software for their product and that a salesman will be able to choose the suitable drive for his costumer by means of simulating the application.

6.2. Further Work

6.2.1. Inverter drive

The inverter drive used for the experimentation has so far only been built as a temporary experimental device and is currently operated with an intermediate circuit voltage of 60 or 100V due to the lack of a suitable three phase 400V power supply system. This problem should be overcome. There were also some problems cause by noise, which

appeared to be caused by the prototype state of the PCB's used. The wire-wrap technology with its long connection legs are operating as ideal antennas. This system should be built to a more final stage with proper PCB's, a final housing and a separate supply system.

A further point is the implementation of a torque sensing device for future investigations. Thus a better confirmation of the simulation results could be achieved. The verification of the torque-speed characteristics for this machine are of great interest.

6.2.2. Software

The software MATLAB used was updated three times during this project and the next update is already in the final stage of preparation. Fortunately these updates did not cause any problems, unlike other software, but every update saw a drastic increase in the computing power made available, eg. the limit for the number of elements for a vector was pushed forward and is now only limited by the memory available. The only difficulty caused by the updates was the requirement of an up to date PC.

There are now toolboxes for MATLAB available for different fields of applications. The capabilities of MATLAB illustrated during this project suggest the production of a toolbox for inverter drive technology based on the research work undertaken so far. The fundamentals for the induction machine, PWM-inverters and a vector controlled inverter are there. Future work could expand this to other inverter types and the inclusion of the other machine types. However, for this purpose it is necessary to lay down a clear concept of what to include and what to exclude, because the software allows the inclusion of almost every aspect of the drive system, such as heat, saturation and switching effects and thus the initial objective might be lost. The limit for what to include would basically be set by the computer power made available.

6.2.3. Hardware

The growing capabilities of the new computer and transputer generations becoming available demand constant updating of equipment. This process is made easier by the dramatic price drops taking place. The software available are breaking with the standard of compatibility, that was blocking the advance of computer power by requiring that software be able to run on the first PC's. Thus new software requires more and more computer systems with a certain standard of advanced features. This project started on a PC-286AT with 1Mbyte ram for the simulation and a 386 with 2Mbyte ram for the inverter drive, that was not available for simulation since it was being used by another project. The 386 computer was one of the first types available, consequently it did inherit a lot of bugs and its speed was slow compared to similar 386 computers available today. For a continuation of this project it appears to be essential to provide a modern 386 computer with at least 8 Mbyte RAM or even better a 486DX computer since MATLAB requires the math coprocessor anyway. A 386 computer with a 387 coprocessor should currently be about the same price as a 486DX computer. Taking into account the gain in speed, originated by the design of the 486 with built in coprocessor and the heavy use made of this by MATLAB, and the greater amount of RAM that can be fitted, the purchase of a 486 appears to be the best choice for a future research project. But this is certainly limited by the resources available for research in this college.

The transputer has also seen a rapid growth from the T400 to the T800, up to T9000 and the new generation H1. The transputers used for this project are of the T800 generation. An increase in power and speed would be welcome for the project once the system is brought to full operation power. The implementation of more sophisticated control strategies demanding more calculations will certainly need these capabilities. As the control approaches a true "real-time" implementation, the greater the speed required.

References

1.1.1 Bowers, B., 1982, "A History of Electrical Light and Power", *Peter Peregrinus Ltd.*, Stevenage, UK.

1.1.2 El-Hawary, M. E., 1983, "Electrical Power Systems", *Reston Publishing Company Inc.*, Reston, Virginia, USA.

1.1.3 Bose, B. K., "Power Electronics - A Technology Review", *Proceedings of the IEEE*, August 1992

1.2.1 Sen, P. C., "Electric Motor Drives and Control - Past, Present, and Future", *IEEE Trans. on Industrial Electronics*, Vol. 37, No. 6, December 1990.

1.2.2 Bose, B. K., 1992, "Modern Power Electronics", *IEEE Press*, New York, USA

1.2.3 Bose, B. K., 1981, "Adjustable Speed AC Drive Systems", *IEEE Press*, New York, USA

1.2.4 Jayne, M. G., 1976, "The Application of Communication Principles to Pulse-Width Modulated Inverters", *PhD Thesis*, CNAA.

1.2.5 Enjeti, P. N., Ziogas, P. D., and Lindsay, J. F., "Programmed PWM Techniques to Eliminate Harmonics: A Critical Evaluation.", *IEEE Trans. on Industry Applications*, Vol. 26, No. 2, March/April 1990.

1.2.6 Bowes, S. R., and Midoun, A., "Suboptimal switching strategies for microprocessor-controlled PWM inveter drives", *IEE Proceedings*, Vol. 132, Pt. B, No.3, May 1985.

1.2.7 Murphy, J. M. D., and Turnbull, F. G., 1989, "Power Electronic Control of AC Motors", *Pergamon Press plc* , Oxford, UK

1.3.1 Blaschke, F., 1973, "Das Verfahren zur Feldorientierung zur Regelung der Drehfeldmaschine", *Dr.-Ing. Thesis*, Braunschweig, Germany.

1.3.2 Leonhard, W., 1990, "Control of Electrical Drives", *Springer Verlag*, Berlin, Heidelberg, Germany.

1.3.3 Gabriel, R., Leonhard, W., and Norby, C., "Microprocessor Control of Induction Motors Employing Field Coordinates", *IEE, 2nd Int Conf. on Electrical Variable -Speed Drives*, London, September 1979.

1.3.4 Gabriel, R., Leonhard, W., and Norby, C., "Field-Oriented Control of a Standard AC Motor Using Microprocessors", *IEEE Trans. on Industry Applications*, Vol. IA-16, No. 2, March/April 1980.

1.3.5 Leonhard, W., "Field-Orientation for Controlling AC-Machines - Principle and Application", *IEE, 3rd Int Conf. on Power Electronics and Variable-Speed Drives.*

1.3.6 Schuhmacher, W., and Leonhard., W., "Transistor-Fed AC-Servo Drive with Microprocessor Control", *IPEC-Tokyo '83.*

1.3.7 Sen, P. C., Trezise, J. C., and Sack, M., "Microprocessor Control of Induction Motor with Flux Regulation", *IEEE Trans. on Ind. El. and Cont.Instrum.*, Vol. IECI-28, No. 1, February 1981.

1.3.8 Ito, T., Yamaguchi, T., Ueda, R., Mochizuki, T., and Takata, S., "Analysis of Field Orientation Control of Current Source Inverter Drive Induction Motor System", *IEEE Trans. on Industry Applications*, Vol. IA-19, No. 2, March/April 1983.

1.3.9 Harashima, F., Kondo, S., Ohnishi, K. Kajita, M., and Susono, M., "Multiprocessor-Based Control System for Quick Response Induction Motor Drive", *IEEE Trans. on Industry Applications*, Vol. IA-21, No. 4, May/June 1985.

1.3.10 Matsuo, T., and Lipo, T., "A Rotor Parameter Identification Scheme for Vector Controlled Induction Motor Drive", *IEEE Trans. on Industry Applications*, Vol. IA-21, No. 4, May/June 1985.

1.3.11 Lorenz, R. D., "Tuning of Field-Oriented Induction Motor Controllers for High-Performance Applications", *IEEE Trans. on Industry Applications*, Vol. IA-22, No. 2, March/April 1986.

1.3.12 Koyama, M., Yano, M., Kamiyama, I., and Yano, S., "Microprocessor-Based Vector Control System for Induction Motor Drives with Rotor Time Constant Identification Function", *IEEE Trans. on Industry Applications*, Vol. IA-22, No. 3, May/June 1986.

1.3.13 Sugimoto, H., Koyama, M., Yano, M., and Ohno, E., "A new Transfer Function of an Induction Motor Driven by Variable Frequency Source", *IEEE Power Electronics Special Conf. Rec. 1983.*

1.3.14 Kubo, K., Watanbe, M., Ohmae, T., and Kamiyama, K., "A Fully Digitalized Speed Regulator using Multiprocessor System for Induction Motor Drives", *IEEE Trans. on Industry Applications*, Vol. IA-21, No. 4, July/August 1985.

1.3.15 Murata, T., Tsuchiya, T., and Takeda, I., "Vector Control for Induction Machine on the Application of Optimal Control Theory", *IEEE Trans. on Industry Electronics*, Vol. 37, No. 4, August 1990.

1.3.16 Lessmeier, R., Schumacher, W., and Leonhard, W.," Microprocessor-Controlled AC-Servo Drives with Synchronous or Induction Motors: Which is Preferable", *IEEE Trans. on Industry Applications*, Vol. IA-22, No. 5, September/October 1986.

1.3.17 Mishkin, E. and Braun, L., 1961, "Adaptive Control Systems", *McGraw-Hill Book Company*, New York, USA.

1.3.18 Tou, J. T., 1964, "Modern Control Theory", *McGraw-Hill Book Company*, New York, USA.

1.3.19 Garés, L. J., "Parameter Adoption for the Speed-Controlled Static AC Drive with a Squirrel-Cage Induction Motor", *IEEE Trans. on Industry Applications*, Vol. IA-16, No. 2, March/April 1980.

1.3.20 Onishi, K., Ueda, Y., and Miyachi, K., "Model Reference Adaptive System Against Rotor Resistance Variation in Induction Motor Drive", *IEEE Trans. on Industrial Electronics*, Vol. IE- 33, No.3, August 1986.

1.3.21 Nielsen, R., and Kažmierkowski, M. P., "Reduced-order observer with parameter adaption for fast rotor flux estimation in induction machines", *IEE Proceedings*, Vol. 136, Pt. D, No.1, January 1989.

1.3.22 Bose, B. K., "An Adaptive Hysteresis-Band Current Control Technique of a Voltage-Fed PWM Inverter for Machine Drive System", *IEEE Trans. on Industrial Electronics*, Vol. 37, No.5, October 1990.

1.3.23 Bose, B. K., 1986, "Power Electronics and AC drives", *Prentice Hall Inc.*, London, UK.

1.3.24 Kirschen, D. S., Novotny, D. W., and Lipo, T. A., "On-Line Optimization of a Variable Frequency Induction Motor Drive", *IEEE Trans. on Industry Applications*, Vol. IA-21, No. 4, May/June 1985.

1.3.25 Brickwedde, A., "Microprocessor-Based Adaptive Control for Electrical Drives", *IFAC Control in Power Electronics and Electrical Drives*, Lusanne, Switzerland, 1983.

1.3.26 Brickwedde, A.,"Microprocessor-Based Adaptive Speed and Position Control for Electrical Drive", *IEEE Trans. on Industry Applications*, Vol. IA-21, No. 5, September/October 1985.

1.3.27 Johnson, B. W., and Aylor, J. M., "Design of an Adaptive Controller for Microcomputer Implementation", *IEEE Trans. on Industrial Electronics*, Vol. IE-33, No. 1, February 1986.

1.3.28 Consoli, A., Fortuna, L., and Gallo, A., "Induction Motor Identification by a Microcomputer-Based Structure", *IEEE Trans. on Industrial Electronics*, Vol. IE-31, No. 4, November 1987.

1.3.29 Zhong, H. Y., Messinger, H. P., and Rashad, M. H., "A new Microcomputer-Based Direct Torque Control System for Three-Phase Induction Motor", *IEEE Trans. on Industry Applications*, Vol. IA-27, No. 2, March/April 1991.

2.2.1.1 Alger, P. L., 1970, "Induction Machines", *Gordon and Breach Science Publisher*, New York, USA.

2.2.2.1 Brosch, P. F., 1989, "Moderne Stromichterantriebe", *Vogel Buchverlag*, Würzburg, Germany.

2.2.2.2 Jones, C. V., 1967, "The Unified Theory of Electrical Mashines", *Butterworths*, London, UK.

2.2.2.3 Adkins, B., and Harley, R. G., 1979, "The General Theory of Alternating Current Machines", *Chapman and Hall*, London, UK.

2.2.2.4 O'Kelly, D., and Simmons, S, 1968, "Generalized Electrical Machine Theory", *McGraw-Hill Publishing Company*, London, UK.

2.2.2.5 Jayawant, B. V., 1968, "Induction Mashines", *McGraw-Hill Publishing Company*, London, UK.

2.2.2.6 Kreyszig, E., 1979, "Advanced Engineering Mathematics", *John Wiley & Sons*, New York, USA.

2.2.2.7 Krause, P. C., and Thomas, C. H.,"Simulation of Symmetrical Induction Machinery", *IEEE Trans. on Power Apparatus and Systems*, Vol. PAS-84, No.11, November 1965.

2.2.2.8 Krause, P. C., "Method of Multiple Reference Frames Applied to the Analysis of Symmetrical Induction Machinery", *IEEE Trans. on Power Apparatus and Systems*, Vol. PAS-87, No. 1, January 1986.

2.2.2.9 Osheba, S. M., Abdel-Kader, F. M., "Dynamic performance analysis of reluctance motors using damping and synchronising torques", *IEE Proceedings*, Vol. 137, Pt.B., No. 4,July 1990.

2.2.2.10 Ho, E. Y. Y., and Sen, P. C., "Digital Simulation of PWM Induction Motor Drives for Transient and Steady-State Performance", *IEEE Trans. on Industrial Electronics*, Vol. IE- 33 No.1, February 1986.

2.2.2.11 Bowes, S. R., and Clements, R. R., "Computer-aided design of PWM inverter systems", *IEE Proceedings*, Vol. 129, Pt. B., No.1, January 1982.

2.2.2.12 Hindmarsh, J., 1984, "Electrical Machines and their Applications", *Pergamon Press*, Oxford, UK.

2.2.2.13 Seely, S., 1962, "Electromechanical Energy Conversion", *McGraw-Hill Book Company*, New York, USA.

2.2.2.14 Bowes, S. R., and Clare, J., "Steady-state performance of PWM inverter drives", *IEE Proceedings*, Vol. 130, Pt. B, No. 4, July 1983

2.2.2.15 Luk, C. K. P., Jayne, M. G., Rees, D. and Schaper, D. W., "A Digital Model for Three-phase Induction Motor Drives using a Personal Computer (PC) Software Package", 5th *IFAC Symposium on Computer Aided Design in Control Systems*, Swansea, UK, Pergamon Press, 1991

2.3.1 Jayne, M. G., Bowes, S. R., and Bird, B. M., "Developments in PWM inverters", *Proceedings of 2nd IFAC Symposium on Control in Power Electronics*, Düsseldorf, October 1975.

2.4.1 Ramierez, R. W., 1985, "The FFT Fundamentals and Concepts", *Prentice Hall Inc.*, London, UK.

2.4.2 Oran Brigham, E., 1988, "The Fast Fourier Transform and its Application", *Prentice Hall Inc.*, London, UK.

2.4.3 Thrane, N., 1979, "Discrete Fourier Transform and FFT Analyzers", *Brüel & Kjær Technical Review* , Søborg, Denmark.

2.5.1 Onishi, K., Suzuki, H., Miyachi, K., and Terashima, M. "Decoupling Control of Secundary Flux and Secondary Current in Induction Motor Drive with Controlled Voltage Source and Its Comparison with Volts/Herts Control", *IEEE Trans. on Industry Applications*, Vol. IA-27, No.1, January/February 1985.

4.3.1 Luk, C. K. P., 1992, "The Transputer Control of Induction Motor Drives", *PhD Thesis*, CNAA, UK.

4.4.1 Atzler, T., and Dude, J., 1986, "Aufbau eines Prüfstandes für umrichtergespeiste Maschine", *Dipl.-Ing.(FH) Thesis*, Hannover, Germany.

4.4.2 Münzebroek, A., 1990, "Drehfeldmessung und Drehfelddarstellung", *Dipl.-Ing.(FH) Thesis*, Hannover, Germany.

Appendix

Appendix A: The motor data

The machine used was a 2.2 kW, 3-Phase, 4 Pole machine fitted with an encoder with 1024 pulses/rev and forced ventilation at the non-drive end. The supply voltage is 240V/415V and the slip is 4.91% at 50 Hz.

The manufacturer supplied the following information about the machine:

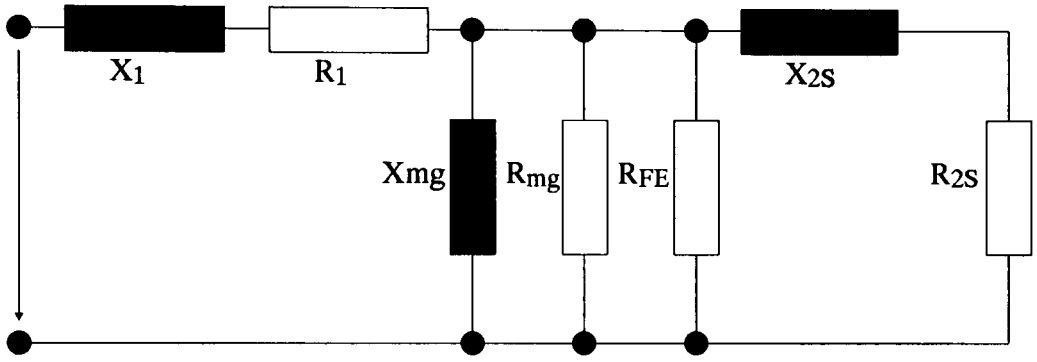

Fig. 85: The equivalent circuit from Manufacturer

X_1, stator leakage inductance	: 3.661Ω
R_1, stator resistance	: 3.76Ω
X_{mg}, magnetising reactance	: 84.2Ω
R_{mg}, equivalent resistance for mechanical losses	: 1387Ω
R_{FE}, equivalent resistance for iron losses	: 1153Ω
X_{2S}, rotor leakage inductance (referred to stator)	: 8.765Ω
R_{2S}, rotor resistance (referred to stator)	: 2.571Ω

Appendix B: Program listings

1. Supply modules

Sinusoidal voltage wave module

```
%sinus.m
%ver 21.05.90
%calculates sinwave

fm=input('frequency                    : ');
Tm=1/fm;
n =input('samplepoints per halfcycle : ');
ck=input('number of cycles             : ');
m=240*sqrt(2);
N=2*n;
Nc=N*ck;

%generating sinewaveout

  for i=1:Nc;
    pa(i)=m*sin((i-1)*2*pi/N); %sinewave Phase A
    pb(i)=m*sin((i-1)*2*pi/N+pi*2/3); %sinewavePhase B
    pc(i)=m*sin((i-1)*2*pi/N+pi*4/3); %sinewave Phase C
  end;

end
```

Regular Sampled Symmetric PWM voltage wave module

```
%rsm.m
%vers 18.03.90
%generates regular sampled symmetric PWM

fm=input('Modulating frequency                    = ');
R =input('Frequency ratio                         = ');
```

```
m =input('Modulating index                                    = ');
n =input('Number of samplingpoints per carrier halfcycle = ');
t=1/fm;
z=-1;
ck=input('Number of cycles                                    = ');
vz=240*sqrt(2);
N=2*n*R;
Nc=N*ck;

% Calculation of carrier and modulation wave

  for i=1:Nc;
    mga(i)=m*sin((i-1)*2*pi/N);
    mgb(i)=m*sin((i-1)*2*pi/N+2*pi/N);
    mgc(i)=m*sin((i-1)*2*pi/N+4*pi/N);

      if rem(i,n)==1
        z=z+1;
      end;

      if rem(i,(2*n))==1
        ma(i)=mga(i);
        mb(i)=mgb(i);
        mc(i)=mgc(i);
      else
        ma(i)=ma(i-1);
        mb(i)=mb(i-1);
        mc(i)=mc(i-1);
      end;

    a(i)=i-(z*n);
      if rem(z,2)==0
        c(i)=1-(2*(a(i)-1)/n);
          if c(i)>ma(i)
            pa(i)=-vz;
          else
            pa(i)=vz;
          end;
```

```
            if c(i)>mb(i)
              pb(i)=-vz;
            else
              pb(i)=vz;
            end;
            if c(i)>mc(i)
              pc(i)=-vz;
            else
              pc(i)=vz;
            end;
        else
          c(i)=(2*(a(i)-1)/n)-1;
            if c(i)<ma(i)
              pa(i)=vz;
            else
              pa(i)=-vz;
            end;
            if c(i)<mb(i)
              pb(i)=vz;
            else
              pb(i)=-vz;
            end;
            if c(i)<mc(i)
              pc(i)=vz;
            else
              pc(i)=-vz;
            end;
        end;
    end;

end
```

Regular Sampled Asymmetric PWM voltage wave module

```
%rsm.m
%vers 18.03.90
%generates regular sampled symmetric PWM
```

```
fm=input('Modulating Frequency                                    = ');
R =input('Frequency ratio                                         = ');
m =input('Modulating index                                        = ');
n =input('Number of samplingpoints per carrier halfcycle = ');
ck=input('Number of cycles                                        = ');
N=2*n*R;
Nc=N*ck;
Tm=1/fm;
z=-1;
vz=240*sqrt(2);

% Calculation of carrier and modulation wave

for i=1:Nc;
    mga(i)=m*sin((i-1)*pi/n/R);
    mgb(i)=m*sin((i-1)*pi/n/R+pi*2/3);
    mgc(i)=m*sin((i-1)*pi/n/R+pi*4/3);
      if rem(i,n)==1
        z=z+1;
      end;
      if rem(i,n)==1
        ma(i)=mga(i);
        mb(i)=mgb(i);
        mc(i)=mgc(i);
      else
        ma(i)=ma(i-1);
        mb(i)=mb(i-1);
        mc(i)=mc(i-1);
      end;
    a(i)=i-(z*n);
      if rem(z,2)==0
        c(i)=1-(2*(a(i)-1)/n);
          if c(i)>ma(i)
            pa(i)=-vz;
          else
            pa(i)=vz;
          end;
          if c(i)>mb(i)
```

```
            pb(i)=-vz;
          else
            pb(i)=vz;
          end;
          if c(i)>mc(i)
            pc(i)=-vz;
          else
            pc(i)=vz;
          end;
        else
          c(i)=(2*(a(i)-1)/n)-1;
          if c(i)<ma(i)
            pa(i)=vz;
          else
            pa(i)=-vz;
          end;
          if c(i)<mb(i)
            pb(i)=vz;
          else
            pb(i)=-vz;
          end;
          if c(i)<mc(i)
            pc(i)=vz;
          else
            pc(i)=-vz;
          end;
        end;

end
```

2. Three phase to two phase transformation module

```
%cabctdq.m
%ver 10.05.90
%calculation of d-q (stator) voltages
```

```
Konst=[1 -1/2 -1/2;0 -1/2*sqrt(3) 1/2*sqrt(3);1 1 1]';
const=inv(Konst);

 for i=1:Nc+1;
   vpwm=[pa(i) pb(i) pc(i)]';
   vqd=const*vpwm;vqd=vqd';
   vd(i)=vqd(1);
   vq(i)=vqd(2);
 end;

end
```

3. Direct on line startup module

```
%dol.m
%ver 10.07.90
%direct on line

dt=Tm/N;
j=sqrt(-1);
Ls =0.27965;  %input('Xs  : ');
Lr =0.2959;   %input('Xr  : ');
Lm=0.268;     %input('Xsr : ');
Rs =3.76;     %input('Rs  : ');
Rr =2.571;    %input('Rr  : ');
Wr(1)=0;
kf=0.001;
J=0.2;

A1=[0 0 0 0]';
G=[0 0 0 0;0 0 0 0;0 Lm 0 Lr;-Lm 0 -Lr 0];
Re=[Rs 0 0 0;0 Rs 0 0;0 0 Rr 0;0 0 0 Rr];
X=[Ls 0 Lm 0;0 Ls 0 Lm;Lm 0 Lr 0;0 Lm 0 Lr];

 for k=1:Nc;
   time(k)=(k-1)*dt;
```

```
    F=inv(X)*((Wr(k)*G)+Re);
    A=-F;
    B=inv(X);
    [Phi,Gamma]=c2d(A,B,dt);
    u=[vd(k) vq(k) 0 0]';
    A2=Phi*A1+Gamma*u;
    A1=A2;
    psis(k)=A1(1)+j*A1(2);
    Ids(k)=A1(1);
    Iqs(k)=A1(2);
    Idr(k)=A1(3);
    Iqr(k)=A1(4);
    IM=[Ids(k) Iqs(k) 0]';
    Iabc=Konst*IM;
    Ia(k)=Iabc(1);
    Ib(k)=Iabc(2);
    Ic(k)=Iabc(3);
    Te(k)=3*Lm*(Idr(k)*Iqs(k)-Ids(k)*Iqr(k));
    k0=dt*(2/J)*(Te(k)-kf*Wr(k));
    k1=dt*(2/J)*(Te(k)-kf*(Wr(k)+k0/2));
    k2=dt*(2/J)*(Te(k)-kf*(Wr(k)+k1/2));
    k3=dt*(2/J)*(Te(k)-kf*(Wr(k)+k2));
    Wr(k+1)=Wr(k)+k0/6+k1/3+k2/3+k3/6;
  end;

end
```

4. Steady state solution module using with Park vector

```
%park.m
%ver 10.07.90
%calculation of flux with park vector

km=N/6;
dt=Tm/N;
j=sqrt(-1);
```

```
Ls =0.27965;
Lr =0.2959;
Lm =0.268;
Rs =3.76;
Rr =2.571;
Speed=input('Speed  : ');
Wr=Speed*pi/15;

G=[0 0 0 0;0 0 0 0;0 Lm 0 Lr;-Lm 0 -Lr 0];
Re=[Rs 0 0 0;0 Rs 0 0;0 0 Rr 0;0 0 0 Rr];
X=[Ls 0 Lm 0;0 Ls 0 Lm;Lm 0 Lr 0;0 Lm 0 Lr];
F=inv(X)*((Wr*G)+Re);
A=-F;
B=inv(X);

[Phi,Gamma]=c2d(A,B,dt);
a=real(exp(j*pi/3));
b=imag(exp(j*pi/3));
M=[a -b 0 0;b a 0 0;0 0 a -b;0 0 b a];
sumu=[0;0;0;0];

  for k=1:km
    u=[vd(k) vq(k) 0 0]';
    sumu=Phi*sumu+Gamma*u;
  end;

A1=inv(M-Phi^(km))*sumu;
xinit=A1;
isis(1)=A1(1)+j*A1(2);
Ids(1)=A1(1);
Iqs(1)=A1(2);
Idr(1)=A1(3);
Iqr(1)=A1(4);

  for k=1:(Nc-1)
    u=[vd(k) vq(k) 0 0]';
    A2=Phi*A1+Gamma*u;
    A1=A2;
```

```
    isis(k+1)=A1(1)+j*A1(2);
    Ids(k+1)=A1(1);
    Iqs(k+1)=A1(2);
    Idr(k+1)=A1(3);
    Iqr(k+1)=A1(4);
  end;

sis(Nc+1)=isis(1);

  for kt=(N+1):Nc
    Ids(kt)=Ids(kt-N);
    Iqs(kt)=Iqs(kt-N);
  end;

  for i=1:Nc
    IM=[Ids(i) Iqs(i) 0]';
    Iabc=Konst*IM;
    Ia(i)=Iabc(1);
    Ib(i)=Iabc(2);
    Ic(i)=Iabc(3);
  end;

end
```

5. Calculation module of motor characteristic

```
%kar.m
%ver 18.07.90
%calculation of machine characteristic

Xmr =84.2;
Xsr =3.661;  %input('Xs  : ');
Xrr =8.765;  %input('Xr  : ');
Rs =3.76;  %input('Rs  : ');
Rr =2.571; %input('Rr  : ');
vl=240;
```

```
s=1;
f=input('Supply Frequency  : ');
Xm=Xmr*f/50;
Xs=Xsr*f/50;
Xr=Xrr*f/50;
v=vl*Xm/sqrt(Rs^2+(Xs+Xm)^2);

  for i=1:99;
     Speed(i)=(1-s)*f*30;
     Te(i)=(3/(pi*f))*v^2/(((Rs+Rr/s)^2)+(Xs+Xr)^2)*Rr/s;
     s=s-0.01;
  end;

Speed(100)=f*30;
Te(100)=0;

end
```

6. Fast Fourier Transformation module

```
ta=length(pa);
y=fft(pa,ta);
Y=y .*conj(y)/(ta^2);
z=sqrt(Y)*2;
f=(0:1:(ta/2));
tx=[f;f;f];
tx=tx(:);
ya=[zeros(1,fix(ta/2+1));z(1:ta/2+1);zeros(1,fix(ta/2+1))];
ya=ya(:);
plot(tx,ya)
```

7. Vector field control module with ideal VVVF

```
%start presets
x0=[0 0 0 0]';
theta=0;
wr(1)=0;
t(1)=0;
sa=0;
sb=0;
sc=0;

for i=1:n
  %controller every 1ms and pwm
    if rem((i-1),10)==0
      Tt=gain*(wrt-wr(i));
      iqt=Tt*Lr/(Lm*Lm*idt);
      wsl=iqt*fac1;
      vdt=idt*Rs-iqt*Lsi*we;
      vqt=iqt*Rs+idt*Ls*we;
      v=sqrt(vdt^2+vqt^2);
      vm(i)=v;
      ang=atan2(vqt,vdt);
      theta=theta+we*dt;
      we=wr(i)+wsl;
    else
      vm(i)=v;
      theta=theta+we*dt;
    end;
    va(i)=v*sin(theta+ang);
    vb(i)=v*sin(theta+ang+2*pi/3);
    vc(i)=v*sin(theta+ang+4*pi/3);
    A=-B*(wr(i)*G+R);
    [phi,gam]=c2d(A,B,dt);
    %apply data  to motor
    u=C*[va(i) vb(i) vc(i)]';
    u=u';
    x1=phi*x0+gam*[u(1) u(2) 0 0]';
    Te(i)=3*Lm*(x1(3)*x1(2)-x1(1)*x1(4));
```

```
    k0=dt*(2/J)*(Te(i)-kf*wr(i));
    k1=dt*(2/J)*(Te(i)-kf*(wr(i)+k0/2));
    k2=dt*(2/J)*(Te(i)-kf*(wr(i)+k1/2));
    k3=dt*(2/J)*(Te(i)-kf*(wr(i)+k2));
    wr(i+1)=wr(i)+k0/6+k1/3+k2/3+k3/6;
    x0=x1;
    t(i+1)=t(i)+dt;
    pt=t(i)/n/dt;
    clc;
    %disp(pt, vm(i), wr(i));
  end;

end
```

8. Vector field control module with PWM

```
%vector field control
%ver 15.5.91

%startup inputs
idt=input('Direct axis current :');
vn=input('DC-Link voltage : ');
nrt=input('Speed          :');
wrt=nrt*2*pi/60/2;
n=input('Number of points : ');
gain=input('gain          :');
kf=input('friction factor  :');
dt=input('time increment   :');

%motor data
Rs=3.76;
Rr=2.571;
Lm=0.268;
Ls=0.27965;
Lr=0.2959;
```

```
Lsi=(Ls*Lr-Lm^2)/Lr;
J=0.02;

%Matrix Equations of Motor
C=(2/3)*[1 -1/2 -1/2;0 -sqrt(3)/2 sqrt(3)/2;1/2 1/2 1/2];
L=[Ls 0 Lm 0;0 Ls 0 Lm;Lm 0 Lr 0;0 Lm 0 Lr];
R=[Rs 0 0 0;0 Rs 0 0;0 0 Rr 0;0 0 0 Rr];
G=[0 0 0 0;0 0 0 0;0 Lm 0 Lr;-Lm 0 -Lr 0];
B=inv(L);

%Startup Data
x0=[0 0 0 0]';
theta=0;
wr(1)=0;
we=0;
t(1)=0;

%preset to simplify colculation, to be changed if idt gets changed
fac1=Rr/Lr/idt;

  for i=1:n
    %Vector Field Control
    k=(i-1)*10+1;
    Tt=gain*(wrt-wr(k));
    iqt=Tt*Lr/(Lm*Lm*idt);
    wsl=iqt*fac1;
    we=wr(k)+wsl;
    vdt=idt*Rs-iqt*Lsi*we;
    vqt=iqt*Rs+idt*Ls*we;
    %Transform Control Inform. to Supply
    v=sqrt(vdt^2+vqt^2);
    ang=atan2(vqt,vdt);
    theta=theta+we*10*dt;
    ph=theta+ang;

      %prepararion of PWM
      M=v/vn;
      if M>1
```

```
M=1;
end;
fm=we/2/pi;
R=33;
Tc=1/R/fm;
 %generation of pwm
werta=sin(ph)+sin((pi/R)+ph);
ta(1)=(Tc/2)*(1+(M/2)*werta);
wertb=sin(ph+2/3*pi)+sin((pi/R)+ph+2/3*pi);
tb(1)=(Tc/2)*(1+(M/2)*wertb);
wertc=sin(ph+4/3*pi)+sin((pi/R)+ph+4/3*pi);
tc(1)=(Tc/2)*(1+(M/2)*wertc);
  for q=2:2*R+1
    werta=sin((pi*(q-1)/R)+ph)+sin((pi*q/R)+ph);
    ta(q)=ta(q-1)+(Tc/2)*(1+((-1)^(q-1))*(M/2)*werta);
    wertb=sin((pi*(q-1)/R)+ph+2/3*pi)+sin((pi*q/R)+ph+2/3*pi);
    tb(q)=tb(q-1)+(Tc/2)*(1+((-1)^(q-1))*(M/2)*wertb);
    wertc=sin((pi*(q-1)/R)+ph+4/3*pi)+sin((pi*q/R)+ph+4/3*pi);
    tc(q)=tc(q-1)+(Tc/2)*(1+((-1)^(q-1))*(M/2)*wertc);
  end;
td=0;
ja=1;
jb=1;
jc=1;
tca=Tc/2;
tcb=Tc/2;
tcc=Tc/2;

  for ki=(i-1)*10+1:i*10
    td=td+dt;
    %sampling pwm
    %phase a
      if rem(ja,2)==0
        if td<=ta(ja)
          va=vn;
        else
          va=-vn;
            if td>=tca
```

```
            tca=tca+Tc/2;
            ja=ja+1;
        end;
    end;
else
    if td<=ta(ja)
        va=-vn;
    else
        va=vn;
        if td>=tca
            tca=tca+Tc/2;
            ja=ja+1;
        end;
    end;
end;
%phase b
if rem(jb,2)==0
    if td<=tb(jb)
        vb=vn;
    else
        vb=-vn;
        iftd>=tcb
        tcb=tcb+Tc/2;
        jb=jb+1;
    end;
    end;
else
    if td<=tb(jb)
        vb=-vn;
    else
        vb=vn;
        if td>=tcb
            tcb=tcb+Tc/2;
            jb=jb+1;
        end;
    end;
end;
%phase c
```

```
        if rem(jc,2)==0
          if td<=tc(jc)
            vc=vn;
          else
            vc=-vn;
              if td>=tcc
                tcc=tcc+Tc/2;
                jc=jc+1;
              end;
          end;
        else
          if td<=tc(jc)
            vc=-vn;
          else
            vc=vn;
              if td>=tcc
                tcc=tcc+Tc/2;
                jc=jc+1;
              end;
          end;
        end;
%D/Q Transformation of Supply Voltage
u=C *[va vb vc]';
u=u';
%Mathematical Transformation for State variable
A=-B*(wr(ki)*G+R);
%Digitazitation of State Equation and Solution of Eq.
[phi,gam]=c2d(A,B,dt);
x1=phi*x0+gam*[u(1) u(2) 0 0]';
Te(ki)=3*Lm*(x1(3)*x1(2)-x1(1)*x1(4));
%Speed Integration ala Runge Kutta
k0=dt*(2/J)*(Te(ki)-kf*wr(ki));
k1=dt*(2/J)*(Te(ki)-kf*(wr(ki)+k0/2));
k2=dt*(2/J)*(Te(ki)-kf*(wr(ki)+k1/2));
k3=dt*(2/J)*(Te(ki)-kf*(wr(ki)+k2));
%updating for next go
wr(ki+1)=wr(ki)+k0/6+k1/3+k2/3+k3/6;
x0=x1;
```

```
        t(ki+1)=t(ki)+dt;
      end;
    end;

end
```

Appendix C: Direct-online start-up with sinusoidal supply

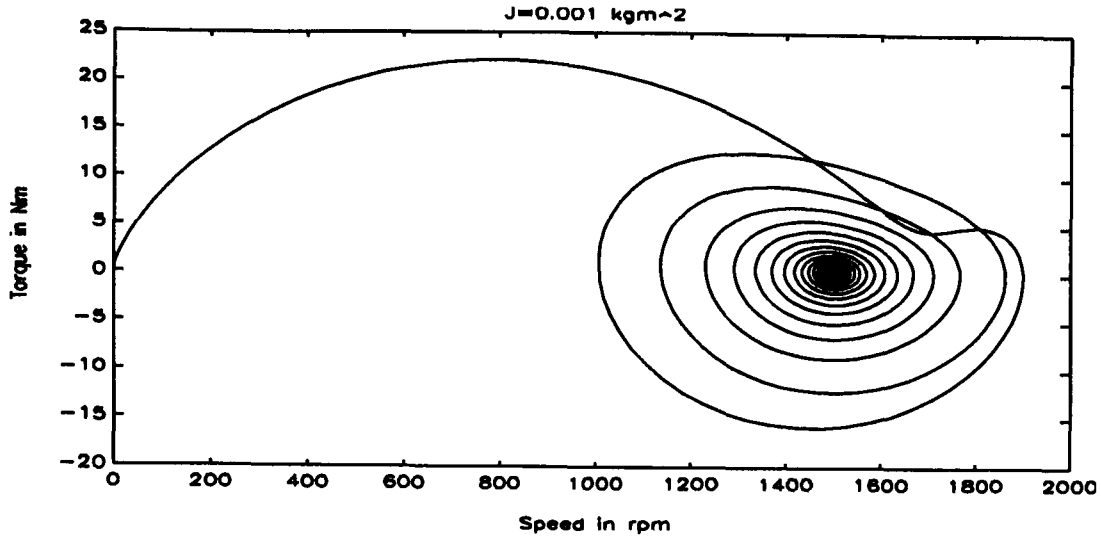

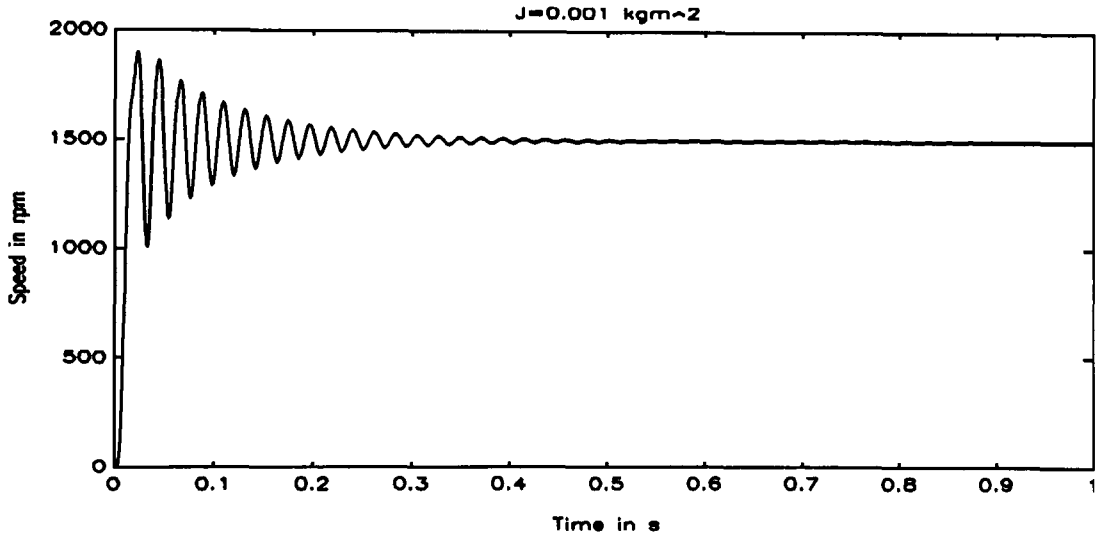

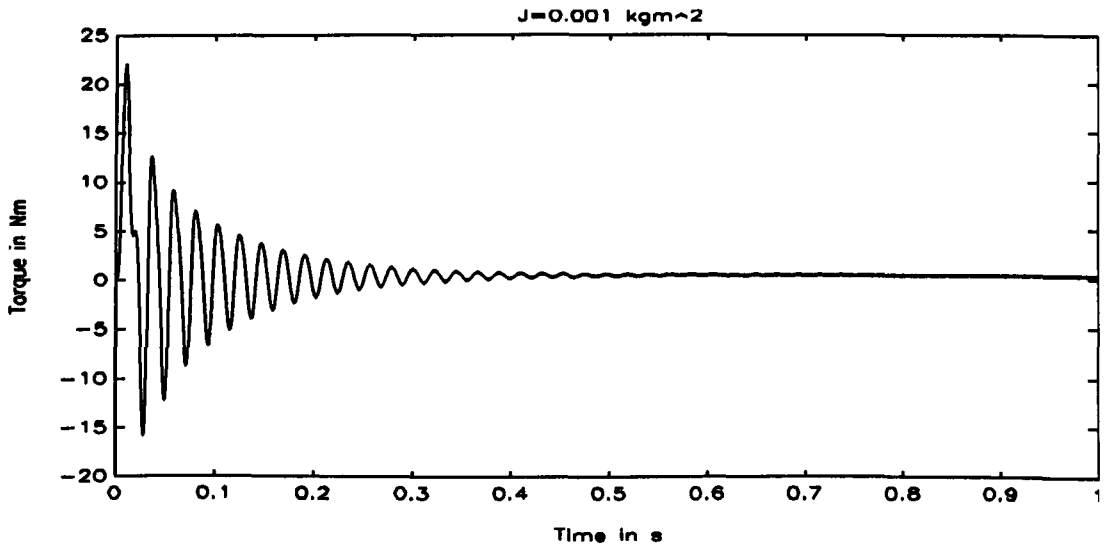

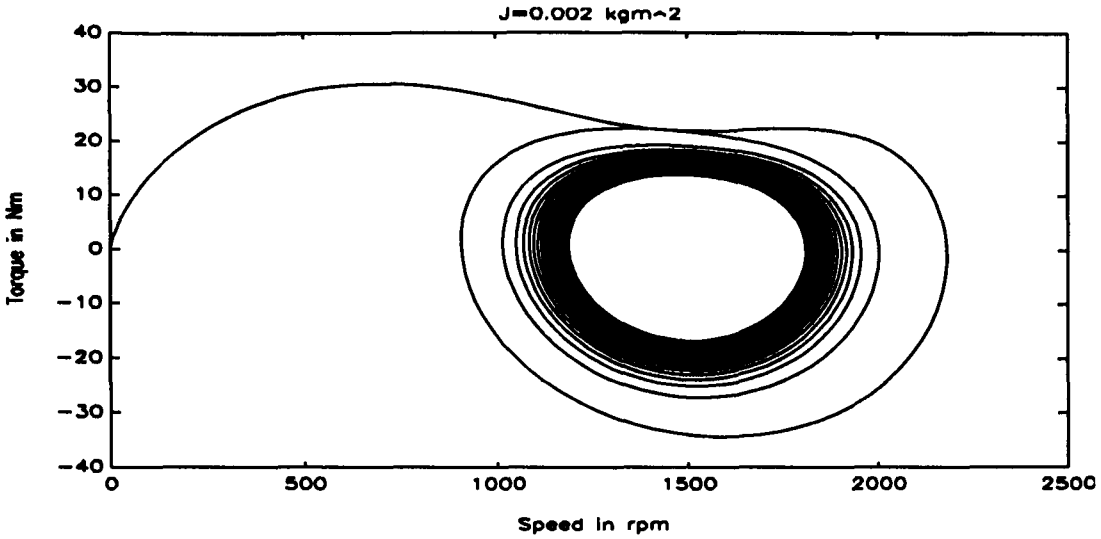
J=0.002 kgm^2
Torque in Nm
Speed in rpm
40
30
20
10
0
-10
-20
-30
-40
0
500
1000
1500
2000
2500

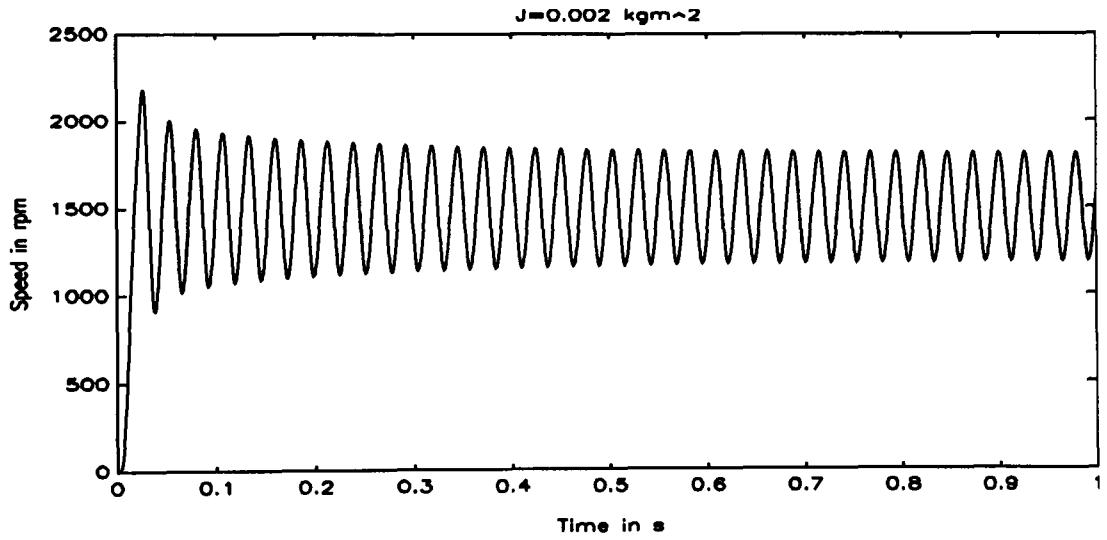
J=0.002 kgm^2
Speed in rpm
Time in s
2500
2000
1500
1000
500
0
0.1
0.2
0.3
0.4
0.5
0.6
0.7
0.8
0.9

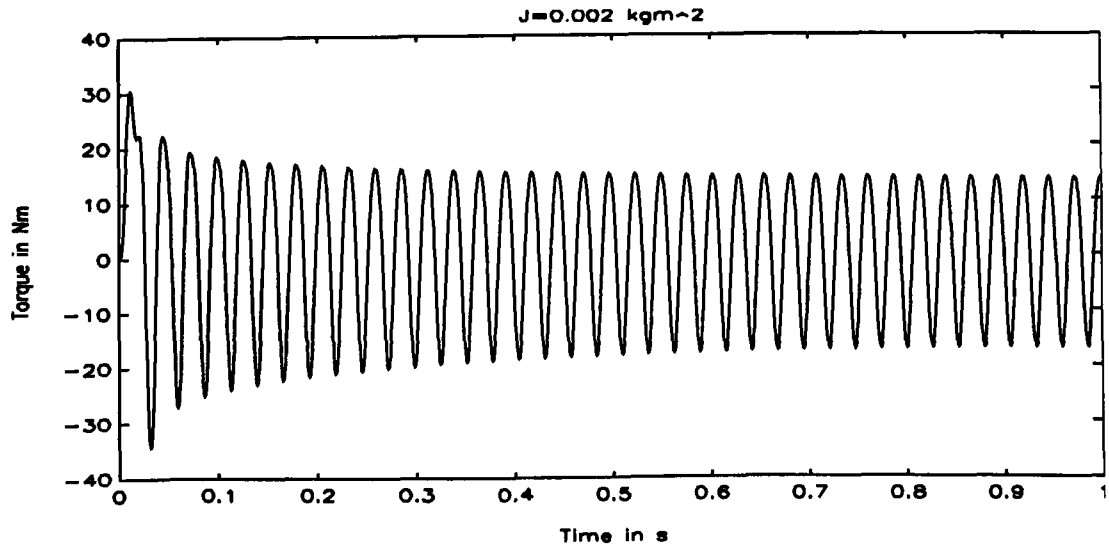
J=0.002 kgm^2
Torque in Nm
Time in s
40
30
20
10
0
-10
-20
-30
-40
0
0.1
0.2
0.3
0.4
0.5
0.6
0.7
0.8
0.9

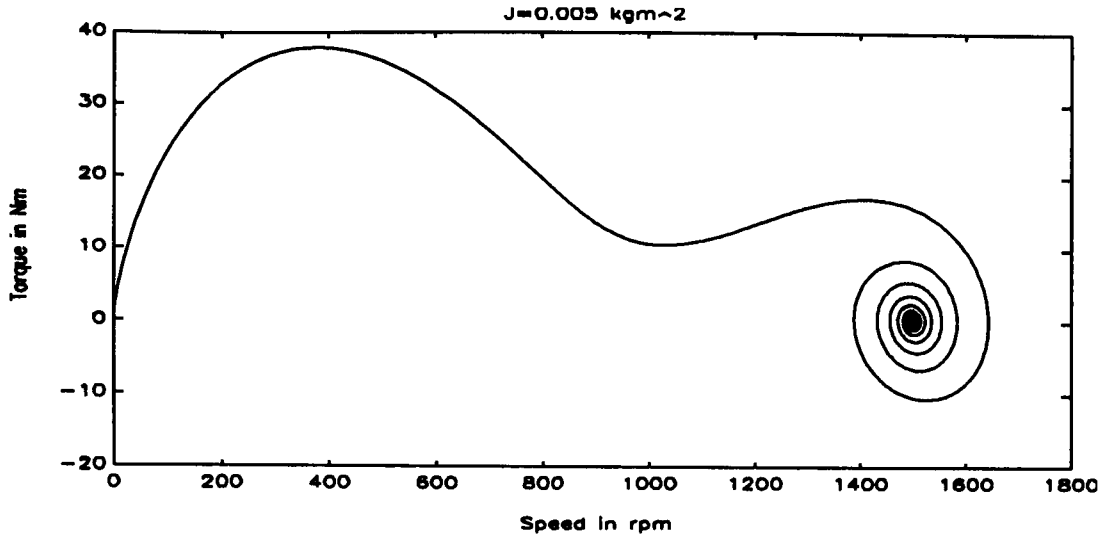
J=0.005 kgm^2
Torque in Nm
Speed in rpm
40
30
20
10
0
−10
−20
0
200
400
600
800
1000
1200
1400
1600
1800

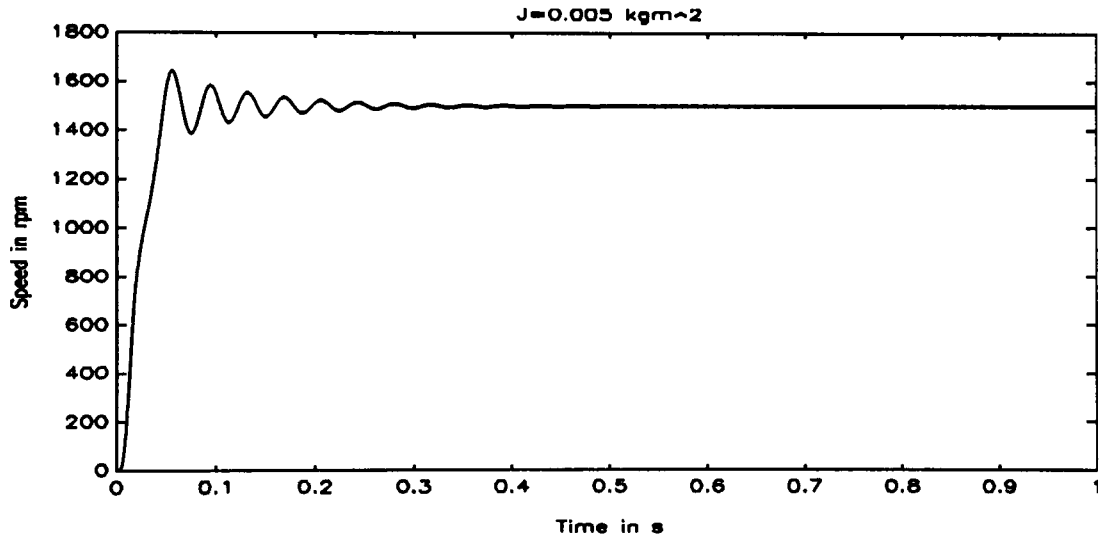
J=0.005 kgm^2
Speed in rpm
Time in s
1800
1600
1400
1200
1000
800
600
400
200
0
0
0.1
0.2
0.3
0.4
0.5
0.6
0.7
0.8
0.9

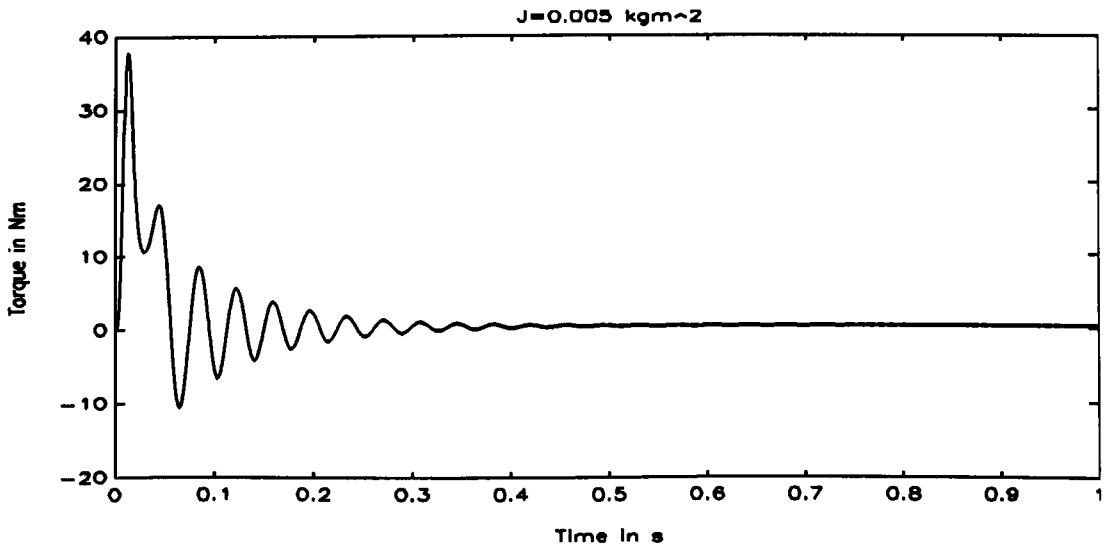
J=0.005 kgm^2
Torque in Nm
Time in s
40
30
20
10
0
−10
−20
0
0.1
0.2
0.3
0.4
0.5
0.6
0.7
0.8
0.9

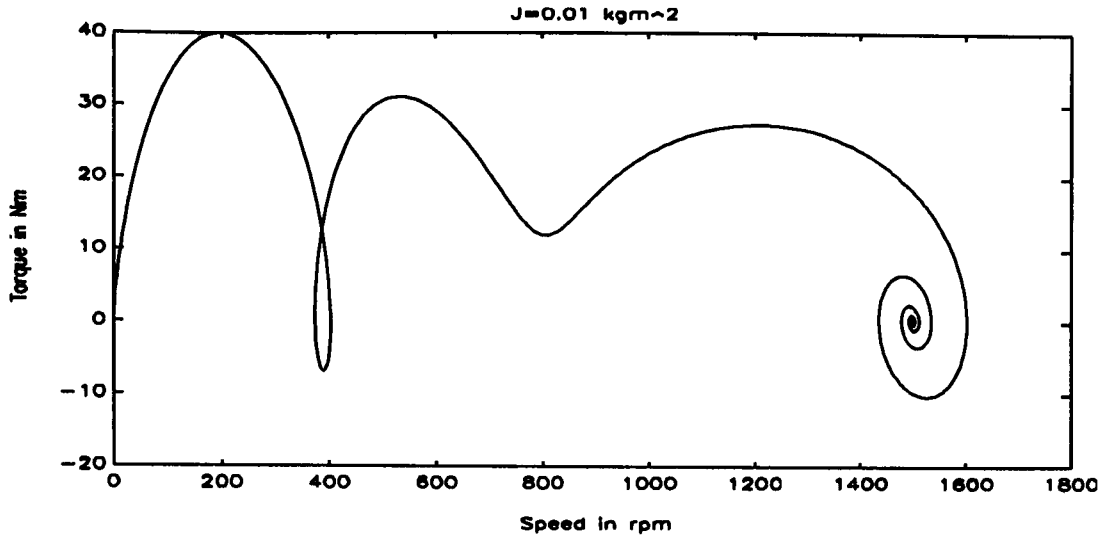
J=0.01 kgm^2
Torque in Nm
Speed in rpm
40
30
20
10
0
−10
−20
0
200
400
600
800
1000
1200
1400
1600
1800

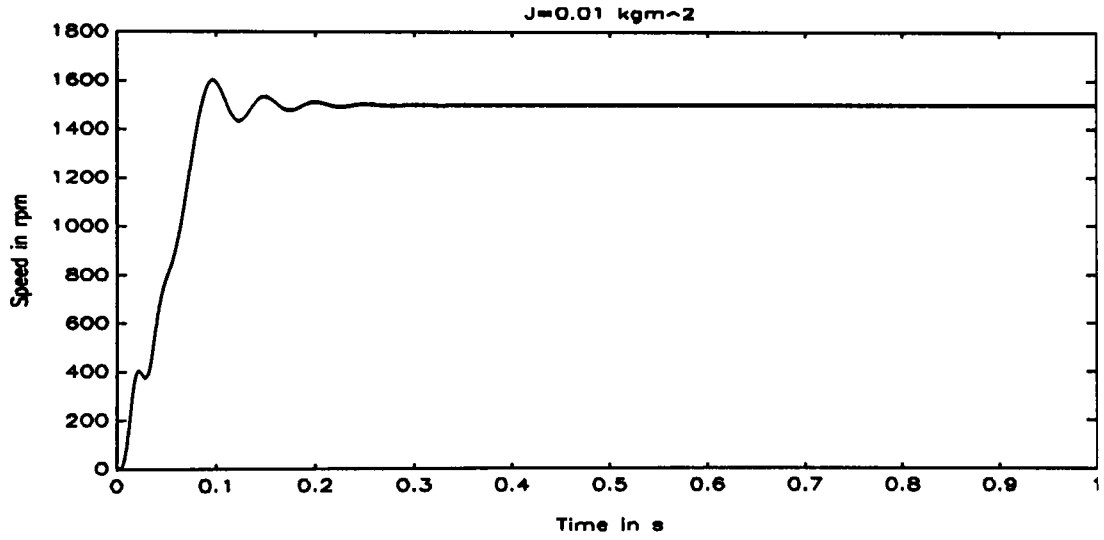
J=0.01 kgm^2
Speed in rpm
Time in s
1800
1600
1400
1200
1000
800
600
400
200
0
0
0.1
0.2
0.3
0.4
0.5
0.6
0.7
0.8
0.9

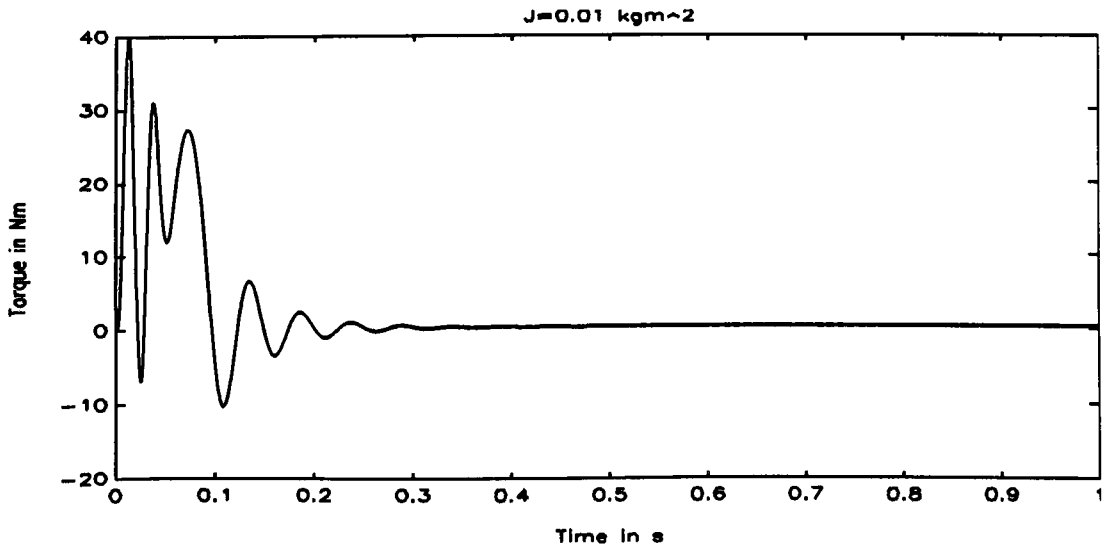
J=0.01 kgm^2
Torque in Nm
Time in s
40
30
20
10
0
−10
−20
0
0.1
0.2
0.3
0.4
0.5
0.6
0.7
0.8
0.9

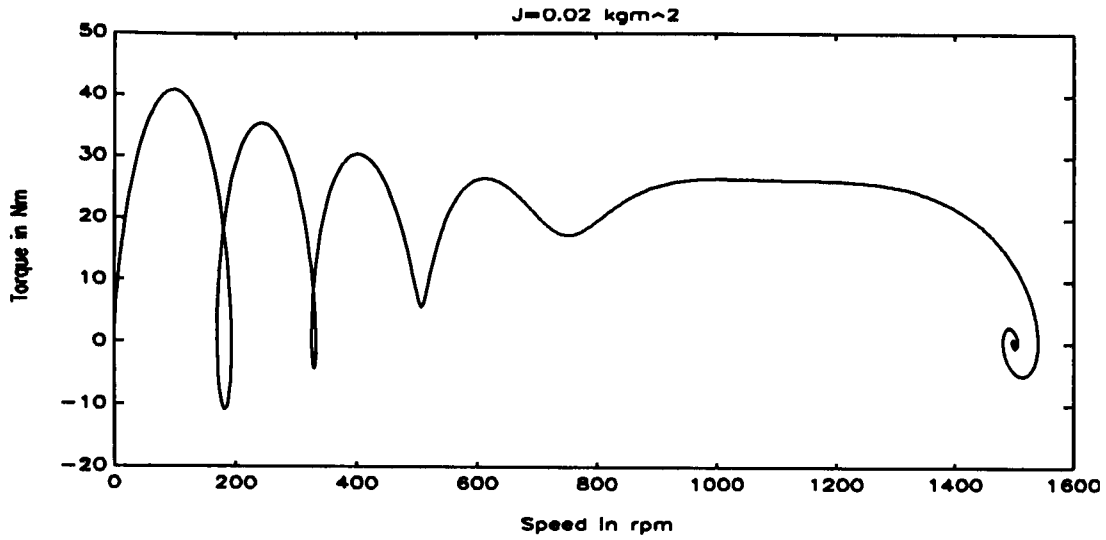
J=0.02 kgm^2
Torque in Nm
Speed in rpm
50
40
30
20
10
0
−10
−20
0
200
400
600
800
1000
1200
1400
1600

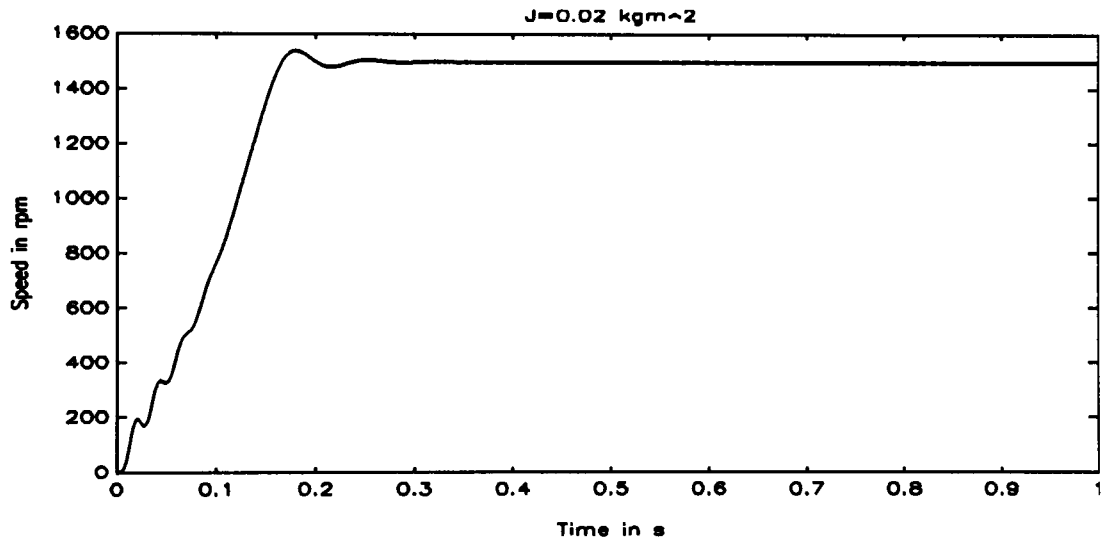
J=0.02 kgm^2
Speed in rpm
Time in s
1600
1400
1200
1000
800
600
400
200
0
0
0.1
0.2
0.3
0.4
0.5
0.6
0.7
0.8
0.9

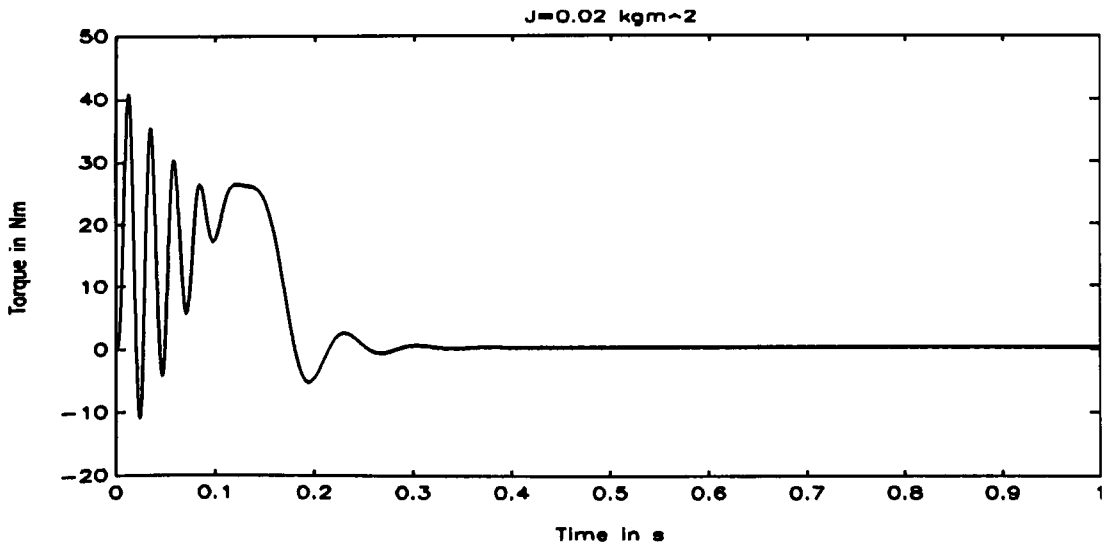
J=0.02 kgm^2
Torque in Nm
Time in s
50
40
30
20
10
0
−10
−20
0
0.1
0.2
0.3
0.4
0.5
0.6
0.7
0.8
0.9

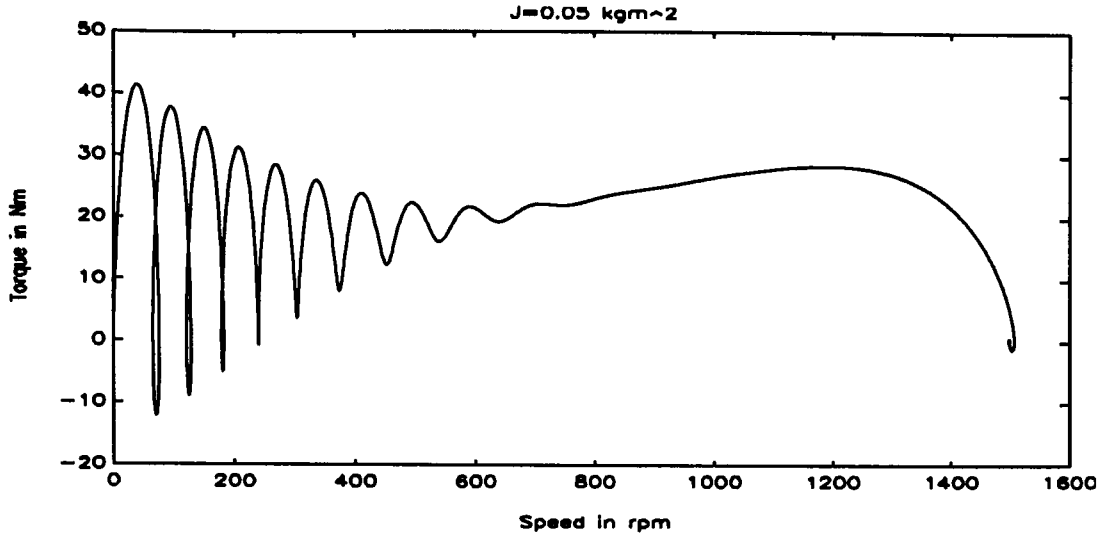
J=0.05 kgm^2
Torque in Nm
Speed in rpm
50
40
30
20
10
0
−10
−20
0
200
400
600
800
1000
1200
1400
1600

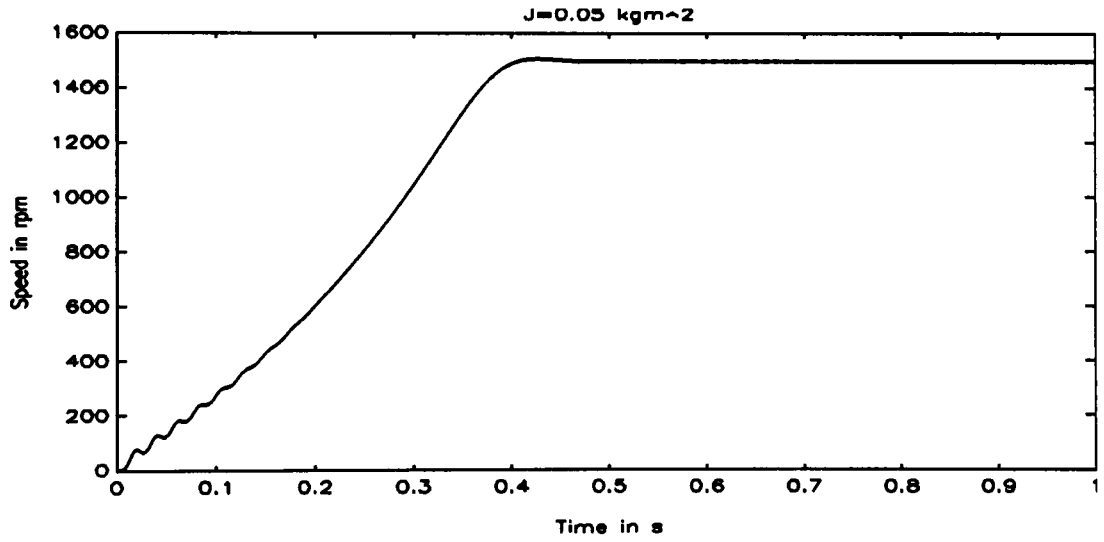
J=0.05 kgm^2
Speed in rpm
Time in s
1600
1400
1200
1000
800
600
400
200
0
0
0.1
0.2
0.3
0.4
0.5
0.6
0.7
0.8
0.9

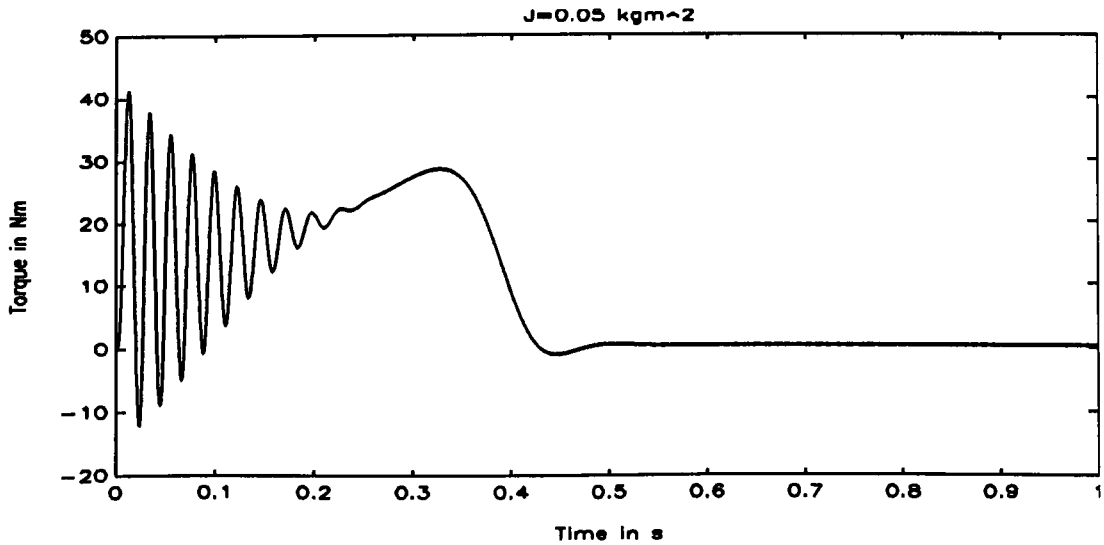
J=0.05 kgm^2
Torque in Nm
Time in s
50
40
30
20
10
0
−10
−20
0
0.1
0.2
0.3
0.4
0.5
0.6
0.7
0.8
0.9

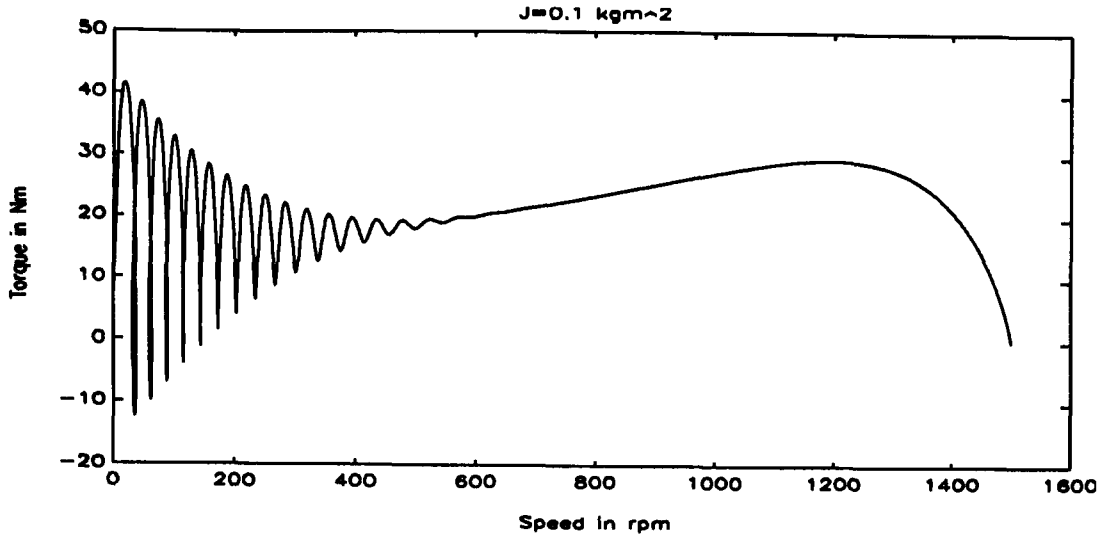
J=0.1 kgm^2
Torque in Nm
Speed in rpm
50
40
30
20
10
0
−10
−20
0
200
400
600
800
1000
1200
1400
1600

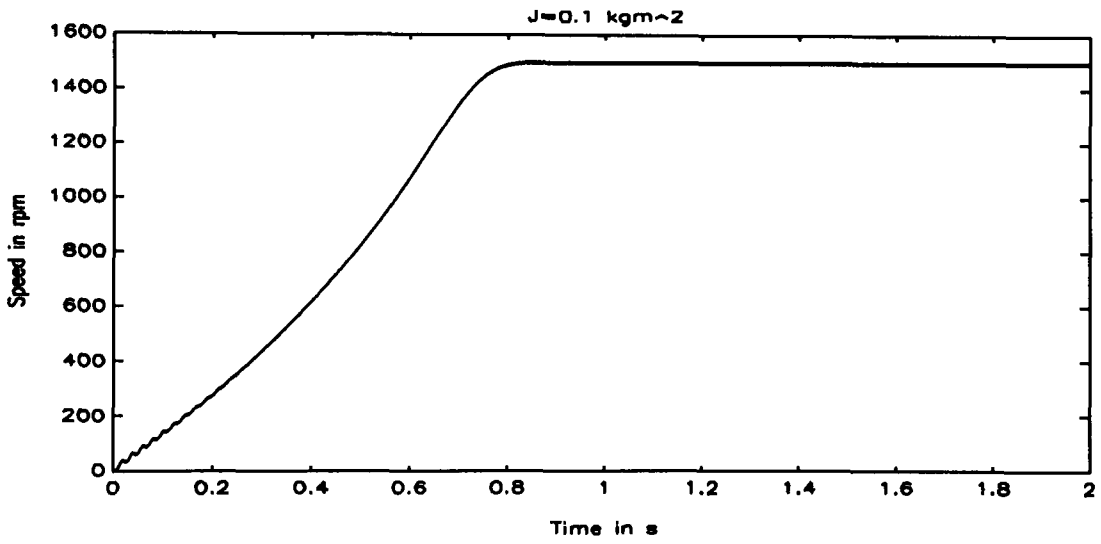
J=0.1 kgm^2
Speed in rpm
Time in s
1600
1400
1200
1000
800
600
400
200
0
0
0.2
0.4
0.6
0.8
1
1.2
1.4
1.6
1.8
2

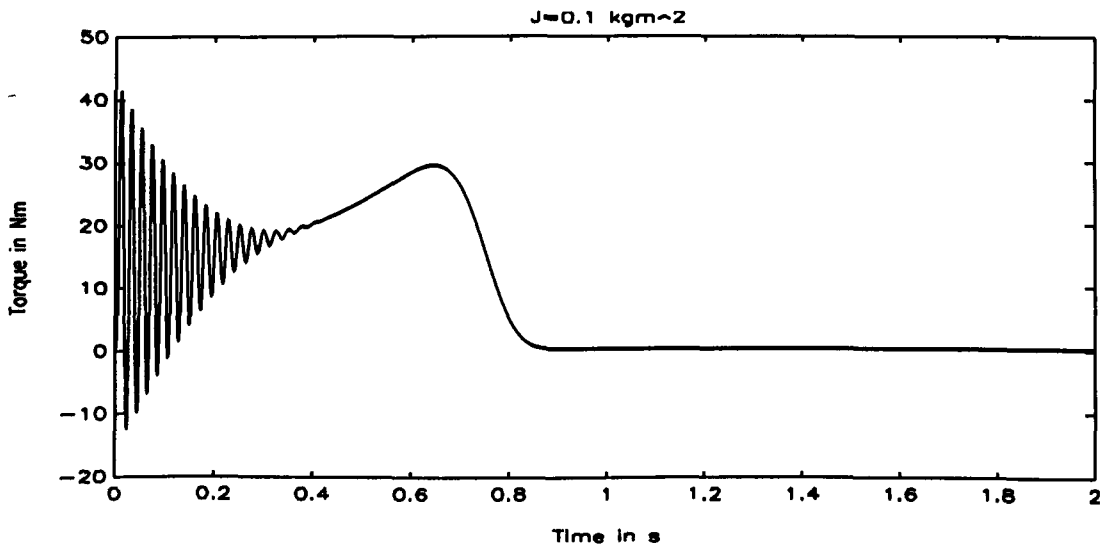
J=0.1 kgm^2
Torque in Nm
Time in s
50
40
30
20
10
0
−10
−20
0
0.2
0.4
0.6
0.8
1
1.2
1.4
1.6
1.8
2

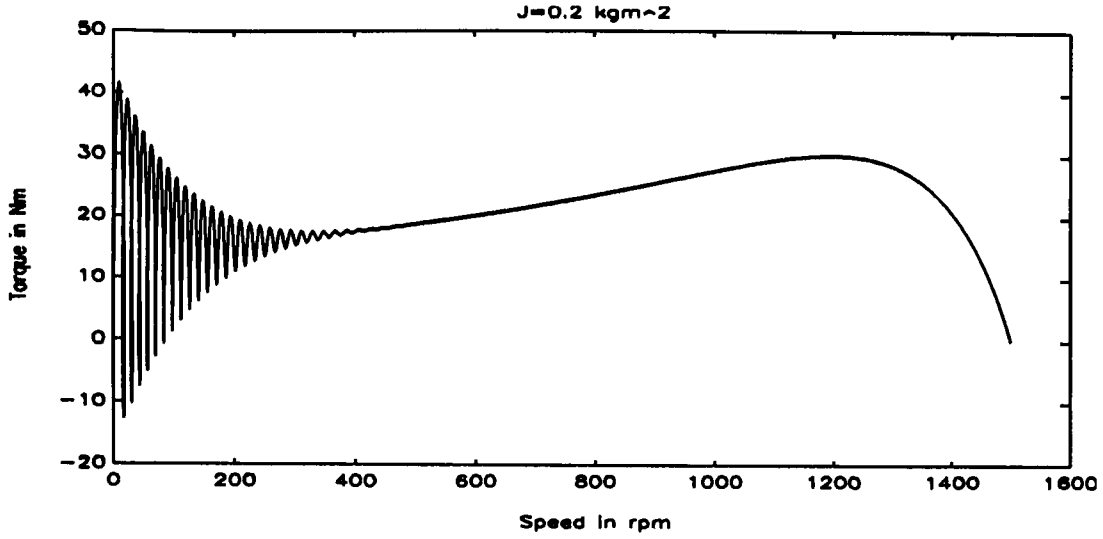
J=0.2 kgm^2
Torque in Nm
Speed in rpm
50
40
30
20
10
0
−10
−20
0
200
400
600
800
1000
1200
1400
1600

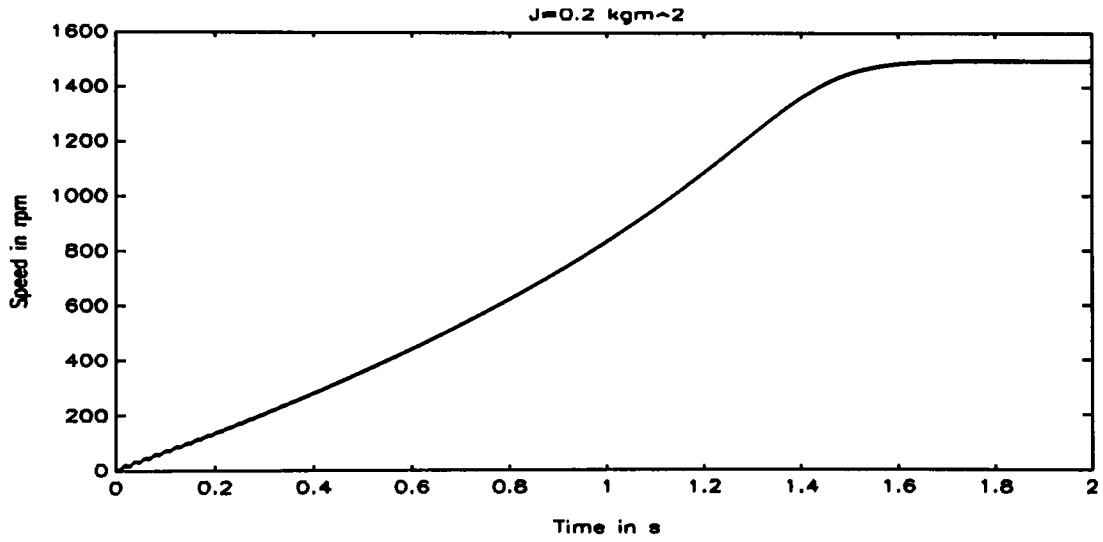
J=0.2 kgm^2
Speed in rpm
Time in s
1600
1400
1200
1000
800
600
400
200
0
0
0.2
0.4
0.6
0.8
1
1.2
1.4
1.6
1.8
2

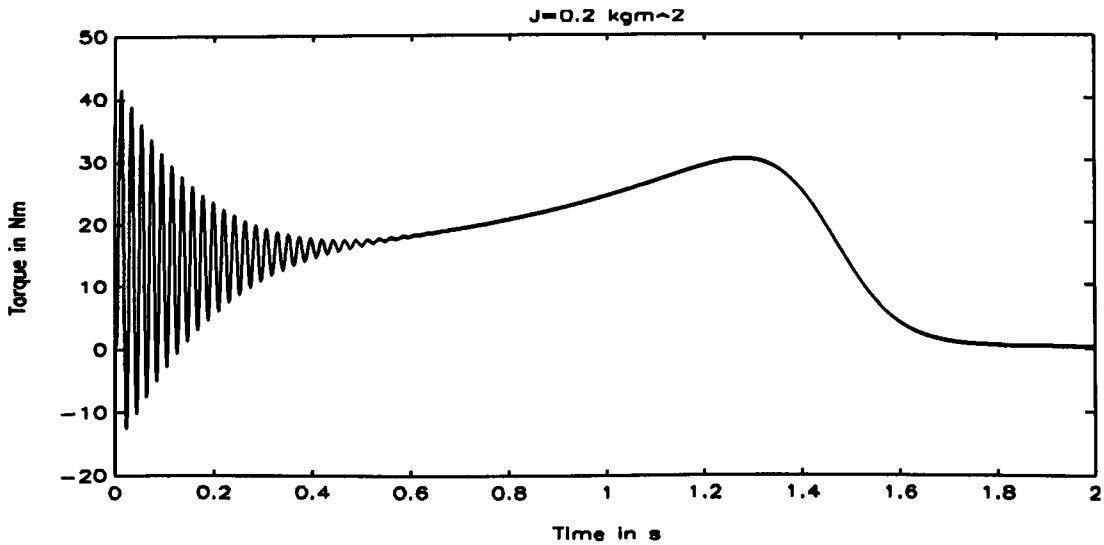
J=0.2 kgm^2
Torque in Nm
Time in s
50
40
30
20
10
0
−10
−20
0
0.2
0.4
0.6
0.8
1
1.2
1.4
1.6
1.8
2

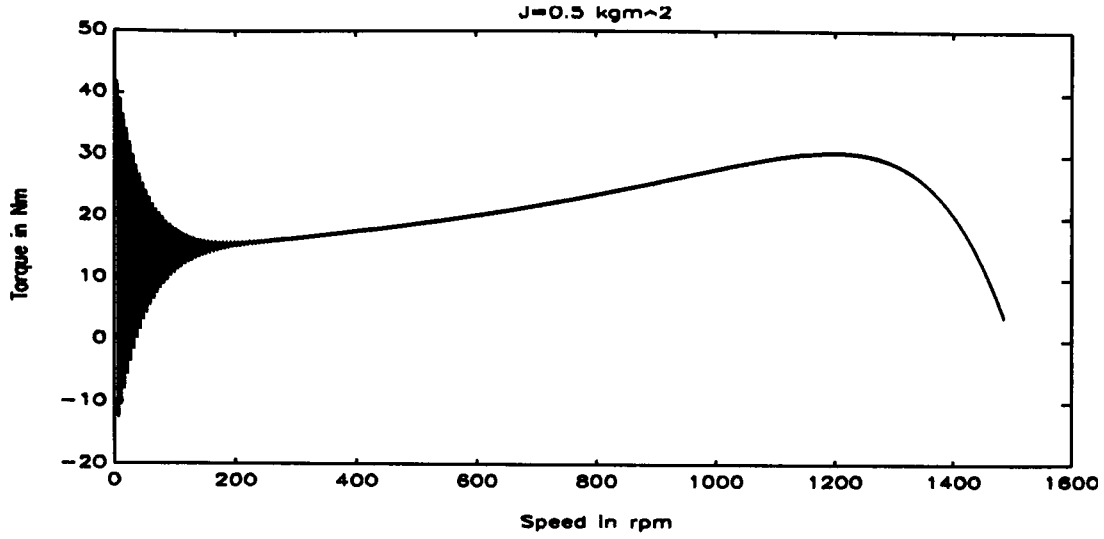
J=0.5 kgm^2
Torque in Nm
Speed in rpm
50
40
30
20
10
0
−10
−20
0
200
400
600
800
1000
1200
1400
1600

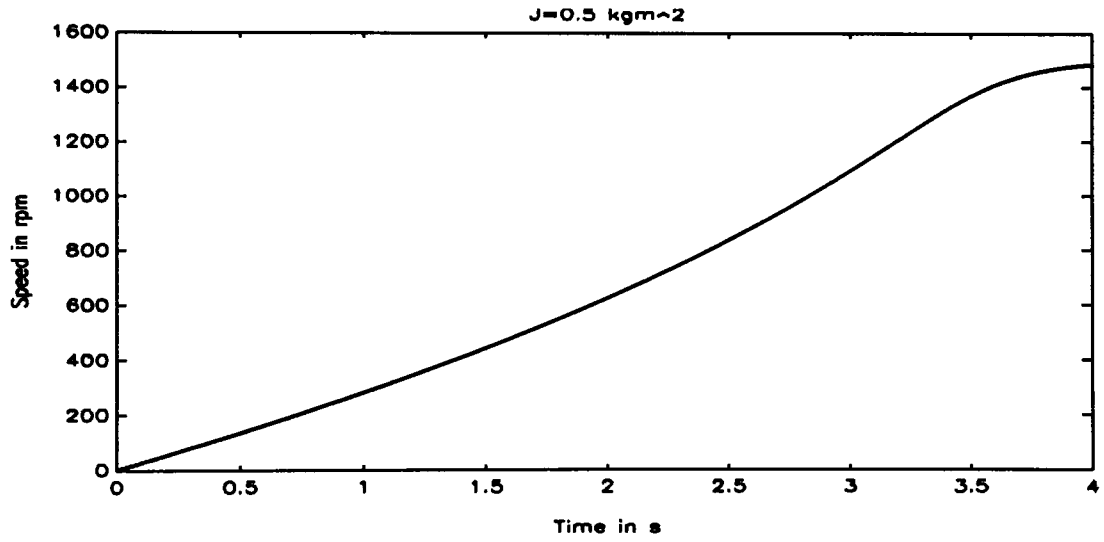
J=0.5 kgm^2
Speed in rpm
Time in s
1600
1400
1200
1000
800
600
400
200
0
0
0.5
1
1.5
2
2.5
3
3.5
4

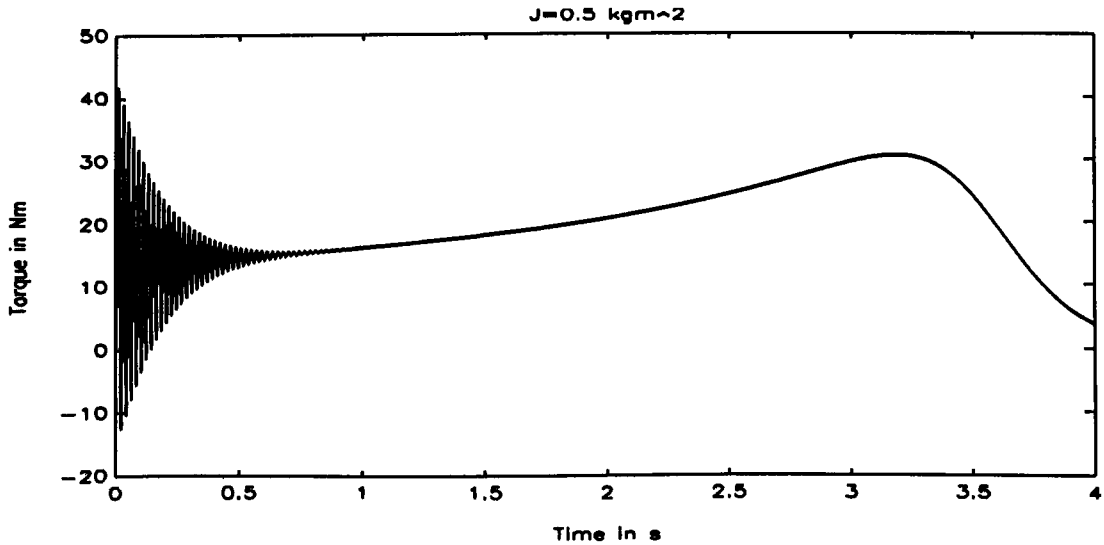
J=0.5 kgm^2
Torque in Nm
Time in s
50
40
30
20
10
0
−10
−20
0
0.5
1
1.5
2
2.5
3
3.5
4

Appendix D: Simulation results of the FFT of PWM

1. Comparison of Regular Sampled Symmetric and Aysmmetric PWM

The following figures show the results of the Fast Fourier Transform of the line to DC-link neutral voltage. In each figure Regular Sampled PWM is used, the modulation index is 1 and the modulation frequency 50 Hz. From the harmonic content the superiority of Asymmetric PWM over Symmetric PWM can be seen.

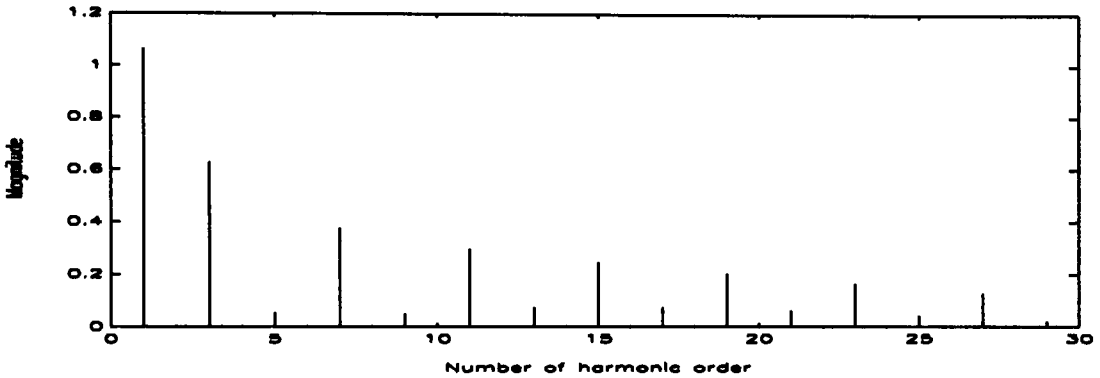

Frequency Ratio = 3, Asymmetric PWM

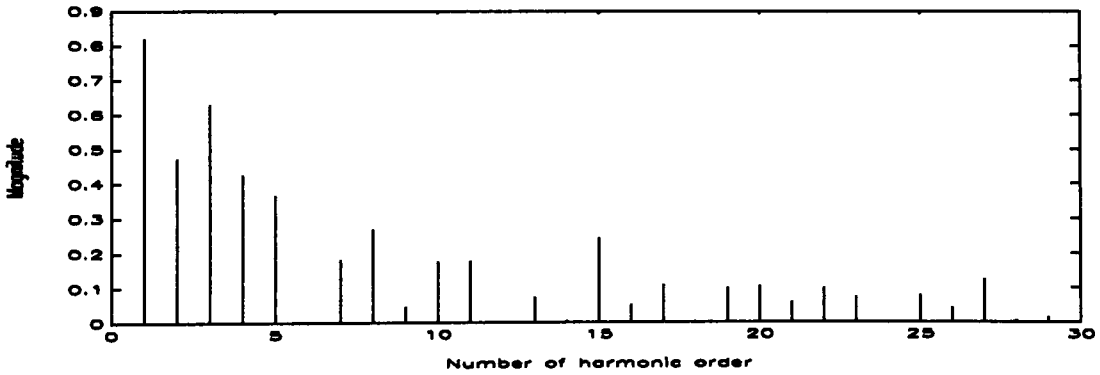

Frequency Ratio = 3, Symmetric PWM

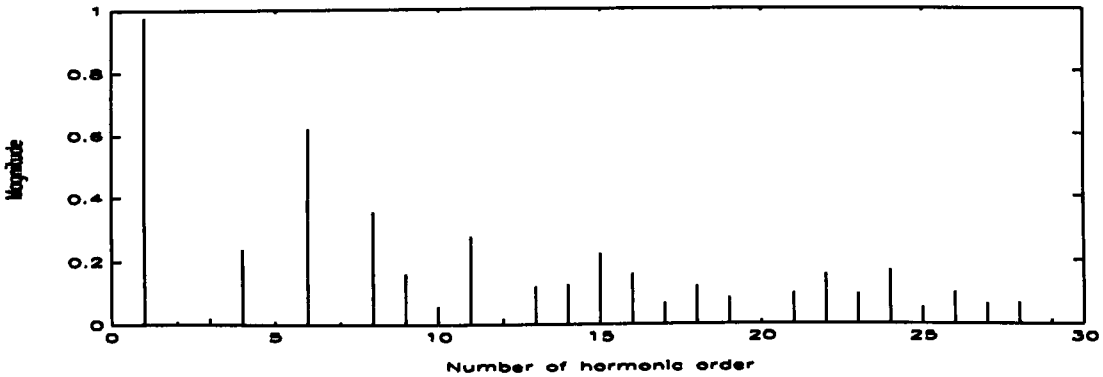

Frequency Ratio = 6, Asymmetric PWM

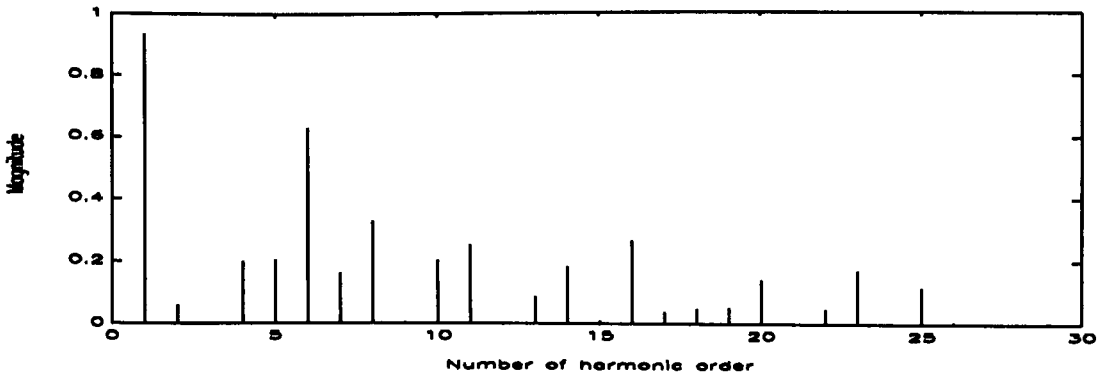

Frequency Ratio = 6, Symmetric PWM

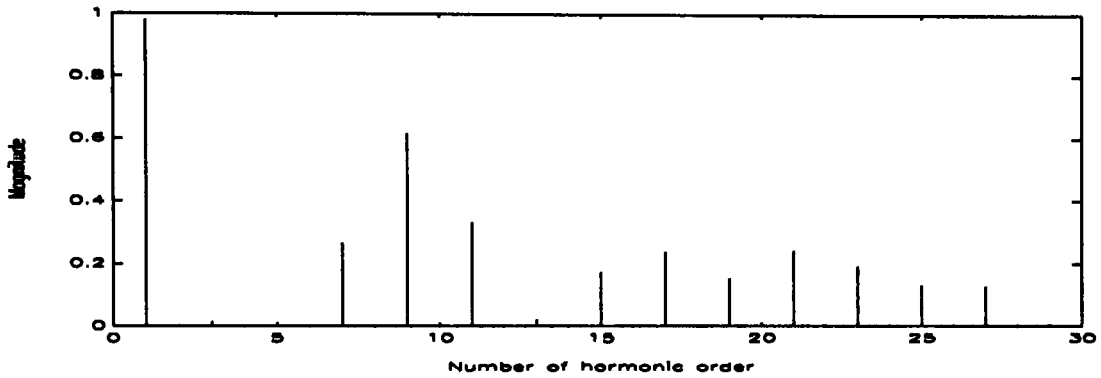

Frequency Ratio = 9, Asymmetric PWM

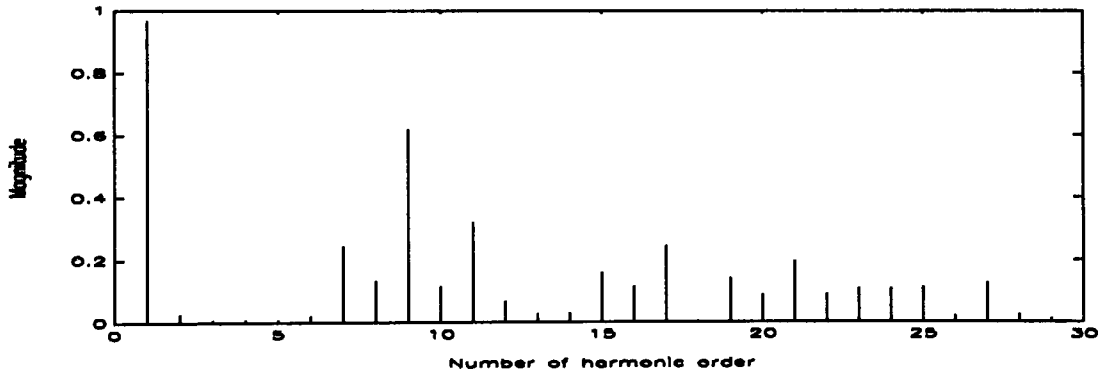

Frequency Ratio = 9, Symmetric PWM

2. Comparision of different Ratios

The following figures show the result of the FFT. In all figures Regular Sampled Asymmetric PWM was used, the modulating index is 1 and the modulation frequency 50 Hz.

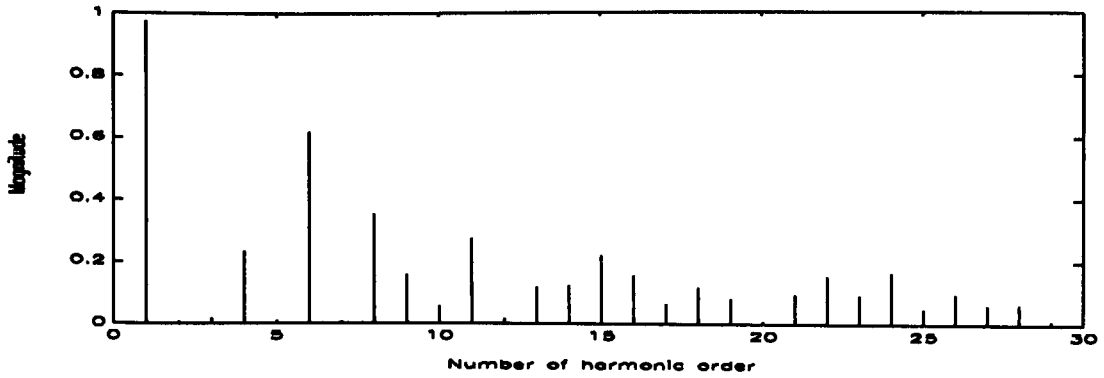

Frequency Ratio = 6

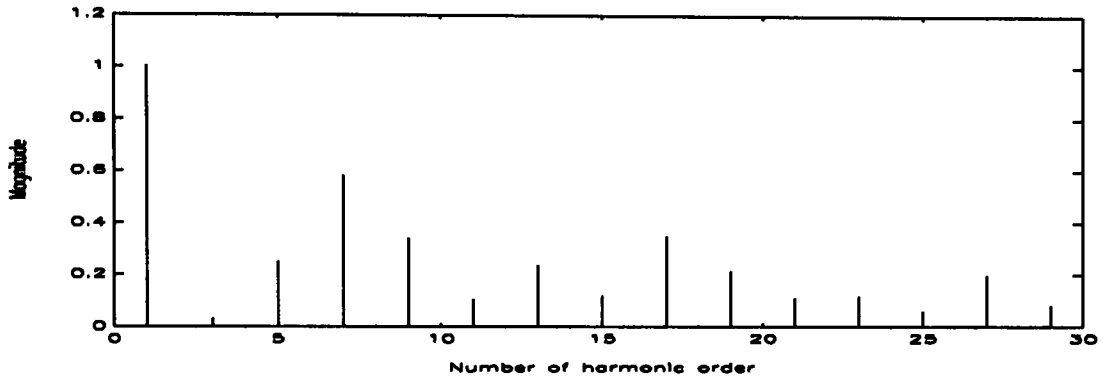

Frequency Ratio = 7

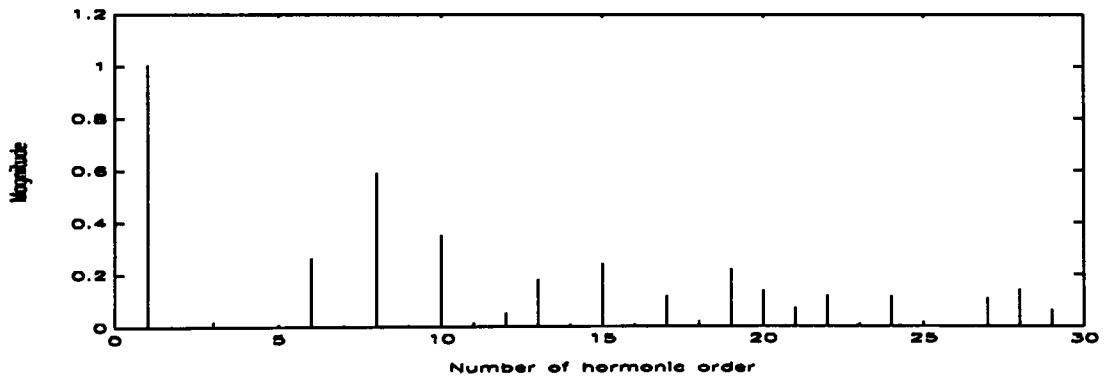

Frequency Ratio = 8

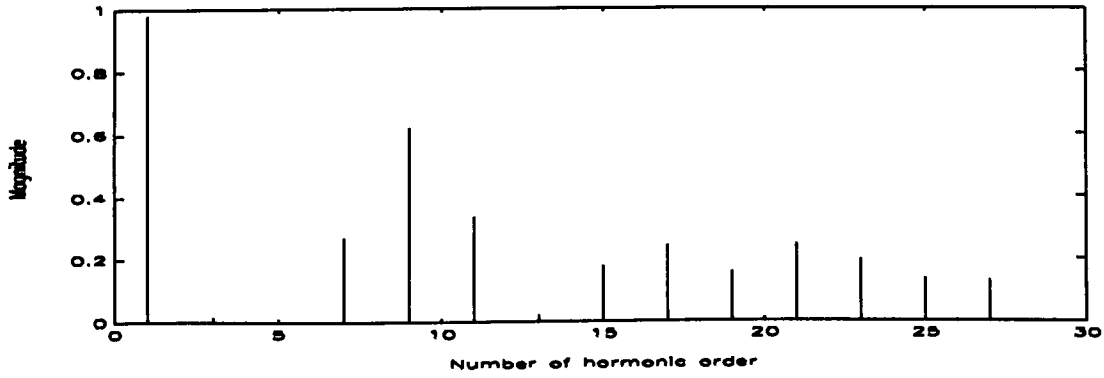

Frequency Ratio = 9

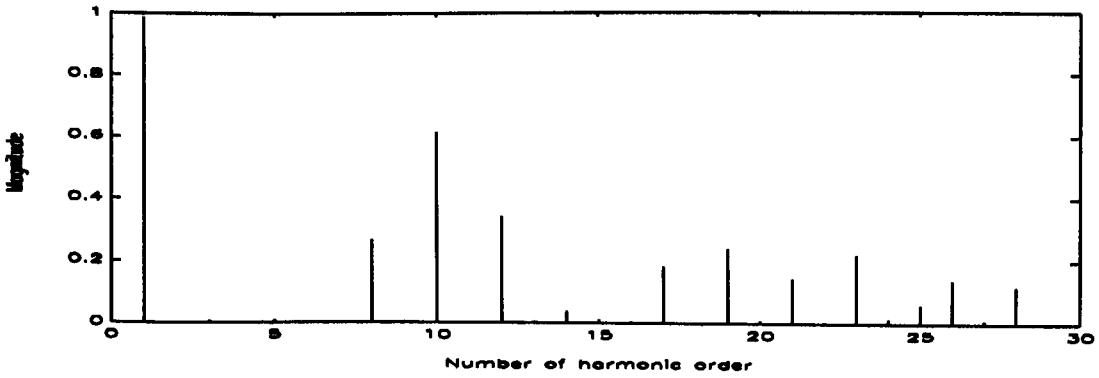

Frequency Ratio = 10

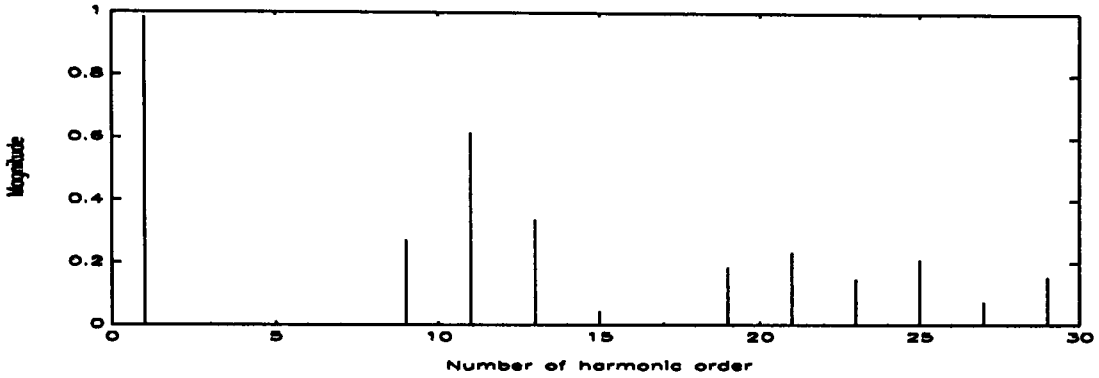

Frequency Ratio = 11

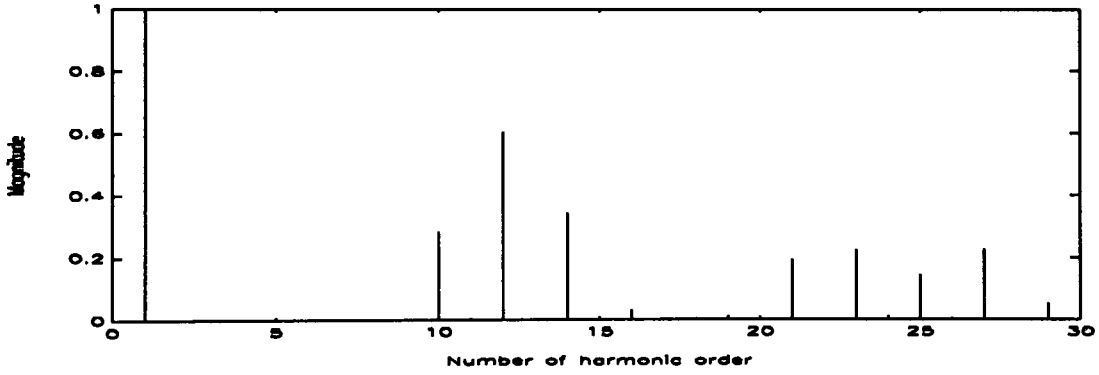

Frequency Ratio = 12

3. Comparison of different Frequency Ratios multiples of 3

The following figures show the harmonic content of Regular Sampled Asymmetric PWM for frequency ratios that are multiples of 3.

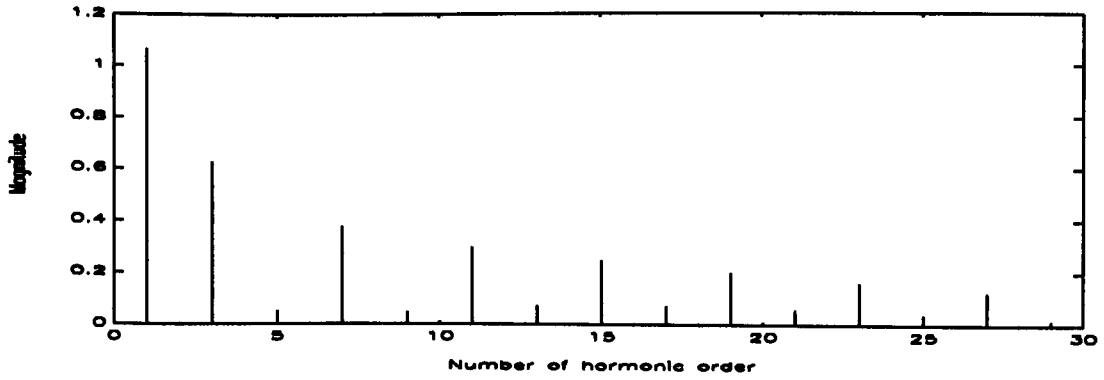

Frequency Ratio = 3

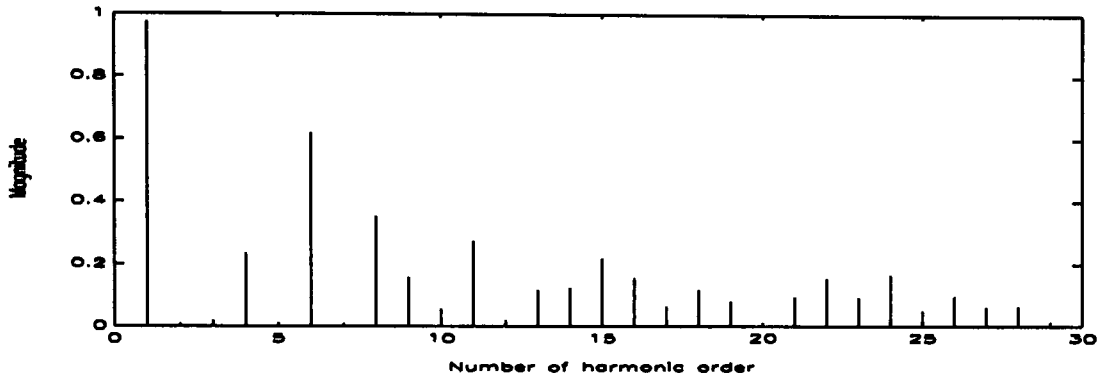

Frequency Ratio = 6

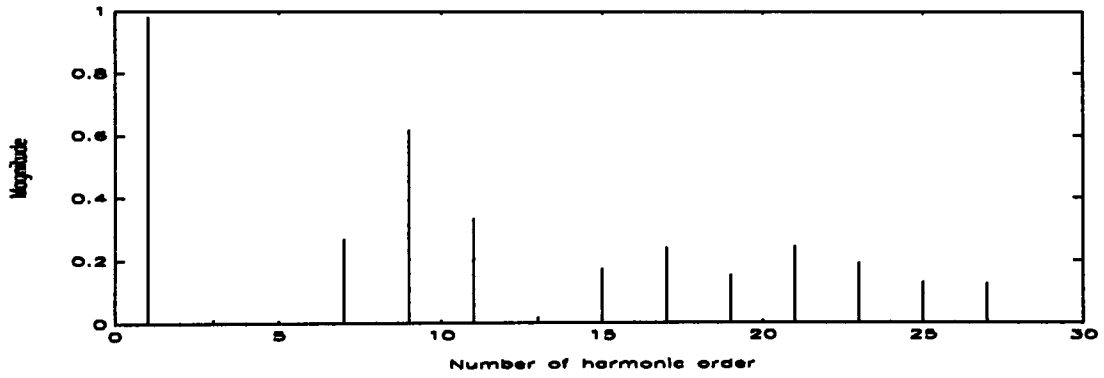

Frequency Ratio = 9

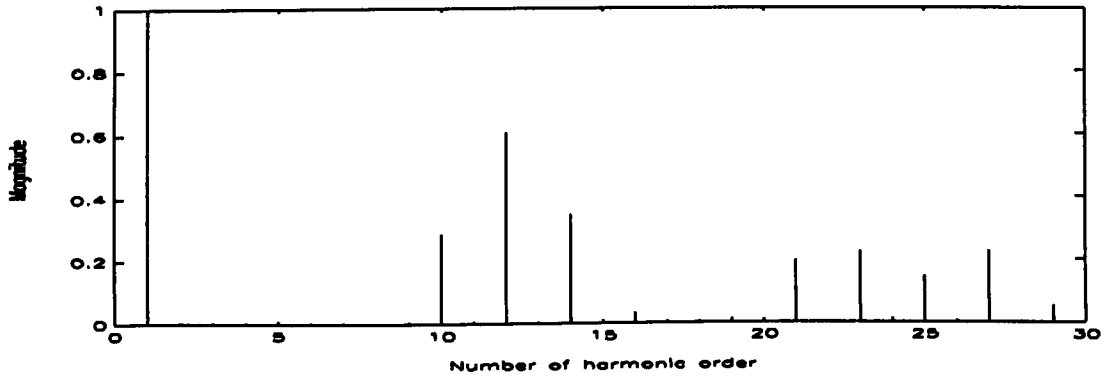

Frequency Ratio =12

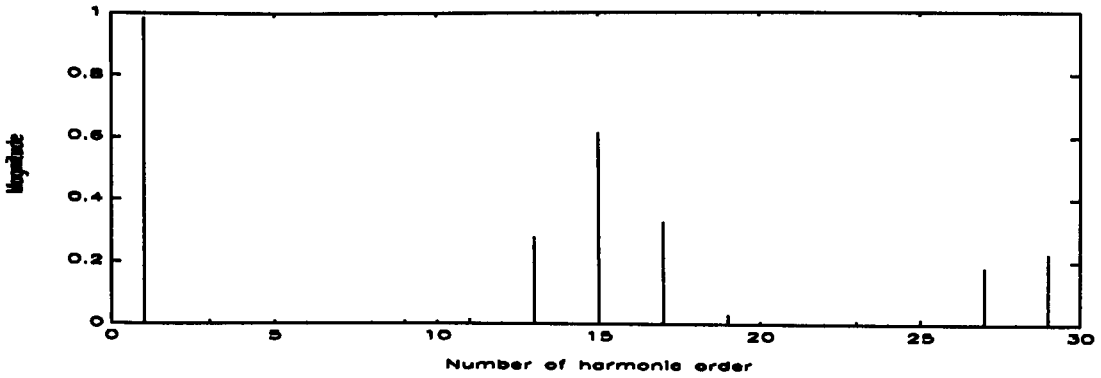

Frequency Ratio = 15

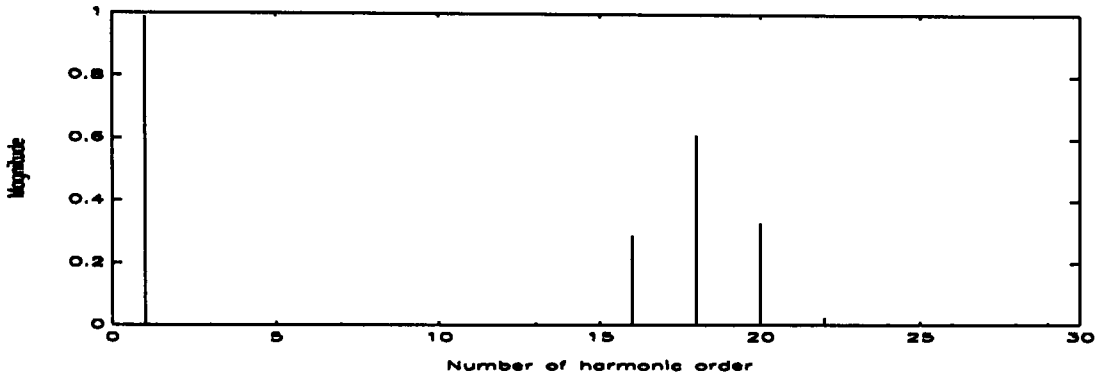

Frequency Ratio = 18

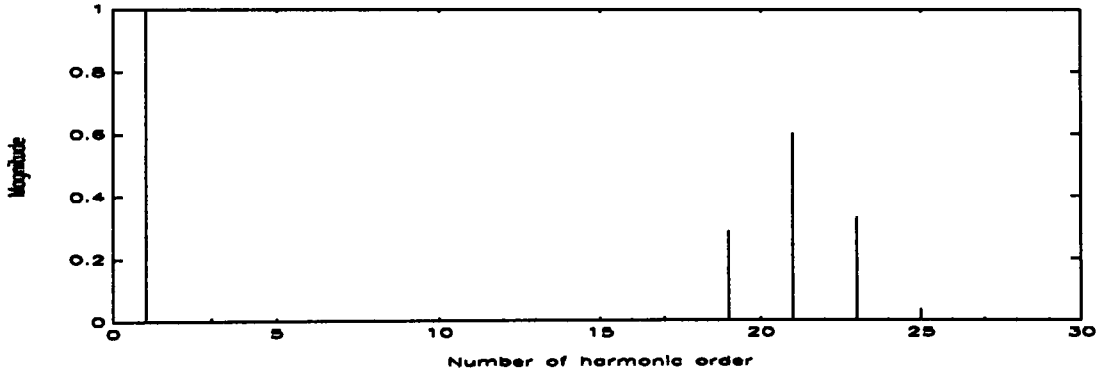

Frequency Ratio = 21

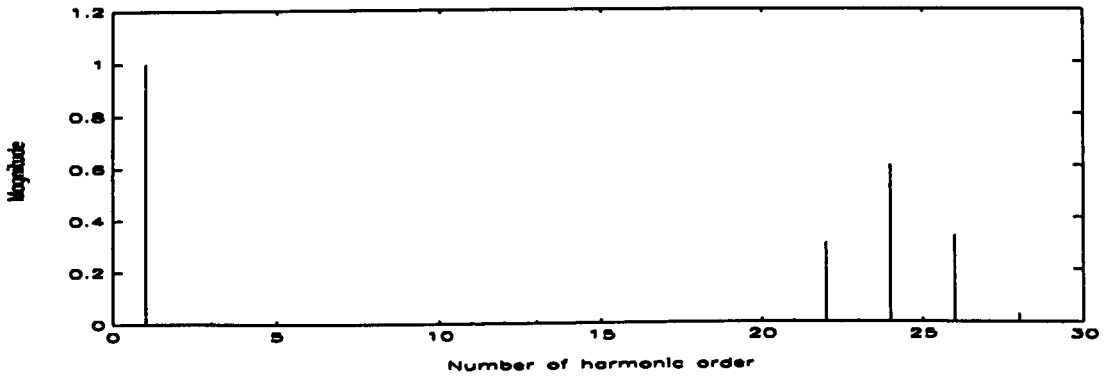

Frequency Ratio = 24

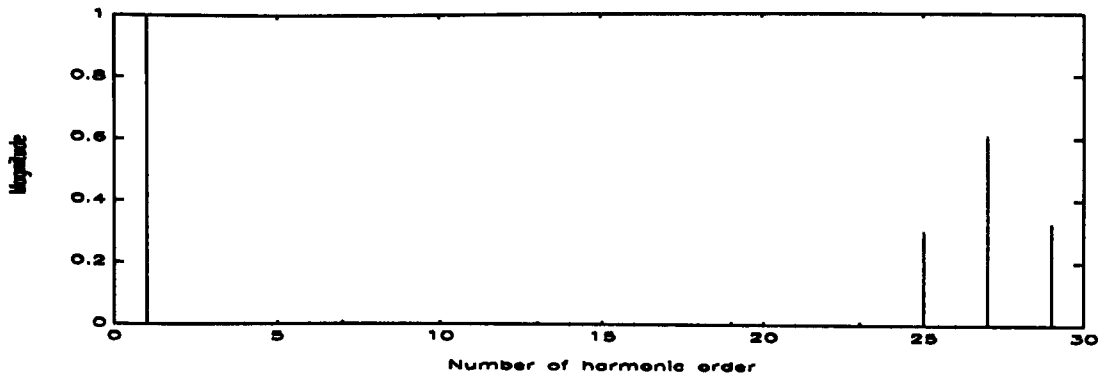

Frequency Ratio = 27

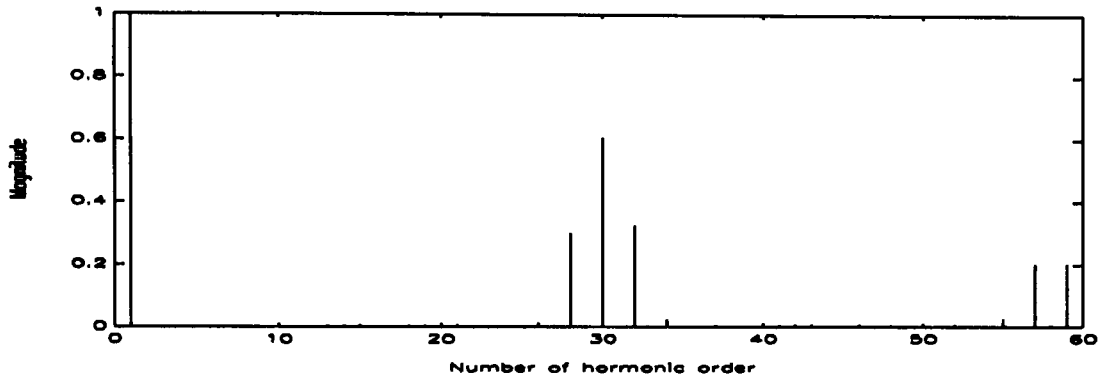

Frequency Ratio = 30

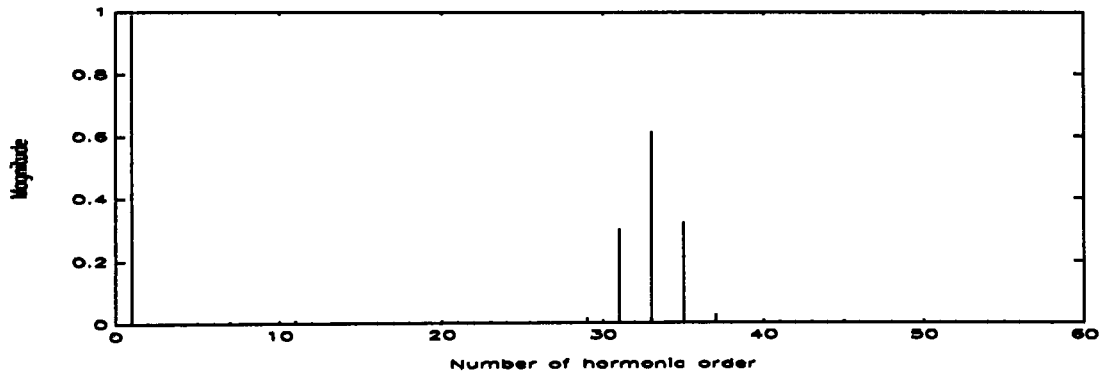

Frequency Ratio = 33

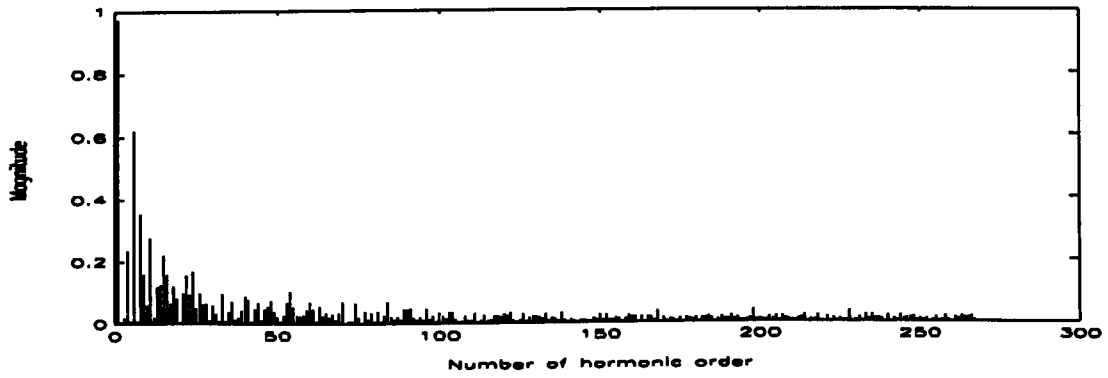

Frequency Ratio = 6

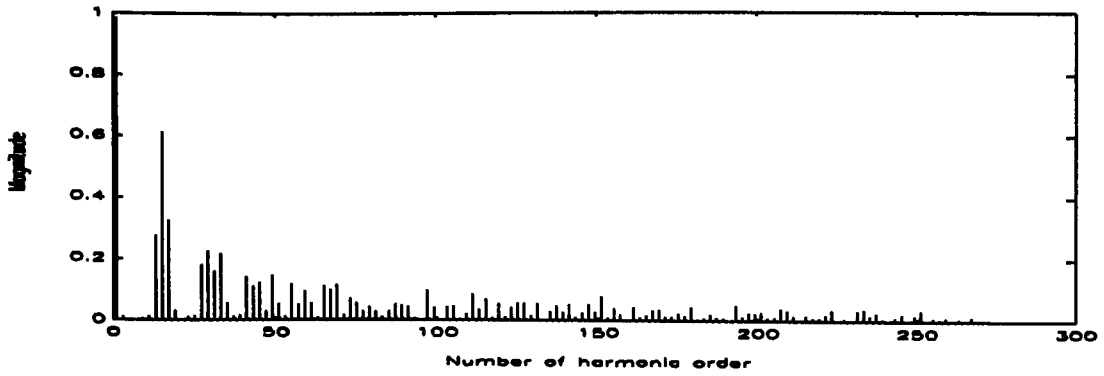

Frequency Ratio = 15

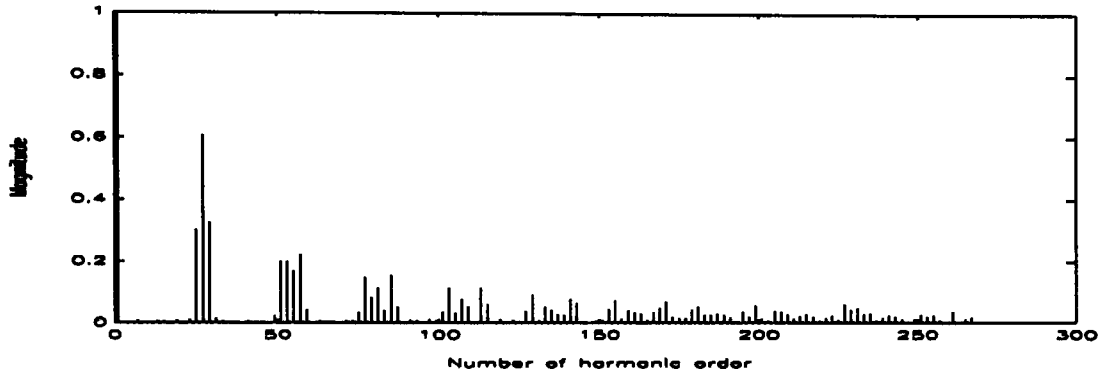

Frequency Ratio = 27

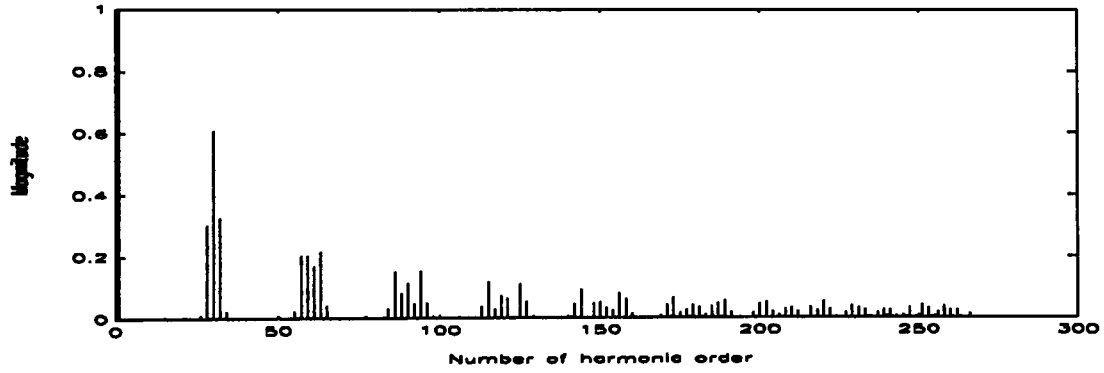

Frequency Ratio = 30

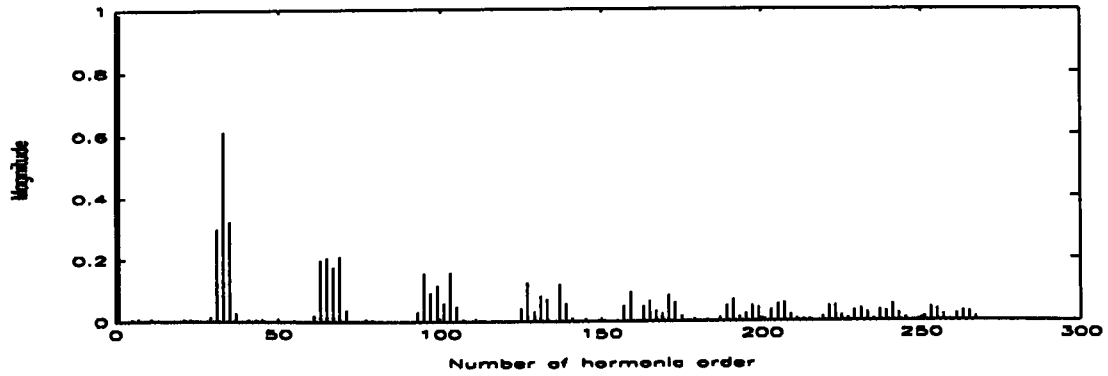

Frequency Ratio = 33

4. Elimination of triplen harmonics in the line to phase voltage

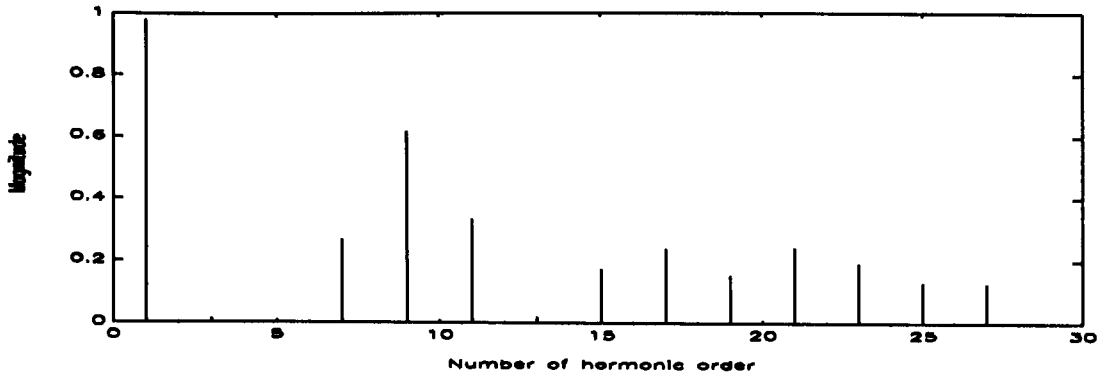

FFT for Line to DC-link nutral point Voltage R = 9

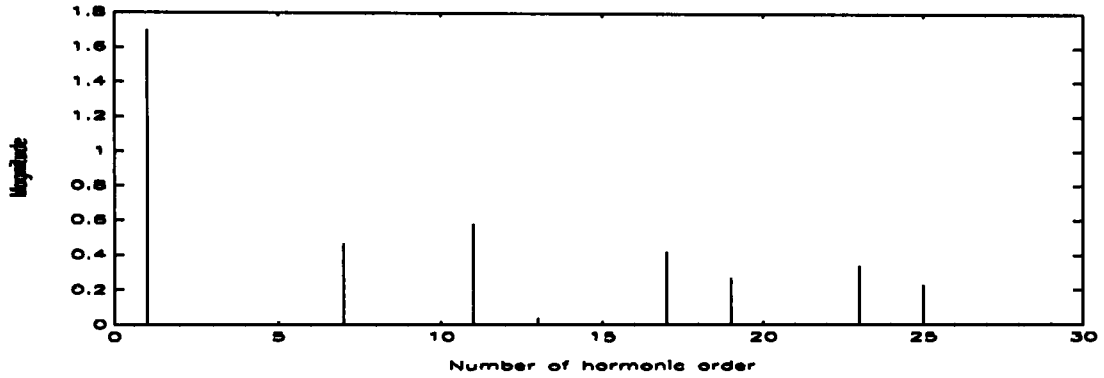

FFT Line to Line Voltage R = 9

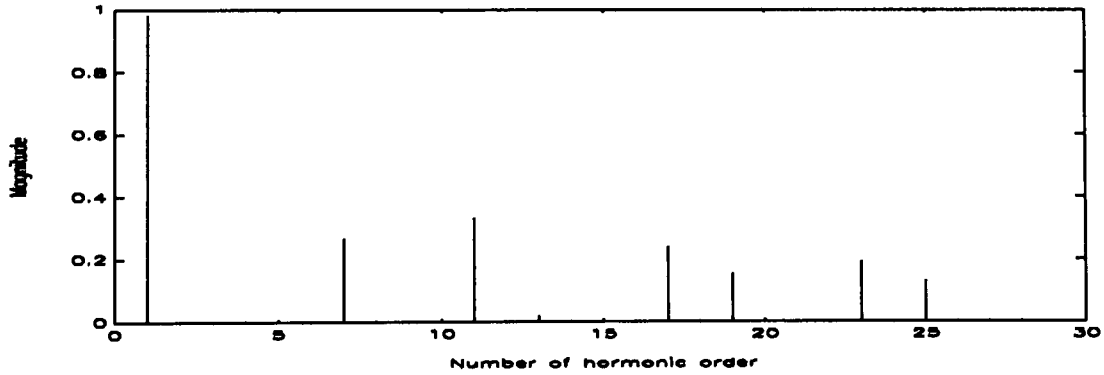

FFT Line to Starpoint Voltage R = 9

Appendix E: Flux trajectories

The following figures show the flux trajectory and the direct and quadrature flux ψ_d and ψ_q. With the supply voltage starting from square wave, going to Regular Sampled Asymmetric PWM with frequency rations 3, 6, 9, 12, 15, .., 33 and ending with sinusoidal wave.

flux trajectory

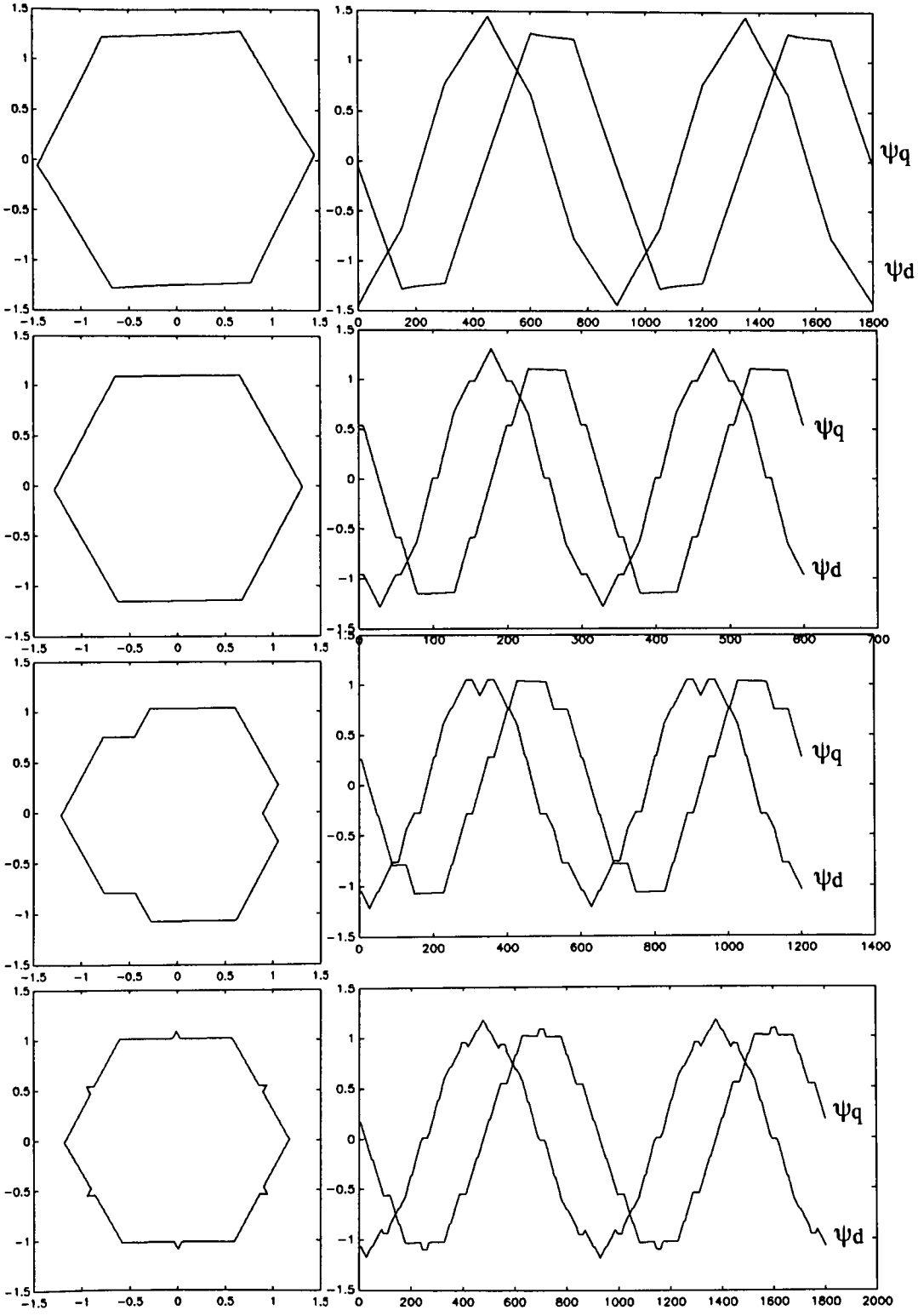

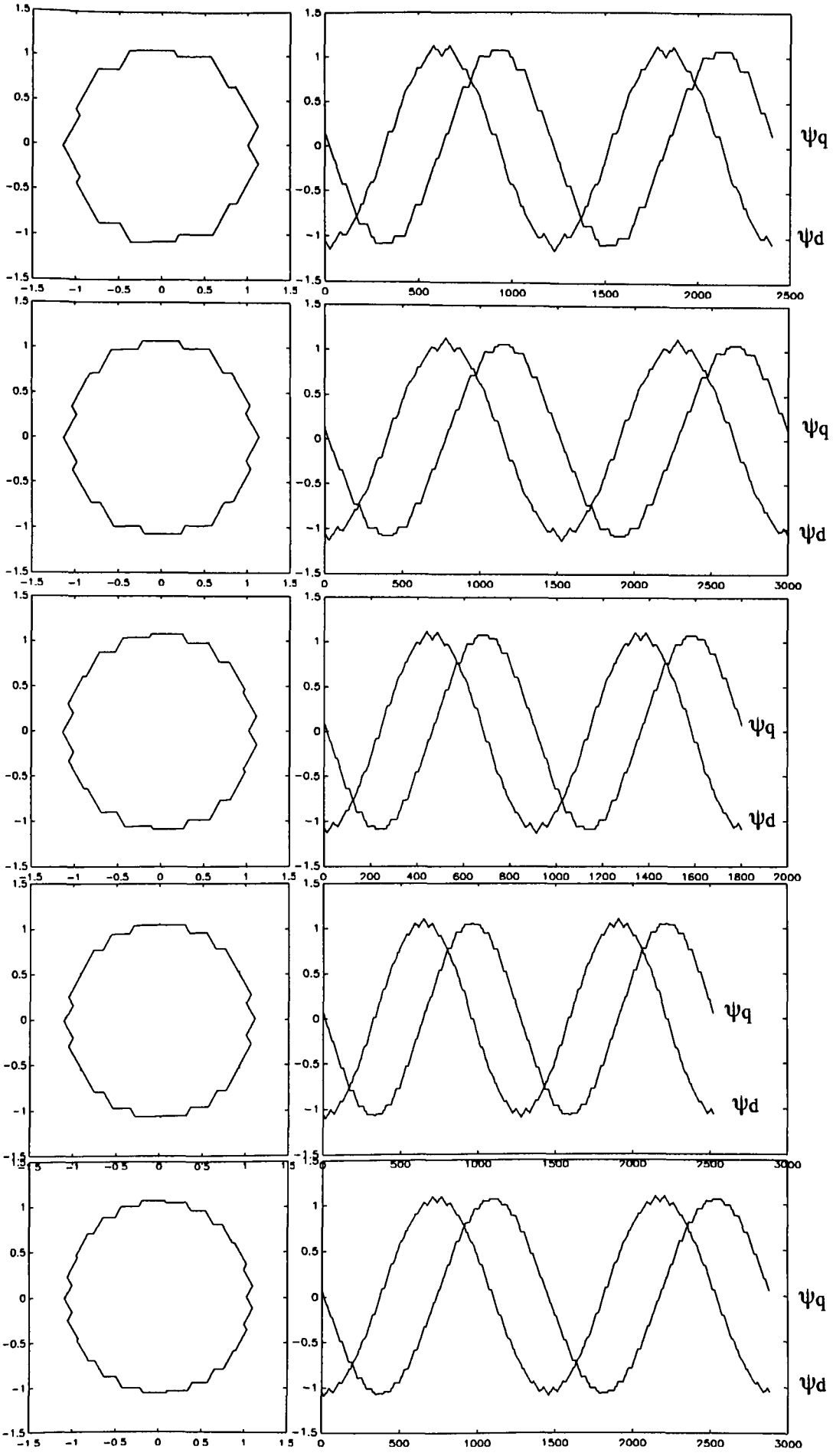
ψq
ψd
ψq
ψd
ψq
ψd
ψq
ψd
ψq
ψd

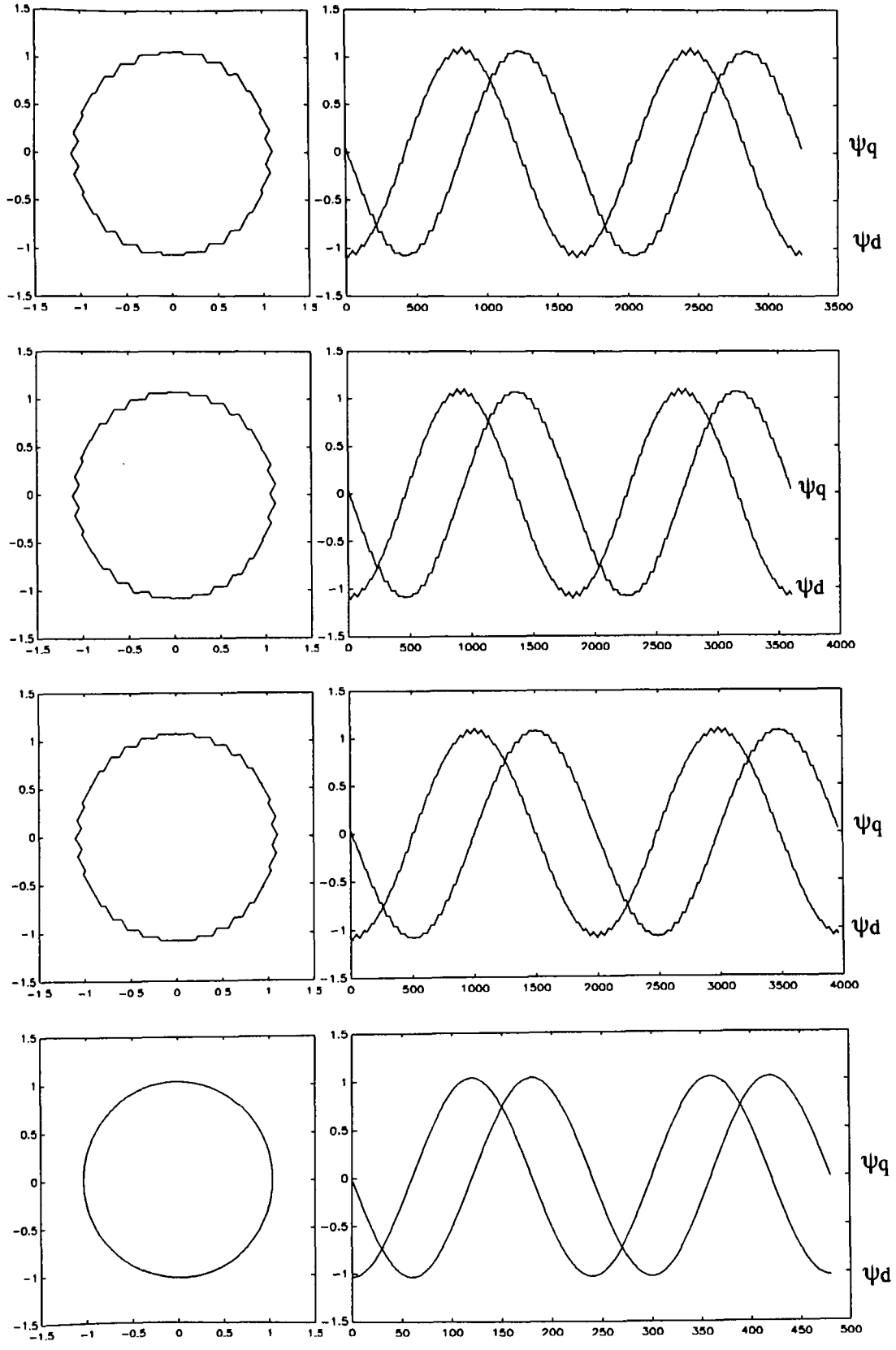
ψq
ψd
ψq
ψd
ψq
ψd
ψq
ψd

Appendix F: Publication

The following paper is related to this project.

A DIGITAL MODEL FOR A THREE-PHASE INDUCTION MOTOR DRIVE USING A PERSONAL COMPUTER (PC) SOFTWARE PACKAGE

C.K.P.Luk , M.G.Jayne, D.Rees, D.W.Schaper

Department of Electronics and Information Technology, Polytechnic of Wales,
Treforest, Pontypridd, Mid Glamorgan CF37 1DL, U.K.

Abstract. A discrete state variable method is used to develop a digital model for a three-phase induction motor drive. It is shown that the computation required in solving the fifth-order non-linear differential equation of the motor is greatly simplified by the exclusive use of matrices. The model can be adapted to the study of steady state as well as dynamic performance of the machine when fed from an inverter. Pulse-width -modulated (PWM) waves are used to test the model which is based on *d-q* transformations of the motor equations. The validity of the model is confirmed by experimental results obtained from a transputer-based PWM inverter drive system.

Keywords. a.c.motors, discrete systems,electric drives, Fourier transforms, matrix algebra, modelling, power converter, simulation, transputer.

INTRODUCTION

The operational advantages of using PWM techniques for the control of induction motors over alternative methods are reflected by the considerable research effort that has been described in the literature over recent years. An essential part of these developments has been the requirement for an efficient and accurate model of the motor in order to examine the performance of a diversity of inverter control strategies. Such a model, results in the general solution of a non-linear, fifth-order differential equation with an input structure which is non-sinusoidal (Bose, 1986). This, together with the subsequent Fourier analysis of various waveforms, requires both good mathematical knowledge and a considerable amount of computing power. Because the majority of a.c. machines in the past were supplied with sinusoidal or near sinusoidal waveforms, frequency domain methods were preferred as system analysis tools (Jacovides, 1973; Murphy, 1976; Jain, 1984). With the number of induction motor drives fed from non-sinusoidal variable frequency supplies increasing, there has been an obvious incentive to use a time domain analysis where all quantities are expressed explicitly instead of the sum of infinite series, as required in the case of frequency domain methods. The classic paper presented by *Lipo* (Lipo, 1977) has shown that even the simulation of a quasi-square inverter in the time domain requires very intensive computation. It has been further demonstrated that (Bowes and Clare, 1983), although accuracy is gained by using time-domain methods, the mathematical complexity involved may dissuade an engineer from adopting such an approach.

In an attempt to demonstrate that the state variable method is one of the most useful means to model a non-linear, multiple-input multiple-output (MIMO) motor model, the authors used a discrete state-variable method which involved only matrix manipulations. With the facilities provided by a personal computer (PC) software package which gives access to a library of subroutines for matrix manipulations, considerable computational simplification is achieved. It is also believed that such a digital model in state-variable form, provides a basis for further development of a modern real-time digital controller in which state-variable methods are commonly used.

MODELLING OF POWER CONDITIONING STAGE

The power conditioning stage is achieved by a 3-phase pulse-width moduated (PWM) inverter. There are numerous PWM generation schemes available (Jayne, Bowes and Bird, 1977). However, only the regular sampled asymmetric modulated PWM waveform is discussed here due to its wide popularity and ease of generation by a digital computer. The method described below for the generation of a discrete PWM waveforms from a continuous one applies to any PWM scheme with known switching angles.

Computation Of Switching Time

The analytical expression for the pulse-width of the n^{th} pulse of the phase *a* of a 3-phase regular sampled asymmetric modulated PWM waveform, is given by (Bowes and Clements, 1982),

$$t_a(n)=(Tc/2)*[1+(-1)^{n+1}*(M/2)*(\sin a_n+\sin a_{n+1})] \qquad (1)$$

where Tc is the period of the carrier wave, M is the modulation index, $a_n=\pi n/R$, and R is the frequency ratio of the carrier wave to the modulating wave. The corresponding pulse-widths for phase *b* and *c* can be found by replacing a_n by b_n and c_n in eqn.(1) respectively, where $b_n=a_n-120°$ and $c_n=a_n-240°$.

It is found that in the real-time generation of a three phase PWM waveform, a more efficient method is to modify eqn.(1) to :

$$ta'(n) = \begin{cases} Tc/4*[1-M*\sin a_n] \text{ , for n is odd} & (1a) \\ Tc/4*[1+M*\sin a_n] \text{ , for n is even} & (1b) \end{cases}$$

These equations were used in both the simulation and in the generation of the real-time PWM waveforms described in the paper at a later stage.

Discretizing the PWM Waveforms

The choice of sampling period,T_s, is basically influenced by two factors - accuracy and computational time. The higher the sampling frequency, the closer is the discretized model to its continuous analogue model, and the longer becomes the

computational time. On the other hand, the sampling period should be small compared with the dominant time constant of the system. The continuous PWM waveform described by eqn.(1a) and (1b) is discretized by means of the sampling process illustrated in Fig.1(a). The fictitious carrier waveform is shown here for reference. $S(n)$ is the sampling pulse in discrete time domain and $h_a(n)$ is the resulting discretized PWM waveform. Fig.1(b) shows the program written in the simulation programming language (discussed later) for the discretization of the PWM waveform. In the program, S and h_a are matrix vectors. The variable p indicates the corresponding element in the matrix. The first two lines in the program are used to generate the sampling pulse chain matrix vector S. The number of samples (N) over half of the carrier cycle ($Tc/2$) can be chosen by the user. The following sections of the program describe the sampling process. It is evident from Fig.1(a) that, if the pulse-width of the PWM waveform is less than T_s, that pulse may not be sampled. For the regular sampled asymmetric modulated PWM waveform, and in fact most of the PWM schemes, there is no switching at the instants corresponding to the apexes of the (fictitious) carrier waveform if the modulating index is less than 1. Thus, to ensure that those pulses with pulse-width less than the sampling period are sampled, it is necessary not only to have an integral number of pulses per half carrier cycle, but also to synchronize the sampling pulse chain with the apexes of the carrier wave. It was found that in this iuvestigation, if the number of samples taken was 10 per half carrier cycle, a good compromise between accuracy and computational time was acheived.

MODELLING OF MACHINE

The operation of a three phase induction motor, for purposes of analysis, is basically the interaction between two sets of coils with relative motion as shown in Fig.2(a). The associated equations are represented in compact matrix form as,

$$v = Ri + \omega_r G\, i + L\, di/dt \qquad (2)$$

where R, L and G are 6×6 square matrices of the winding coefficients; v and i are 6-element column matrices; and ω_r is the rotor speed.

To improve computational efficiency, eqn.(2) is usually transformed into a d-q axis fixed either on the stator or the rotor or rotating in synchronism with the applied voltages. The transformation referred to the stator is chosen and can be divided into two steps as shown in Fig.2(b)and 2(c).

The first step involves the three-phase to two-phase transformation with no change of space-frame, as shown in Fig.2(b). The current transformation from frame (A,B,C) to (D,Q,Γ) for the stator , and (a,b,c) to (α,β,χ) for rotor, can be expressed in matrix forms as,

$$i_{DQ\Gamma} = D\, i_{ABC} \qquad (3)$$

$$i_{\alpha\beta\chi} = D\, i_{abc} \qquad (4)$$

Similar relationships are true for voltages. The second step involves the change of space-frame for the rotor, as shown in Fig.2(c). The current transformation from frame (α,β,χ) to (d,q,χ), can be expressed in matrix forms as,

$$i_{dq\chi} = S\, i_{\alpha\beta\chi} \qquad (5)$$

Combining (4) and (5) gives,

$$i_{dq\chi} = S\, i_{\alpha\beta\chi} = S\, D\, i_{abc}$$

$$or, \qquad i_{dq\chi} = C\, i_{abc} \qquad (6)$$

Similar relationships are true for the voltages.The matrices D, S and C are as defined in the Appendix.

The motor equation in d-q form referred to the stator may therefore be expanded as,

$$\begin{bmatrix} v_{ds} \\ v_{qs} \\ v_{dr} \\ v_{qr} \end{bmatrix} = \begin{bmatrix} R_s+L_s\mathrm{p} & 0 & pM & 0 \\ 0 & R_s+L_s\mathrm{p} & 0 & pM \\ \mathrm{p}M & \omega_r M & R_r+L_r\mathrm{p} & \omega_r L_r \\ -\omega_r M & pM & \omega_r L_r & R_r+L_r\mathrm{p} \end{bmatrix} \bullet \begin{bmatrix} i_{ds} \\ i_{qs} \\ i_{dr} \\ i_{dr} \end{bmatrix} \qquad (7a)$$

If this equation is put into the form of eqn.(2), the order of the matrices will be reduced by 2 as a result of the d-q transformations. Thus, R,L and G become 4×4 matrices, and v,i are 4-element column matrices. The electromagnetic torque T_e is given by,

$$T_e = \mathrm{n}\, i\, G\, i^T \qquad (7b)$$

where n is the number of pole-pairs and i^T is the transpose of i. Eqn.(7a) and Eqn.(7b) may be combined together to form a fifth-order equation,

$$\begin{bmatrix} v_{ds} \\ v_{qs} \\ v_{dr} \\ v_{qr} \\ T_e \end{bmatrix} = \begin{bmatrix} R_s+L_s\mathrm{p} & 0 & pM & 0 & 0 \\ 0 & \mathrm{R}_s+L_s\mathrm{p} & 0 & pM & 0 \\ \mathrm{p}M & \omega_r M & R_r+L_r\mathrm{p} & \omega_r L_r & 0 \\ -\omega_r M & pM & \omega_r L_r & R_r+L_r\mathrm{p} & 0 \\ i_{qr}M & i_{dr}M & i_{dr}L_r & -i_{qr}L_s & J\mathrm{p}+R_F \end{bmatrix} \bullet \begin{bmatrix} i_{ds} \\ i_{qs} \\ i_{qr} \\ i_{dr} \\ \omega_r \end{bmatrix} \qquad (8)$$

where J is the moment of inertia of the rotating mass, and R_F is a mechanical coefficient representing dissipation due to friction and windage.

DEVELOPMENT OF THE SIMULATION

Simulation Software Package *PC-MATLAB* [1]

The *PC-MATLAB* is a high-level user-friendly programming software package suitable for the design and analysis of control systems. As the abbreviated name (*MAT*rix *LAB*oratory) implies, the software handles data exclusively in matrix form and is hosted by a PC with a maths co-processor. A subroutine library consisting of many useful matrix functions such as Fourier Transforms and the solution of the state-transition matrix in exponential form. It can also import programs written in C or Fortran. The graphic output facility contains standard output format such as Hewlett Packard Graphic Language (HPGL) so that output data can be transferred with great ease.

Solution of State Variable Equation

Digitizing the state variable equation. The machine equation described by eqn.(7a) can be written in standard state-variable form as,

$$\dot{x} = Ax + Bu \qquad (9)$$

[1] *PC-MATLAB* User's Guide, 1988.

where x is the state variable of the transformed current vector and u is the PWM input vector to the d-q frame; and A, B are as defined in the Appendix.

The discrete form of eqn.(9) is given by,

$$x(n+1) = \Phi x(n) + \Gamma u(n) \qquad (10)$$

where, $\Phi = e^{ATs} = I + ATs + (1/2!)A^2Ts^2 + ..$

$$\Gamma = \int_0^{Ts} e^{A\tau}\, d\tau\, B$$

Since the PWM input $u(nT_s)$ over the period, $nT_s < \tau < (n+1)T_s$, is constant, then,

$$\Gamma = [\, I\, T_s + (1/2!)AT_s^2 + \ldots \,]\, B$$

The transformation from eqn.(9) to (10) is achieved by a command called ***c2d*** (continuous to discrete) provided by *MATLAB*. The sampling time T_s is chosen to be the same as in the discretization of the PWM waveform.

Initial condition. The inherent symmetry of the induction motor voltage and current waveforms when supplied from a balanced source can be used to find the initial conditions of eqn.(10). Depending on the symmetry of the waveform, one of the following relations may be used (Bowes and Clare, 1983).

For waveforms with no half-wave symmetry,

$$x(t+T/3) = S_1\, x(t) \qquad (11a)$$

And for waveforms with half-wave symmetry,

$$x(t+T/6) = S_2\, x(t) \qquad (11b)$$

where T is the period of the waveform, and S_1 and S_2 are as defined in the Appendix.

Thus, for a half-wave symmetrical model, if the p^{th} sample is at T/6, then from eqn.(10), the following equations may be obtained.

$$x(1) = \Phi x(0) + \Gamma u(0) \qquad (12a)$$

$$\vdots$$

$$x(i) = \Phi x(i-1) + \Gamma u(i-1) \qquad (12b)$$

$$\vdots$$

$$x(p) = \Phi x(p-1) + \Gamma u(p-1) \qquad (12c)$$

By multiplying equations (12a), ...(12b), ...(12c), with Φ^{p-1},... Φ^{p-i},...,I respectively, and through the process of summation and elimination the following equation for $x(0)$ can be obtained.

$$x(0) = [S_2 - \Phi^p]^{-1} \sum_{i=0}^{p-1} \Gamma \Phi^i u(p-1-i) \qquad (13)$$

Once the initial vector $x(0)$ is obtained, the complete solution for the state equation of the motor currents can then be found as a matter of routine by means of eqn.(10). Fig.3 shows one of the phase currents with the PWM voltage waveform at the sampling points over one-sixth of its cycle. These sampled currents $I(0)$,..$I(i)$,..$I(p)$ can be found by inverse transformation of the discrete state variables $x(0)$,..$x(i)$,..$x(p)$ by means of eqn.(3).

Spectrum Analysis of the Waveforms

Two Fourier transform commands are provided by *PC-MATLAB* - the discrete Fourier Transform (***dft***) and the fast Fourier Transform (***fft***). Quantities represented in the time domain stored in a row or column matrix T can be transformed to the frequency domain and stored in another matrix, F. Thus,

$$F = fft(T) \quad or \quad F = dft(T)$$

The number of samples to be used in the ***fft*** should be equal to 2^n(where n is an integer value). A matrix with a number of terms less than 2^n will be filled up with zeros before the transform is performed. The number of samples chosen is restricted by the condition required to synchronize the sampling pulses with the apexes of the carrier waveform (see Fig.1a). This means that if the frequency ratio R is not equal to 2^n itself, then the number of samples N, which is equal to the number of sample per period of carrier wave, say k, times the frequency ratio R, cannot be a 2^n number either. In such cases, k should be chosen such that $k \times R$ is near to 2^n to avoid unacceptable errors due to the filled zeros in the matrix. Alternatively, the ***dft*** may be used at the expense of an increase in the computational time. In this paper, the ***dft*** was used for values of R not equal to 2^n.

SIMULATION RESULTS

PWM Inverter Voltage Waveforms

The common method of controlling the induction motor by keeping the ratio of voltage-to-frequency (or modulation index to frequency) constant is illustrated in Fig.4 and 5. It may be noted that at higher frequency operations, low frequency ratios (see Fig.5) are used to limit the switching frequency and associated inverter losses. At lower frequency operations, the modulation index is small and voltage pulses are widely separated, resulting in high harmonic distortion. Therefore, higher frequency ratios (see Fig.4) are used to improve the harmonic content of the inverter output voltage. The process of changing from one pulse number per cycle to another is commonly known as 'gear changing'.

Motor Current and Voltage Waveforms

The transformed PWM stator voltages (v_{ds}, v_{qs}) and stator currents (i_{ds}, i_{qs}) in the d-q frame are shown in Fig.6. It can be shown that v_{ds} represents the line voltage and v_{qs} is a scaled version of the phase voltage (Bowes and Clements, 1982). By plotting the q-quantities against the d-quantities, the locus of the phasor voltage or current waveforms can be obtained. Fig.7 shows the locus of the voltage phasor for the PWM inverter at a frequency ratio (R) of 21. It should be noted that as the frequency ratio increases, the locus of the phasor will approach a circle. Fig.8 shows the typical motor phase currents, which were found by inverse transformation of i_{ds} and i_{qs}.

Spectrum Analysis of Current And Voltage Waveforms

The harmonic spectrum of the PWM inverter voltage waveforms illustrated in Fig.4 and Fig.5 are shown in Fig.9 and Fig.10 respectively. It can be seen that, by comparing Fig.9 and Fig.10, the magnitude of the fundamental frequency component is proportional to the modulation index. The lower harmonics which are more harmful to the motor, are either greatly reduced or canceled when high values of frequency ratio R are used.

Electromagnetic Torque

The simulation results show that the ripples of the electromagnetic torque generated is largely influenced by the value of the frequency ratio used. The magnitude of the ripples reduces as the frequency ratio increases. Fig.11 shows the waveform of a typical electromagnetic torque when a low frequency ratio is used.

EXPERIMENTAL RESULTS

The results presented in this section were obtained from a transputer-based PWM inverter system (Fig.12). Due to its fast processing speed, the transputer was used to generate a 3-phase PWM waveform in real-time, using the same expressions as described in eqn.(1a) and (1b). The programs were coded in

OCCAM, a programming language closely assocaited with the transputer. The resulting PWM signals were fed to a 3-phase metal-oxide semiconductor field-effect transistor (MOSFET) inverter via an interface circuit. A 2.2kW 3-phase cage rotor induction motor was used for the test. The instrument used to display the results in the *d-q* frame consisted of a 3-phase to 2-phase transformer employing operational amplifiers and R-C circuits. It is shown that the experimental results compare favourably with the simulation results (see Fig.13-16).

CONCLUSION

It has been shown that the solution of the discretized state variable formulated machine model of a 3-phase induction motor is greatly simplifed by the use of matrices. The software package, *PC-MATLAB*, has proved itself as an ideal tool to provide a solution to the problem of machine simulation described in this paper. It allows engineers to analyze machine models in state-variable form without involving considerable mathematical complexity, and also provides computing power at an affordable cost as in contrast to main-frame or mini-computers. It is believed that with the ever-increasing computing power offered by microprocessors, simulation of machine at PC level will become more cost effective and popular in the future.

REFERENCES

Bose,B.K.(1986) "Power Electronics and AC Drives," Prentice Hall.

Jacovides,L.J.(1973) "*Analysis of induction motor drives with noninusoidal supply voltages using Fourier analysis*," IEEE Trans. Ind. Appl., vol. IA-9, pp. 741-747.

Murphy,J.D.M.(1976) "*Analysis of inverter fed induction motors*," Int. J. Elec. Eng. Educ., vol. 13, pp. 359-369.

Jain,G.C.(1984) "*The effect of voltage waveshape on the performance of a 3-phase induction motor*," IEEE Trans. Power App. Syst., vol. Pas-83, pp. 561-566.

Lipo,T.A. and Turnbull,F.G. (1975) "*Analysis and Comparison of Two Types of Square-Wave Inverter Drives*," IEEE Transactions on Industry Applications, Vol. IA-11, No. 2.

Bowes,S.R. and Clare,J. (1983) "*Steady-state performance of PWM inverter drives*," IEE Proceedings, Vol. 130, Pt. B, No. 4.

Jayne,M.G.,Bowes,S.R. and Bird,B.M. (1977) "*Developments in PWM Inverters*," Proceedings of 2nd IFAC Symposium on Control in Power Electronics, Düsseldorf.

Bowes,S.R. and Clements,R.R. (1982) "*Computer-aided design of PWM inverter systems*," IEE Proc., Vol. 129, Pt. B, No. 1.

APPENDIX

List Of Symbols.

p	=	differential operator
R_s	=	stator resistance
R_r	=	rotor resistance
L_s	=	stator leakage inductance
L_r	=	rotor leakage inductance
M	=	mutual inductance
ω_r	=	angular speed of rotor (electrical)

Matrices D, S, C, S_1 and S_2. The matrices D, S and C used in the transformations of frame are defined as:

$$D = \sqrt{2/3}\begin{bmatrix} 1 & 1/2 & 1/2 \\ 0 & -3/2 & 3/2 \\ 1/\sqrt{2} & 1/\sqrt{2} & 1/\sqrt{2} \end{bmatrix} \qquad S = \begin{bmatrix} \cos\omega_r t & \sin\omega_r t & 0 \\ -\sin\omega_r t & \cos\omega_r t & 0 \\ 0 & 0 & 1 \end{bmatrix}$$

$$C = \sqrt{2/3}\begin{bmatrix} \cos\omega_r t & \cos(\omega_r t+120^\circ) & \cos(\omega_r t-120^\circ) \\ -\sin\omega_r t & -\sin(\omega_r t+120^\circ) & -\sin(\omega_r t-120^\circ) \\ 1/\sqrt{2} & 1/\sqrt{2} & 1/\sqrt{2} \end{bmatrix}$$

The matrices S_1 and S_2 used to express the inherent symmetry of the motor waveform are defined as:

$$S_1 = \begin{bmatrix} -1/2 & \sqrt{3}/2 & 0 & 0 \\ \sqrt{3}/2 & -1/2 & 0 & 0 \\ 0 & 0 & -1/2 & -\sqrt{3}/2 \\ 0 & 0 & \sqrt{3}/2 & -1/2 \end{bmatrix} \qquad S_2 = \begin{bmatrix} 1/2 & \sqrt{3}/2 & 0 & 0 \\ -\sqrt{3}/2 & 1/2 & 0 & 0 \\ 0 & 0 & 1/2 & \sqrt{3}/2 \\ 0 & 0 & -\sqrt{3}/2 & 1/2 \end{bmatrix}$$

State Variable Equation For Induction Motor. The equations for the general induction machine model in *d-q* frame with the usual assumptions can be expressed in matrix form as:

$$v = Ri + L\,p\,i + \omega_r G\,i \qquad \text{(i)}$$

where $v = [v_{ds} \quad v_{qs} \quad v_{dr} \quad v_{qr}]^T$

$i = [i_{ds} \quad i_{qs} \quad i_{dr} \quad i_{qr}]^T$

v^T = transpose of the matrix v

$$R = \begin{bmatrix} R_s & 0 & 0 & 0 \\ 0 & R_s & 0 & 0 \\ 0 & 0 & R_r & 0 \\ 0 & 0 & 0 & R_r \end{bmatrix} \quad L = \begin{bmatrix} L_s & 0 & 0 & 0 \\ 0 & L_s & 0 & 0 \\ 0 & 0 & L_r & 0 \\ 0 & 0 & 0 & L_r \end{bmatrix} \quad G = \begin{bmatrix} 0 & 0 & 0 & 0 \\ 0 & 0 & 0 & 0 \\ 0 & M & 0 & M \\ -M & 0 & -M & 0 \end{bmatrix}$$

Rearranging (i) gives,

$$v = (R + \omega_r G)i + Lpi$$

$$\text{or,} \quad pi = -(R + \omega_r G)L^{-1} + IL^{-1}v \qquad \text{(ii)}$$

Thus, by comparing (ii) with the standard state-variable equation (iii),

$$\dot{x} = Ax + Bu \qquad \text{(iii)}$$

it gives A and B, which are defined as in (iv),

$$A = -(R + \omega_r G)L^{-1}$$
$$B = IL^{-1} \qquad \text{(iv)}$$

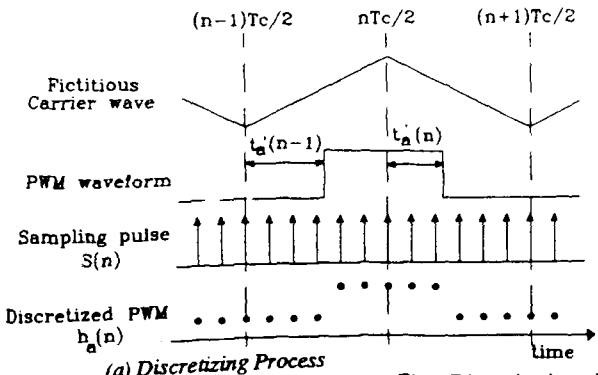

(a) Discretizing Process

```
Ts=(Tc/2)/N;
S=0:Ts:N*Ts*(2*R);
p=1;q=1;
for q=1:2*R;
  for p=N*(q-1)+1:N*q;
    if rem(q,2) >0
      if S(p)<ta'(q)+(q-1)*(Tc/2)
        ha(p)=-1;
          else
        ha(p)=1;
      end,
      else
      if S(p)<ta'(q)+(q-1)*(Tc/2)
        ha(p)=1;
          else
        ha(p)=-1;
      end,
    end,
  end,
end
```

(b) Program

Fig.1 Discretization of PWM Waveform

Fig. 2 Transformation of Induction Motor Windings to *d-q* frame

Fig. 3 Sampled Phase Current over one-sixth of Cycle

Fig. 4 Voltage Waveforms of Inverter with f=50Hz, M/f=0.02, R=9

Fig. 5 Voltage Waveforms of Inverter with f=35Hz, M/f=0.02 and R=15.

Fig.6 PWM stator voltages and currents waveforms in *d-q* frame with f=50Hz, M=0.99 and R=15 and slip=0.02.

Fig.7 Locus of Stator Phasor of PWM Waveform (f=35Hz,M=0.99,R=21)

Fig.8 Motor Phase Currents with f=50Hz,M=0.99,R=15,slip=0.2

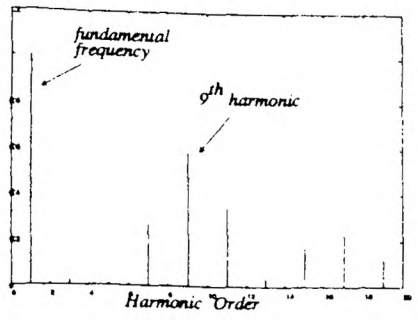

Fig. 9 Harmonic Spectrum of PWM Wave corresponding to Fig.4

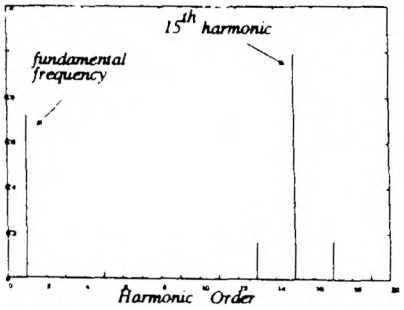

Fig. 10 Harmonic Spectrum of PWM Wave corresponding to Fig.5

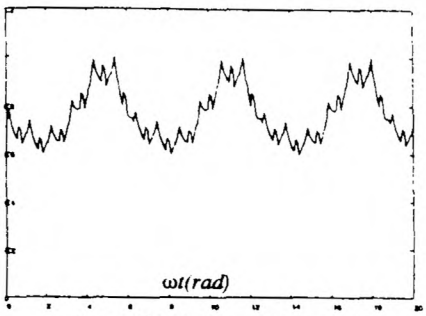

Fig. 11 Electromagnetic Torque (f=50Hz,M=0.99,R=6,slip=0.02)

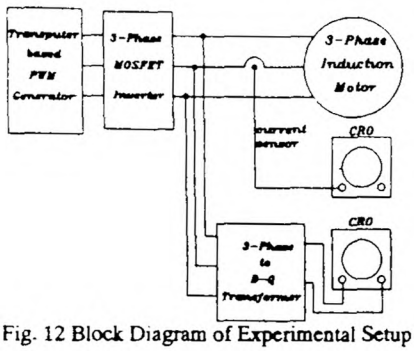

Fig. 12 Block Diagram of Experimental Setup

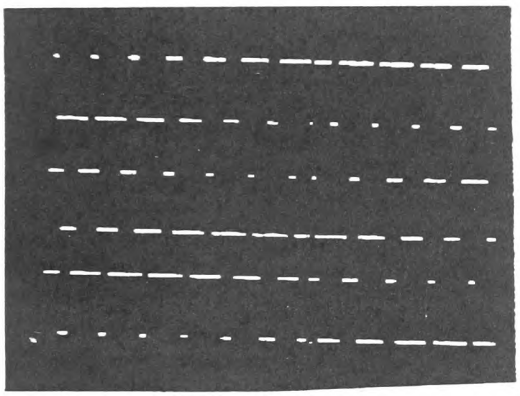

Fig. 13 Experimental Result corresponding to Fig. 5

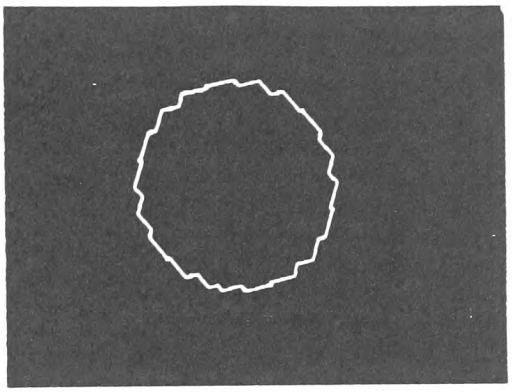

Fig. 14 Experimental Result corresponding to Fig.7

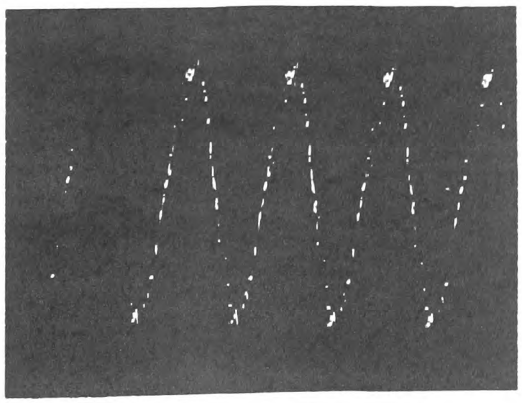

Fig. 15 Experimental Result corresponding to Fig.8

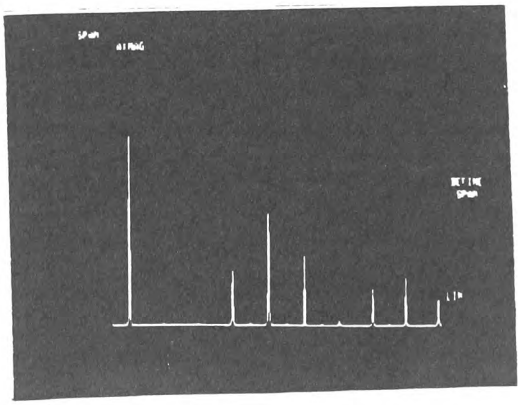

Fig. 16 Experimental Result corresponding to Fig. 9